The consequences of Cannabinoid receptor 2 expression in HER2+ breast cancer

Nicolas Jaime Roth

April 2023

Submitted in partial fulfilment of the requirements of the Degree of Doctor of Philosophy

Queen Mary University of London

William Harvey Research Institute

Centre for Endocrinology

John Vane Science Centre

Charterhouse Square London EC1M 6BQ

In loving memory of Alan Francis Blake

1927-2016

Be healthy, be happy

Declaration

I, Nicolas Jaime Roth, confirm that the research included within this thesis is my own work or that where it has been carried out in collaboration with, or supported by others, that this is duly acknowledged below and my contribution indicated. Previously published material is also acknowledged below.

I attest that I have exercised reasonable care to ensure that the work is original, and does not to the best of my knowledge break any UK law, infringe any third party's copyright or other Intellectual Property Right, or contain any confidential material.

I accept that the College has the right to use plagiarism detection software to check the electronic version of the thesis.

I confirm that this thesis has not been previously submitted for the award of a degree by this or any other university. The copyright of this thesis rests with the author and no quotation from it or information derived from it may be published without the prior written consent of the author.

Signature: Nicolas Jaime Roth

Date: 4th April 2023

Publications

Relton EL, **Roth NJ**, Yasa S, Kaleem A, Hermey G, Minnis CJ, Mole SE, Shelkovnikova T, Lefrancois S, McCormick PJ, Locker N. The Batten disease protein CLN3 is important for stress granules dynamics and translational activity. J Biol Chem. 2023 Mar 23:104649. doi: 10.1016/j.jbc.2023.104649. PMID: 36965618.

Tomas Bort E, Joseph MD, Wang Q, Carter EP, **Roth NJ**, Gibson J, Samadi A, Kocher HM, Simoncelli S, McCormick PJ, Grose RP. Purinergic GPCR-integrin interactions drive pancreatic cancer cell invasion. *Elife*. 2023 Mar 21;12:e86971. doi: 10.7554/eLife.86971. PMID: 36942939.

Israeli H, Degtjarik O, Fierro F, Chunilal V, Gill AK, **Roth NJ**, Botta J, Prabahar V, Peleg Y, Chan LF, Ben-Zvi D, McCormick PJ, Niv MY, Shalev-Benami M. Structure reveals the activation mechanism of the MC4 receptor to initiate satiation signaling. *Science*. 2021 May 21;372(6544):808-814. doi: 10.1126/science.abf7958. PMID: 33858992.

Sarott RC, Westphal MV, Pfaff P, Korn C, Sykes DA, Gazzi T, Brennecke B, Atz K, Weise M, Mostinski Y, Hompluem P, Koers E, Miljuš T, **Roth NJ**, Asmelash H, Vong MC, Piovesan J, Guba W, Rufer AC, Kusznir EA, Huber S, Raposo C, Zirwes EA, Osterwald A, Pavlovic A, Moes S, Beck J, Benito-Cuesta I, Grande T, Ruiz de Martı N Esteban S, Yeliseev A, Drawnel F, Widmer G, Holzer D, van der Wel T, Mandhair H, Yuan CY, Drobyski WR, Saroz Y, Grimsey N, Honer M, Fingerle J, Gawrisch K, Romero J, Hillard CJ, Varga ZV, van der Stelt M, Pacher P, Gertsch J, McCormick PJ, Ullmer C, Oddi S, Maccarrone M, Veprintsev DB, Nazaré M, Grether U, Carreira EM. Development of High-Specificity Fluorescent Probes to Enable Cannabinoid Type 2 Receptor Studies in Living Cells. *J Am Chem Soc*. 2020 Oct 7;142(40):16953-16964. doi: 10.1021/jacs.0c05587. PMID: 32902974.

Acknowledgements

First and foremost, I would like to thank my supervisors Peter and Richard for their advice and guidance through the years. They both were integral to not only the successful completion of my PhD, but also to the enjoyment of being in the lab. I would like to thank Peter for providing many opportunities for collaborations mentorship. And to Richard, thank you for the encouragement and motivation to help your students to strive to achieve their best. Thank you to the Medical Research Council for funding the Doctoral Training Programme.

I am very grateful for the opportunity to carry out my PhD in Tumour Biology. It was an incredibly supportive, helpful and friendly department to join. Thank you to the lab support staff who kept Tumour Biology running despite all the difficulties. To Eamonn and Debbie, thank you for all the necessary hard work this entailed. I would also like to thank the other lockdown lab Owls, Fred John, Demi and Elena for their support during those difficult months. Thank you to Demi, Shayin, Reza, Elena, Amelia, Litsa, Lauren, Josie, Lucy, Lakshmi, Jesus, Gabriel and Lucia who helped make Tumour biology a fun and social environment to work in and a great group to wind down in the pub with. To Rachel and Christine, thank you for your joviality and helping me hone my terrible jokes.

Thank to Endocrinology lab members for their help in many aspects of my PhD project, especially Georges, Zara, Dillon and James who helped my design, set up and run many experiments. Thank you to Natasa Tomasevic for her hard work in difficult circumstances.

I would like to extend my gratitude to Barrie and Stephanie for their role as my 9-month and 18-month examiners and offering productive feedback and insight through my entire PhD, especially Barrie's inputs, help with metabolic data analysis and career guidance.

It would be hard to overstate my gratitude towards the entire Grose group, both the past and present members, for their support, encouragement, insight and good humour. Both during meetings and in the lab, they provided invaluable feedback to my scientific work and outside the lab a wonderful group of friends. Thank you to the post docs Ed, Lucia, Kubra, Chris and Abi for their wisdom and technical knowledge, and especially to Ed for always having an answer for my many questions.

To Shayin, Demi, Elena and Reza, the PhD journey would not have been the same without you all. You have all helped keep me sane through all highs and lows and I will be forever grateful for your friendship. Reza, thank you for helping me to not Jez everything up. Elena, thank you. Thank you for your all help, support and kindness.

A big thank you to Smashed Crab Studio for very generously providing me with a laptop during the writing of this thesis, you made a hard grind that much easier.

And finally, thank you to my wonderful and supportive family for their encouragement, understanding and the many, many cups of tea.

Abstract

Overexpression of the receptor tyrosine kinase HER2 (*ERBB2*) leads to an aggressive form of breast cancer. In the past two decades many HER2-targeted therapies have been developed that have increased patient survival, however, metastatic patients often develop resistance to these treatments. HER2 expression has been shown to induce the expression of cannabinoid receptor 2 (CB_2), which relates to a more aggressive phenotype, increased rates of metastasis, and a worse prognosis. Targeting CB_2 in HER2+ breast cancer represents a novel way to decrease protumourigenic signalling and overcome HER2-target treatment resistance.

To understand the role of CB_2 in promoting tumourigenesis and its potential as a therapeutic target, I engineered a CB_2 expression system in HER2+ breast cancer cell lines. Using this system in 2D and 3D models, I demonstrate that CB_2 expression increases migration and invasion, which is abrogated with cannabinoid treatment. CB_2 expression leads to metabolic rewiring, increased ATP production and increased protection against oxidative stress. The resulting metabolic phenotype reproduces that of cancer stem cells (CSCs), and we observed CB_2-dependent increased stemness, shown by mammosphere formation, which was reduced upon cannabinoid treatment. Moreover, CB_2 increased Wnt/β-catenin signalling, leading to the expression of the stem cell marker ALDH1A1. We also report that CB_2 expression increases PYK2, AKT, and PDL1, driving 3D invasion and immune escape. Taken together, these data suggest that CB_2 expression in HER2+ breast cancer induces a migratory CSC-like phenotype that is highly invasive and potentially facilitates immune evasion, thereby promoting metastasis. The expression of CB_2 could be an important biomarker for a less favourable prognosis in HER2+ breast cancer. Using CB_2-targeting therapies in conjunction with traditional treatments could lead to reduced metastasis, reduced tumour recurrence and improved patient outcomes.

Contents

Table of Figures

Acronyms and abbreviations

2-AG	2-arachidonoyl glycerol
ABC	ATP-binding cassette
ADC	Antibody-drug conjugates
ADCC	Antibody-dependent cell cytotoxicity
ADH	Atypical ductal hyperplasia
AEA	Arachidonoyl ethanolamide
ALDH	Aldehyde dehydrogenase
APC	Adenomatous polyposis coli
ATP	Adenosine triphosphate
APS	Ammonium persulfate
BCS	Breast-conserving surgery
BSA	Bovine serum albumin
CAF	Cancer-associated fibroblasts
cAMP	Cyclic adenosine monophosphate
CB1	Cannabinoid receptor 1
CB2	Cannabinoid receptor 2
CBD	Cannabidiol
CBN	Cannabinol
CK1	Casein kinase 1
CNS	Central nervous system
COX2	Cyclooxygenase 2
CSC	Cancer stem cell
CSF1	Colony stimulating factor 1
CTC	Circulating tumour cell
CTCF	Corrected total cell fluorescence

CTG	Cell Titre Glow
CTLA4	Cytotoxic T-lymphocyte-associated protein 4
DAGL	Diacylglycerol lipase
DAPI	4′,6-diamidino-2-phenylindole
DC	Dendritic cell
DCIS	Ductal carcinoma *in situ*
DNM1P46	Dynamin 1 pseudogene 46
Dox	Doxycycline
DTC	Disseminated tumour cell
ECAR	Extracellular acidification rate
ECM	Extracellular matrix
ECS	Endocannabinoid system
EGFR	Epidermal growth factor receptor
EMT	Epithelial-mesenchymal transition
ER	Endoplasmic reticulum
ER	Oestrogen receptor
FAAH	Fatty acid amide hydrolase
FACS	Fluorescence-activated cell sorting
FAO	Fatty acid oxidation
FBS	Foetal bovine serum
FCCP	Carbonyl cyanide-p-trifluoromethoxyphenylhydrazone
FISH	Fluorescence in situ hybridization
G6P	Glucose-6-phosphate
GBM	Glioblastoma
GPX	Glutathione peroxidase
GSK3	Glycogen synthase kinase 3
HA	Hemagglutinin

HER2	Human Epidermal Growth Factor Receptor 2
HK3	Hexokinase 3
HKDC1	Hexokinase domain containing 1
HGF	Hepatocyte growth factor
IDC	Invasive ductal carcinoma
IDO	Indoleamine 2,3-dioxygenase
IGFR1	Insulin-like growth factor 1 receptor
IHC	Immunohistochemistry
IL-10	Interleukin 10
LDHB	Lactate dehydrogenase B
MAGL	Monoacylglycerol lipase
MAPK	Mitogen-activated protein kinase
MET	Mesenchymal-to-epithelial transition
MFE	Mammosphere formation efficiency
MMP	Matrix metalloproteinase
MS	Multiple sclerosis
MTS	3-(4,5-dimethylthiazol-2-yl)-5-(3-carboxymethoxyphenyl)-2-(4-sulfophenyl)-2H-tetrazolium
NAD	Nicotinamide adenine dinucleotide
NAPE	N-arachidonoyl phosphatidyl ethanol
OCR	Oxygen consumption rate
PBS	Phosphate buffered saline
PGC-1α	Peroxisome proliferator-activated receptor gamma coactivator 1-alpha
PD1	Programmed cell death protein 1
PDL1	Programmed death-ligand 1
PI3K	Phosphoinositide 3-kinase
PIP2	Phosphatidyl inositol bis-phosphate

PLCß	Phospholipase C ß
PPARG	Peroxisome proliferator-activated receptor gamma
PR	Progesterone receptor
RA	Retinoic acid
RAR	Retinoic acid receptor
RSEM	RNA-seq by Expectation Maximisation
RT	Room temperature
RTKi	Receptor tyrosine kinase inhibitor
rtTA	Reverse tet-transactivator
RXR	Retinoid X receptor
SDS	Sodium dodecyl sulfate
TAE	Tris-acetate-EDTA
TAM	Tumour-associated macrophages
TBS	Tris buffered saline
TCA	Tricarboxylic acid cycle
TCGA	The Cancer Genome Atlas
T-DM1	Trastuzumab emtansine
TEMED	Tetramethylethylenediamine
TBGß	Transforming growth factor beta
THC	Δ9-tetrahydrocannabinol
TIMP	Tissue inhibitors of metalloproteinase
TNBC	Triple-negative breast cancer
TNM	Tumour-node-metastasis
TRE	Tetracycline response element
Treg	Regulatory T cell
TRP	Transient receptor potential
WT	Wild type

Chapter 1 Introduction

1.1 Breast cancer

Breast cancer is a leading cause of death among women worldwide and has become the most frequently diagnosed cancer, with 2.3 million diagnoses reported in 2020[1]. Documentation of breast cancer dates back to antiquity, with the earliest descriptions of breast cancer in ancient Egypt[2]. The visible manifestation and palpability of late-stage breast cancer allowed for easy identification and documentation of the disease in ancient texts such as the Edwin Smith Surgical Papyrus from 3500 BCE. The ancient Greek physician Hippocrates also describes breast cancer around 400 BCE. In accordance with his Humoral theory of medicine, Hippocrates postulated that breast cancer is caused by an excess of black bile and suggested treatment through restoring the balance of humours[3]. During this period, Hippocratic physicians used the phrase *krakinoma*, or carcinoma, derived from the Greek word for crab, *krakinos*, to describe the crab-like appearance of tumours and their associated blood vessels[2].

In the 1st century CE, Leonides provides the first documented description of a mastectomy with removal of the tumour and surrounding tissue through alternating incision and cautery to control bleeding, which became the surgery standard for over 1500 years[4,5]. Development of the radical mastectomy surgery by William Halsted at the end of the 19th century, revolutionised the surgical treatment of breast cancer and soon became the criterion standard. Radical mastectomy decreased recurrence rates by removing the surrounding breast tissue, the pectoralis major and minor and axillary lymph nodes[6].

The advancement of surgical practices and the understanding of breast cancer through the 20th and into the 21st century broadened surgical options. The radical mastectomy has since undergone adaptations, with the current standard-of-care 'modified mastectomy' developed by John Madden in 1972[7]. Furthermore, breast-conserving surgery (BCS), which leaves the majority of breast tissues intact rather than complete

removal of the breast through mastectomy, is now an option for many patients[8]. Alongside these advances in surgical practices was increased understanding of the biology and causes of breast cancer.

1.1.1 Risk factors for breast cancer

Throughout the history of breast cancer, much effort has been invested in understanding its origins. Observations that breast cancer incidence changed with lifestyle factors such as celibacy, age at marriage and number of children have been recorded for hundreds of years[9]. In 1926 Janet Elizabeth Lane-Claypon published risk factors for breast cancer implicating the age at menarche, age at first birth, number of children, age at menopause and months of breastfeeding as significant risk factors that are still relevant today [10]. Additionally, various extrinsic factors have now been linked with increased breast cancer incidence, such as high-fat diet, lack of physical activity and alcohol consumption[11].

Further research into the causes of breast cancer identified inherited genetic mutations in two tumour suppressor genes, *BRCA1*[12] and *BRCA2*[13]. Carriers of *BRCA1* and *BRCA2* mutations were found to have an increased incidence of breast and ovarian cancers, with up to 80% increased risk of breast cancer by 70 years of age[14]. Missense and nonsense mutations in these breast cancer susceptibility genes increase the risk of breast cancer through impaired DNA repair, genomic instability and loss of cell cycle control[15]. Screening for these genes has enabled women at very high risk of developing breast cancer to take early preventative steps, such as prophylactic mastectomy[16].

BRCA mutations have also been recognised as a risk factor in the development of male breast cancer[17]. While the incidence of male breast cancer is considerably lower than female breast cancer, contributing to less than 1% of all breast cancer diagnoses, male breast cancer is becoming more frequently diagnosed[18]. Furthermore, many risk factors

associated with female breast cancers are similar amongst men, such as age, hormonal imbalance and obesity[19]. However, due to the differences in biology, gene expression, subtypes and survival rates between male and female breast cancer[20], this thesis solely focuses on breast cancer in women.

1.1.2 Breast cancer development

Cancer of the breast prominently occurs in the breast duct, the vessel that carries milk from the lobules to the nipple, with around 80% of breast cancer cases diagnosed as ductal carcinoma[21]. Lobular breast cancer is less common, making up 10-15% of breast cancer diagnoses[21], and is not covered in this thesis. The breast duct comprises an inner layer of polarised luminal epithelial cells and an outer layer of myoepithelial cells that act as a supportive barrier and provide contractile forces for milk expulsion[22] (Figure 1.1.1). This ductal bilayer of cells is surrounded by the basement membrane, primarily made up of collagen, laminin, nidogen and proteoglycans[23].

The initial formation of breast cancer and its progression to invasive and metastatic cancer involves both cell-intrinsic (e.g. genetic mutations) and cell-extrinsic processes (e.g. ECM remodelling)[24]. Initial aberrant growth starts with intra ductal hyperplasia, leading to atypical ductal hyperplasia (ADH), abnormal but non-cancerous growth within the lumen[24]. ADH precedes ductal carcinoma *in situ* (DCIS), where the abnormal growth becomes cancerous, and cells continue to proliferate within the ductal lumen. DCIS is a non-invasive form of breast cancer confined to the lumen by the anti-tumoural action of myoepithelial cells and the basement membrane[25]. However, DCIS is a non-obligate precursor to invasive ductal carcinoma (IDC), so whilst some patients may remain with DCIS for life with a favourable prognosis, some patients will progress to IDC, which has a significantly poorer prognosis[26] (Figure 1.1.1).

Pre-invasive DCIS can lead to alterations of the surrounding microenvironment to support tumour growth and progression, such as increased angiogenesis, increased leukocyte infiltration and protumoural alterations of the myoepithelial cells[27]. Interestingly, transcriptome analysis revealed high levels of similarity in gene expression changes in epithelial cancer cells between DCIS to IDC[28], indicating genetic alterations are not the cause of DCIS progression. There are, however, significant changes in non-cancerous myoepithelial cell gene expression, likely caused by epigenetic modifications[29].

Progression from DCIS to IDC requires cancer cells to escape the ductal environment through the loss of the myoepithelial layer and the basement membrane. The population of myoepithelial cells becomes heterogenous, with some losing their anti-tumourigenic properties and promoting neoplastic growth. These 'altered' myoepithelial cells have significantly different gene expression compared to myoepithelial cells from normal tissue[29]. Alterations in myoepithelial gene expression leads to the loss proteins involved in maintaining differentiation, such as cytokeratin 7, 14 and 17, and the oxytocin receptor, decreasing their ability to provide a barrier that can prevent invasion into the surrounding tissue[30]. Altered myoepithelial cells also exhibit increased expression of CXCL12 and CXCL14, chemokines that regulate cell proliferation, migration and invasion, increasing the potential for DCIS to invade into the surrounding tissue[30]. Moreover, altered myoepithelial expression of different collagen isoforms and proteases, such as matrix metalloproteinase-2 (MMP2) and cathepsins, lead to the remodelling of the extracellular matrix (ECM), facilitating cancer invasion[27,31]. Furthermore, increased myoepithelial MMP2 expression has been linked to increased angiogenesis and worse patient outcomes[32].

In addition to altered myoepithelial cells increasing the risk of IDC, other stromal cells have altered phenotypes in DCIS that contribute to tumour progression. Cancer-associated fibroblasts (CAFs) secrete chemokines and growth factors such as CXCL12

and hepatocyte growth factor (HGF), promoting cell proliferation and angiogenesis[33,34]. Similarly to myoepithelial cells, the alterations in the stromal compartment that influence the phenotypic change are due to the epigenetic regulation of gene expression[35]. Importantly, breast cancer patients with high levels of Human epidermal growth factors receptor 2 (HER2), whose disease is more likely to progress to IDC, have been observed to have a higher frequency of epigenetic modifications in stromal cells, than patients with low HER2 expression[36].

Alterations in the myoepithelial and stromal cells also leads to increased leukocyte recruitment, with an increased level of macrophage infiltration often accompanying the progression from DCIS to IDC. Tumour-associated macrophages (TAMs) promote tumourigenesis through ECM remodelling, cytokine and proangiogenic factor secretion and inhibition of anti-tumour immune response, increasing the risk of DCIS progression. Moreover, cytotoxic chemotherapy has been shown to increase the recruitment of TAMs through increased cancer cell production of colony stimulating factor 1 (CSF1), a potent chemokine for macrophages[37]. TAMs may therefore be used as a prognostic marker to determine the likelihood of progression[38].

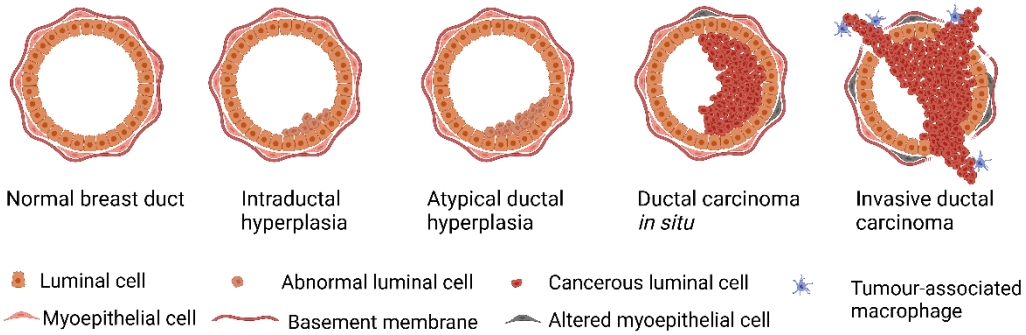

Figure 1.1.1: Breast cancer progression

The development of breast cancer from the normal duct to the preliminary aberrant non-cancerous growth of intraductal hyperplasia and atypical ductal hyperplasia (ADH). ADH precedes the formation of ductal carcinoma *in situ* (DCIS), a pre-invasive form of breast cancer, with initial changes to the surrounding microenvironment, including alterations to the myoepithelial cells. DCIS can progress to invasive ductal carcinoma (IDC), where cancer cells escape the ductal environment and invade the surrounding tissue. IDC is often accompanied by further alterations to the myoepithelial cells and the recruitment of tumour-associated macrophages (TAMs), leading to the degradation of the basement membrane and tumour invasion.

1.1.3 Breast cancer progression

The progression of DCIS to IDC is an important stage of breast cancer, with the 10-year overall survival of patients decreasing from around 98% with DCIS to less than 80% with IDC, attributable to their increased risk of metastasis[39,40]. Most deaths from breast cancer are due to such metastases[41], as breast cancer commonly metastasises to critical organs such as the lung, brain, and liver[21]. Clinically, the Tumour-node-metastasis (TNM) staging system is used to describe the size of the tumour (T), the presence of lymph node metastasis (N) and the extent of its metastatic spread (M). Overexpression of HER2 in breast cancer is associated with higher TNM grading, indicating the increased chance of HER2+ cancers to progress to IDC and metastasise[42].

For IDC to progress into metastatic breast cancer, tumour cells undergo a multistep process known as the metastatic cascade[43] (Figure 1.1.2). The first step requires a single cancer cell, or a cluster of cancer cells, to disseminate from the primary tumour. These disseminated tumour cells (DTCs) invade the surrounding tissue and then intravasate into the circulatory system through blood or lymph vessels. Whilst in the circulatory system, DTCs are termed circulating tumour cells (CTCs) until their extravasation at distant sites[44]. To survive the circulatory system and spread throughout the body, CTCs need to initially detach from the ECM and survive anoikis, an anchorage-dependent form of apoptosis[45]. Further, CTCs need to evade the immune system through the expression of immune checkpoint proteins such as PDL1 and CTLA4 and interactions with platelets in the blood[46]. Upregulation of cell surface proteins such as P-selectin on CTCs facilitates platelet binding and contributes survival of haemodynamic shear forces encountered in blood vessels[46].

For the formation of secondary tumour sites, CTCs need to leave the circulatory system through extravasation, which can be aided by arresting of CTCs in the

microvasculature. Once at a secondary site, tumour cells need to outcompete the surrounding tissue for available resources to proliferate and form clinically relevant metastases. Metastasis can be a relatively slow and inefficient process due to its multistep nature and the harsh environments of blood vessels and secondary sites, with only around 1% of CTCs successfully establishing macrometastases[47].

Once at a secondary site, DTCs can remain dormant, where the level of proliferation is not sufficient to facilitate the formation of macrometastses[48]. These dormant micrometastases formed of small groups of DTCs, or even single cells, can have latency periods from weeks to years, depending on tumour grade[49]. Due to the low levels of proliferation, and the genetic heterogeneity between metastases and the primary tumour, cytotoxic chemotherapy and targeted therapies can fail to eliminate the dormant metastases, leading to their eventual awakening, growth into macrometastases and patient relapse[50].

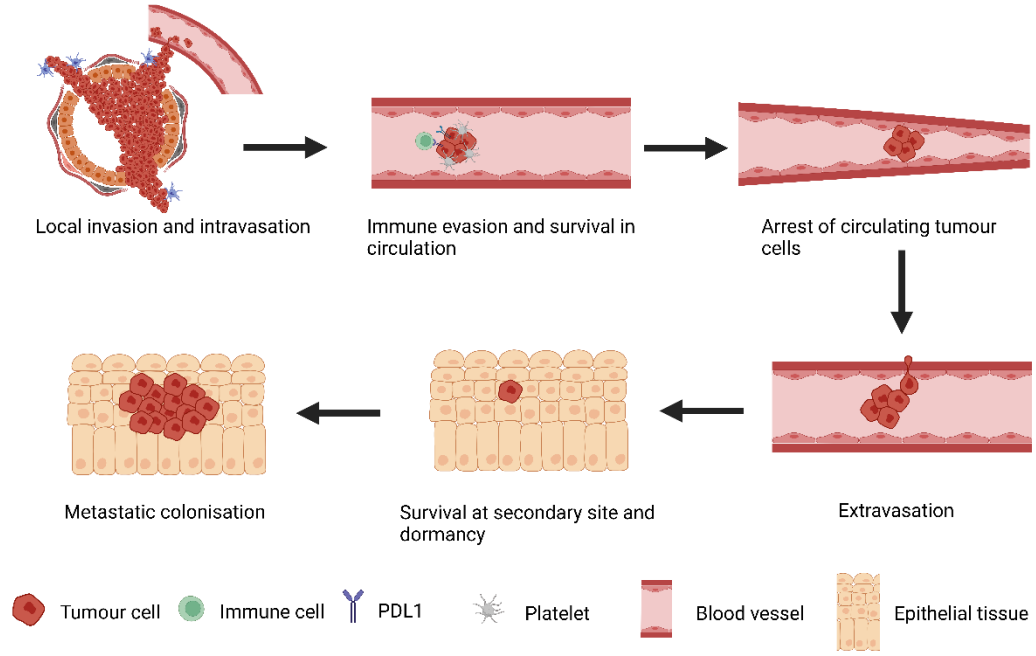

Figure 1.1.2: The metastatic cascade

Metastatic progression from invasive cancer begins with intravasation into the circulatory system. Once in circulation, cancer cells need to evade the immune system through the expression of immune checkpoint proteins and interactions with platelets. Circulating tumour cells arrest at distant sites throughout the body and extravasate into the surrounding tissue. At the secondary site, metastatic tumour cells adapt to compete with normal cells to access the required nutrients for proliferation. Micrometastases can remain dormant and not rapidly proliferate for extended periods. Tumour recurrence can occur when dormant metastases awaken, leading to the metastatic colonisation of secondary tumour sites and relapse.

1.1.4 The subtypes of breast cancer

Breast cancer is considered a highly heterogenous disease, with patient outcomes varying significantly. The classification of patients into subtypes began after the ground-breaking studies by Perou *et al.* in 2000, in which patient tumour gene expression signatures were profiled using microarrays[51]. Cancers were categorised as either luminal A, luminal B, basal-like or HER2+ using intrinsic gene expression profiles. The division of breast cancer into subtypes has aided the accurate determination of patient prognosis, their response to specific treatments, and the potential for targeted therapy[52].

Luminal breast cancer

Breast cancers that display expression of luminal epithelial markers, such as cytokeratin 8 and 18, are classified as luminal subtype and are further subdivided into luminal A and luminal B, which differ in terms of prognosis, marker expression and treatment options[51]. Luminal A breast cancer is characterised by the expression of the oestrogen receptor (ER) and the progesterone receptor (PR) and a lack of HER2 expression. Luminal A cancers often display low levels of proliferation markers such as Ki67 and therefore have a low proliferation index[53] and account for the highest proportion of breast cancers, around 50-60% of all diagnoses[54]. Patients diagnosed with luminal A have the best prognosis of all subtypes, with an overall survival rate of 95% after 5 years[55]. Patients are often treated with endocrine therapies, such as tamoxifen, which can significantly increase their long-term survival[56].

Luminal B breast cancers are ER+, with or without PR expression and typically negative for HER2, and account for 15-20% of breast cancer diagnoses[54]. Luminal B cancers are differentiated from luminal A due to their characteristic high levels of Ki67 and expression of other proliferation markers such as MYBL2 and cyclin-B1, resulting

in a high proliferative index[57]. Hence, luminal B is an aggressive subtype of breast cancer resulting in poor patient outcomes, with only 88.7 % of patients surviving for 5 years[55]. Moreover, luminal B cancers are less responsive to endocrine therapies, neoadjuvant paclitaxel, and doxorubicin-based chemotherapies[54].

Basal breast cancer

The basal subtype is characterised by the expression of basal epithelial markers cytokeratin 5, cytokeratin 17 and integrin β4[51], and accounts for 10-20% of breast cancer diagnoses[58]. Basal breast cancers are poorly differentiated and have a high histological grade and proliferative index[59]. Patients with basal breast cancer typically suffer from poor prognoses with a high chance of relapse and increased rates of metastasis[60], with only 78.5% of patients surviving to 5 years[55]. Basal cancers often lack detectable ER, PR or HER2 expression by immunohistochemistry (IHC) and are therefore termed triple-negative breast cancer (TNBC). However, not all basal breast cancers are triple negative. As the basal subtype is defined through microarray analysis of gene expression and TNBC is classed through IHC, there is only around an 80% concordance of these two classifications[54]. Basal cancers often exhibit overexpression of oncogenic proteins such as EGFR, Ki67 and cyclin-E[61]. Interestingly, patients that have mutations in BRCA1 are more likely to be diagnosed with basal-like breast cancer than other subtypes[54].

HER2+ breast cancer

HER2+ breast cancer, the focus of this thesis, is a highly proliferative subtype, comprising approximately 20% of diagnoses[62] and is characterised by overexpression of HER2, which is defined by high IHC and fluorescence *in situ* hybridization (FISH) scores of tumour biopsies[63]. Patients diagnosed with HER2+ breast cancer typically

have poor prognoses with an overall survival rate of 85.6% at 5 years[55]. HER2+ breast cancer often has low or no expression of ER and PR, although in some cases, luminal breast cancers can show HER2 expression (discussed later). Furthermore, HER2 expression is observed in some breast cancers with basal gene expression profiles[64].

HER2 is a receptor tyrosine kinase in the ErbB family of receptors, comprising four receptors, epidermal growth factor receptor (EGFR), HER2, HER3 and HER4, which upon ligand binding, can homo- and heterodimerise to regulate signalling pathways[65]. HER2 has no known ligand; however, due to its strong kinase activity, it is the preferential dimerisation partner of the other members of the ErbB family, commonly forming HER2-EGFR, HER2-HER3 and HER2-HER4 heterodimers[66,67]. Activation of HER2 leads to signalling through the mitogen-activated protein kinase (MAPK) and phosphoinositide 3-kinase (PI3K)[68] pathways resulting in cell proliferation, survival, invasion and angiogenesis. In breast cancer, HER2 can heterodimerise with any member of the ErbB family. However, the HER2-HER3 heterodimer results in the most potent protumoural signalling[69]. Moreover, unlike other ErbB family members, overexpression of HER2 allows for ligand-independent homodimerisation and activation without the need for any growth factor ligands, resulting in the rapid, uncontrolled growth that is characteristic of HER2+ breast cancer[70]. Whilst HER2+ cancers are highly proliferative, they often lack upregulation of the proliferation markers PCNA and Ki67 which are commonly observed in other aggressive breast cancers, such as TNBC[71]. However, HER2+ cancers commonly have mutations in p53 and increased cell cycle activation[72].

Overexpression of HER2 in breast cancer is commonly caused by gene amplification events, such as polysomy of chromosome 17, where the HER2 gene, *ERBB2*, is located[73]. Moreover, whilst relatively rare, hyperactivating mutations of HER2 can lead to tumourigenesis. A mutation that is present in around 5% of HER2+ breast cancers is the in-frame deletion of exon 16 of *ERBB2* (delta 16 HER2), resulting in

constitutive homodimerisation and activation of HER2[74]. Another hyperactive HER2 mutant is p95HER2, a truncation of the HER2 protein that lacks the extracellular domain whilst retaining a constitutively active form of the intracellular domain, contributing to increased tumour growth[75].

Other subtypes of breast cancer

Whilst most patients can be classified into the previously mentioned subtypes, there are rarer subtypes with distinct phenotypes. The normal breast-like subtype accounts for around 5-10% of breast cancer diagnoses and displays gene profiles similar to normal breast tissue[54]. Normal breast-like cancers do not express ER, PR and HER2 and are thus classified as a subset of TNBC. However, they lack expression of basal markers such as cytokeratin 5 and EGFR, preventing classification into the basal subtype[54]. Another subset of TNBC is the claudin-low breast subtype. These tumours display low levels of the cell-cell adhesion proteins claudin 1, 3, 4 and 7. Claudin low tumours often have an epithelial-mesenchymal transition (EMT) phenotype and poor patient outcomes[76].

Expression of HER2 is also occasionally seen in luminal breast cancer, termed the luminal-HER2 subtype[71]. These cancers are HER2+ and ER+, often with low PR expression. Patients with luminal-HER2 cancer are less responsive to endocrine therapy such as tamoxifen and show increased rates of tumour recurrence[77,78].

Subtyping of breast cancer has become an invaluable clinical tool to determine patient prognosis and treatment plans. IHC analysis of patient tissue is often sufficient for subtype diagnosis; however, differentiating between subtypes can be difficult due to arbitrary cut-offs, poor inter-lab reproducibility and different antibody selections used in staining classifications[54]. More reliable diagnosis can be achieved through gene expression analysis using clinical RT-qPCR panels such as MammaPrint[79] and

Oncotype Dx[80]. The ability to differentiate between breast cancer subtypes allows for prognostic assessments, patient stratification and the tailoring of personalised therapies. The discrimination between cancers of different grades enables rapid aggressive treatment regimens to be implemented whilst sparing patients with low-grade cancers from the side effects of unnecessary treatment.

1.2 Treatment and resistance in HER2+ breast cancer

1.2.1 HER2+ breast cancer treatment

Although *ERBB2* is a potent oncogene and its over expression relates to poor patient outcomes, the presence of HER2 on the cancer cell surface allows for HER2-targeted therapies. In 1998, the development of the humanised anti-HER2 monoclonal antibody trastuzumab (Herceptin) revolutionised the treatment of HER2+ breast cancer. Trastuzumab binds to the extracellular juxtamembrane region of HER2, preventing HER2 homodimerisation, disrupting the formation of HER2-HER3 heterodimers and abrogating signalling through the MAPK and PI3K pathways[81–83]. Trastuzumab also triggers HER2 internalisation and degradation via c-Cbl, initiates cell cycle arrest and leads to apoptosis[84]. Furthermore, trastuzumab interacts with Fc receptor family expressed on the patient's immune cells and mediates cancer cell killing through to antibody-dependent cell cytotoxicity (ADCC), primarily through the action of natural killer cells[85,86].

Trastuzumab is indicated for early-stage breast cancer in both adjuvant and neoadjuvant settings, in combination with chemotherapy and as a monotherapy[87,88]. Combination trastuzumab with paclitaxel or anthracycline chemotherapies has become the mainline therapy for patients with HER2+ breast cancer[89]. Trastuzumab has dramatically improved the outcome of HER2+ breast cancer patients since the

start of its clinical use, with adjuvant trastuzumab treatment reported to increase 5-year disease-free survival by around 12%[90].

Since the advent of trastuzumab, other therapies targeting HER2 have been developed. Lapatinib, a small molecule receptor tyrosine kinase inhibitor (RTKi) of HER2 and EGFR, acts as a competitive inhibitor of the adenosine triphosphate (ATP) binding site, preventing the kinase activity and subsequent signal transduction[91]. Lapatinib has been approved for clinical use in patients with metastatic breast cancer and can significantly extend patient survival[92]. Additionally, lapatinib can improve the progression-free and disease-free survival in patients that have developed resistance to trastuzumab[93] and the combination therapy of trastuzumab and lapatinib is more effective than either alone[94].

Other combinations have also been shown to increase therapeutic response, with trastuzumab, pertuzumab (another HER2-targeted monoclonal antibody) and the chemotherapy docetaxel prescribed for metastatic HER2+ breast cancer significantly increasing patient survival[93]. The development of effective therapeutic anti-HER2 antibodies also allows the target delivery of cytotoxic agents in the form of antibody-drug conjugates (ADCs). Trastuzumab emtansine (T-DM1) and trastuzumab deruxtecan are well-tolerated ADC therapies used in unresectable metastatic breast cancer patients[95] and significantly increase their survival[96,97]. In these ADCs, trastuzumab binds to HER2-expressing cancer cells and induces receptor internalisation to deliver the cytotoxic payload. Once inside the cell, emtansine inhibits microtubule assembly, preventing cell division[98], whereas deruxtecan acts as a topoisomerase inhibitor, blocking DNA replication, both resulting in cell death[99]. Moreover, cancer cells killed through the action of ADCs can subsequently release the cytotoxic component into the surrounding milieu, resulting in the death of cells that may have been resistant to trastuzumab binding, via the bystander effect[100].

1.2.2 Treatment resistance in HER2+ breast cancer

HER2+ breast cancer patients are at a higher risk of tumour recurrence than HER2- patients due to the increased capacity of HER2-expressing cancer cells to establish metastases[101]. This is compounded due to the high rates of treatment resistance in HER2+ breast cancer, with over two-thirds of patients displaying intrinsic resistance or acquiring resistance over the course of HER2-targeted treatment[102]. Although trastuzumab and other HER2-targeted treatments are initially effective therapies for most HER2+ patients, there are many resistance mechanisms that cancer cells use to prevent HER2 inhibition.

Intrinsic resistance to trastuzumab can occur in patients with mutated forms of HER2. For example, the p95HER2 mutant, which lacks the extracellular portion of HER2, no longer contains the trastuzumab binding site, whilst the intracellular side remains constitutively active[75]. Additionally, the delta 16 HER2 mutant, which still includes the trastuzumab binding site, confers resistance through its potent HER2 dimerisation, overcoming the inhibitory effects of trastuzumab[103]. However, this remains controversial as some report delta 16 HER2 mutant cells are still sensitive to trastuzumab action[104]. In addition to HER2 mutations blocking trastuzumab binding, the increased expression of MUC4 glycoprotein has been shown to contribute to resistance by binding to the extracellular domain of HER2, physically blocking the trastuzumab binding site and preventing HER2 inhibition[105].

Further, mutations in the signalling pathways downstream of HER2 can also lead to resistance. The intracellular kinase AKT is commonly mutated in invasive breast cancers, with over 30% of patients displaying hyperactivating mutations, reducing the efficacy of HER2 inhibition[69]. Moreover, loss of PTEN function through nonsense mutations or deletion events imparts resistance to blocking HER2 function by preventing the negative regulation of PI3K signalling[106]. Likewise, gain of function

mutations in PIK3CA allow for the circumvention of HER2 inhibition through constitutive downstream signalling and is involved in the resistance of many anti-neoplastic agents[107].

The alternative activation of these downstream pathways through the compensatory upregulation of different receptors is another common form of anti-HER2 treatment resistance. Overexpression of the other HER family members and increased heterodimerisation with HER2 is seen in cancers that have developed resistance to HER2 therapies, along with an increase in the ligands for EGFR, HER3 and HER4, further contributing to anti-HER2 therapy resistance[108]. The overexpression of non-HER family member cell surface receptors can maintain protumourigenic signalling via activating the same intracellular signalling pathways. HER2 inhibition can lead to compensatory increases insulin-like growth factor 1 receptor (IGFR1) or MET expression[69], and increased concentrations of their ligands can bypass the action of trastuzumab or lapatinib through the activation of AKT and MAPK signalling pathways[109]. Interestingly heterotrimerisation has been reported between HER2, HER3 and IGF1R in response to the inhibition of HER2, highlighting the diverse mechanisms of HER2 therapy resistance[110].

Furthermore, the overexpression of apoptosis and cell cycle regulators can reduce the efficacy of HER2 inhibition. Upregulation of cyclin-E is observed in trastuzumab-resistant patients[111], as well as the anti-apoptotic factors BIM and SURVIVIN, preventing both cell death and decreases in proliferation in response to HER2 inhibition[112,113]. Additionally, polymorphisms in the FCGRIIa receptor have been shown to impair trastuzumab binding and therefore limit the efficacy of trastuzumab-mediated cytotoxicity through defective ADCC[114,115].

1.2.3 Overcoming resistance

As a result of the numerous and diverse mechanisms of treatment resistance, patient relapse is a common event with over 30% of HER2+ patients suffering tumour recurrence[116]. Therefore, many patients are treated with combination therapies that aim to delay the onset of resistance and circumvent resistance once it has developed. Understanding the cause of a specific patient's resistance is valuable in deciding which combination treatment would be most successful. As such, cancers resistant to trastuzumab might still be sensitive to HER2 inhibition with small molecule RTK inhibitors due to their different mechanism of action. The increases efficacy of trastuzumab and lapatinib combination therapy for metastatic breast cancer patients indicates that the dual targeting HER2 can re-sensitise resistant cancers[117]. Additionally, the neoadjuvant polytherapy of trastuzumab, lapatinib and paclitaxel was significantly more effective than either trastuzumab or lapatinib alone, reinforcing the potential of combination therapies for combating resistance[118].

Trastuzumab used in conjunction with other anti-HER2 antibodies, such as pertuzumab or 19H6-Hu, which recognise different epitopes on HER2, can overcome HER2 mutations or steric hindrances that prevent the binding of a single antibody [109]. ADCs, as discussed earlier (Section 1.2.1), can combat resistance through the combination of HER2 inhibition and their cytotoxic action which is enhanced through the bystander effect. However, resistance to ADCs such as T-DM1 can occur through impaired HER2 internalisation; as such, there is a new generation of anti-HER2 ADCs under development that have distinct binding sites to trastuzumab and different cytotoxic drug cargoes. The ADCs ARX788 and XMT-1522.ARX788, anti-HER2 monoclonal antibodies conjugated to the tubulin polymerisation inhibitor amberstatin[119], are showing promising pre-clinical results in cancers resistant to T-DM1 and are shown to be an effective anti-neoplastic agent in *in vivo* mouse xenograft models using HER2+ breast cancer cell lines BT474 and HCC1954[120–122].

However, whilst there are effective strategies to combat resistance, hyperactivated downstream signalling networks still pose a significant therapeutic hurdle to overcome. Whilst inhibitors of AKT, PI3K, mTOR and other downstream signalling molecules have been used clinically, the blockade of these intracellular kinases is poorly tolerated and leads to adverse side effects[123]. Due to this, and the dynamic nature of cancer evolution, there is still an unmet need for further understanding of the mechanisms of resistance and the identification of alternate pathways and targets that could be used to prevent resistance development. One such system receiving increasing research interest as a potential target for anti-cancer drugs is the endocannabinoid system (ECS). Pre-clinical data have demonstrated that targeting the ECS with well-tolerated cannabinoids could aid in preventing metastasis, treatment resistance and tumour recurrence[124].

1.3 Targeting the endocannabinoid system in breast cancer

1.3.1 The endocannabinoid system

The endocannabinoid system (ECS) is a complex signalling system that regulates diverse processes throughout the body[125]. The ECS is evolutionarily ancient and has been found to regulate the feeding response in primitive *Cnidaria* prior to the evolution of bilateral animals[126] and is involved in many behavioural systems in complex vertebrates[127]. In humans, the ECS consists of the two main GPCR cannabinoids receptors (CB), CB_1 and CB_2, as well as less well-characterised receptors such as the orphan receptor GPR55, ion channels in the transient receptor potential (TRP) family and peroxisome proliferator-activated receptors (PPARs) (Figure 1.3.1). In addition to these receptors, the ECS comprises endogenous ligands, termed endocannabinoids, the enzymes responsible for endocannabinoid synthesis and degradation, and endocannabinoid membrane transporters[128].

1.3.2 Endocannabinoid ligands

The ligands of the ECS, endocannabinoids, are lipid-based molecules that exist as precursors in the cell membrane[125]. Unlike other signalling molecules, such as neurotransmitters, endocannabinoids are not synthesised in advance and stored in vesicles but are produced on demand through enzymatic modification of phospholipids on the inner leaflet of the cell membrane[129]. The two central and most well studied endocannabinoids are 2-arachidonoyl glycerol (2-AG) and arachidonoyl ethanolamine (AEA), which have distinct biosynthetic and degradation pathways. 2-AG is produced primarily from the precursor phosphatidyl inositol bis-phosphate (PIP_2) through the action of phospholipase C β (PLCβ) and diacylglycerol lipase (DAGL) enzymes[130]. After signalling, 2-AG is transported back across the cell membrane and can be degraded by monoacylglycerol lipase (MAGL) and cyclooxygenase 2 (COX2), resulting in a hydrolysed or oxidised product, respectively[131,132]. Degradation of 2-AG by COX2 produces prostaglandin glycerol ethers, an important step in prostaglandin synthesis[125].

Similarly, AEA is synthesised from N-arachidonoyl phosphatidyl ethanol (NAPE) by different enzymes such as NAPE-phospholipase C and NAPE phospholipase D. AEA can be degraded through the action of fatty acid amide hydrolase (FAAH) into ethanolamine[131] or by COX2 into prostaglandin E2[133], highlighting the interrelation between endocannabinoid signalling and other cellular pathways[125]. These endocannabinoids have differing affinities for CB_1 and CB_2, which can influence the cellular response. 2-AG is considered a full agonist for CB_1 and CB_2, whilst AEA has lower affinity for both receptors and acts as a partial agonist for these receptors[134]. In addition to 2-AG and AEA, there are many less well-characterised endocannabinoids, such as noladin, virodhamine, oleamide, and N-arachidonyoldopamine, that are less potent modulators of the ECS[135].

1.3.3 Phytocannabinoid ligands

Cannabinoids from the plant *Cannabis sativa*, so-called phytocannabinoids, are the group of molecules that mediate their biological effects through interaction with the ECS[125,128]. The cultivation of *Cannabis* for these effects has been recorded since the neolithic era, with documented medicinal, recreational and spiritual use dating back around 6000 years[136]. Whilst over 100 phytocannabinoids have been described, the effect of only a handful of these has been extensively studied. The most potent and well-known phytocannabinoid is Δ9-tetrahydrocannabinol (THC), the component of *Cannabis* responsible for its psychoactive effects through CB_1 binding[125]. In addition to its psychotropic action, THC acts as a sedative, appetite stimulant and analgesic through interactions with CB_1 in the brain[134].

Additionally, the phytocannabinoid cannabidiol (CBD), whilst not psychoactive, has many physiological effects, acting as an effective anxiolytic, antioxidant and anti-convulsant[137]. Interestingly, CBD does not bind to the orthosteric site of CB_1 or CB_2 and is thought to mediate some of its effects by acting as an allosteric modulator of these receptors[138] and through the action of TRPV and PPARs[134]. However, there is growing evidence that CBD can act as an inverse agonist for CB_1 and CB_2 and hence balances some of the psychoactive effects of THC[139].

1.3.4 Cannabinoid receptors

CB_1 and CB_2 are the major receptors through which both endo and phytocannabinoids mediate their effects. Whilst both receptors are found on tissues throughout the body, CB_1 is primarily located in the central nervous system (CNS) and CB_2 on immune cells and tissues[140]. CB_1 is localised to the cerebellum, basal ganglia, hippocampus and cortex of the brain[141], where it regulates sleep, appetite, mood, memory, cognition, circadian rhythm, stress and pain perception[125,128,134]. CB_1 mediates these wide-ranging

effects by regulating the firing of GABAergic, glutamatergic and cholinergic neurons, amongst others[141]. A major role of CB_1 on these neurons is inhibiting the continued firing of the pre-synaptic neuron, with CB_1 expression localised to the terminal end of neurons. Endogenous cannabinoids produced by the post-synaptic neuron signal to CB_1 in a retrograde manner, inhibiting further neurotransmitter release[142]. In addition to its diverse role in regulating normal brain function, CB_1 is also essential during brain development. CB_1 mRNA expression has been observed in the foetal brain from week 20 of gestation[143], with roles in establishing axonal connections, which continue into adulthood. Hence, adolescent use of *Cannabis* has been theorised to interfere with proper brain development by disrupting CB_1 function[128].

As most CB_2 expression is located on immune cells and organs such as the spleen, CB_2 activation with phytocannabinoids does not result in psychotropic effects[144,145]. Moreover, compared to the stable expression of CB_1 in the CNS, the expression of CB_2 in the immune compartment is highly inducible, with significant increases in CB_2 expression during tissue injury and in inflammatory states[146,147]. Activation of CB_2 by endocannabinoids typically has anti-inflammatory effects; however, CB_2 signalling can also promote inflammation, highlighting CB_2 as an important regulator of immune function[144]. CB_2 regulates the migration of immune cells to areas of infection and modulates their function through the production of cytokines such as IL-6 and IL-10 to mediate the inflammatory response[148,149]. Due to the importance of cannabinoid signalling in regulating inflammation, dysregulation of the ECS can result in inflammatory and autoimmune diseases[150,151]

Signalling through the CB_2 GPCR, usually results in the coupling to inhibitory Gαi/o G-proteins[152]; however, they less commonly associate Gαs G-proteins[148]. After ligand binding and signal transduction, active Gαi inhibits adenyl cyclase, leading to decreased cyclic adenosine monophosphate (cAMP) levels, which leads to the activation of AKT and MAPK pathways[148,153]. Moreover, CB_2 activation leads to β-

arrestin recruitment and subsequent receptor internalisation and arrestin-mediated signalling events[153]. Furthermore, the various cannabinoid ligands have displayed biased signalling through cannabinoid receptors, further fine-tuning their physiological function through the engagement with different G-proteins and differing degrees of G-protein activation[154,155]. Additionally, many synthetic cannabinoids have been developed that have high specificity and high affinity for CB_2 that has enabled its functional isolation[156]. Interestingly, further refinement of cannabinoid signalling occurs through receptor dimerisation with other GPCRs, such as CB_2 dimerisation with the chemokine receptor CXCR4 to meditate the migration of cancer cells[157].

1.3.5 Dysregulation of the endocannabinoid system in disease

Due to the wide-ranging functions of the ECS and its involvement in other major signalling pathways, it is unsurprising that perturbations of the ECS are a common cause of human disease. In fact, ECS is involved in many neurological disorders, including schizophrenia, Parkinson's, Alzheimer's, multiple sclerosis (MS), amyotrophic lateral sclerosis and epilepsy, as well as non-neurological conditions such as glaucoma, obesity, autoimmune disorders, and cancer[135,150,158–160]. Furthermore, manipulating ECS function through the medicinal application of *Cannabis* or its derivatives has proved successful in treating many of these conditions.

Nabilone, a synthetic analogue of THC, has been indicated for the relief of chemotherapeutic side effects[161], and Sativex (a cannabinoid preparation of 1:1 THC and CBD) is prescribed to patients with MS[162]. Furthermore, the ingestion of *Cannabis* is a recognised treatment for intraocular hypertension associated with glaucoma[163,164]. Moreover, much research has investigated the use of cannabinoids for palliative care for cancer patients due to their anti-emetic, anti-cachexic, and anti-nociceptive effects[165]. Now, however, increasing studies strongly suggest that dysregulation of the

ECS is common in various cancer types and that cannabinoids can have anti-tumourigenic effects in *in vitro*, *in vivo* and clinical research[166].

1.3.6 The role of the endocannabinoid system in cancer

The ectopic expression of CB_1 or CB_2 has been observed in many different cancers, including bone, brain, breast, gastrointestinal, lung, prostate and skin cancers[134,135,167–169]. Expression of the cannabinoid receptors in these cancers has been related to increased cancer cell growth, migration, invasion and angiogenesis[134,166,168]. In breast cancer, CB_2 is commonly expressed and linked to poor patient prognosis in most subtypes[170]. However, some report that CB_2 expression in ER+ breast cancer has been linked with improved patient survival[171]. Indeed, CB_2 expression correlates with breast cancer grade, with more aggressive cancers such as TNBC, luminal B and HER2+ breast cancer having higher CB_2 expression[134].

HER2+ breast cancers have the highest proportion of CB_2 expression of any subtype, with over 95% of HER2+ breast cancer patients displaying CB_2 expression with 75% having high CB_2 expression, with negligible expression of CB_2 observed in the surrounding normal breast tissue[172]. Moreover, HER2+ patients with high CB_2 expression are also more likely to have decreased overall survival and increased rates of relapse and metastasis[172]. Additionally, activation of the MAPK-ELK pathway through HER2 signalling has been shown to increase CB_2 expression[173]. It has been reported that CB_2 and HER2 receptors interact at the membrane and form a GPCR-RTK receptor heteromer[173]. Whilst GPCR-GPCR heteromers are relatively common in nature[174], comparatively few GPCR-RTK heteromers have been described[175]. The presence of the HER2-CB_2 heteromer in patient tissue correlates with poor survival and increased tumour recurrence[173].

1.3.7 Anti-cancer mechanisms of cannabinoids

The expression of the CB receptors in an array of cancers and their diverse physiological effects highlight the potential of targeting these receptors with cannabinoids to modulate cancer cell growth. The anti-proliferative effects of cannabinoids have been known since 1975 when Albert Munson and colleagues demonstrated that THC and cannabinol (CBN), another phytocannabinoid, reduced the *in vivo* growth of Lewis lung adenocarcinoma[176]. Since then, much research has been invested into elucidating the anti-cancer mechanisms of cannabinoids.

Most research into these mechanisms has been conducted in glioma cells, which commonly display upregulated expression of CB_1 and CB_2[124]. In these cells, the addition of cannabinoids such as THC and CBD can cause cancer cell death through autophagy-mediated apoptosis. Activation of the cannabinoid receptors leads to increased ceramide production, resulting in endoplasmic reticulum (ER) stress and inhibition of AKT via p8 and TRIB3[177]. Inactive AKT can no longer activate mTORC1, preventing the mTORC1-mediated inhibition of autophagy, leading to autophagic cell death[177]. Moreover, concurrent treatment with cannabinoids and the main line treatment of glioma, temozolomide, results in increased cancer cell death compared to either therapy alone[178]. This mechanism of cannabinoid-induced cell death has been observed wholly or partially in many other cancer types, including breast, pancreatic, liver and melanoma cancers[124].

However, autophagic cell death is not the only anti-cancer mechanism of cannabinoids. Cannabinoids have also been shown to reduce cancer cell migration, invasion, angiogenesis and metastasis *in vivo*[179]. Cannabinoid treatment prevents tumour growth through the inhibition of the cell cycle via decreased expression of CDK2 and decreased angiogenesis via a reduction in VEGF expression[179,180]. Moreover, exogenous cannabinoids can interact with COX enzymes, leading to

reduced expression of metastasis-related genes, inhibition of the cell cycle and ROS generation[166]. In addition, cannabinoids can decrease the activity of the potent tumourigenic β-catenin/Wnt pathway by reducing the activation and nuclear localisation of β-catenin[181]. Importantly, these cell death mechanisms appear to be unique to cancer cells. Normal cells expressing cannabinoid receptors are unaffected by cytotoxic activity of cannabinoid treatment, and the reason for this difference is yet to be elucidated[124].

However, it is important to note that some reports have documented protumoural effects of cannabinoids[179]. This biphasic signalling of cannabinoid receptors appears to be regulated by cannabinoid concentration, with low concentrations leading to increased proliferation and high concentrations preventing tumour growth and progression[179]. This biphasic signalling is observed under the normal function of CB_1 and CB_2, with endocannabinoid concentration impacting cellular response. For example, at high concentrations of AEA, there is an decrease in CB_2 expressing leukocytes' ability to phagocytose, whilst at low AEA concentrations, phagocytosis is enhanced[182]. Biphasic signalling is also observed with THC binding CB_1, with anxiolytic and anxiogenic effects at low and high concentrations, respectively[182]. Similarly to biased signalling with different cannabinoid ligands, the biphasic effect of ligand concentration could also be mediated by differential G-protein activation[182]. Furthermore, it is important to note that CB_2 activation in normal physiology often results in the opposite of CB_2 activation in cancer, through yet to be elucidated mechanisms. For instance, the activation of CB_2 in neuronal cells leads to increased cell survival via the BAX/BCL2 axis. However, in cancer cells CB_2 expression correlates with cell survival, and subsequent activation of CB_2 leads to apoptosis via BAX activity. In cancer, CB_2 expression, but not activation with exogenous cannabinoids, has the same effect as CB_2 activation in normal tissue.

In breast cancer, cannabinoids have been shown to lead to cell death via AKT inhibition and reduce expression of the breast cancer risk factor gene *BRCA1* via MAPK inhibition[166]. Experiments in the MMTV-neu mouse model of HER2+ breast cancer demonstrated that the addition of the CB_2-specific synthetic cannabinoid JWH133 or the phytocannabinoid THC reduced tumour burden by decreasing the number of tumours generated, increasing the latency time before tumour onset and reducing the number of lung metastases[183]. Moreover, cannabinoid-treated mice had increased staining for cleaved caspase 3, indicating apoptosis, as well as decreased tumour vascularisation, MMP2 expression, AKT activity and increased cell cycle arrest[124,184,185]. Furthermore, in HER2+ breast cancer, HER2-CB_2 heteromer-expressing cells treated with the THC *in vitro* lead to HER2 degradation by the proteasome, and once separated from HER2, CB_2 activation promotes autophagy-induced apoptosis[186]. This anti-tumour effect is also seen in mouse models of the HER2-CB_2 heteromer, with THC administration reducing tumour growth *in vivo*[186].

Whilst CB_2 expression in HER2+ breast cancer leads to increased protumoural signalling, the exact mechanisms are still undetermined. Moreover, as cannabinoids have strong anti-neoplastic properties, are well tolerated and can be designed with high receptor specificity, they have high therapeutic potential. Therefore, understanding CB_2's mechanistic role in HER2+ breast cancer and how cannabinoids affect tumour growth in this setting could lead to the development of cannabinoid-based therapies for HER2+ patients.

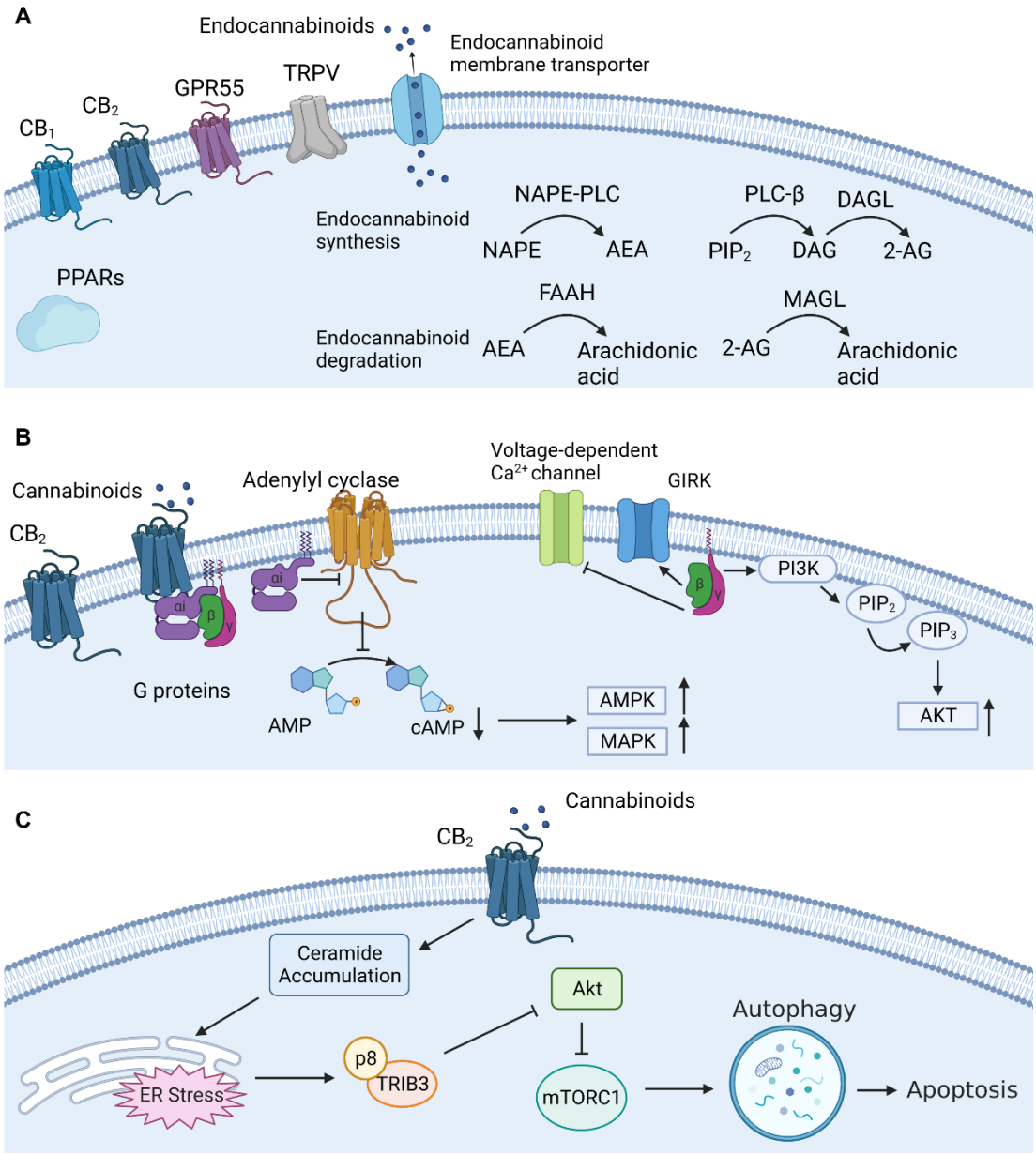

Figure 1.3.1: The endocannabinoid system.

(A) An illustration of the endocannabinoid system (ECS) containing of the cannabinoid receptors CB_1 and CB_2, orphan receptors such as GPR55, peroxisome proliferator activated receptors (PPARs) and the vanilloid transient receptor potential (TRPV) ion channels. The two major ligands for the cannabinoid receptors, endocannabinoids arachidonoyl ethanolamine (AEA) and 2-arachidonoyl glycerol (2-AG) are synthesised from phospholipid precursors in cell membranes via N-acyl phosphatidylethanolamine (NAPE) and phosphatidylinositol 4,5-bisphosphate (PIP_2), respectively. NAPE-phospholipase D (NAPE-PLD) converts NAPE to AEA and phospholipase C β (PLC-β) and diacylglycerol lipase (DAGL) convert PIP_2 to diacylglycerol (DAG) and subsequently 2-AG. Endocannabinoids are then transported out of the cellvia endocannabinoid membrane

transporters to activate cannabinoid receptors. After signalling, AEA and 2-AG are transported back into the cell where they are degraded to arachidonic acid by fatty acid amide hydrolase (FAAH) and monoacylglycerol lipase (MAGL), respectively. (B) Canonical signalling pathways of CB_2 in normal tissue. After activation with cannabinoid ligands CB_2 couples with Gαi G proteins, leading to inhibition of adenylyl cyclase, decreased cAMP accumulation leading to increased AMPK and MAPK activity. The Gβγ complex can further signal, inhibiting Ca^{2+} ion channels, activating G protein-coupled inwardly rectifying potassium channels (GIRKs) and activating the PI3K-AKT signalling pathway. (C) Mechanism of CB_2-mediated cancer cell cytotoxicity. Activation of CB_2 expressed on cancer cells leads to accumulation of ceramides, causing ER stress and activation of the ER stress related proteins, p8 and TRIB3, leading the inhibition of AKT. Reduced AKT activity leads to decreased mTORC1 function, resulting in increased autophagy, leading to apoptosis.

1.4 Hypothesis and aims

Whilst HER2+ breast cancer has effective targeted treatments, it still has a relatively poor survival rate, high rates of resistance and metastasis. Therefore, further research into mechanisms of disease progression, resistance development and new therapeutic targets is vital.

CB_2 expression is linked with decreased survival in many cancers, including HER2+ breast cancer. CB_2 therefore highlights a potential biomarker for patient stratification and a promising drug target.

I hypothesise that the that CB_2 expression contributes to decreased patient survival in HER2+ breast cancer patients via increasing metastatic potential. Therefore, the primary aim for this thesis was to examine the protumourigenic effects of CB_2 expression in HER2+ breast cancer and determine the efficacy of cannabinoid-based therapy in this context.

To address this, the main objectives are:

- Develop an inducible CB_2 expression system in HER2+ breast cancer cell lines.
- Use the inducible exp
- ression to examine changes in gene expression upon CB_2 expression.
- Using 2D and 3D models investigate phenotypic changes that lead to increased metastatic potential.
- Use synthetic cannabinoids to functionally validate the role of CB_2 in the context HER2+ breast cancer.
- Evaluate the suitability of using cannabinoids targeting CB_2 therapeutically.

Chapter 2 Materials and Methods

2.1 Cell culture

HCC1954[187] (ATCC) cells were cultured in RPMI-1640 medium (Gibco, 21875-034) supplemented with 10% foetal bovine serum (FBS) (Sigma, F9665) and grown at 37°C in 5% CO_2. SKBR3[188] (ATCC) cells were culture in McCoy's 5a medium (Sigma, M4892) supplemented with 10% FBS (Sigma, F9665) and grown at 37°C in 5% CO_2. BT474[189] (ATCC) cells were culture in DMEM-F12 (Sigma, D8437) supplemented with 10% FBS (Sigma, F9665) and grown at 37°C in 5% CO_2. HEK293T[190] (ATCC) cells were used for lentivirus production and were cultured in DMEM (Gibco) supplemented with 10% FBS (Sigma, F9665) and grown at 37°C in 5% CO_2. For preparing experiments, cells were harvested by washing in phosphate buffered saline (PBS) (Severn Biotech, 20-7461-01) and dissociated from culture vessel with 1 x trypsin (Gibco, 15400054) and gentle tapping. Cells were counted with a Countess II (Invitrogen) and plated as appropriate. Cells were tested for mycoplasma every 6 months and were confirmed to be negative.

2.2 Gateway cloning

The *CNR2* gene was cloned into the pINDUCER20 (Addgene) plasmid using the Gateway method[191]. BP clonase and LP clonase (Invitrogen) were used to generate the entry vector and expression clones, respectively, containing HA-tagged *CNR2*, according to the manufacturer's instructions. AttB flanked 3xHA-*CNR2* PCR product was produced in a PCR reaction, using NEB Q5 polymerase, with the 3xHA-*CNR2*-pcDNA3.1 vector as a template and AttB primers (Table 1), according to the manufacturer's instructions. The PCR reaction was set up as follows: 100 ng of template DNA was combined with 5 µl Q5 reaction buffer, 0.5 µl 10 mM dNTPs, 1.25 µl of 10 mM forward and reverse CB_2 AttB primers (Table 1), 2.5 µl Q5 high-fidelity DNA polymerase and d.H_2O to a final volume of 25 µl. The reaction was mixed, and

the PCR carried out in a Veriti 96-Well Fast Thermal Cycler (Applied Biosystems). Initial denaturation was performed at 98°C for 30 s, followed by 98°C for 10 s, 60°C for 30 s and 72°C for 30s, for 30 cycles. Final extension was performed at 72°C for 2 min.

The AttB PCR product was run on an agarose DNA gel (2.4 DNA gels), to ensure resolution at the correct size (1200 bp). The AttB PCR product was then excised from the DNA gel for purification using the Monarch® DNA Gel Extraction Kit (New England Biolabs, T1020) following the manufacturer's instructions. Briefly, the excised portion of gel was weighed and transferred to a 2 ml centrifuge tube. 400 µl of Monarch Gel Dissolving buffer was added per 100 mg of gel, then incubated at 55°C, with occasional inversion and vortex until gel fully dissolved (around 15 min). Dissolved gel was then transferred to spin column and centrifuged at 16,000 x g for 1 min. Flow-through was discarded and 200 µl DNA Wash Buffer added before a second centrifugation. The spin column was then transferred to a clean 1.5 ml centrifuge tube and 6 µl DNA elution buffer added to the spin column membrane and incubated for 1 min. A final centrifuge was performed to elute the purified DNA containing the AttB PCR product. The pure AttB PCR product is then incubated with the donor vector (pDONR) and BP clonase in TE buffer (pH 8) for 1 hour at room temperature (RT). 1 µl proteinase K was added to terminate the reaction. Correct insertion of *HA-CNR2* was verified by BsrG1 restriction enzyme digestion (Section 2.3).

The LR reaction was performed by combining the entry vector (*CNR2*-pDONR) and the destination vector (pINDUCER20) with the LR Clonase in TE buffer (pH), at RT for 1 hour. The reaction was terminated by the addition of 1 µl proteinase K. After LR reaction the correct insertion corroborated with BsrGI digestion (Section 2.3)

For plasmid propagation, NEB 10-Beta bacteria (New England BioLabs, C3019H) were transformed with plasmid, according to manufacturer's instruction. Briefly, bacteria for transformation were defrosted on ice. 1 µl of plasmid was added to 50 µl

of bacteria and incubated for 20 min on ice. Bacteria were heat shocked at 42°C for 30 s, then transferred to ice for 2 min. 750 µl of NEB 10-Beta outgrowth medium was added to the bacteria and incubated at 37°C for 1 hour. Bacteria were spread onto agar plates containing antibiotics (Zeocin 50µg/ml or Ampicillin, 1 µg/ml) and left to grow overnight at 37°C. Colonies that grew were picked and expanded in 5 ml LB broth containing antibiotics (Zeocin 50µg/ml or Ampicillin 1 µg/ml) and cultured in a shaker at 150 rpm at 37°C for 12-16 hours. To check the for the presence of *CNR2* in bacterial colonies, colony PCR was performed by dabbing the pipette tip used to pick colony into nuclease free water. Using the NEB Q5 PCR kit, PCR was performed as above and the PCR product was run on a 1% agarose gel (Section 2.4) to ensure the correct size of the plasmid. Plasmid DNA was harvested using the Monarch Plasmid Miniprep Kit (New England BioLabs, T1010S), following manufacturer's instructions. Briefly, 4.5 ml bacterial suspension was centrifuged at 1500 x g for 15 min to pellet. Bacterial pellet was resuspended in 200 µl Plasmid Resuspension Buffer then lysed by the addition of 200 µl Plasmid Lysis Buffer and mixed by inversion. Lysis was neutralised by the addition of 400 µl Plasmid Neutralization Buffer and incubated at RT for 2 min. Lysed cells were then centrifuged for 5 min at 16,000 x g. Supernatant was then transferred to spin column and centrifuged at 16,000 x g for 1 min. The flow through was discarded and spin column washed with 200 µl Wash Buffer 1 and centrifuged at 16,000 x g for 1 min. Flow through was discarded and spin column washed in 400 µl Wash Buffer 2 then centrifuged at 16,000 x g for 1 min. Spin column was transferred to a clean 1.5 ml centrifuge tube. 30 µl Elution Buffer was added to the membrane of the spin column and incubated for 1 min at RT. Plasmid DNA was then eluted by a final centrifuge at 16,000 x g for 1 min.

For the bulking up of plasmids for maxiprep, 150 µl of transformed bacteria was added to 150 ml LB broth containing the relevant antibiotic (Zeocin 50µg/ml or Ampicillin 1 µg/ml) and cultured in a shaker at 150 rpm at 37°C for 12-16 hours. Plasmid was

harvested using ZymoPURE II Maxiprep kit, following manufacturer's instructions. Briefly, bacterial broth was centrifuged to pellet bacteria. The bacterial pellet was then resuspended in 14 ml of the ZymoPURE P1 buffer. Bacteria was then lysed with 14 ml of the ZymoPURE P2 buffer. The reaction was neutralised with 14 ml of the ZymoPURE P3 buffer, creating a precipitate. The reaction was transferred into a syringe filter and incubated for the precipitate to settle to the top. The clear lysate was filtered into a clean 50 ml centrifuge tube and combined with 14 ml Binding buffer. The mixture was transferred to a 50 ml reservoir attached to the Zymo-spin column and placed onto a vacuum manifold, before being washed three times with wash buffers. DNA was then eluted in 400 µl nuclease free water through centrifugation into a 1.5 ml centrifuge tube at 16,000 x g for 1 min.

Table 1: Primer sequences

Primer	Sequence
AttB *CNR2* Fw	5' TGGTCTAGAGCTAGCATGTACCCATACGATGT 3'
AttB *CNR2* Rv	5' CCGATTTAAATTCGAATTCTCAGCAATCAGAGAGG 3'
CNR2 Fw	5' CGGAAGCCCTCATACCTGTTC 3'
CNR2 Rv	5' GTCACGCTGCCAATCTTCAG 3'
CNR1 Fw	5' GGGATGCGAAGGGATTGCC 3'
CNR1 Rv	5' CCACGTACAGGAGGTCAGTG 3'
MMP13 CHIP Fw	5' CACAGGCCACTTGAGAGGTT 3'
MMP13 CHIP Rv	5' AAGGTTGGTGGTGAAAGTGAGA 3'
HK3 Fw	5' CTGCTTGTCCAGATGACTTCGG 3'
HK3 Rv	5' CTGCTTGTCCAGATGACTTCGG 3'
HKDC1 Fw	5' GTTTGCGGTCCACTTGATGG 3'
HKDC1 Rv	5' GTGGGCAACATCTTCACTGC 3'
LDHB Fw	5' CTGCTTGTCCAGATGACTTCGG 3'
LDHB Rv	5' CTGCTTGTCCAGATGACTTCGG 3'
SOX2 Fw	5' GGATAAGTACACGCTGCCC 3'
SOX2 Rv	5' CATGTGCGCGTAACTGTC 3'
KLF4 Fw	5' CCCTGGGTCTTGAGGAAG 3'
KLF4 Rv	5' CATGAGCTCTTGGTAATGGAGC 3'
OCT4 Fw	5' GTAGTCCCTTCGCAAGCCC 3'
OCT4 Rv	5' GAG AAG GCG AAA TCC GAA GC 3'
WNT10A Fw	5' GTGCTCCTGTTCTTCCTACTG 3'
WNT10A Rv	5' CTGGCAATGTTAGGCACACTG 3'
ALDH1A1 Fw	5' CACGCCAGACTTACCTGTCC 3'
ALDH1A1 Rv	5' GCAGAGCTCCTCCTCAGTTG 3'
CD44 Fw	5' CCTCAGCTCATACCAGCCAT 3'
CD44 Rv	5' TTGCAGTAGGCTGAAGCGTT 3'
CD274 Fw	5' TGCCGACTACAAGCGAATTACTG 3'
CD274 Rv	5' CTGCTTGTCCAGATGACTTCGG 3'

2.3 BsrG1 digestion

DNA digestion by BsrG1 (New England BioLabs, R3575) was carried out according to the manufacturer's instructions. Briefly, 1 µg of target DNA for digestion was combined with 5 µl NEB CutSmart Buffer, 1 µl BsrG1 restriction enzyme and combined with nuclease free H_2O to a total volume of 50 µl. The reaction was incubated at RT for 15 min. The reaction was heat inactivated at 80°C for 20 min.

2.4 DNA gels

TAE agarose gels for DNA separation were made in 1x tris-acetate-EDTA (TAE) buffer (Severn Biotech) with 1% agarose (Invitrogen, 11553277). For a single gel 300 µg agarose was combined with 30 ml 1x TAE buffer and microwaved at 50% power for 2.5 min, or until all agarose had dissolved. Gel was allowed to cool slightly, then GelRed (Biotium, 41003) was added at 1:10,000 dilution, and gels poured and allowed to set. DNA samples were combined with Gel Loading Dye, Purple (6X) (New England BioLabs, B7024) (1:6 dilution) and the gels were run at 100V for 30-45 min. Gels were imaged on a BioSpectrum Imaging System (Ultra-Violet Products Ltd.).

2.5 Lentivirus generation

Lentivirus containing the *HA-CNR2*-pINDUCER20were generated in HEK293T cells. The pINDUCER20 expression clones were combined with pMD2.G and pCMVΔR8.74 packaging lentivirus plasmids and transfected into HEK293T cells using FuGENE HD (Promega, E2311) according to the manufacturer's instructions. Briefly, packaging plasmids and *HA-CNR2*-pINDUCER20were combined with 50 µl FuGENE HD reagent and incubated at RT for 15 min before being added to HEK293T cells. Transfected HEK292T cells were incubated for 24 hours at 37°C in 5% CO_2, before medium was refreshed. After a further 24 hours the supernatant

containing lentivirus was harvested, centrifuged to remove cell debris and stored at -80°C until use.

2.6 Transduction and selection

The HA-tagged CB_2 inducible expression plasmid (*HA-CNR2*-pINDUCER20, (Section 2.2) was transduced into HCC1954, SKBR3 and BT474 cells using a lentivirus vector (Section 2.5). Briefly, cells were cultured in 6 cm^2 cell culture dishes, after 1 day of culture 1 ml of lentivirus vector was added on top of the cell culture media. The following day cell culture medium was refreshed. Cells were incubated for a further 24 hours before neomycin selection. Cells containing the *HA-CNR2*-pINDUCER20plasmid ($HCC1954^{iCB2}$, $SKBR3^{iCB2}$, $BT474^{iCB2}$) were subsequently selected in growth medium containing 5 mg/ml neomycin (Sigma, N-6386) for 7 days. For the induction of CB_2, expression $HCC1954^{iCB2}$, $SKBR3^{iCB2}$ and $BT474^{iCB2}$ cells were treated with 1 μg/ml doxycycline (dox) (ThermoFisher, J60422-06).

2.7 Neomycin kill curve

$HCC1954^{iCB2}$, $SKBR3^{iCB2}$ and $BT474^{iCB2}$ cells were plated into a flat bottom 96 well plate at 5000 cells/well, in the appropriate cell culture media for each cell line (Section 2.1). Triplicate wells containing 200 μl of each media were added to calculate baseline values. The next day cell culture medium was removed and replaced with media containing increasing concentrations of neomycin. Cells were cultured at 37°C in 5% CO_2 for 2 days. Cell viability was measured using the 3-(4,5-dimethylthiazol-2-yl)-5-(3-carboxymethoxyphenyl)-2-(4-sulfophenyl)-2H-tetrazolium (MTS) assay, following the manufacturer's instructions. Briefly, cell culture media was removed and replaced with 100 μl fresh cell culture media, followed by the addition of 20 μl MTS reagent. The

plate was incubated at 37°C in 5% CO_2 for two hours before reading at 490 nm on the Clariostar plate reader (BMG Labtech).

2.8 RNA extraction and RT-PCR

RNA was harvested using Monarch® Total RNA Miniprep Kit (New England BioLabs, T2010S), following the manufacturer's instructions. Briefly, plates containing cells for RNA extraction were washed in PBS and then the PBS removed. 350 µl RNA Lysis Buffer was added to each well and cells were scraped to remove from plate. Lysed cells were added to the gDNA columns then centrifuged for 30 s at 16,000 x g. Flow through was retained and mixed with 350 µl 100% ethanol and transferred to RNA purification columns and centrifuged for 30 s at 16,000 x g. Flow through was discarded and spin column membranes were treated with DNase I (5 µl + 75 µl DNase reaction buffer) and incubated for 15 min at RT. 500 µl Priming buffer was added to the column and then centrifuged for 30 s at 16,000 x g. Flow through was discarded and 500 µl RNA Wash buffer was added then centrifuged for 30 s at 16,000 x g. Flow through was discarded and another 500 µl RNA Wash buffer was added, before a 2 min centrifuge to dry the spin column membrane. Spin columns were then transferred to clean 1.5 ml centrifuge tube and 50 µl of nuclease free water added to the membrane. mRNA was eluted with a final centrifuge for 30 s at 16,000 x g. Concentration of mRNA was determined using a Nanodrop One spectrophotometer (ThermoFisher). mRNA was converted to cDNA using NEB LunaScript® RT SuperMix Kit (New England BioLabs, E3010), following the manufacturer's instrcutions. Briefly, 1 µg of mRNA was combined with 4 µl LunaScript RT SuperMix and nuclease free water up to a total volume of 20 µl. The reverse transcription reaction was performed on a Veriti 96-Well Fast Thermal Cycler (Applied Biosystems). Initially, samples were heated to 25°C for primer annealing, followed by cDNA synthesis at 55°C for 10 min and final heat inactivation at 95°C for 1 min. RT-qPCR

was carried out using the NEB Luna® Universal qPCR Master Mix (New England BioLabs, M3003L), according to the manufacturer's instructions. Briefly, primer master mixes were prepared with 5 µl Luna Universal qPCR Master Mix, 0.25 µl 10 mM forward and reverse qPCR primers (Table 1), and 3.5 µl nuclease free water, for each primer pair. Master mixes were added to 96-well RT-qPCR plates (Applied Biosystems, 4306737) and 1 µl (50 ng) of cDNA added to appropriate wells. Each condition was plated in technical triplicate, as well as including beta actin house-keeping gene and non-template controls. Plate was sealed with MicroAmp Optical Adhesive Film (Applied Biosystems, 4360954) and RT-qPCR analysis was carried out using the StepOnePlus™ Real-Time PCR System (Applied Biosystems) with the following temperature cycles. Initial denaturation was carried out at 95°C for 1 min, followed by 40 cycles of denaturation at 95°C for 10 s, then extension at 60°C for 30s. Data was analysed using QuantStudio™ and GraphPad Prism 9 software, with $2^{-\Delta\Delta Ct}$ values used for relative quantification.

2.9 Western blotting

Polyacrylamide gels for electrophoresis were prepared in two parts, the resolving gel and the stacking gel. For a single 10% gel the resolving gel was prepared as follows, 4.8 ml d.H_2O was combined with 3 ml resolving buffer (500 ml d.H_2O + 90.9 g Tris-base + 10 ml 20% sodium dodecyl sulfate (SDS) (Sigma, 436143), pH 8.8), 4 ml 30% acrylamide (BioRad, 1610156), 120 µl 10% SDS, 96 µl 10% ammonium persulfate (APS) (ThermoFisher, 17874) and 12 µl tetramethylethylenediamine (TEMED) (Sigma, T9281)**.** The resolving gel was poured into a gel cassette (Invitrogen, NC2015) and 500 µl 100 % isopropanol was added on top to flatten the gel surface and remove bubbles. Gels were allowed to polymerise at RT, before the removal of the isopropanol and addition of the stacking gel. The stacking gel was prepared with 1.8 ml d.H_2O, 750

µl stacking buffer (500 ml d.H_2O, 30.29 g Tris-HCl (Sigma, T3253), 10 ml 20% SDS, pH 6.8), 375 µl 30% acrylamide, 30 µl 10% SDS, 60 µl 10% APS and 6 µl TEMED).

Lysates for western blotting were prepared by lysing cells in ice cold radioimmunoprecipitation assay (RIPA) buffer (1% Triton X, 0.5% sodium deoxycholate (Sigma, D5670), 0.1% SDS, 50 mM Tris (Sigma, T1503), 150 mM NaCl (Fisher, BF358-1), adjusted to pH 8.0) supplemented with NaF (Sigma, S6776) and $NaVO_4$ (Sigma, S6508) and protease inhibitors (Calbiochem, 539131). Lysates were centrifuged at 16,000 x g for 15 min at 4°C to remove insoluble protein. Protein concentration was calculated using the Bradford assay (Bio-Rad, 5000114). Samples containing 20 µg of protein per well were boiled in Laemmli sample buffer (Sigma, S3401) for 5 min. For the analysis for HA-tagged CB_2 protein, samples were incubated in Laemmli sample buffer for 1 hour at RT . Proteins were separated by SDS PAGE on a 10% gel, and then transferred onto a nitrocellulose membrane (Amersham, 10600003) using the Mini Trans-Blot® Cell system (Bio-Rad, 1703930) containing transfer buffer (700 ml d.H_2O, 100 ml 10x Tris-glycine (Severn Biotech, 20-6300-10), 200 ml methanol (Fisher, AC326950025)) for 1 hour at 100 V. Membranes were blocked in 5% milk Tris buffered saline + 0.05% Tween 20 (TBST) for 1 hour at RT. Membranes were incubated with anti-HA (Invitrogen, 26183), anti-ALDH1A1 (Invitrogen, PA5-11537), anti-phospho-AKT (S473) (Cell Signalling Technologies, 92715), anti-total-AKT (Cell Signalling Technologies, 2920S), anti-PDL1 (Cell Signalling Technologies, 13684T), anti-alpha-tubulin (Sigma, T5168) or anti-HSC70 (Santa-Cruz, SC7298) antibodies (Table 2: Antibodies), diluted to 1:5000 in 5% BSA, overnight at 4°C. Horseradish peroxidase (HRP)-conjugated secondary antibodies anti-mouse-HRP (Dako, P0447), anti-rabbit-HRP (Dako, P0448), diluted to 1:2000 (Table 2: Antibodies) in 5% milk TBST were incubated for 1 hour at RT. Membranes were incubated with Immobilon Western HRP substrate (Merck Millipore, WBLUF0500) and images were captured using the Amersham AI600 Imager (GE

Healthcare). For phospo- and total-AKT blotting, membranes were initially developed using anti-phospho-AKT antibodies, and then stripped using Re-Blot Plus Mild Solution (Merck Millipore, 2502) (1:10 in d.H_2O) for 10 min under agitation, then re-blocked in 5% milk TBST for 1 hour, before staining with anti-total-AKT antibody, as above.

2.10 Immunofluorescence

Cells for immunostaining were seeded on coverslips in a 6 well plate (Corning, 3598). After appropriate treatments, coverslips were washed in PBS prior to fixation in 4% formaldehyde (Thermo Scientific, 28908) for 10 min at RT. Coverslips were washed 3 times in PBS and permeabilised for 10 min at RT using 0.1% Triton-X in PBS (Alfa Aesar, A16046). Cover slips were blocked using 5% bovine serum albumin (BSA) (Sigma, A8022) in PBS for 1 hour at RT and were incubated in anti-HA (Invitrogen, 26183, 1:500 dilution), anti-HER2 (Cell Signalling Technologies, 2242S, 1:500) anti-vimentin (Sigma SAB5700070, 1:100) anti E-cadherin (Cell Signalling Technologies, 3195S, 1:1000), anti-ALDH1A1 (Invitrogen, PA5-11537, 1:50 dilution) or anti-β-catenin (Cayman Chemical, 100029, 1:300 dilution) antibodies (Table 2: Antibodies), diluted in 5% BSA PBS overnight at 4°C. The following day, coverslips were washed 3 times in PBS and incubated in anti-mouse AF488 (Invitrogen, A21202) and/or anti-rabbit AF546 (Invitrogen, A11035) antibodies, diluted 1:500 and 1:250, respectively, (Table 2: Antibodies) in 5% BSA PBS for 1 hour at RT. Coverslips were washed 3 times in PBS, dried, and mounted on microscope slides using ProLong™ Gold Antifade Mountant with DAPI (Invitrogen, P36931).

For immunofluorescence of spheroids, gels were removed from the culture plate, washed in PBS and fixed in 4% formaldehyde for 30 min at RT. Gels were washed 3 times in PBS and spheres permeabilised with 0.1% Triton-X in PBS for 1 hour at RT,

then blocked in immunofluorescence (IF) buffer (130mM NaCl (Fisher, BF358-1), 7 mM Na_2HPO_4 (Sigma, S9390), 3.5 mM NaH_2PO_4 (Sigma, S0751), 7.7 mM NaN_3 (Sigma, S2002) , 0.1% BSA, 0.2% Triton X-100, 0.05% Tween-20 (Sigma, P9416), 10% horse serum (Gibco, 16050-130)) for 1 hour under agitation. Anti-PDL1 (Cell Signalling Technologies, 13684T) and anti-HA (Invitrogen, 26183) antibodies were diluted in IF buffer at 1:200 and incubated with gels for 48 hours at 4°C under agitation. Gels were washed in IF buffer and incubated anti-mouse AF568 (Invitrogen, A11031) and anti-rabbit AF488 (Invitrogen, A11008) antibodies, diluted 1:500 and 1:200, respectively, in IF buffer, for 2 hours at RT in the dark under agitation. Gels were washed 3 times in IF buffer and stained in 4′,6-diamidino-2-phenylindole (DAPI) (Sigma, D9542) for 10 min at RT. Gels were placed onto microscope slides that had been prepared with two layers of electrical tape with the centre of the tape excised to allow space for the thickness of the gels, before being mounted using Mowiol (Calibio Chem, 475904) and coverslips that cover the electrical tape. All immunofluorescence images were captured on an LSM 710 confocal microscope (Zeiss).

2.11 Bioinformatics

Overall survival plots were generated with the Kaplan-Meier plotter web tool at kmplots.com[192]. The Cancer Genome Atlas database was used for patient data, using all available Breast Cancer mRNA gene chip datasets. *CNR2* (Affymetrix ID 206586) was selected with auto select best cut-off, HER2 status, and lymph node status were selected as positive or negative where appropriate.

For differential expression analysis, cBioPortal[193,194] was used to select HER2+ patient data from Breast Cancer Invasive PanCancer dataset of TCGA and separate into upper (n = 20 patients) and lower (n = 19 patients) quartiles of *CNR2* mRNA expression. Genes of interest were selected and differential expression data between quartiles was

downloaded and graphed in GraphPad Prism 9. For *CNR2* co-expression correlation analyses, cBioPortal was used to select HER2+ patient data from Breast Cancer Invasive PanCancer dataset of TCGA. The expression of genes of interest were compared to *CNR2* expression and data was downloaded and graphed in GraphPad Prism 9.

2.12 Hanging drop spheroid culture

Spheroids were generated by resuspending HCC1954^{iCB2} or BT474^{iCB2} cells in media containing 2.5% methylcellulose at 25,000 cells/ml (Sigma, M0512). Droplets of 20 µl containing 500 cells were pipetted on to the underside of a 15 cm culture dish (Thermo, 130183) lid, with PBS in the bottom of the dish and left at 37°C in 5% CO_2 overnight to form spheroids. The following day, gel composed of 2 mg/ml collagen I (Corning, 354249), 2 mg/ml Matrigel (Corning, 356234), 12.5 µM HEPES (Sigma, H3375), 10 µM NaOH (Fisher, J/7620/15) was prepared. Wells of low attachment 96 well plates (Greiner, 655970) were coated with 40 µl gel and set at 37°C. Spheroids were harvested from the hanging drops, washed in medium to removed methylcellulose and resuspended in the collagen-Matrigel gel mix. Gel containing spheroids was added to precoated wells at 50 µl/well, with approximately 6 spheroids per well. Plates were incubated for 45 mins at 37°C for the gels to set before 200 µl of medium was added, containing 1 µg/ml dox, 100 nM JWH133 (Tocris, 1343), 1 µM CP55940 (Tocris, 0949), 100 nM Defactinib (Tocris, 7305), 100 nM AKT1/2 inhibitor (Sigma, A6730), or DMSO (Fisher, D-4120-PB08) vehicle control, as appropriate. 100 nM JWH133 was added daily. Spheroids were incubated at 37°C in 5% CO_2 for 3 days. Images of spheroids were captured using an Axiovert 13S light microscope (Zeiss). Invasion was quantified on ImageJ and % invasion was calculated using the following equation:

$$\%\ Invasion = \left(\frac{Area_{total} - Area_{central}}{Area_{central}}\right) x100$$

2.13 Incucyte assays

For Incucyte proliferation assays, 5000 cells per well were plated in flat bottomed 96 well plates (Costar, 3599), +/- 1 µg/ml dox, and cultured for up to 5 days at 37°C in 5% CO_2, with images captured every 4 hours. Incucyte S3 software was used to determine the percentage confluency at each time point.

For migration assay, cells were washed in serum free RPMI-1640, harvested and resuspended to 5000 cells per well in serum free RPMI-1640. Cells in 40µl serum free medium were plated in the top well of the Incucyte® Clearview 96-well Plate for Chemotaxis, 8 µm pore size, (Sartorius, 4648) +/- 1 µg/ml dox. Full growth medium containing 10% FBS was added to the bottom of the Chemotaxis transwell plate, 175 µl/well. Cells were incubated in the Incucyte for 4 days, with pictures being taken every 4 hours. Incucyte chemotaxis software was used to analyse the area of cells in focus on the top side of the transwell membrane, versus the bottom side of the membrane to calculate level of migration.

2.14 Lapatinib dose response

To test the effect of CB_2 on lapatinib sensitivity, HCC1954^{iCB2}and BT474^{iCB2} cells were plated at 1000 cells / well in a flat bottom 96-well plate (Costar, 3599) and cultured at 37°C in 5% CO_2. Cells were then treated with 1 µg/ml dox for 24 hours, followed by increasing concentrations of lapatinib or DMSO vehicle control for 7 days. Cell viability was tested using the MTS assay following the manufacturer's instructions, as outlined in Section 2.7. The plate was incubated at 37°C in 5% CO_2 for two hours before reading at 490 nm.

2.15 Cell Titre Glo assay

HCC1954^{iCB2} and BT474^{iCB2} cells were plated into white 96 well clear bottom plates (Greiner, 655083) at 3000 cells / well in RPMI-1640 + 10% FBS +/- 1 μg/ml dox. Cells were cultured for 4 days before analysis by Cell Titre Glo (Promega, G7571). Cell Titre Glo was performed according to the manufacturer's instructions. Briefly, cell culture plates were removed from incubator and equilibrated to RT for 30 min. 100 μl of cell culture medium was removed and 100 μl of Cell Titre Glo reagent was added. Plates were mixed on a plate shaker for 2 min at RT and incubated at RT for a further 10 min and luminescence was recorded on Clariostar plate reader (BMG Labtech).

2.16 Seahorse XF Cell Energy Phenotype assay

The measurement of oxidative phosphorylation and glycolysis rates in HCC1954^{iCB2} and BT474^{iCB2} cells was carried out using the Agilent Seahorse XF Cell Energy Phenotype Kit (Agilent, 103325-100) using the Agilent Seahorse XFe 96 Analyzer, according to the manufacturer's instructions. Briefly, HCC1954^{iCB2} and BT474^{iCB2} cells were plated into the Seahorse XF Cell Culture Microplate (Agilent, Seahorse XFe96 FluxPak, 102416-100). Cell density was optimised by test concentrations of 5000-30,000 cells/well. The following day cell medium was removed and medium +/- 1 μg/ml dox was added. The Agilent Seahorse XFp Sensor Cartridge (Agilent, Seahorse XFe96 FluxPak, 102416-100) was hydrated with Agilent Seahorse XF Calibrant (Agilent, 100840-000) a day prior to the assay and incubated in a non-CO_2 incubator at 37°C overnight. The following day Seahorse XF RPMI Assay medium (Agilent, 103681-100) was supplemented with 1 mM pyruvate, 2 mM glutamine, and 10 mM glucose (Agilent, 103681-100) and warmed to 37°C. The cell culture plate was washed twice in Seahorse XF Assay medium, with the final wash volume of 180 μl per well, then incubated in a non-CO_2 incubator at 37°C for 1 hour. Oligomycin and Carbonyl cyanide-p-trifluoromethoxyphenylhydrazone (FCCP) were reconstituted to

concentrations of 10 μM and 5 μM, respectively (Agilent, 103275-100). FCCP concentration was titrated for optimal oxygen consumption rate (OCR) response. 20 μl of Oligomycin and FCCP were added to the drug ports of the previously hydrated Agilent Seahorse XFp Sensor Cartridge. The metabolic phenotype was measured using the Cell Energy Phenotype assay template using the Agilent Seahorse XFe 96 Analyzer. Data were normalised by protein concentration using the Protein Assay kit (Biorad #5000116). GraphPad Prism 9 was used for data presentation and statistical analysis using the unpaired Student's t-test.

2.17 MitoTracker staining

Cells for mitochondria content analysis were plated on coverslips in a 6 well cell culture plate (Corning, 3587) +/- CB_2 induction. Staining was carried out using MitoTracker™ Red CMXRos (Invitrogen, M7512) according to manufacturer's instructions. Briefly, cells were treated with 250 nM MitoTracker for 30 minutes. Coverslips were then washed in PBS and fixed in 4% formaldehyde for 10 min at room temperature RT. Coverslips were washed 3 times in PBS and then mounted onto microscope slides using ProLong™ Gold Antifade Mountant with DAPI (Invitrogen, P36931). Images were captured on an LSM 710 confocal microscope (Zeiss). Quantification of mitochondrial content was carried out in ImageJ (Section 2.23).

2.18 Metabolite extraction

$HCC1954^{iCB2}$ cells were plated into a 6-well plate (Costar, 3516) at 250,000 cells /ml. The following day cells were treated +/- 1 μg/ml dox. After 24 hours cell culture medium was changed with either glucose free and glutamine free RPMI (kindly

donated by Katiuscia Bianchi) containing 11.1 mM ^{13}C glucose (CK Isotopes, CLM-481) and 2 mM ^{15}N glutamine (CK, Isotopes, NLM-557) or glutamine free RPMI (Gibco, 21870076) containing 2 mM ^{13}C glutamine (CK Isotopes, CLM-1822-H). After 8 hours, one well of each 6 well plate was counted to determine volume of extraction solution (50% LC-MS grade Methanol (Sigma, 1060020500), 30% LC-MS grade Acetonitrile (Sigma, 1.00029) and 20% LC-MS grade Water (Thermo, 51140)) required (1 ml per 10^6 cells). After the cell counting, the medium was aspirated and the 6-well plates placed on ice, then wash 3x with ice cold PBS. After the last wash all remaining PBS was removed from the well. Appropriate volume of extraction buffer was added to each well and incubated for 15 minutes on dry-ice and methanol. The cells were then scraped and transferred into Eppendorf tubes. Eppendorf tubes were then agitated for 15 mins at 4°C using a Thermomixer, then incubated for 1hour at -20 °C. Following this, tubes were centrifuged for 10 minutes at 4°C, at 16,000 x g for 15 min and the supernatant collected. This centrifugation step was then repeated to remove insoluble debris. Finally, the supernatant was transferred into autosampler vials and stored at -80 °C until further analysis. Analysis was performed by the BCI mass spectrometry facility.

2.19 Mammosphere formation assay

Mammospheres were produced as described in Lombardo *et al.* (2015)[195]. Briefly, cells were counted and diluted from 500 to 5000 cells/ml for cell titration, or 1000 cells/ml for experimentation in RPMI 1640 medium + 10% FBS +/- 1 μg/ml dox, ensuring a single cell suspension and were seeded into an ultra-low attachment 24 well plate, 1ml/well (Corning, 3473) in triplicate wells per condition. Plates were incubated at 37°C in 5% CO_2 for 7 days to allow mammospheres to form and treated with 100 nM JWH133 or DMSO vehicle treatments every other day. Mammosphere images were

captured using an Axiovert 13S light microscope (Zeiss). Mammosphere forming efficiency (MFE) was determined as in Lombardo *et al.* (2015). Briefly, mammospheres that measured 40 µm in diameter or larger were counted and the average number of mammospheres per well per condition were calculated. The MFE was then calculated using the following formula:

$$MFE\ \% = \frac{average\ number\ of\ mammospheres\ per\ well}{number\ of\ cells\ seeded\ per\ well}\ x\ 100\%$$

2.20 TOPFlash assay

HCC1954^{iCB2} cells were plated in 96-well flat bottom plates at 5000 cells/well, +/- 1 µg/ml dox, then were cotransfected with the TOPFlash (1500 ng) and Renilla (10 ng) plasmids using Lipofectamine 3000 (Invitrogen, L3000001), according to the manufacturer's instructions. Briefly, for the transfection of a single well of a 96-well plate 5 µl Opti-MEM (Gibco, 31985062) was combined with 0.3 µl Lipofectamine reagent. In a separate tube, 5 µl Opti-MEM was combined with 0.4 µl P3000 reagent and the above concentrations of DNA. The diluted Lipofectamine 3000 and the diluted P3000 and DNA was combined into a single tube and incubated at RT for 15 min. 10 µl of the transfection mix was added to the appropriate wells and incubated at 37°C in 5% CO_2. 72 hours after transfection, luminescence was detected using the Dual Luciferase Kit (Promega, E1910) on the FLUOstar Omega plate reader (BMG Labtech).

2.21 Flow cytometry

Cells for flow cytometry analysis were harvested using TrypLE (Gibco, 12604013) and gentle scraping with a cell scraper, centrifuged at 450 x g for 3 mins and washed in PBS. Dead cells were stained with Zombie Violet (Biolegend, 423113) 1:1000 in PBS,

20 min at RT. The staining reaction was quenched by the addition of FACS buffer (PBS + 5% FBS + 1 mM EDTA (Invitrogen, AM9261) + 0.1% NaN_3 (Sigma, S2002)) and cells centrifuged again, as above. For cell surface staining, cells were resuspended in 100 µl anti-PDL1 (Cell Signalling Technologies, 13684T) antibody (Table 2: Antibodies), diluted 1:500 in FACS buffer and incubated with cells for 1 hour at 4°C, then washed 3 times in FACS buffer. Secondary staining was performed in 100 µl anti-rabbit AF546 secondary antibody (Table 2: Antibodies) (Invitrogen, A11035), diluted 1:500 in FACS buffer, and incubated for 1 hour at 4°C, then cells were washed 3 times in FACS buffer. Stained cells were fixed with 4% formaldehyde for 10 min at RT before the final 3 x FACS buffer washes and resuspension in FACS buffer ready for acquisition. For intracellular Ki-67 staining, cells were fixed in 4% formaldehyde for 10 min at RT and permeabilised using 0.1% Triton-X for 10 min at RT, prior to antibody staining with 100 µl anti-Ki67 antibody (Abcam, ab15580) at 1:500 dilution and 100 µl anti-rabbit AF546 antibody (Invitrogen, A11035) at 1:500 dilution (Table 2: Antibodies) using FACS buffer containing 0.1% Triton-X. Flow cytometry data were acquired on the BD LSRFortessa (BD Biosciences). Flow cytometry analysis was performed using FlowJo™ v10.8 Software (BD Life Sciences).

2.22 Statistical analysis

The appropriate statistical tests were performed using GraphPad Prism 9 software. See figure legends for specific tests and statistical significance.

2.23 ImageJ fluorescence quantification

Quantification of fluorescence was performed using ImageJ software[196]. For corrected total cell fluorescence (CTCF) 'area integrated intensity' and mean grey value were selected in 'select measurements'. Greyscale images were opened and using the

polygon select tool the outline of a cell to be analysed were traced and measurements collected. This was repeated for all the cells to be analysed. Background is then selected using the circle select tool and measured in the same way, with equal numbers of cells and background measurements taken. CTCF was then calculated with the following formula:

$$CTCF = (Integrated\ density - (Area\ of\ selected\ cell\ x\ Mean\ fluoresence\ of\ background)$$

For β-catenin analysis the same method was used but only the nuclear area was selected, as determined by DAPI staining. For PDL1 spheroid fluorescence quantification, the same method was used, selecting either the total spheroid or invasive protrusion, as appropriate.

Table 2: Antibodies

Antibody	Species (Class)	Use (Dilution)	Supplier (Catelogue #)
Anti-ALDH1A1	Rabbit (polyclonal)	Western blot (1:5000) Immunofluorescence (1:50)	Invitrogen (PA5-11537)
Anti-Alpha Tubulin	Mouse (monoclonal)	Western blot (1:5000)	Sigma (T5168)
Anti-ß-catenin	Rabbit (polyclonal)	Immunofluorescence (1:300)	Cayman Chemical (100029)
Anti-E-cadherin	Rabbit (monoclonal)	Immunofluorescence (1:1000)	Cell Signalling Technologies (3195S)
Anti-HA-tag	Mouse (monoclonal)	Western blot (1:5000) Immunofluorescence (1:500, 1:200 spheroid)	Invitrogen (26183)
Anti-HER2	Rabbit (polyclonal)	Immunofluorescence (1:500)	Cell Signalling Technologies (2242S)
Anti-HSC70	Mouse (monoclonal)	Western blot (1:5000)	Santa-Cruz (SC7298)
Anti-Ki67	Rabbit (polyclonal)	Flow cytometry (1:500)	Abcam (ab15580)
Anti-Mouse-AF488	Donkey (polyclonal)	Immunofluorescence (1:500)	Invitrogen (A21202)
Anti-Mouse-AF568	Goat (polyclonal)	Immunofluorescence (1:500)	Invitrogen (A11031)
Anti-Mouse-HRP	Goat (polyclonal)	Western blot (1:2000)	Dako (P0447)
Anti-PDL1	Rabbit (monoclonal)	Western blot (1:5000) Immunofluorescence (1:200 spheroid) Flow cytometry (1:500)	Cell Signalling Technologies (13684T)

Anti-Phospho-AKT (Ser473)	Rabbit (polyclonal)	Western blot (1:5000)	Cell Signalling Technologies (92715)
Anti-Rabbit-AF488	Goat (polyclonal)	Immunofluorescence (1:200)	Invitrogen (A11008)
Anti-Rabbit-AF546	Goat (polyclonal)	Immunofluorescence (1:250) Flow cytometry (1:500)	Invitrogen (A11035)
Anti-Rabbit-HRP	Goat (polyclonal)	Western blot (1:2000)	Dako (P0448)
Anti-Total-AKT	Mouse (monoclonal)	Western blot (1:5000)	Cell Signalling Technologies (2920S)
Anti-Vimentin	Rabbit (polyclonal)	Immunofluorescence (1:100)	Sigma (SAB5700070)

Chapter 3 Development of an inducible CB_2 expression system

3.1 Inducible CB_2 expression

To investigate CB_2 function in HER2+ breast cancer *in vitro* inducible expression system was developed, enabling study of genotypic and phenotypic changes upon CB_2 expression and activation. Many expression systems have been designed for inducible expression, such as Tet-on and Tet-off, Tamoxifen-inducible, Cumate-inducible and even light-switchable[197]. In the case of Tet-on and Tet-off systems, tetracycline, also known as doxycycline (dox), induces or represses the expression of the gene of interest. Moreover, this expression system can be translated *in vivo* by supplementing feed or water with dox to induce expression of the gene of interest.

For this thesis project the pINDUCER20 vector was chosen due to ease of use, negligible leakiness and potential for translation to *in vivo* systems[198]. pINDUCER20 is a Tet-on based system of inducible expression; without dox, a reverse tet-transactivator (rtTA) protein, encoded on the pINDUCER20 plasmid, cannot bind to the tetracycline response element (TRE) DNA region of pINDUCER20 to initiate transcription. Transcription can be initiated with the addition of dox, which binds the rtTA and facilitates interactions with TRE allowing transcription of the gene of interest (Figure 3.1.1)[197,198].

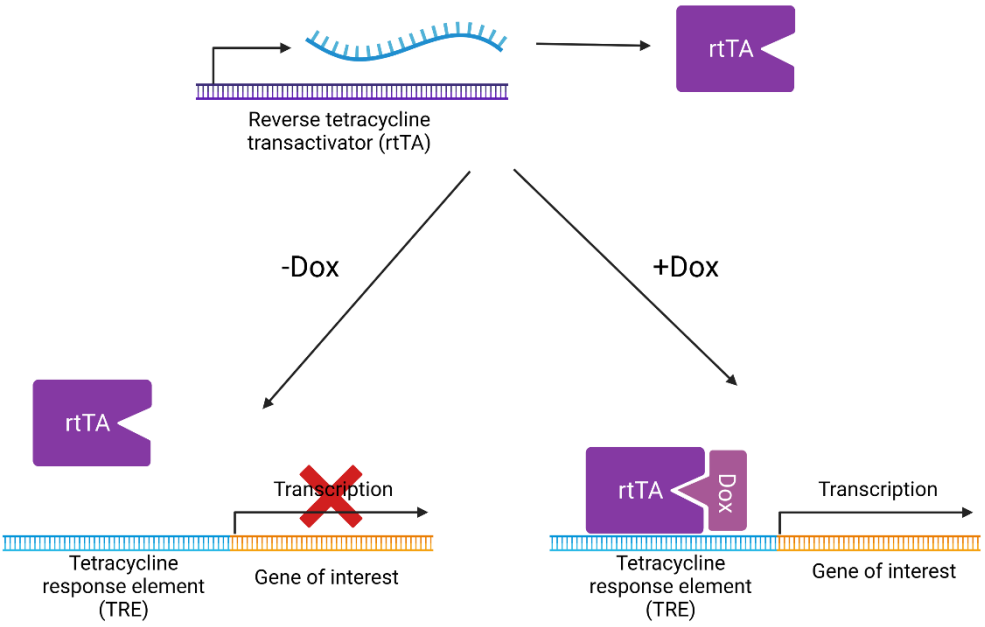

Figure 3.1.1: The Tet-on system of inducible gene expression in the pINDUCER20 plasmid.

The pINDUCER20 plasmid encodes reverse tetracycline transactivator (rtTA) protein that regulates the transcription of the gene of interest. Without tetracycline, also known as doxycycline (dox), rtTA cannot bind to the tetracycline-response element (TRE) to regulate transcription. When dox is added it binds to rtTA, which allows rtTA to interact with the TRE and initiates transcription of the gene of interest.

3.2 Cloning *CNR2* with the Gateway system

Gateway cloning was used to insert the *CNR2* gene into the pINDUCER20 plasmid using two enzymatic recombination reactions[199]. *CNR2* was amplified by PCR using primers containing DNA sequence termed AttB. The template for the AttB PCR reaction was a pcDNA3.1 vector containing *CNR2* with a 5' sequence for a 3x hemagglutinin (HA) tag (to allow for antibody detection of the CB_2 protein) (Appendix figure 1). *HA-CNR2* was amplified by PCR using primers that contained the AttB sequence (Table 1), resulting in a PCR product of *HA-CNR2*, flanked by two AttB sequences. During the first recombination reaction the enzyme BP clonase inserts *HA-CNR2* into the pDONR plasmid, replacing the bacterial death gene, *ccdB*, which encodes for a DNA gyrase inhibitor, causing DNA damage and bacteria death[200]. Bacteria transformed with pDNOR plasmids that still retain the *ccdB* gene and not *HA-CNR2* fail to form colonies. Six bacterial colonies were picked and verified to contain *CNR2* by colony PCR using *CNR2* qPCR primers (Table 1). Confirmation of the correct *CNR2* amplicon size was observed at the expected size of 146 bp after separation on an 1% agarose TAE gel (Appendix figure 2).

Correct *HA-CNR2* insertion into pDONR was confirmed by digestion with the restriction enzyme bsrG1 (Figure 3.2.1). After digestion with bsrG1, the pDONR-*HA-CNR2* yielded two bands on an agarose gel, indicating the plasmid was only cut twice (Appendix figure 4) and hence *HA-CNR2* had been inserted, removing the third bsrG1 site. Furthermore, *CNR2* resolved at the correct size (~1200 bp) in all four colonies (1-4), confirming its presence in the pDONR plasmid (Figure 3.2.1 A).

The LR reaction was performed on plasmid DNA isolated from Colony 1, inserting *HA-CNR2* into the destination vector, pINDUCER20 (Appendix figure 4). The *HA-CNR2*-pINDUCER20 plasmid was transformed into competent bacteria, and another six colonies (A-F) were picked. Confirmation of the correct amplicon size for *CNR2*

was confirmed by colony PCR (Appendix figure 2), with colonies E and F having the strongest band.

The pINDUCER20 plasmid contains 4 bsrG1 cut sites, losing one during the LR reaction. BsrG1 digestion of the *HA-CNR2*-pINDUCER20 yielded three distinct bands, indicating the correct insertion of *HA-CNR2*, with *CNR2* resolving at the correct size (Figure 3.2.1 B). However, there was detection of a faint fourth band in all samples, possibly suggesting the presence of pINDUCER20 lacking *HA-CNR2* insertion. The *HA-CNR2*-pINDUCER plasmid isolated from Colony F was sent for sequencing at SourceBioscience for final confirmation of successful cloning.

The *HA-CNR2*-pINDUCER20 plasmid was packaged into lentivirus particles using HEK293T cells. The harvested lentivirus containing *HA-CNR2*-pINDUCER20 was used to transduce the HER2+ breast cancer cell lines HCC1954, SKBR3 and BT474. The *HA-CNR2*-pINDUCER20 plasmid contains a neomycin resistance gene for selection, therefore a neomycin dose response was performed in wild type (WT) cells ($HCC1954^{WT}$, $SKBR3^{WT}$ and $BT474^{WT}$) before transduction to determine an appropriate concentration of neomycin for selection. The lowest neomycin concentration that achieved maximal cell death was 5 mg/ml achieved maximal cell death in all WT cell lines (Figure 3.2.2). After transduction with *HA-CNR2*-pINDUCER20, HCC1954, SKBR3 and BT474 cells ($HCC1954^{iCB2}$, $SKBR3^{iCB2}$ and $BT474^{iCB2}$) were grown in media containing 5 mg/ml neomycin for 7 days for selection of successfully transduced cells.

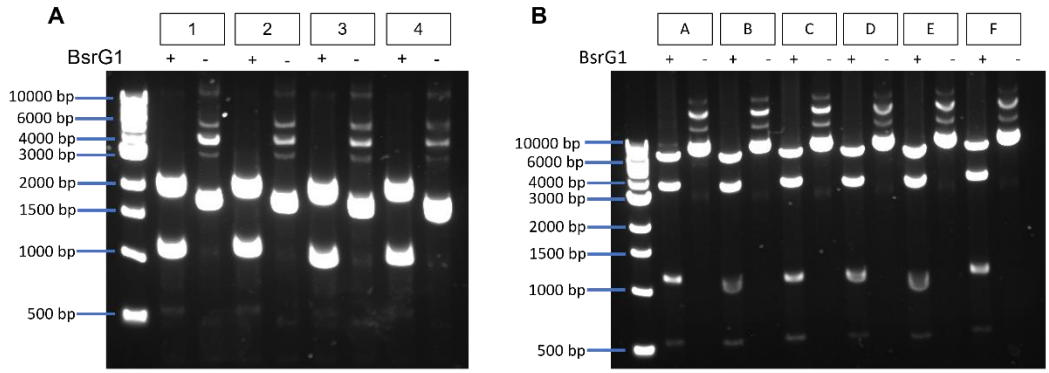

Figure 3.2.1: BsrG1 digestion of the BP and LR reaction products containing *HA-CNR2.*

(A) Plasmid isolated from colonies 1-4 run on a 1% agarose TAE gel with and without digestion by the restriction enzyme bsrG1. Bands in bsrG1 digestion lanes represent the digestion products, two linear DNA sequences. The band at ~1200 bp represents the *HA-CNR2* gene fragment. The larger band at ~2000 bp is the remaining pDONR fragment. The lanes containing undigested pDONR-*HA-CNR2* bands representing the different conformations of circular plasmid DNA. (B) Plasmid isolated from colonies A-F with and without digestion by the restriction enzyme bsrG1. Bands in bsrG1 digestion lanes represent the three linear DNA digestion products. The band at ~1200 bp represents the *HA-CNR2* gene fragment. The larger bands at ~2500 and ~4000 bp are the remaining pINDUCER20 fragments. The lanes containing undigested *HA-CNR2*-pINDCUER20 bands representing the different conformations of circular plasmid DNA. The small fragment at ~500 bp represents presence of digestion pINDUCER20 plasmid containing four bsrG1 digestions site, indicating presence of pINDUCER20 plasmid without *HA-CNR2* insert.

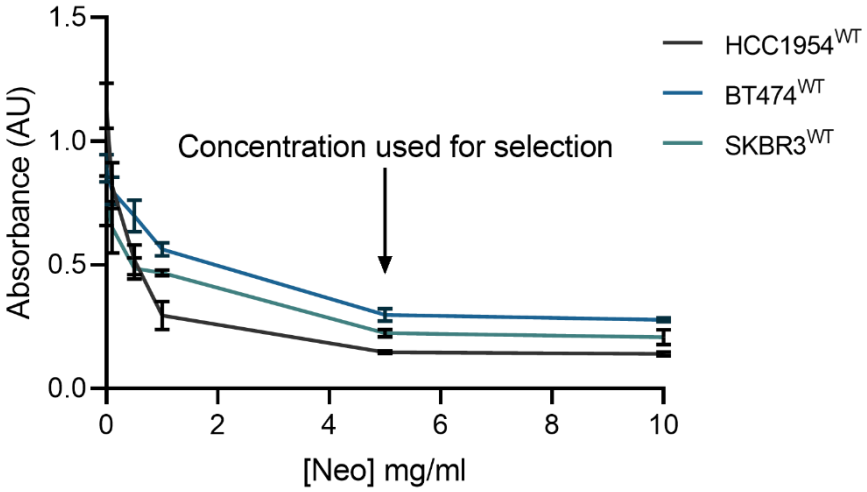

Figure 3.2.2: Neomycin kill curve.

Absorbance values of HCC1954, SKBR3 and BT474 wild type (WT) cells grown in increasing concentrations of neomycin after 5 days, measured in with the MTS assay. Decreasing levels of viability are inferred by decreasing absorbance.

3.3 Validation of inducible CB_2 expression in HER2+ cell lines

Initially, the dox inducible expression of *CNR2* was determined by qPCR in HCC1954^{iCB2}, SKBR3^{iCB2} and BT474^{iCB2} cells. Dox (1 μg/ml) increased the expression of *CNR2* mRNA 630-fold, 380-fold and 360-fold in HCC1954^{iCB2}, SKBR3^{iCB2} and BT474^{iCB2} cells, respectively (Figure 3.3.1 A). As CB_2 and CB_1 share 44% amino acid homology identity[134], qPCR using *CNR1* primers was performed to determine endogenous CB_1 expression was not confounding *CNR2* detection (Figure 3.3.1 B). Only minimal *CNR1* mRNA was detected across all three cell types (Ct values >30).

Finally, qPCR was performed using genomic DNA primers for *MMP13* to confirm that contamination with genomic DNA (gDNA) was the source of *CNR2* detection in HCC1954^{iCB2} and BT474^{iCB2} cells, with negligible amounts of gDNA detected (Appendix figure 5).

Subsequently, dox-inducible CB_2 protein expression was analysed. All three cell lines showed CB_2 expression after 24-hour dox treatment, detected by western blot using an anti-HA antibody. There was no detectable HA-antibody stain in WT cells with or without dox treatment (Figure 3.3.2 A). HCC1954^{iCB2}, SKBR3^{iCB2} and BT474^{iCB2} cells also showed a dox dose-dependent increase in CB_2 expression (Figure 3.3.2 B). HCC1954^{iCB2} cells displayed increased CB_2 expression with increasing dox concentrations, peaking at 1 μg/ml dox. SKBR3^{iCB2} cells showed little CB_2 expression until 1 μg/ml dox, which decreased by 10 μg/ml. BT474^{iCB2} cells had strong CB_2 expression at 50 ng/ml dox, and CB_2 expression remained stable with increasing concentrations. Taken together, the qPCR and western blot data indicate slight differences in CB_2 induction across the three cell lines. HCC1954^{iCB2} cells displayed the greatest expression of *CNR2* mRNA and the most tunability of CB_2 expression with different concentrations of dox. However, all cell lines showed significant expression of CB_2 with 1 μg/ml dox, which was used for subsequent experimentation.

Further analysis of CB_2 protein expression via immunofluorescence using an anti-HA antibody revealed heterogeneity in cells expressing CB_2 across all three cell lines, particularly in $SKBR3^{iCB2}$ cells (Figure 3.3.3), possibly down to differences in the transduction efficiencies of each cell line. To achieve more homogenous CB_2 expression, cells were induced for CB_2 expression with 1 μg/ml dox and fluorescently stained. Cells were then sorted using fluorescence-activated cell sorting (FACS). Positively stained cells were sorted into medium and high populations of the top 50% and top 10% of fluorescent cells, respectively. Immunofluorescence was performed to assess CB_2 expression level and heterogeneity in sorted populations (Figure 3.3.4). Some heterogeneity remained in the high populations across the cell lines. However, the number of cells that displayed little CB_2 expression decreased. Subsequent experiments used the high populations of each cell line unless otherwise stated. CB_2 expression was tested by RT-qPCR, western blotting and IF throughout the project, whilst CB_2 expression remained high, some heterogeneity was still observed in subsequent IF experiments.

Finally, immunofluorescence was performed with and without cell permeabilisation to determine whether CB_2 was successfully localising to the cell membrane (Figure 3.3.5). As the HA-tag was located on the 5' end of the *CNR2* gene, when translated, the HA-tag is at the N-terminus, on the extracellular side. Non-permeabilised cells displayed staining with the anti-HA antibody, indicating localisation to the cell surface. This validation confirms that a dox-inducible system of CB_2 expression has been established in the three HER2+ breast cancer cell lines: HCC1954, SKBR3 and BT474, enabling interrogation into the role of CB_2 on the progression of HER2+ breast cancer, and the potential of targeting CB_2 therapeutically.

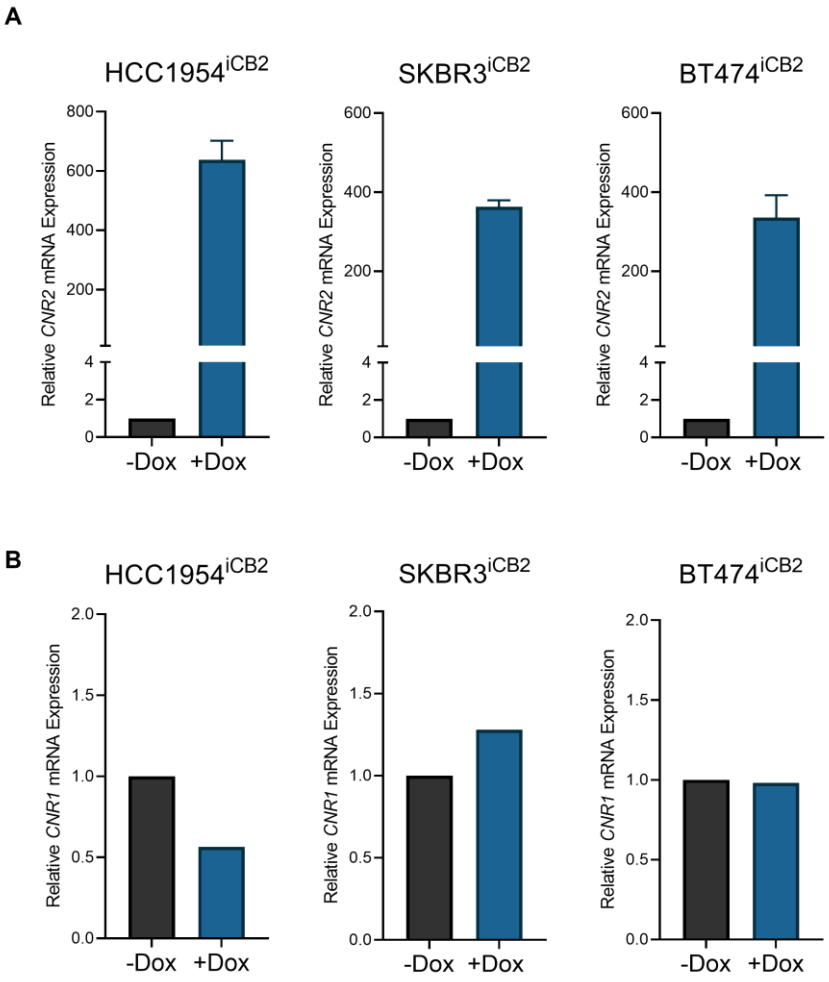

Figure 3.3.1: Inducible expression of *CNR2* mRNA.

(A) RT-qPCR analysis of *CNR2* mRNA expression in HCC1954^{iCB2}, SKBR3^{iCB2} and BT474^{iCB2} cells after 24 hours +/- 1 µg/ml doxycycline (dox), n=2. Relative mRNA expression normalised to *ACTB* (β-actin) mRNA expression. (B) Relative expression of *CNR1* mRNA in HCC1954^{iCB2}, SKBR3^{iCB2} and BT474^{iCB2} cells, 24 hours after +/- 1µg/ml dox, n=1.

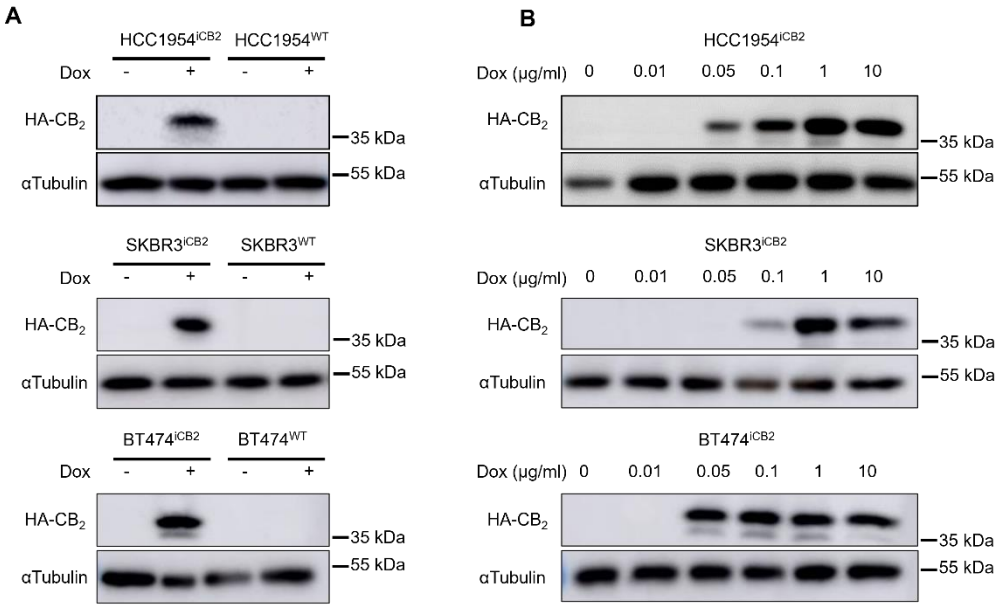

Figure 3.3.2: Doxycycline inducible CB_2 protein expression.

(A) Western blot analysis of whole cell lysates isolated from HCC1954, SKBR3 and BT474 inducible CB_2 (iCB2) or wild type (WT) cells using αHA tag antibody +/- 1 µg/ml doxycycline for 24 hours. αTubulin was used as a loading control (representative image of n=3 biological replicates). (B) Western blot of whole cell lysates isolated from $HCC1954^{iCB2}$, $SKBR3^{iCB2}$ and $BT474^{iCB2}$ after 24-hour treatment with increasing concentration of doxycycline using αHA-tag antibody. αTubulin was used as a loading control (n=1).

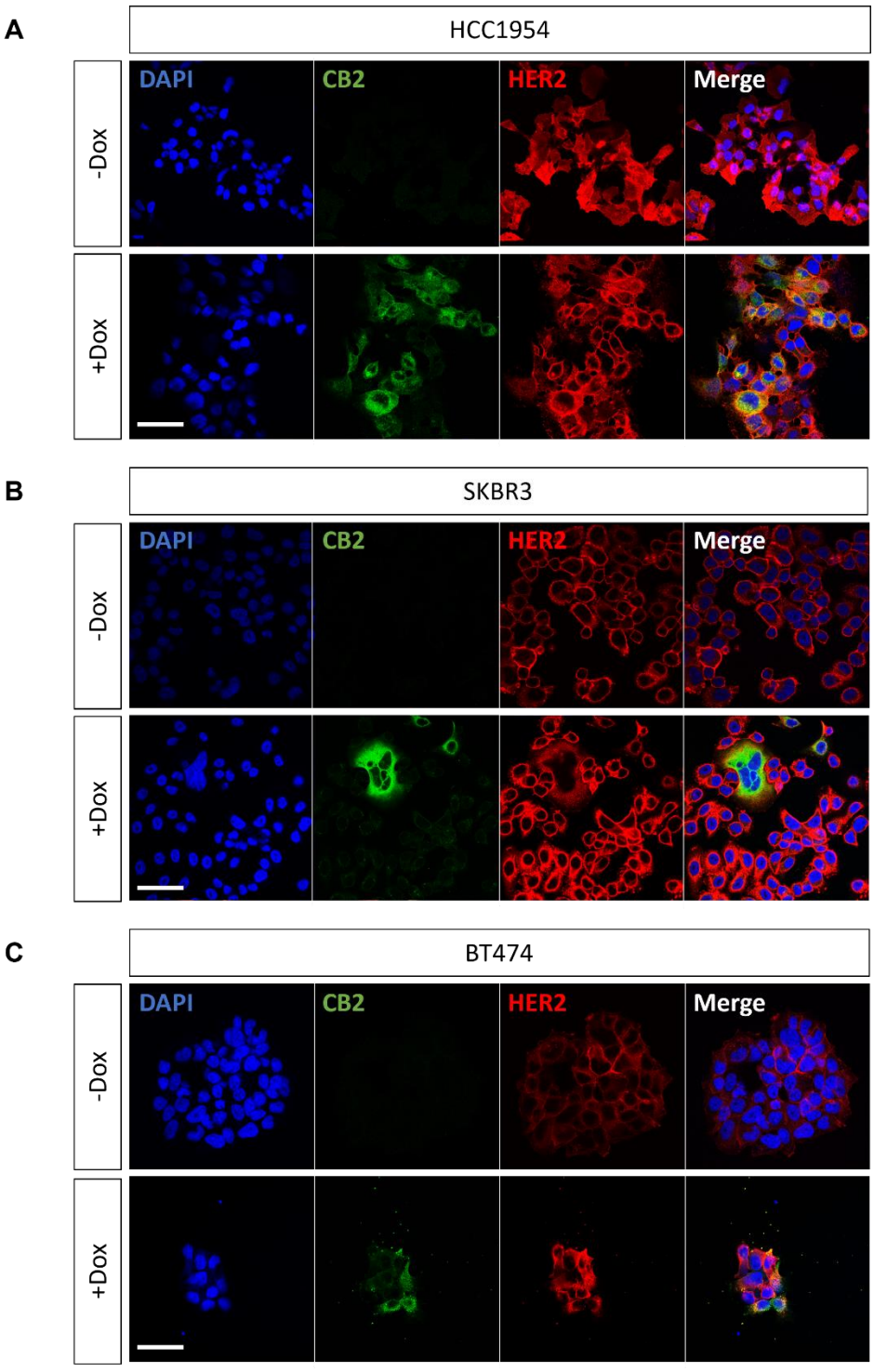

Figure 3.3.3: Heterogenous CB_2 expression after induction.

Immunofluorescence of HA-CB_2 (green) and HER2 (red) using anti-HA tag and anti-HER2 antibodies, respectively, in (A) HCC1954^{iCB2}, (B) SKBR3^{iCB2} and (C) BT474^{iCB2} cells with and without 24-hour 1µg/ml dox treatment (representative image of n=3 biological replicates). Scale bar 50µm.

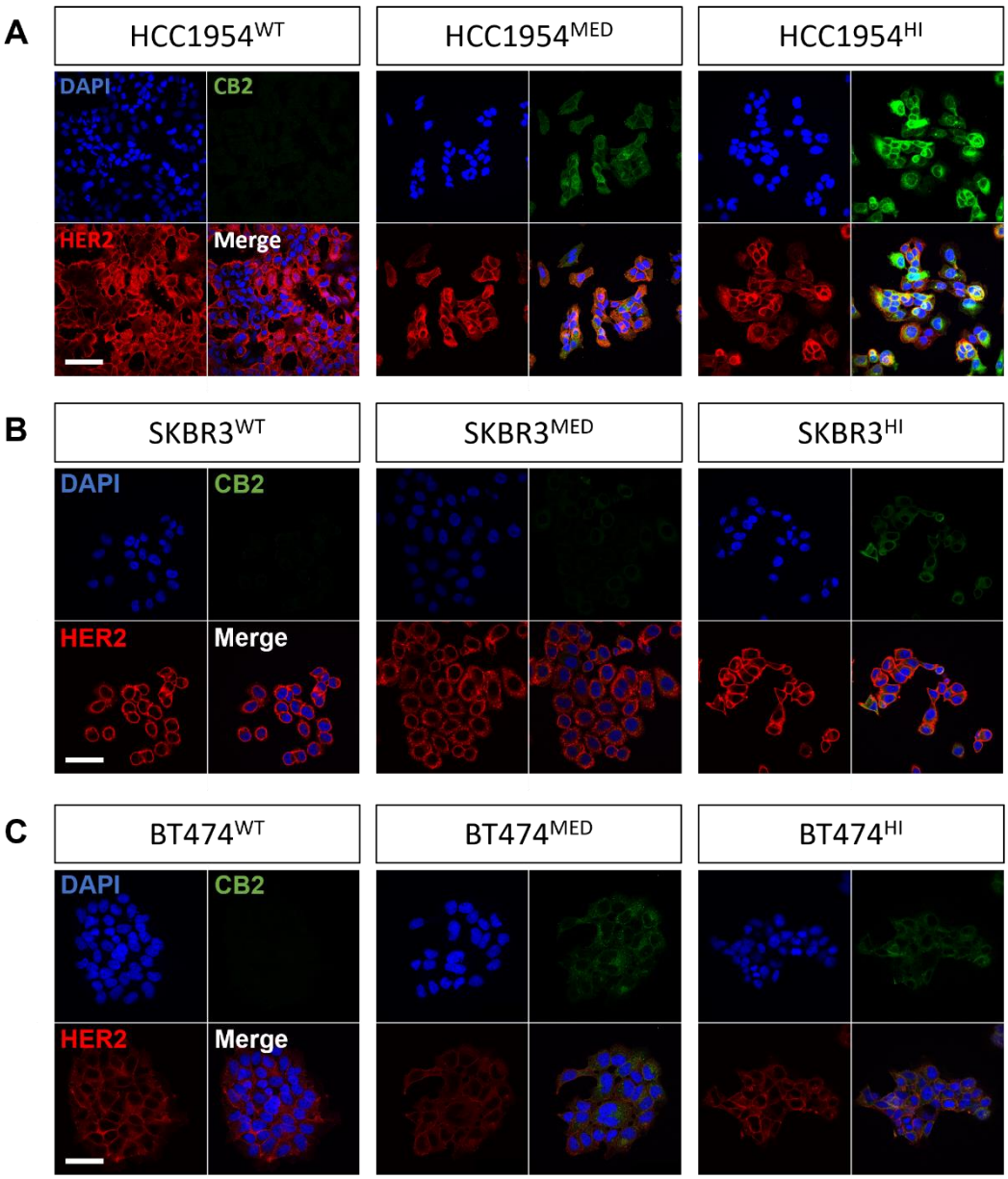

Figure 3.3.4: Heterogeneity of CB_2 expression is reduced after FACS sorting.

Immunofluorescence HA-CB_2 (green) and HER2 (red) in wild type (WT), top 50% of CB_2 expressing cells (CB_2 MED) and top 10% of CB_2 expressing cells (CB_2 HI), in (A) HCC1954, (B) SKBR3 and (C) BT474 cells after 24-hour 1 µg/ml dox treatment (representative image of n=3 biological replicates). Scale bar 50 µm.

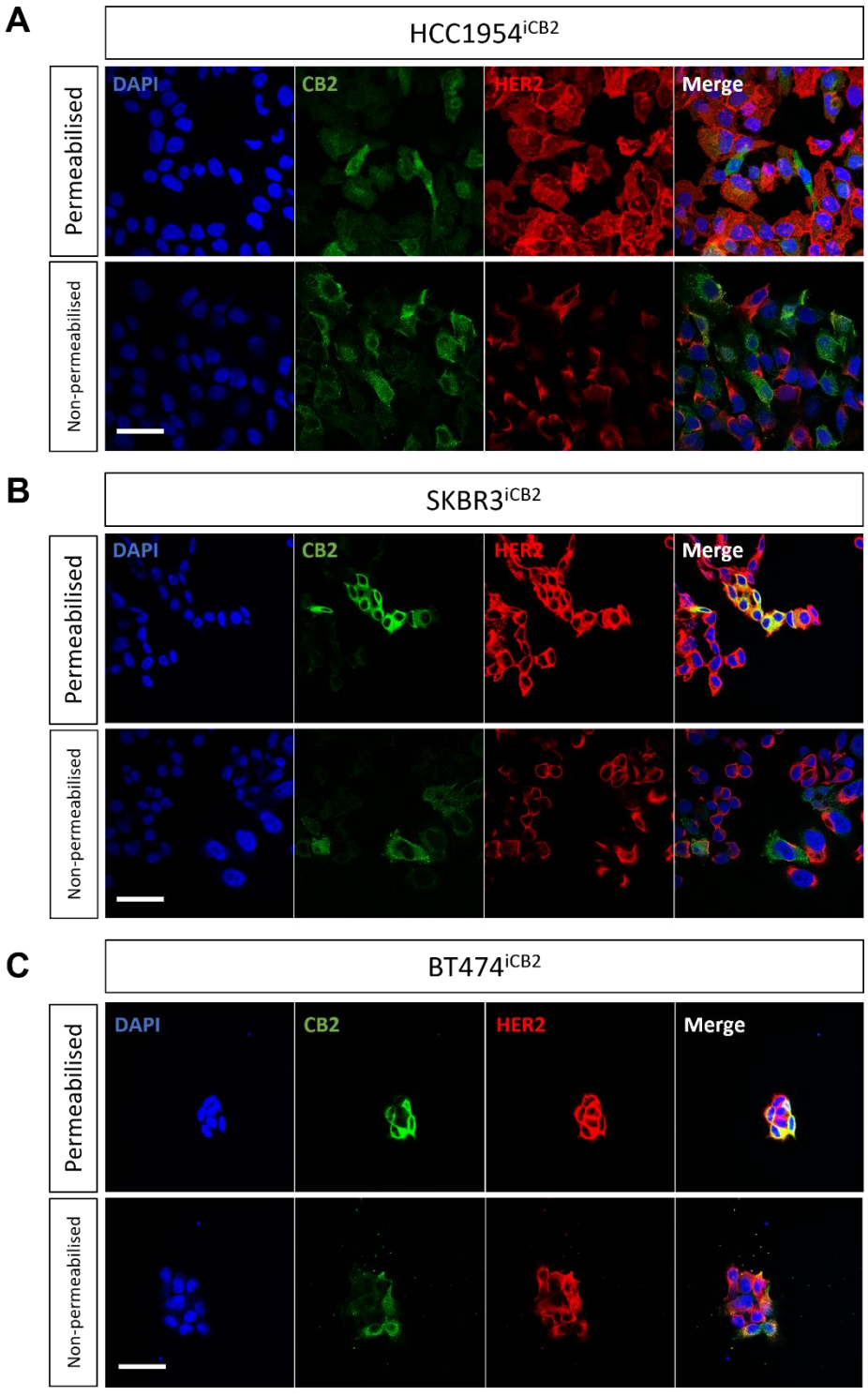

Figure 3.3.5: CB_2 immunofluorescence of permeabilised and non-permeabilised cells.

Immunofluorescence of HA-CB_2 (green) and HER2 (red) with and without permeabilisation with 0.1% Triton X, after 24-hour 1µg/ml dox treatment in (A) HCC1954^{iCB2}, (B) SKBR3^{iCB2} and (C) BT474^{iCB2} cells. Scale bar 50 µm.

3.4 Summary of Results

- Developed a doxycycline inducible CB_2 expression system in the HER2+ breast cancer cell lines HCC1954, BT474, SKBR3.
- Validated CB_2 induction with dox in the above cell lines at mRNA and protein level.
- FACS sorted the highest 10% of CB_2 expressing cells for future experiments to reduce heterogeneity of CB_2 expression.

Chapter 4 The role of CB_2 on HER2+ breast cancer progression

4.1 CB_2 expression impacts patient survival

The palliative use of cannabinoids to treat the symptoms of cancer and chemotherapy is well established; cannabis is an effective anti-emetic, analgesic and appetite stimulant[201]. However, there is growing evidence that phyto and synthetic cannabinoids have anti-tumourigenic properties[202]. In addition, alterations in the ECS are commonly observed in many cancer types[135135]. Specifically, CB_2 expression is seen in cancers of various tissues; non-small cell lung cancer[203], breast cancer[180], colon cancer[204], glioma[205], and renal cell carcinoma[206], amongst others. Whilst ectopic expression of CB_2 is relatively common in cancer, the prognostic implication of its expression is convoluted. CB_2 expression correlates with poor survival in colon cancer[204] and glioma[205], although NSCLC and hepatocellular carcinoma patients with high CB_2 expression have better prognoses[169,203,207]. Regardless of how CB_2 expression affects patient survival in different cancers, cannabinoid treatment in each case can elicit anti-tumourigenic effects, depending on concentration[208–210]. The complexities of CB_2 as a prognostic marker persist even in cancers of the same tissue, with CB_2 relating to better or worse outcomes in different breast cancer subtypes. High CB_2 expression associated with aggressive forms of breast cancer is commonly observed in TNBC, HER2+, and ER- PR- subtypes, with the highest proportion of CB_2 seen in the HER2+ subtype[211]. However, CB_2 expression in ER+, ER- and HER2- subtypes is correlated to better patient outcomes[171].

Over 75% of HER2+ patients display high CB_2 expression, which correlates with decreased survival and increased rates of metastasis and relapse[204]. HER2+ signalling has been reported to induce CB_2 expression via ERK, leading to CB_2-HER2 heteromer formation[186]. The CB_2-HER2 heteromer results in increased protumoural signalling, which is inhibited by THC administration, leading to HER2 poly ubiquitination and degradation via the proteasome[186].

Examination of publicly available data sets[192] confirmed that high CB_2 expression is linked to decreased survival of patients with HER2+ breast cancer but not HER2- breast cancer (Figure 4.1.1 A), indicating that the presence of the CB_2-HER2 heteromer could be responsible for decreased patient survival. Furthermore, HER2- patients have a better prognosis with high levels of CB_2, possibly due to an antitumourigenic effect of CB_2 in the absence of HER2 as seen in ER+ breast cancer[134]. Alternatively, as CB_2 is primarily expressed on immune cells, these cancers could have a higher immune infiltrate, leading to increased survival.

Interestingly, analysis of patient data shows that HER2+ patients with lymph node metastases have significantly worse survival with high CB_2 expression, whilst the survival of HER2+ patients without lymph node metastasis is unaffected by CB_2 expression (Figure 4.1.1 B). This suggests that HER2+ patients expressing high levels of CB_2 are at risk of advanced metastatic disease. Furthermore, CB_2 expression could contribute to a specific increased risk of lymph node metastases through promoting immune evasion. These data also suggest that CB_2 expression only contributes to decreased survival after successful lymph node metastasis.

Metastasis to the lymph nodes is common in breast cancer and a reliable predictor of mortality[212]. Tumours can initiate lymph node metastasis through lymphangiogenesis, stimulating the growth of lymphatic vessels into the tumour[213]. Cancer cells intravasate into the lymphatic lumen, travelling into the lymph node where they can colonise and form a secondary tumour. For colonisation of the lymph node to be successful, metastasising tumour cells must evade immune surveillence[212]. Cancer cells can trigger the anergy and apoptosis of immune cells through the release of immunosuppressive cytokines, and the expression of immune checkpoint proteins such as PDL1, which are commonly observed in lymph node metastases[214,215]. Furthermore, patients with lymph node metastasis struggle to respond to chemotherapy as drug concentrations in axillary lymph nodes are very low after intravenous administration, leading to

increased mortality[216]. Therefore, CB_2 expression could contribute to decreased survival of HER2+ breast cancer patients by promoting metastasis to the lymph nodes.

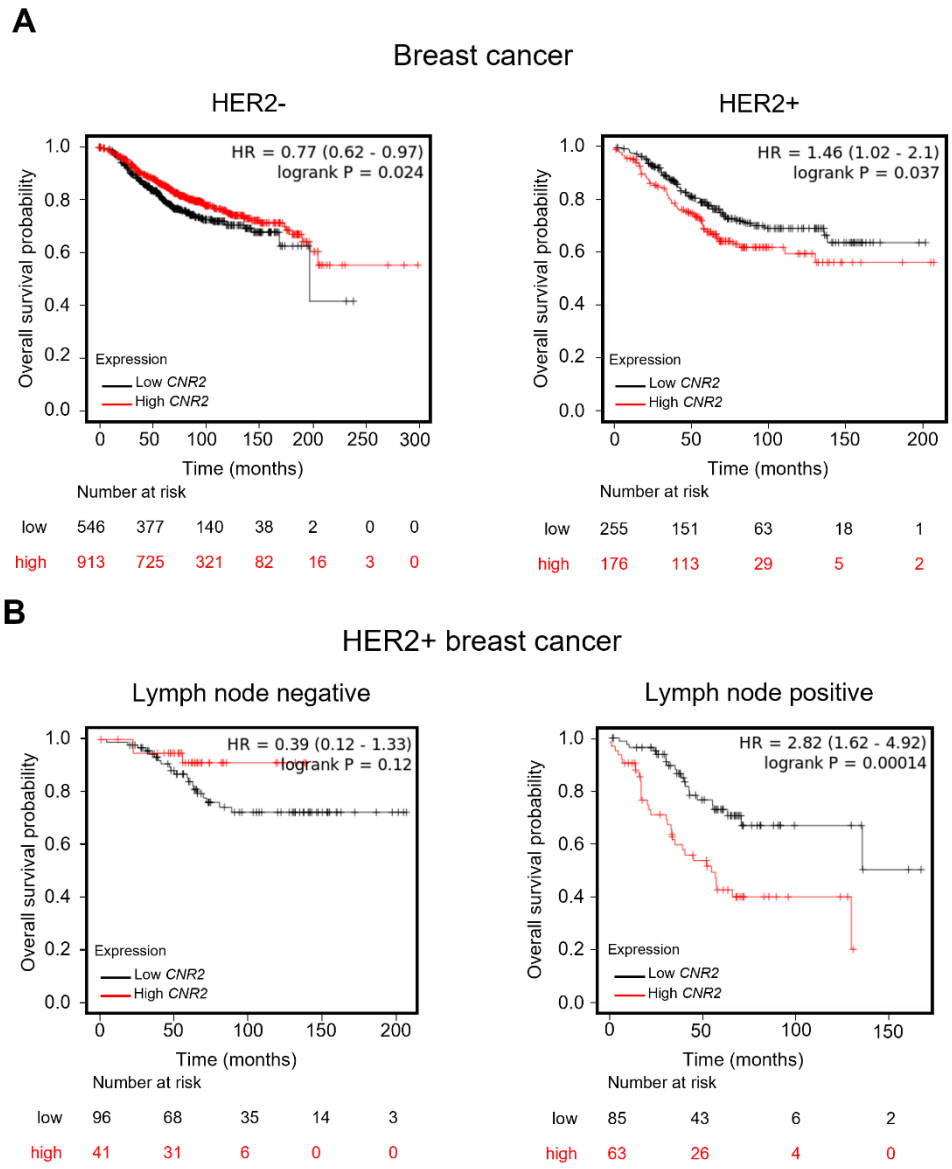

Figure 4.1.1: CB_2 expression impacts HER2+ breast cancer patient overall survival, dependent on lymph node metastases.

(A) Kaplan-Meier overall survival plots of HER2- and HER2+ breast cancer patients with high (red) or low (black) *CNR2* expression. (B) Kaplan-Meier overall survival plots of HER2+ breast cancer patients with or without lymph node metastasis, with high (red) or low (black) *CNR2* expression. Survival plots were made with kmplots.com, using all Breast Cancer mRNA gene chip datasets. *CNR2* (Affymetrix ID 206586) with auto select best cut-off was selected, and lymph node status was selected as positive or negative. HR = hazard ratio, significance logrank $P < 0.05$, using logrank test of survival distribution.

4.2 CB_2 increases metastatic potential of HER2+ breast cancer cells

To investigate the link between CB_2 expression and metastasis in HER2+ breast cancer, I used the inducible CB_2 expression system to model invasion *in vitro*. Several methods to study cancer cell invasion have been established, from simple wound healing assays to complex 3D *in vitro* models. In the wound healing assay, a scratch, or 'wound', is made on a monolayer of cancer cells, and cancer cells' ability to migrate and 'heal' the wound is measured[217]. However, whilst measuring migratory capacity, the 2D nature of this assay does not recapitulate the extracellular environment cancer cells encounter in a tumour.

To simulate the 3D environment of tissue, ECM proteins can be isolated and formed into a matrix for *in vitro* culture. In the organotypic invasion model, cancer cells are seeded on top of a physiomimetic hydrogel composed of collagen, Matrigel or a combination of the two in a transwell insert[218]. Cells penetrate the gel towards a chemoattractant in the bottom of the transwell, and cell invasion is measured qualitatively by degree of cell penetration into the gel or quantitatively by the number of cells on the underside of the insert. While this does imitate the 3D environment of tissue, it does not recapitulate the 3D structure of tumours, as the cells are grown on a monolayer on top of the gel.

For this study, the invasive potential of HCC1954^{iCB2}, SKBR3^{iCB2} and BT474^{iCB2} cells +/- CB_2 induction was determined in a hanging drop spheroid model[219]. This model recapitulates both tumoural 3D ECM using similar phyisomimetic organotypic gels and the 3D structure of tumours using cancer cell spheroids. Spheroids are produced in droplets of cells suspended on the lid of a Petri dish. Methylcellulose in the medium helps cells coalesce into spheroids, which are then harvested from the droplets and embedded into an ECM hydrogel to grow and invade. Spheroids can subsequently be harvested from the gels for further analysis.

Optimisation to ensure reliable spheroid invasion in this model was required. First, the 3D matrix most suitable for invasion was assessed by comparing collagen gels and collagen-Matrigel gels. Collagen gels offer a uniform matrix for the growth of spheroids, as they only contain collagen I, allowing reliability of gel formation between experimental repeats. However, as they consist of only a single ECM protein, they do not reflect the complexity of the ECM found *in vivo*. Alternatively, collagen-Matrigel gels compose numerous matrix proteins, primarily collagen I, laminin, collagen IV, entactin and perlecan, with other components in low abundance, more accurately recapitulating the diverse nature of the ECM[220]. Spheroids containing 1000 HCC1954^{iCB2} cells/sphere were embedded in collagen and collagen-Matrigel gels (Figure 4.2.1) to test which gel was suitable. Gels were imaged at day 1, and collagen-Matrigel gels were determined to be most appropriate, with setting properties resulting in clear, easy to image gels and reliable spheroid invasion.

Next, cell titrations of 500, 1000 and 2000 cells/spheroid were performed to determine the optimal spheroid size for consistent invasion (Figure 4.2.2). For HCC1954^{iCB2} and BT474^{iCB2,} 500 cells/sphere were chosen as spheroids form uniformly, and invasion was observed after only 1 day of culture. SKBR3^{iCB2} cells could not form spheroids, so were not analysed for invasion.

Further, I sought to determine what experimental endpoint was optimal for quantifying spheroid invasion. Spheroids of HCC1954^{iCB2} and BT474^{iCB2} cells were imaged at day 3, 4 and 5, and invasion was quantified (Figure 4.2.3). In HCC1954^{iCB2} spheres, there was significantly higher invasion with CB_2 induction at all time points. However, for BT474^{iCB2}, there was a significant increase in invasion at day 3, and quantification of invasion at day 4 and day 5 still indicated increased invasion after CB_2 induction, although this was not significant. An experimental endpoint at day 3 was chosen for both HCC1954^{iCB2} and BT474^{iCB2} spheroids due to consistent, significant CB_2-driven invasion. In addition, with extended culture periods, spheroids

tend to grow into one another, preventing quantification of invasion of the spheroids (Appendix figure 6). After optimising the hanging drop spheroid model, experiments used collagen-Matrigel gels, containing 2 mg/ml collagen and Matrigel, with 500 cells per spheroid and quantifying invasion at day 3 of culture.

As shown during optimisation, analysis of spheroid invasion revealed a significant increase in the ability of in HCC1954^{iCB2} and BT474^{iCB2} spheroids to invade into surrounding collagen-Matrigel matrix after 3 days of CB_2 induction. Importantly, treatment with the synthetic CB_2-specific cannabinoid JWH133 (100 nM) significantly reduced CB_2-driven invasion in both cell lines (Figure 4.2.4). Furthermore, treatment with a non-specific cannabinoid CP55940 (1 μM) also significantly reduced invasion in HCC1954^{iCB2} spheroids (Figure 4.2.5). These data indicate that CB_2 expression contributes to the invasive potential of the HER2+ cell lines, HCC1954 and BT474, which is abrogated by the activation of CB_2 with cannabinoid ligands.

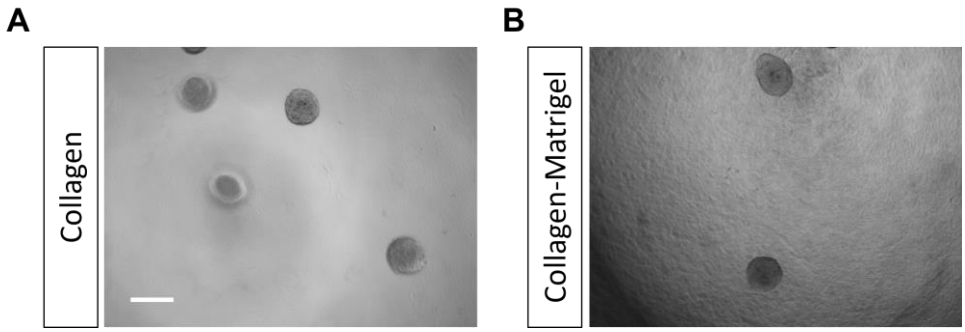

Figure 4.2.1: Comparison of collagen I and collagen-Matrigel matrices.

HCC1954^{iCB2} spheroids embedded into (A) collagen I hydrogel and (B) collagen-Matrigel hydrogel after 1 day of culture. Scale bar 200 µm.

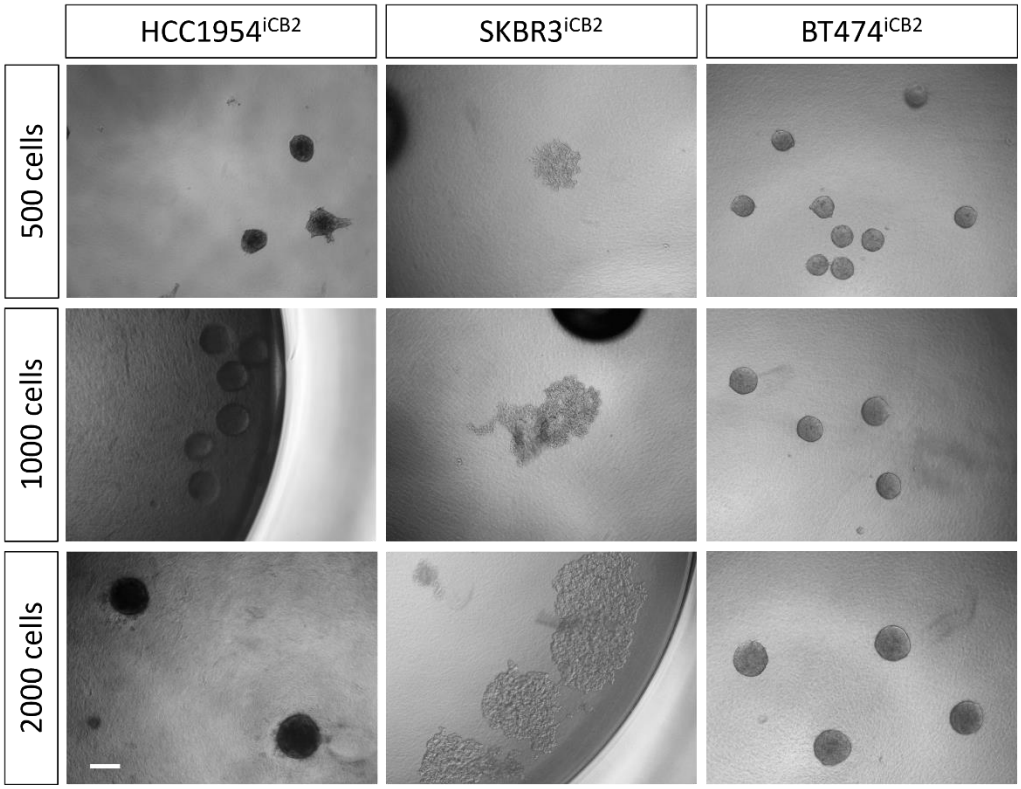

Figure 4.2.2: Comparison of spheroid size.

HCC1954^{iCB2}, SKBR3^{iCB2} and BT474^{iCB2} spheroids, composed of 500 cells/sphere, 1000 cells/sphere or 2000 cells/sphere after 1 day of culture. Scale bar 200 µm.

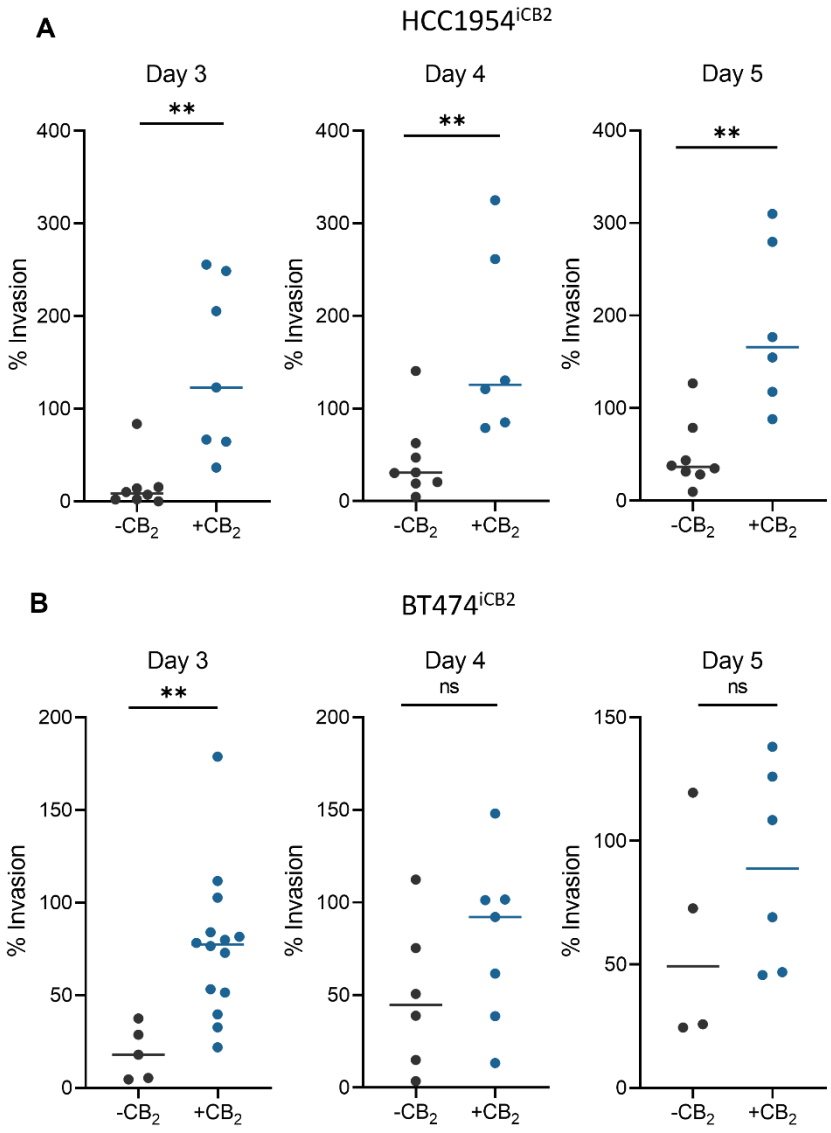

Figure 4.2.3: Hanging drop experimental endpoint optimisation.

Quantification of (A) HCC1954^{iCB2} and (B) BT474^{iCB2} spheroids in a collagen-Matrigel matrix, +/- CB_2 induction and cultured for 5 days, imaged and quantified on day 3, 4 and 5, each point representing a single spheroid and horizontal line represents median % invasion. ** $p < 0.01$.

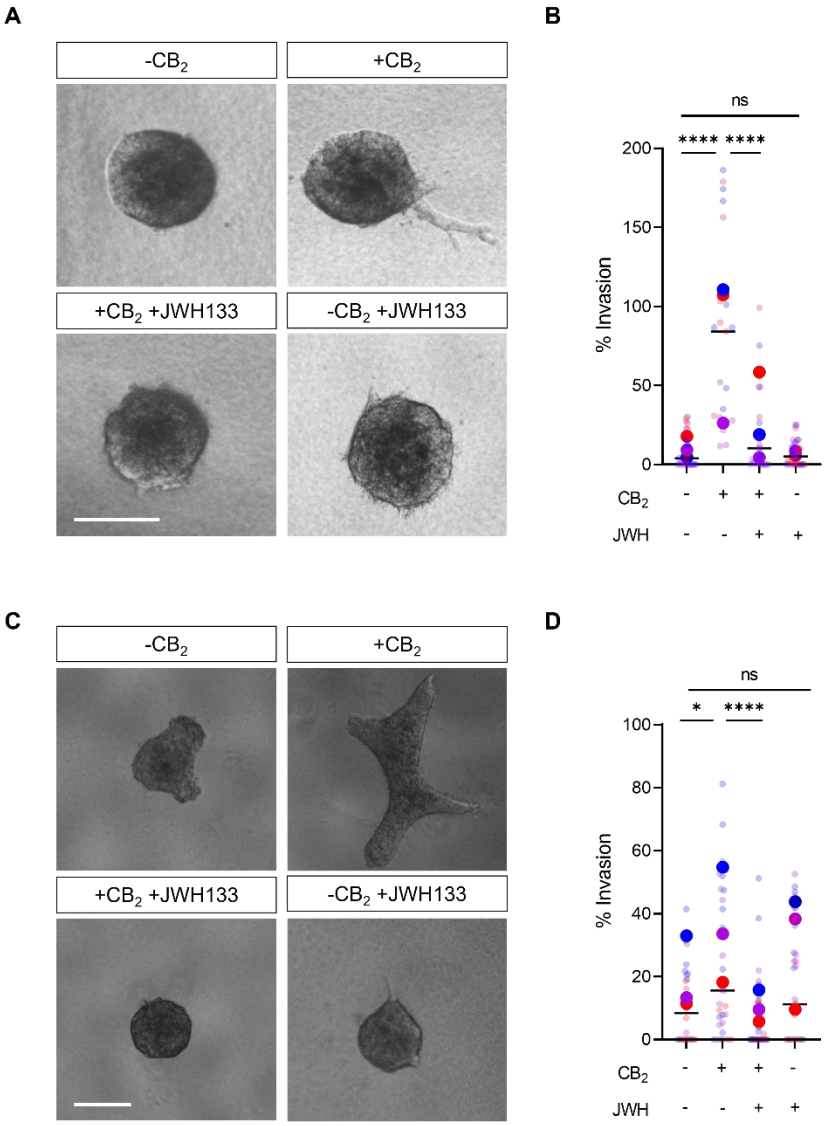

Figure 4.2.4: CB_2 increases 3D spheroid invasion, which is blocked by JWH133.

(A) HCC1954^{iCB2} spheroids in a collagen-Matrigel matrix, +/- CB_2 induction and +/- 100 nM JWH133 or vehicle (DMSO), after 3 days (representative images of n=3). (B) Analysis of invasive potential of CB_2 expressing HCC1954^{iCB2} spheroids from (A), with each colour representing biological repeats, translucent points representing a single spheroid and each larger solid point represents the mean invasion of each experimental repeat, horizontal line represents median % invasion (n=3, ordinary one-way ANOVA). (C) BT474^{iCB2} spheroids in a collagen-Matrigel matrix, +/- CB_2 induction and +/- 100 nM JWH133 or vehicle (DMSO), after 3 days (representative images of n=3). (D) Analysis of invasive potential of CB_2 expressing BT474^{iCB2} spheroids from (C). (n=3, ordinary one-way ANOVA). * $p < 0.05$, **** $p < 0.0001$. Scale bar 200 µm.

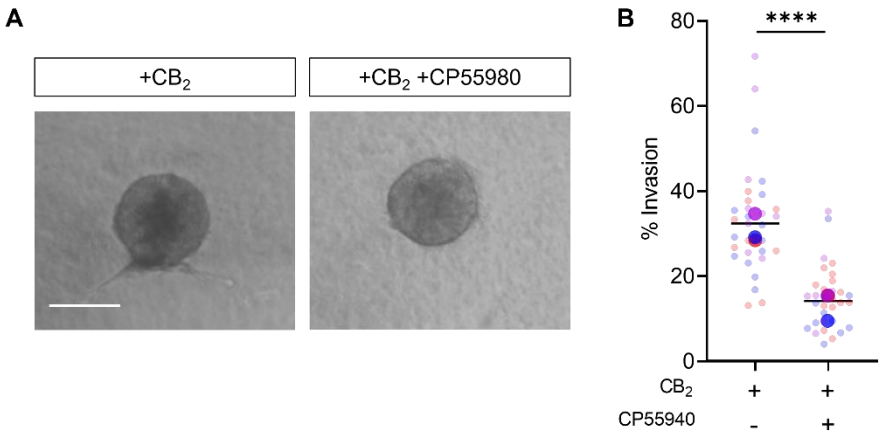

Figure 4.2.5: Non-specific cannabinoid CP-55940 reduces invasion of HCC1954^{iCB2} spheroids.

(A) Light micrographs of HCC1954^{iCB2} spheroids embedded in a collagen-Matrigel matrix, with CB_2 expression and treated with synthetic cannabinoid, CP55940 (1 µM) or vehicle (DMSO) after 3 days (representative images of n=3). (B) Quantification of invasion of CB_2 expressing HCC1954^{iCB2} spheroids into surrounding collagen-Matrigel matrix +/- 1 µM CP55940 (n=3, unpaired t-test). **** $p < 0.0001$. Scale bar 200 µm. Experiment performed by Natasa Tomasevic, Medical University of Vienna, Centre for Physiology & Pharmacology.

4.3 The effect of CB_2 expression on migration and proliferation

As the invasion of cancer cells into tissue is linked to cell migration, I aimed to assess whether CB_2-mediated increase in 3D invasion corresponded to an increase in cell migration. Using a 96-well plate Incucyte chemotaxis Boyden chamber model (+/- CB_2 induction), cell migration of HCC1954^{iCB2} and BT474^{iCB2} towards serum was assayed. Recapitulating the 3D invasion data, CB_2 expressing HCC1954^{iCB2} cells showed significantly higher migration towards an FBS gradient (Figure 4.3.1). However, there was no significant difference in migration in BT474^{iCB2} cells, regardless of CB_2 induction. Moreover, levels of migration of BT474^{iCB2} cells were generally low. This relative static behaviour could be due to BT474 cells having potentially stronger cell-cell adhesion than HCC1954 cells, or their tendency to grow in clumps rather than in a monolayer, reducing the access of cells to the pores of the lower chamber.

Verification that the changes in migration and invasion were not a result of CB_2 increasing proliferation was confirmed by monitoring cell confluency over time in 2D using the Incucyte. Induction of CB_2 in HCC1954^{iCB2} cells had no significant impact on growth. Interestingly, in BT474^{iCB2} cells, CB_2 induction significantly reduced cell proliferation. The difference in proliferative response to CB_2 induction could be due to the genetic and phenotypic differences between HCC1954 and BT474 cell lines, discussed later. This suggests that the increase in invasion observed in HCC1954^{iCB2} and BT474^{iCB2} and increased migration in HCC1954^{iCB2} cells is not due to increased growth but increased cell motility due to CB_2 expression.

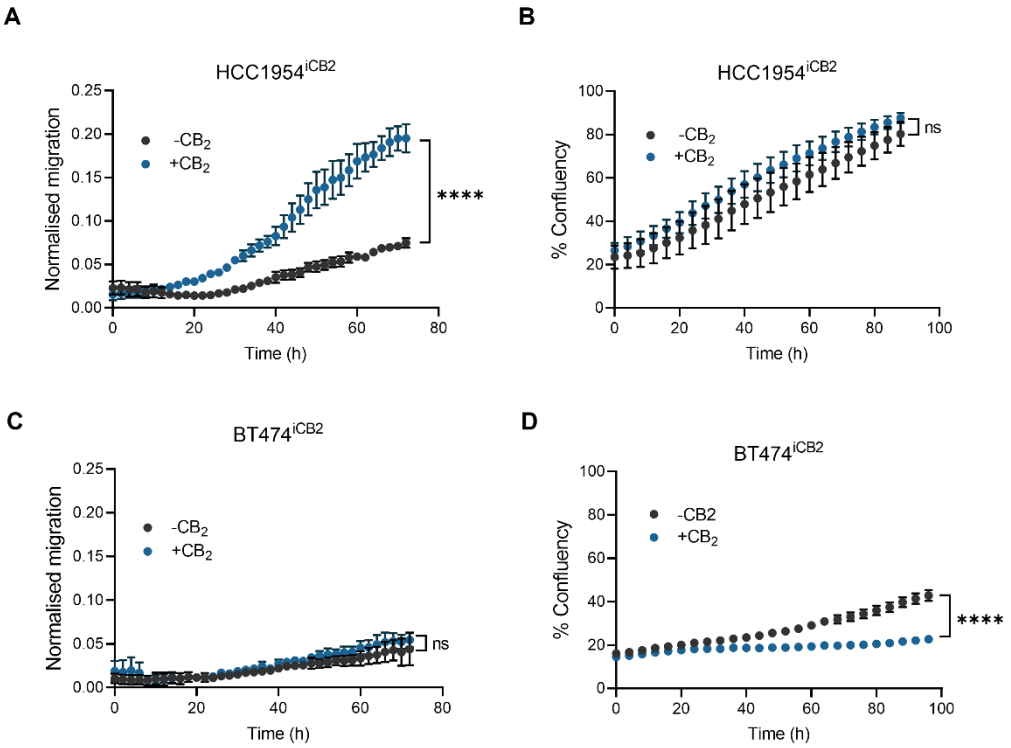

Figure 4.3.1: The impact of CB_2 on HER2+ breast cancer cell migration and proliferation.

(A) Transwell migration of HCC1954^{iCB2} cells towards an FBS gradient measured using the Incucyte chemotaxis assay over 3 days. Migration calculated using phase area on the underside of transwell membrane normalised to initial value on top of the membrane (n=3, unpaired t-test, mean ± SD). (B) Proliferative capacity of HCC1954^{iCB2} cells +/- CB_2 induction, determined by Incucyte growth assay measuring cell confluency over 4 days (n=3, unpaired t-test, mean ± SD). (C) Transwell migration of BT474^{iCB2} cells towards an FBS gradient using the Incucyte chemotaxis assay after 3 days. (n=3, unpaired t-test, mean ± SD). (D) Proliferative capacity of BT474^{iCB2} cells +/- CB_2 induction, determined by Incucyte growth assay measuring cell confluency over 4 days (n=3, unpaired t-test, mean ± SD). **** $p < 0.0001$.

4.4 CB_2 impacts epithelial-to-mesenchymal transition.

Having shown the effect of CB_2 on migration and invasion I sought to determine if the CB_2-dependent migration was due to epithelial-to-mesenchymal transition (EMT). EMT is a normal developmental process during embryogenesis, wound healing and tissue regeneration, where epithelial cells lose cell-to-cell contacts and polarity, converting to a mesenchymal phenotype[221]. Mesenchymal cells then migrate to specific areas before transitioning back into an epithelial phenotype in the reverse process, mesenchymal-to-epithelial transition (MET), regaining cell adhesion[221]. This process of EMT and subsequent MET is hijacked by cancer cells, aiding dissemination into the circulatory system and colonising a suitable niche, forming metastases[222].

Phenotypically, EMT can be characterised by the loss of cellular adhesion protein E-cadherin and increased expression of N-cadherin, fibronectin and vimentin[223,224]. Cancer cells that have undergone EMT become highly invasive, hence EMT is related to poor patient prognosis[225]. Furthermore, EMT in cancer is associated with the formation of cancer stem cells (CSCs), epithelial cancer cells that become mesenchymal-like develop stem cell characteristics[226]**.** In breast cancer, EMT has been associated with HER2 overexpression, increased levels of migration and invasion and resistance to trastuzumab therapy[227–229]. Furthermore, CB_2 has been reported to influence EMT in colon cancer cells, with the EMT transcription factor snail correlating with CB_2 expression[204]. Using the cBioportal Breast Cancer Invasive PanCancer dataset of The Cancer Genome Atlas (TCGA)[193,194], HER2+ patients were selected and split on the level of *CNR2* mRNA expression, and the highest (n=20 patients) and lowest (n=19 patients) quartiles of *CNR2* expression were compared. With this comparison, the gene expression changes in HER2+ breast cancer patients that correlate with high CB_2 expression can be explored. Analysis of TCGA datasets revealed, there was no difference in *SNAI1* mRNA expression, between high and low of *CNR2* expressing HER2+ breast cancer patients, or any significant correlation

between *CNR2* and *SNAI1* expression (Figure 4.4.1 A, B). However, there was a significantly positive correlation with another EMT-regulator, ZEB2 (Figure 4.4.1 C, D), indicating that CB_2 expression may mediate EMT in HER2+ breast cancer, although not via snail.

Therefore, I investigated if CB_2 regulated EMT to increase the metastatic potential observed in HCC1954^{iCB2} and BT474^{iCB2} cell lines. Immunofluorescence of the EMT markers E-cadherin and vimentin in HCC1954^{iCB2} cells revealed that, even without CB_2 expression, HCC1954 cells appeared to be more mesenchymal-like, with low levels of E-cadherin and high vimentin expression, which remained unaffected with the induction of CB_2 expression (Figure 4.4.2). Upon CB_2 induction, E-cadherin staining decreased, and vimentin staining increased, suggesting that CB_2 expression does contribute to EMT in BT474 cells. Therefore, CB_2 expression is sufficient to trigger for EMT in HER2+ cell lines, although is not required as EMT is controlled by many tumourigenic processes.

Interestingly, although HCC1954^{iCB2} cells are already mesenchymal-like in their E-cadherin and vimentin expression, CB_2 induction leads to increased migration (Figure 4.3.1) This suggests that, even in a mesenchymal state, CB_2 induction further increases their migratory capacity through another mechanism. As for BT474^{iCB2} cells, although there is a change in the EMT markers E-cadherin and vimentin, and increased invasion in 3D upon CB_2 induction, this did not lead to increased migration in 2D. Even though there appeared to be differences in the effect of CB_2 between HCC1954 and BT474 cell lines, CB_2 increased the invasiveness of both, which was inhibited through activation of CB_2 with JWH133 and CP55940. Increased invasion is a vital hallmark of metastasising cancer cells, and these data highlight the potential of targeting CB_2 with cannabinoids to reducing cancer's invasive potential.

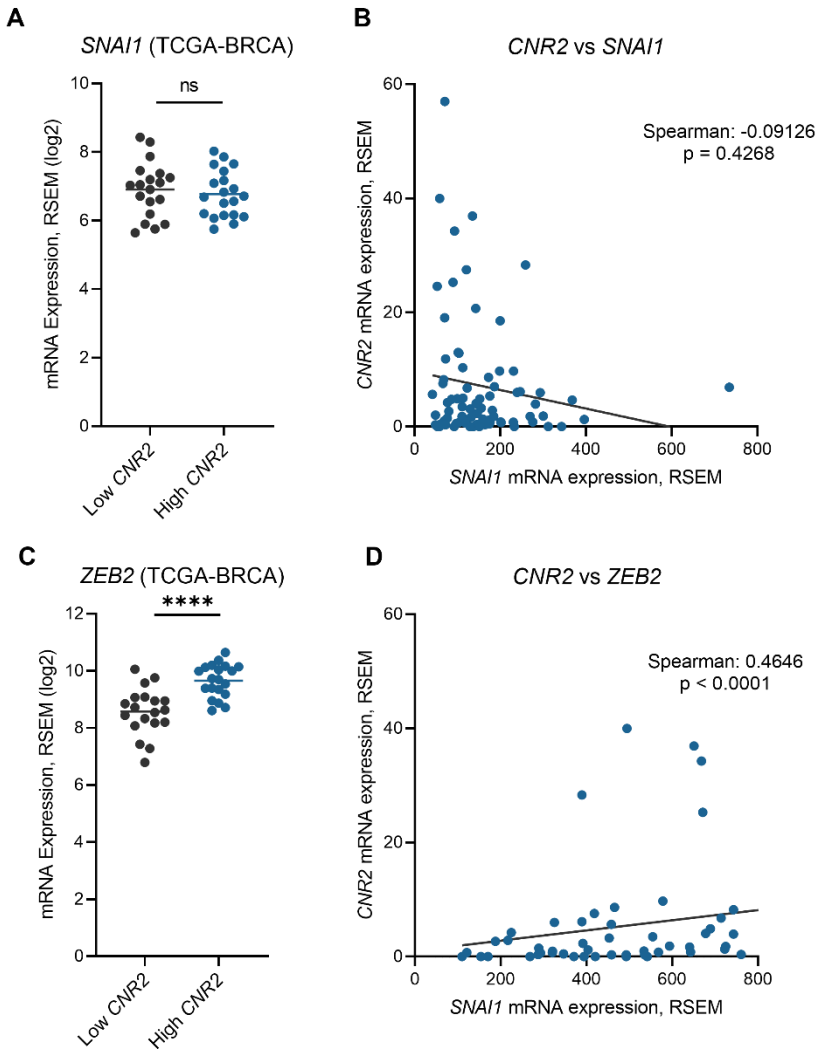

Figure 4.4.1: Correlation with CNR2 expression and regulators of EMT in HER2+ breast cancer patients.

(A) Comparison of *SNAI1* mRNA expression between the upper and lower quartiles of *CNR2* expressing HER2+ patients in the Breast Cancer Invasive TCGA dataset (unpaired t-test). (B) The correlation of mRNA expression between *SNAI1* and *CNR2* in HER2+ breast cancer patients. (C) Comparison of *ZEB2* mRNA expression in high and low *CNR2* expressing HER2+ breast cancer patients and (D) the correlation between *CNR2* and *ZEB2* in HER2+ breast cancer patients. TCGA data generated using RNA-seq by Expectation Maximisation (RSEM).

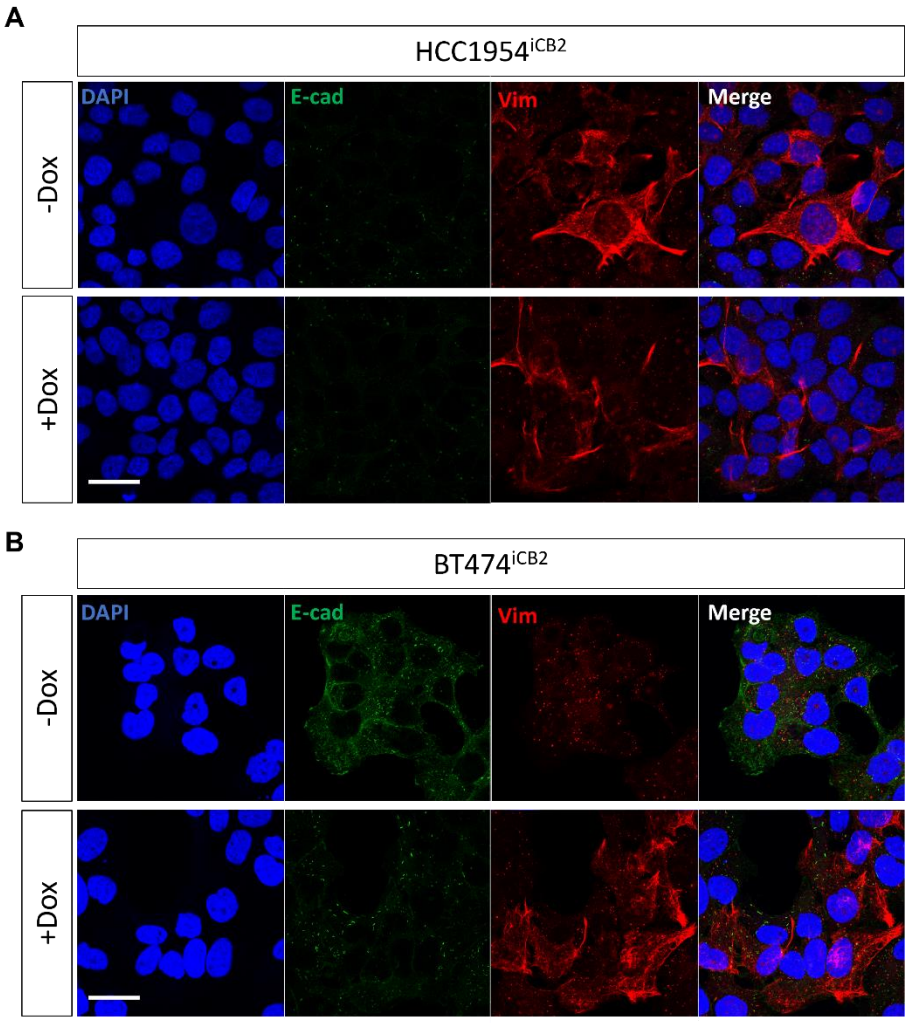

Figure 4.4.2: Immunofluorescence of EMT markers in HCC1954^{iCB2} and BT474^{iCB2} cells.

Immunofluorescence of vimentin (red) and E-cadherin (green) in (A) HCC1954^{iCB2} and (B) BT474^{iCB2} cells +/- 24-hour CB_2 induction (representative image of n=3 biological replicates). Scale bar 50µm.

4.5 Contribution of CB_2 expression in treatment resistance

CB_2 expression is closely associated with worse patient survival in HER2+ breast cancer (Figure 4.1.1). Hence, I wanted to examine if CB_2 was linked to treatment resistance, a common cause of mortality for cancer patients. To this end, I investigated CB_2's impact on resistance to lapatinib, a small molecule receptor tyrosine kinase inhibitor, indicated for metastatic breast cancer patients and used as a combination therapy[93]. Lapatinib is an ATP-competitive inhibitor of both HER2 and EGFR, preventing the autophosphorylation of the tyrosine kinase domains and subsequent signal transduction. Whilst lapatinib is an effective therapy for HER2+ breast cancer, some patients display innate resistance, and others acquire resistance during treatment. As upregulation of compensatory receptors and signalling pathways is a common mechanism of resistance for lapatinib[230], I hypothesised that the expression of CB_2 could lead to compensatory activation of signalling pathways such as MAPK or AKT, preventing lapatinib-induced cell death.

However, I found no difference in sensitivity across a range of lapatinib concentrations, regardless of CB_2 expression in $HCC1954^{iCB2}$ or $BT474^{iCB2}$ cells (Figure 4.5.1, unpaired t-test), suggesting that CB_2 does not decrease patient survival by preventing lapatinib efficacy but through other mechanisms. Unfortunately, I did not have the opportunity to investigate the role of CB_2 expression on trastuzumab resistance. As trastuzumab binds to the extracellular domain of HER2, preventing HER2 activity by blocking homodimerization, the HER2-CB_2 heteromer could interfere with trastuzumab binding, conferring resistance. Investigation into this possibility would be beneficial, however, due to the importance of trastuzumab's ADCC action, analyses in *in vivo* models would be required.

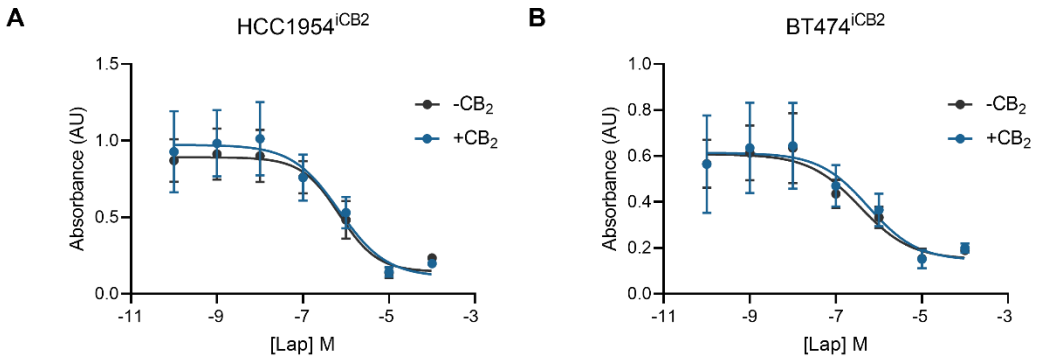

Figure 4.5.1: CB_2 expression does not affect sensitivity to lapatinib.

Viability of (A) HCC1954^{iCB2} and (B) BT474^{iCB2} cells grown in increasing concentrations of lapatinib, +/- CB_2 induction, measured by the MTS assay. n=2 biological replicates, unpaired t-test.

4.6 Summary of Results

- CB_2 is associated with decreased survival in HER+, but not HER2- breast cancer patients.
- Survival of HER2+ patients with lymph node metastases is significantly decreased with high CB_2 expression, which was not observed in HER2+ patients without lymph node metastases.
- CB_2 expression increased *in vitro* 3D invasion, which was blocked by synthetic cannabinoid agonists JWH133 and CP55940.
- HCC1954^{iCB2} and BT474^{iCB2} cell lines displayed differences in migration, proliferation and EMT with CB_2 induction.
- HCC1954^{iCB2} increased migration with CB_2 but not proliferation and displayed a mesenchymal phenotype regardless of CB_2 expression.
- BT474^{iCB2} did not increase 2D migration with CB_2 expression, however, CB_2 decreased proliferation and promoted a more mesenchymal phenotype.
- Increase in the expression of the EMT transcription factor *ZEB2* was observed in patients with high CB_2.
- CB_2 expression did not impact sensitivity to lapatinib in HCC1954^{iCB2} or BT474^{iCB2} cells.

Chapter 5 CB_2 alters the metabolic architecture of HER2+ breast cancer

5.1 CB_2-driven metabolic changes in breast cancer

Metabolic changes are a hallmark of tumourigenesis; cancer cells alter their metabolism to adapt to nutrient availability, aid proliferation and prevent oxidative stress[231–233]. The Warburg effect is a well-established phenomenon where highly proliferative tumours switch their metabolism from oxidative phosphorylation towards aerobic glycolysis[234]. This metabolic shift rapidly produces small amounts of ATP and enables more substrate availability to sustain the rapid growth of cancer[235]. In breast cancer, glycolytic enzymes are often upregulated to increase the rate of glycolysis[236,237] and can even contribute to treatment resistance, with increased enolase 1 expression being linked to tamoxifen resistance[238]. However, due to the energetic demands associated with metastasis, cancer cells will often increase their metabolic output by increasing mitochondrial respiration[239]. Metabolic plasticity such as this is observed during EMT and in CSCs, highlighting the phenotypic link between these two invasive populations of cancer cells and the necessity for sufficient energy production to sustain cellular movement.

As I observed CB_2 increasing rates of invasion and migration, I speculated that CB_2 could increase energy production to increase motility. Cell migration is an energetically demanding process, with cytoskeletal rearrangements requiring high ATP levels. Migrating cells translocate mitochondria to the leading edge, providing a localised increase in ATP[240]. Interestingly, glycolytic enzymes associated with the cytoskeleton can lead to ATP production at the leading-edge during cell migration, similar to the localised mitochondrial ATP production[241]. Moreover, interaction with the cytoskeleton can potentiate the activity of glycolytic enzymes. For instance, PFK-1 has been shown to preferentially bind to filamentous (F)-actin, stabilising the active conformation of PFK-1 and decreasing its allosteric inhibition by ATP, citrate or lactate, leading to increased rates of glycolysis[241].

Furthermore, invasive cancer cells often develop metabolic plasticity, allowing greater ATP generation to aid migration, adaptation to nutrient deprivation and subsequent switching to aerobic glycolysis to support proliferation in a new niche[242]. For example, cancer cells that have undergone EMT and invade require high levels of ATP to take advantage of available nutrients and for cytoskeletal rearrangements[241]. Alternatively, clustered cancer cells do not necessarily share the same metabolic phenotype during collective invasion. Like the mesenchymal invasion of individual cancer cells, the leader cell in collective invasion requires high levels of ATP for movement and degradation of the ECM, compared to follower cells[243]. Due to the intertwined nature of cellular movement and energy availability in cancer invasion I aimed to determine the role of CB_2 on metabolism.

The impact of CB_2 on ATP production in our system was initially investigated using the Cell Titre Glow (CTG) assay. CTG measures ATP abundance using bioluminescence, light generated from the ATP-dependent conversion of luciferin to oxyluciferin by the luciferase enzyme[244]. The amount of ATP in a cell is directly proportional to the amount of light generated. Induction of CB_2 for 24 hours increased ATP accumulation in HCC1954^{iCB2} and BT474^{iCB2} cells (Figure 5.1.1), indicating that CB_2 expressing cells are more metabolically active.

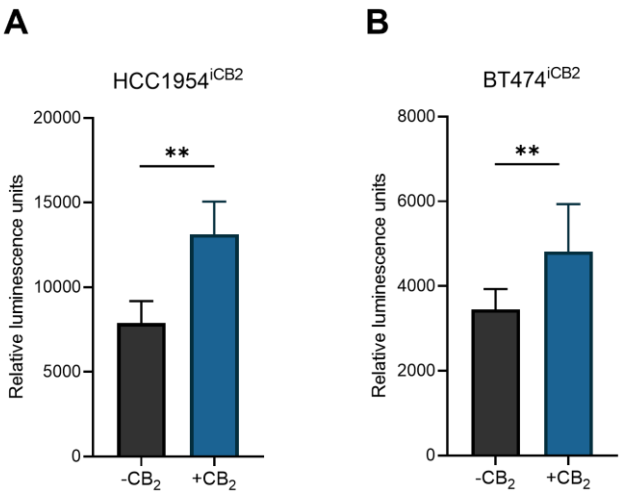

Figure 5.1.1: CB_2 expression increases ATP accumulation in HCC1954^{iCB2} and BT474^{iCB2} cells.

Cell Titre Glo assay measuring ATP content in (A) HCC1954^{iCB2} and (B) BT474^{iCB2} cells, +/- 24-hour CB_2 induction with 1 µg/ml dox. n=3, unpaired t-test, mean ± SD, ** $p < 0.01$.

5.2 Changes in glycolysis and oxidative phosphorylation after CB_2 expression

I utilised the Seahorse XF analyser to elucidate which metabolic pathway is responsible for increased ATP production after CB_2 induction. The Seahorse energetic phenotype assay determines metabolic flux through glycolysis and mitochondrial respiration under basal and stressed conditions to establish the metabolic potential of cells. Using biosensors for H^+ ions and oxygen, Seahorse assays can measure the extracellular acidification rate (ECAR) and the oxygen consumption rate (OCR), respectively. Initially, ECAR and OCR are determined to establish the basal activity of the glycolytic and oxidative phosphorylation pathways. Levels of ECAR and OCR are then measured under stress conditions by the addition of carbonyl cyanide-p-trifluoromethoxyphenylhydrazone (FCCP) and oligomycin to estimate the metabolic potential of a cell line.

FCCP is a protonophore that uncouples the inner mitochondria membrane, allowing protons to flow into the mitochondrial matrix, reducing the membrane potential. The electron transport chain becomes highly active to maintain the electrochemical gradient, pumping protons into the intermembrane space. This results in increased oxygen consumption via complex IV, which consumes oxygen to make water as it pumps protons[245]. Oligomycin is used to ascertain the maximal rate of glycolysis. Oligomycin inhibits ATPsynthase, preventing ATP production through oxidative phosphorylation, causing increased flux through glycolysis to meet the cellular energy demands[246]. When FCCP and oligomycin are added together in the stressed condition, cells undergo maximal ECAR and OCR, displaying their metabolic potential. Using this assay, I sought to determine what effects CB_2 had on the rates of ECAR and OCR in $HCC1954^{iCB2}$ and $BT474^{iCB2}$ cells.

To achieve the best response in the energetic phenotype assay, cell density and FCCP concentration need to be optimised. Firstly, the appropriate seeding density of

HCC1954^{WT} and BT474^{WT} cell lines was verified. Densities of 5000, 10,000, 20,000 and 30,000 cells/well in 96-well plates were plated for both cell lines and basal and stressed ECAR and OCR were determined (Figure 5.2.1). The optimal cell density of HCC1954^{WT} cell that generated the largest signal window of ECAR and OCR was 20,000 cells/ml, while for BT474^{WT} 30,000 cells/well was optimal. Next, FCCP concentration was optimised for both cell lines to establish the concentration that yielded the maximum OCR (Figure 5.2.2). HCC1954 cells displayed the highest levels of OCR with 0.5 μM FCCP, and BT474 cells had the maximal OCR with 1 μM FCCP, resulting in the largest signal window.

Before analysis of the metabolic phenotype in HCC1954^{iCB2} and BT474^{iCB2} cells, it is important to note that dox has been reported to impact cell metabolism[247]. Dox was initially developed as an antibiotic that impedes bacteria growth by inhibiting the 30S ribosomal subunit, preventing protein synthesis[247]. Dox is widely used in *in vitro* and *in vivo* inducible systems, and its physiological effects have been extensively studied. As one of the key processes dox has been shown to affect is metabolism, it is difficult to draw concrete conclusions about metabolic changes whilst using a dox-inducible system. In addition to the effect of dox inhibiting bacterial ribosomes, dox has been shown to have similar effects in eukaryote cells by inhibiting the mitochondrial 70S ribosomes. Non-functional 70S ribosomes prevents the translation of mitochondrial proteins, including components of the electron transport chain, leading to a decrease in mitochondrial function. In a compensatory manner, dox can lead to an increase in glycolysis[247]. However, the extent of these changes can vary depending on the cell line. MCF12A and HEK293T cells displayed increased glycolytic flux, measured by lactate production, and decreased oxygen consumption due to decreased mitochondrial respiration. Yet in the lung squamous cell carcinoma cell line, H157, dox did not change the rate of glycolysis, although there was a 70% decrease in oxidative

phosphorylation[247]. Therefore, it is likely that dox affects cellular metabolism, although this effect is inconsistent across cell lines.

Therefore, to allow the study of metabolism using the dox inducible system without confounding the metabolic data, I tested the effect of dox in HCC1954^{WT} and BT474^{WT} cells. Interestingly, in HCC1954^{WT} and BT474^{WT} cells the addition of 1 μg/ml dox for 24 hours led to a significant decrease in ECAR and OCR (Figure 5.2.3). These results were contrary to previously reported effects of dox on metabolism[247], with differences potentially caused by the variation of genetic background between cell lines.. Whilst I did observe a decrease in OCR, as previously shown, the concomitant reduction in ECAR suggests that there is not a compensatory increase in glycolysis.

After establishing the optimal cell density, FCCP concentration and effect of dox on wild-type cells, I examined how CB_2 expression changes the rate of glycolysis and oxidative phosphorylation. HCC1954^{iCB2} cells had significant upregulation of glycolysis and oxidative phosphorylation, measured by ECAR and OCR, respectively (Figure 5.2.4 A). Likewise, CB_2 expression in BT474^{iCB2} cells led to significantly higher rates of both glycolysis and oxidative phosphorylation (Figure 5.2.4 B); however, there were high levels of variation in ECAR and OCR in the BT474^{iCB2} cell line. Moreover, both HCC1954^{iCB2} and BT474^{iCB2} cells displayed higher metabolic potential when expressing CB_2, indicated by the steeper slope between basal and stressed conditions.

Therefore, this further suggests that CB_2 expression influences a change to a more energetic metabolic phenotype, with increased metabolic potential. Interestingly CB_2 led to an increase in glycolysis and oxidative phosphorylation, demonstrating a possible increase in metabolic plasticity. While increased glycolysis is associated with proliferating cancer cells, increased oxidative phosphorylation is often seen in CSCs[248]. The ability of CSCs to regulate their metabolic flux enables a high-energy, invasive phenotype and a quiescent, low growth phenotype, depending on environmental cues[249]. CB_2 expression may cause an increase in glycolysis in some cells in a

population, whilst others become stem-like and increase ATP generation through oxidative phosphorylation.

Bioinformatic analysis of TCGA datasets was used to corroborate the possible increase in glycolysis observed in HCC1954^{iCB2} and BT474^{iCB2} cell lines using patient data. To understand how CB_2 could lead to increased glycolysis, the change in expression of 30 glycolytic enzymes was examined using the TCGA datasets. There was no significant difference in the expression of most enzymes, regardless of *CNR2* level (Figure 5.2.5 A). However, HER2+ patients with high *CNR2* expression had significant upregulation of HK3, HKDC1, and LDHB mRNA, compared to HER2+ patients with low *CNR2* expression, with the expression of these glycolytic enzymes positively correlating with *CNR2* expression (Figure 5.2.5 B).

The *HK3* gene encodes hexokinase 3 (HK3), an enzyme responsible for the phosphorylation of glucose to glucose-6-phosphate (G6P)[250]. This is the crucial first step of glucose metabolism, preventing glucose from leaving the cell and committing it to glycolysis. The reaction catalysed by HK3, and its isoforms HK1 and HK2, is a rate-limiting step of glycolysis and is inhibited in a negative feedback loop by G6P. Interestingly, HK3 has also been associated with ROS reduction and mitochondria biogenesis[250], suggesting CB_2 could increase both glycolysis and oxidative phosphorylation through HK3 expression. Hexokinase domain containing 1 (HKDC1) is a newly discovered hexokinase isoform, typically expressed during pregnancy[251], with high homology to HK1. HKDC1 catalyses the same reaction as HK3 and is overexpressed in lung cancer[252], where it is associated with increased tumourgenicity[253]. Alternatively, *LDHB* encodes for a subunit of lactate dehydrogenase, the other subunit encoded by *LDHA.* Lactate dehydrogenase catalyses the reversible conversion of lactate and pyruvate and the co-enzyme NAD between its oxidised (NAD^+) and reduced (NADH) forms. LDHB overexpression is implicated in numerous cancer types, enabling the use of lactate in metabolism, contributing to

increased proliferation and the regulation of autophagy[254]. Serum levels of LDHB are a commonly used biomarker for many cancers, including breast cancer, as high serum LDHB is associated with decreased survival[255]. Expression of these three enzymes was further examined in HCC1954^{iCB2} cells; CB_2 induction led to a significant increase in the mRNA expression of *HK3* and *HKDC1* mRNA and an increase in *LDHB* mRNA, although this did not reach significance (Figure 5.2.6). Together, these data indicate that the CB_2 expression is driving increased flux glycolysis through the expression of HK3, HKDC1 and potentially LDHB. Increased levels of HK3 could also lead to increase mitochondria biogenesis and reduced levels of ROS.

Analysis of the above mentioned TCGA datasets also allowed investigation into the observed increase of oxidative phosphorylation. Examination revealed a significant increase in the mRNA of two genes associated with mitochondrial biogenesis, *PPARG* and *DNM1P46*, in patients with high *CNR2* expression, and positive correlations between *PPARG* and *DNM1P46* expression and *CNR2* expression (Figure 5.2.7)[256,257]. *PPARG* encodes for the nuclear receptor, Peroxisome proliferator-activated receptor gamma (PPARγ), which can form heteromers with the retinoid X receptors (RXR) to regulate gene transcription[258]. Activation of PPARγ can lead to increased mitochondrial turnover and reduction of ROS[257]. Interestingly PPARγ is part of then ECS and has been shown to interact with AEA[259], an endocannabinoid, and two of the most abundant phytocannabinoids, THC[258]and CBD[260]. *DNM1P46*, dynamin 1 pseudogene 46, is a GTPase associated with the mitochondrial membrane, and has been implicated in regulating fission during mitochondria biogenesis[256]. Expression of *DNM1P46* has also been shown to be controlled by retinoid signalling, through the receptor RXRA[261].

The increase in *PPARG* and *DNM1P46* expression with high CB_2 in the patient data suggests that CB_2 may lead to increased mitochondrial content, and hence the increase in oxidative phosphorylation. This was explored in HCC1954^{iCB2} cells using the

fluorescent mitochondrial stain MitoTracker™ Red CMXRos (Figure 5.2.8). CB_2 expression in HCC1954^{iCB2} cells led to a significant increase in mitochondrial content, suggesting that the increased OCR detected by the Seahorse assay is due to increased mitochondria biogenesis, possibly through the action of PPARγ and DNM1P46.

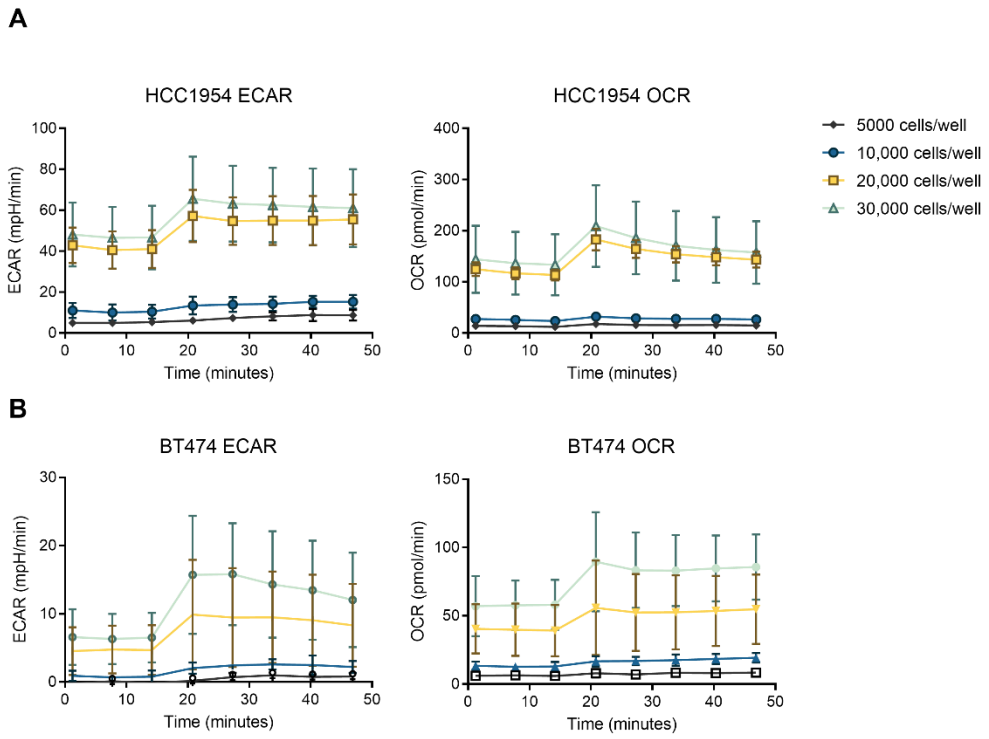

Figure 5.2.1: HCC1954 and BT474 cell number titration for the Seahorse Energetic Phenotype Assay.

(A) HCC1954 and (B) BT474 wild type cells at 5000, 10,000, 20,000, and 30,000 cells/well measuring extracellular acidification rate (ECAR) as a measure of glycolysis rate and oxygen consumption rate (OCR) at basal (prior to Oligomycin and FCCP addition) and maximal (after Oligomycin and FCCP addition) metabolic states (n=3, unpaired t-test, mean ± SD).

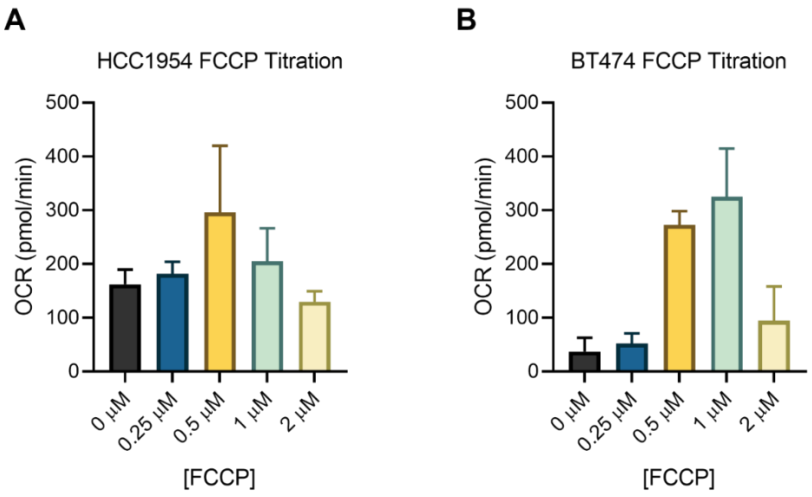

Figure 5.2.2: FCCP titration in the Seahorse Energetic Phenotype Assay in HCC1954 and BT474 cells.

The oxygen consumption rate (OCR) of (A) HCC1954 and (B) BT474 wild type cells at increasing concentrations of FCCP, measured in the Seahorse energetic phenotype assay (n=3).

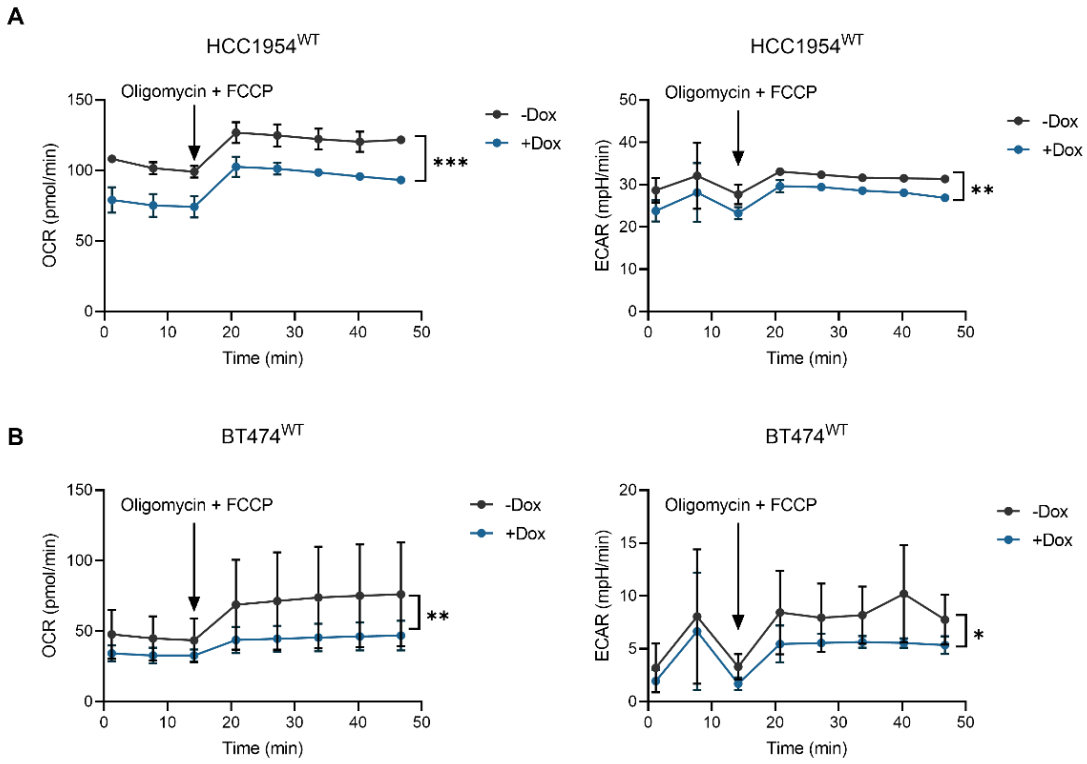

Figure 5.2.3: Doxycycline impacts on OCR and ECAR in HCC1954^{WT} and BT474^{WT} cells.

The extracellular acidification rate (ECAR) and oxygen consumption rate (OCR) measured by the Seahorse energetic phenotype assay in (A) HCC1954 and (B) BT474 wild type (WT) cells after 24 hours +/- 1 µg/ml doxycycline (n=3, unpaired t-test of data at all time points, mean ± SD) * $p < 0.05$, ** $p < 0.01$, *** $p < 0.001$.

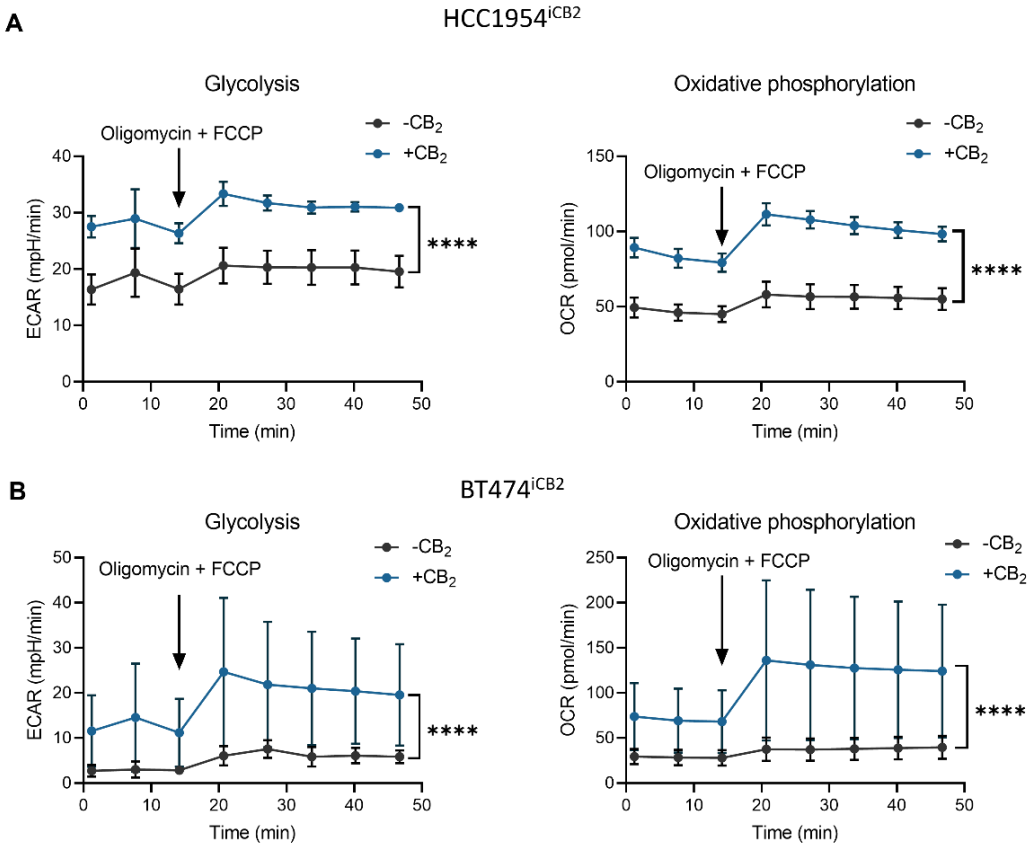

Figure 5.2.4: Seahorse analysis of CB_2 expression on glycolysis and oxidative phosphorylation in HCC1954^{iCB2} and BT474^{iCB2} cells.

(A) Extracellular acidification rate (ECAR) as a measure of glycolysis and oxygen consumption rate (OCR) as a measure of oxidative phosphorylation rate in (A) HCC1954^{iCB2} and (B) BT474$^{iCB"}$ cells at basal (prior to oligomycin and FCCP addition) and maximal (after oligomycin and FCCP addition) metabolic states (n=3, unpaired t-test of data at all time points, mean ± SD). **** $p < 0.0001$.

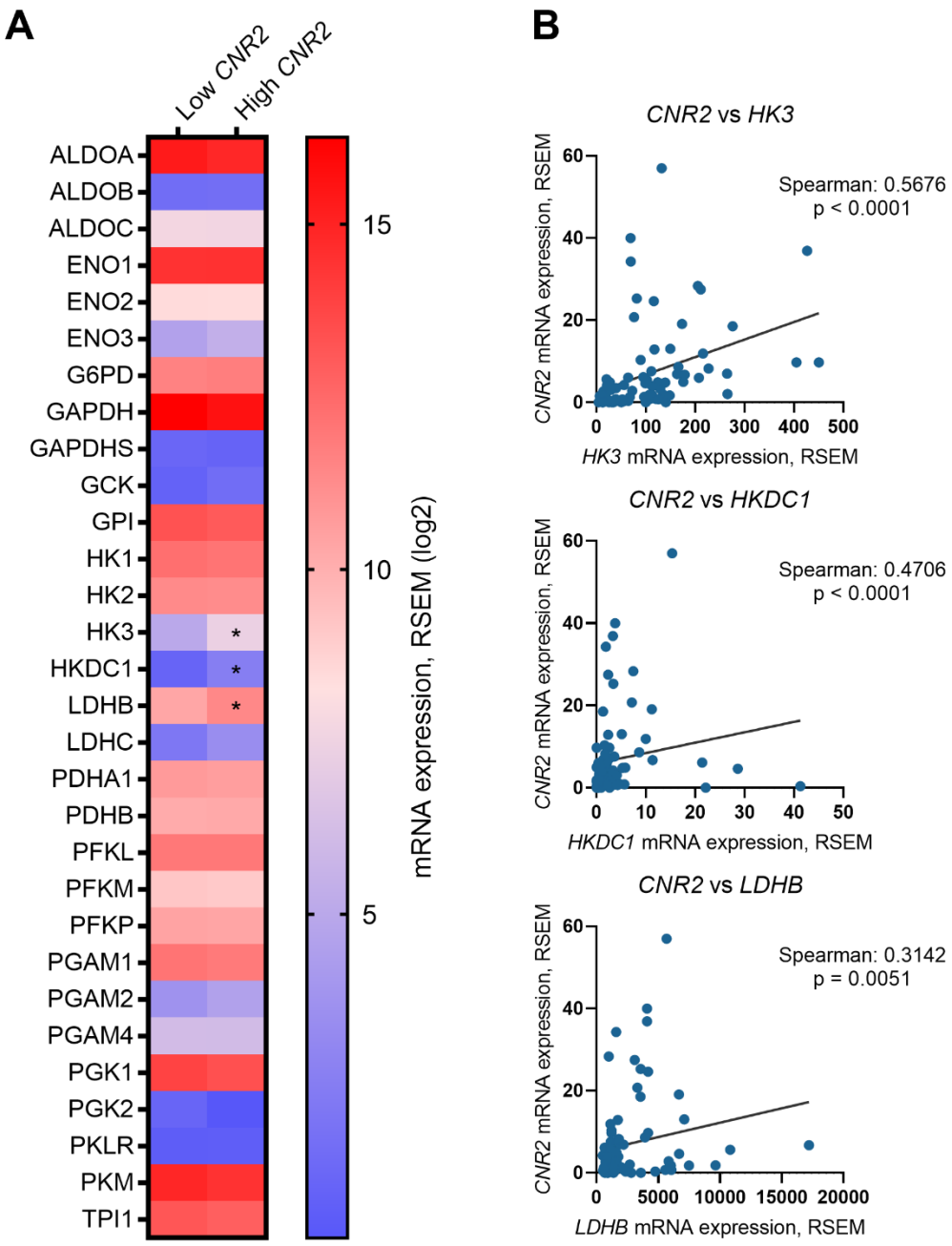

Figure 5.2.5: Expression changes of glycolytic enzymes.

(A) Heatmap of glycolytic enzyme gene expression from HER2+ patients in the Breast Cancer Invasive data set (TCGA, PanCancer Atlas), comparing patients in the lower and upper quartiles of *CNR2* expression. (B) Breast Cancer Invasive TCGA HER2+ patient data of the correlation of mRNA expression between *HK3*, *HKDC1* or *LDHB* and *CNR2*. TCGA data generated using RNA-seq by Expectation Maximisation (RSEM). (* indicates significance of $p < 0.01$).

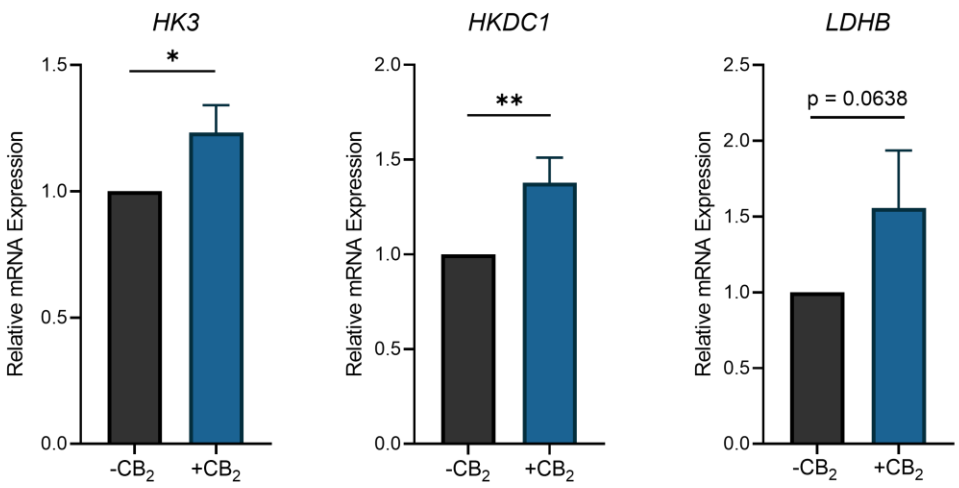

Figure 5.2.6: Changes in glycolytic enzyme expression after CB_2 induction in HCC1954^{iCB2} cells.

RT-qPCR analysis of *HK3*, *HKDC1* and *LDHB* mRNA in HCC1954^{iCB2} cells +/- 24-hour induction of CB_2 expression (n=3, unpaired t-test, mean ± SD). Relative mRNA expression normalised to *ACTB* (β-actin) mRNA expression. * $p < 0.05$, ** $p < 0.01$

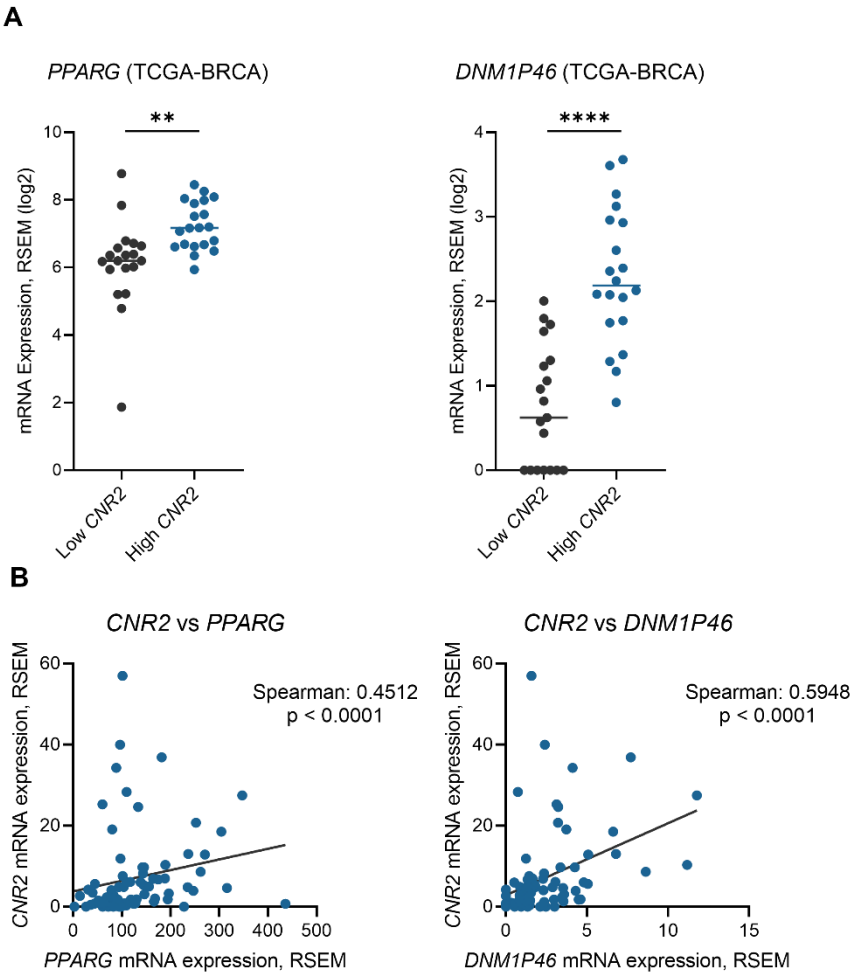

Figure 5.2.7: High CB_2-expressing HER2+ breast cancer patients have increased expression of genes related to mitochondrial biogenesis.

(A) TCGA mRNA expression of *PPARG* and *DNM1P46* from HER2+ patients in the Breast Cancer Invasive TCGA dataset between the upper and lower quartiles of *CNR2* expression (unpaired t-test). (B) Breast Cancer Invasive TCGA HER2+ patient data of the correlation of mRNA expression between *PPARG* or *DNM1P46* and *CNR2*. TCGA data generated using RNA-seq by Expectation Maximisation (RSEM). ** $p < 0.01$, **** $p < 0.0001$.

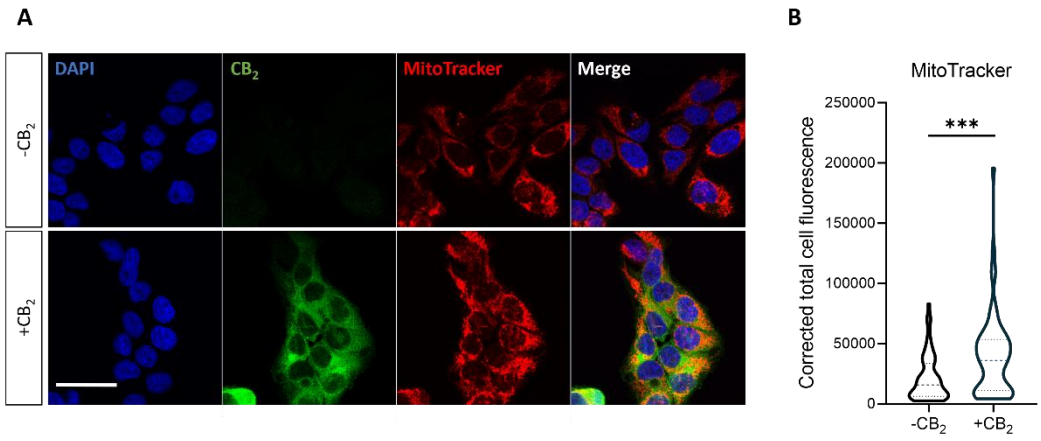

Figure 5.2.8: CB_2-meditated increase in mitochondrial content in HCC1954^{iCB2} cells.

(A) Fluorescent staining of mitochondria using MitoTracker (red) and CB_2 immunofluorescence (green) in HCC1954^{iCB2} cells +/- 24-hour CB_2 induction (representative images of n=3 biological replicates). (B) Corrected total cell fluorescence (CTCF) of mitochondrial staining in HCC1954^{iCB2} cells +/- CB_2 induction from (A), with distribution of CTCF indicated by violin plot thickness. Mean CTCF and upper and lower quartiles indicated by dashed and dotted lines, respectively (n=3 biological replicates, unpaired t-test). *** $p < 0.001$. Scale bar 40 µm.

5.3 Metabolite changes with CB_2 expression: Fluxomic analysis

To further investigate the role of CB_2 on metabolic reprogramming, I performed fluxomic analysis using radiolabelled ^{13}C glucose and ^{13}C glutamine in HCC1954^{iCB2} cells. I used mass spectrometry to analyse changes in 29 common metabolites (Figure 5.3.1). Confirming the increase in ECAR, I observed that most glucose-derived carbon generates lactate (Appendix figure 7). As a result of increased glycolysis, I observed a decrease in the level of the TCA intermediate citrate (Figure 5.3.2 A), indicating decreased carbon from glucose entering the TCA and being converted to citrate. This could lead to decreased *de novo* synthesis of fatty acids, leading to a reliance on uptake of fatty acids and susceptibility to ROS lipid damage. This is supported by the increase in glutathione synthesis through glutamine metabolism, as I saw increased glutamine carbon-derived glutathione (Figure 5.3.2 B). Furthermore, glutathione is used as a substrate for glutathione peroxidase (GPx) enzymes that are important in reducing ROS (Figure 5.3.3). Interestingly, supporting this is the finding that in TCGA, there is a significant increase in *GPX3* expression in high *CNR2* HER2+ patients and *GPX3* expression positively correlates with *CNR2* expression (Figure 5.3.2 C), which is associated with the formation of cancer stem cells[262].

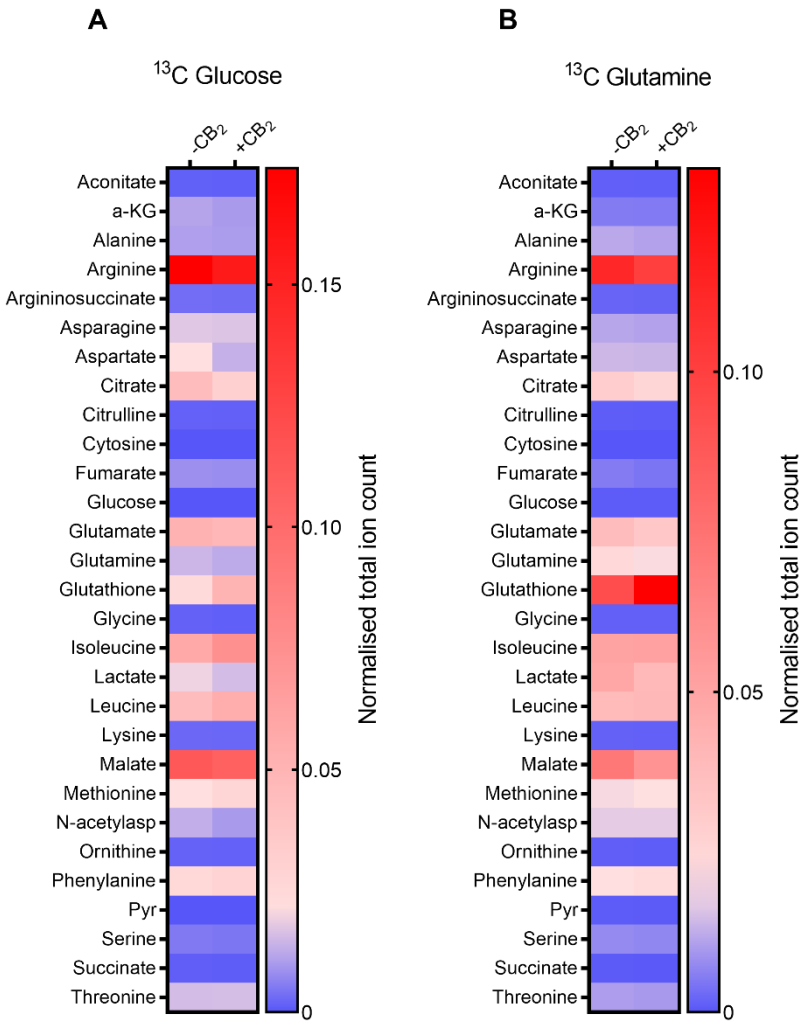

Figure 5.3.1: Changes in metabolites after CB_2 induction.

Heatmaps of metabolite changes using (A) ^{13}C glucose and (B) ^{13}C glutamine detected by mass spectrometry, isolated from HCC1954^{iCB2} cells +/- 24-hour CB_2 induction with 1 µg/ml dox. Data from five technical replicates of one biological replicate.

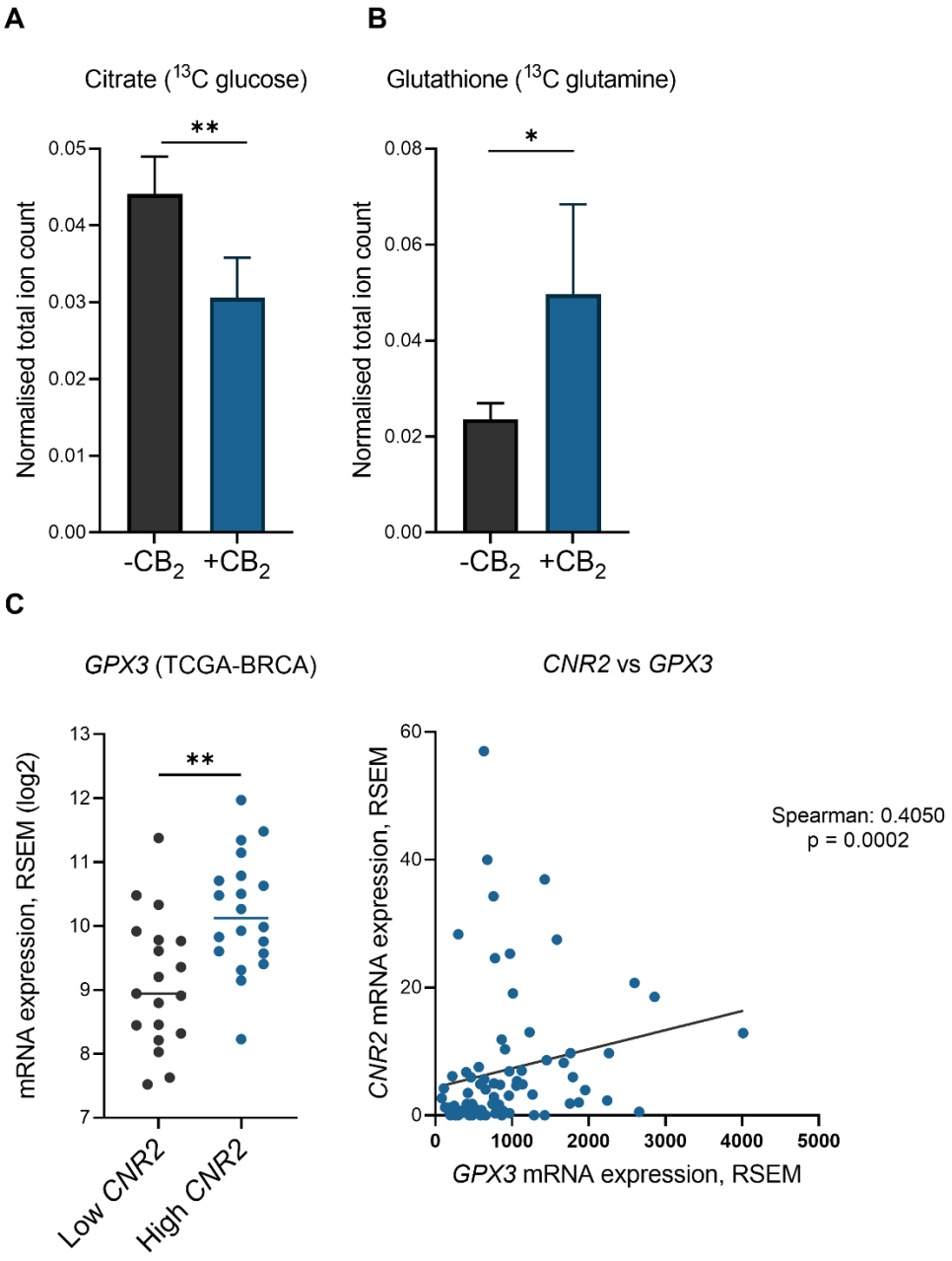

Figure 5.3.2: CB_2 expression causes increased flux through reductive metabolite pathways.

Changes in (A) glucose-derived citrate and (B) glutamine-derived glutathione concentration in HCC1954^{iCB2} cells +/- 24-hour CB_2 induction expression (n=5 technical replicates, unpaired t-test, mean ± SD). (C) Comparison of *GPX3* mRNA expression between the upper and lower quartiles of *CNR2* expressing HER2+ patients in the Breast Cancer Invasive TCGA dataset (unpaired t-test, mean ± SD). and the correlation of mRNA expression between *GPX3* and *CNR2*. TCGA data generated using RNA-seq by Expectation Maximisation (RSEM). * $p < 0.05$, ** $p < 0.01$

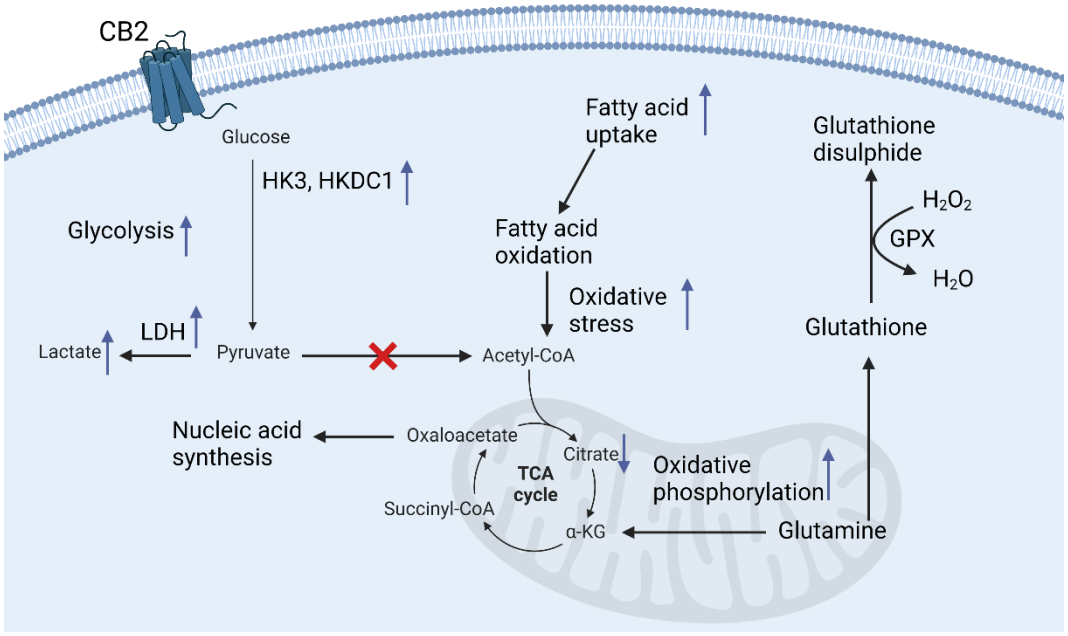

Figure 5.3.3: Theoretical proposed mechanism of the effect of CB_2 cancer cell metabolism

CB_2 leads to the metabolic rewiring of HER2+ cancers cells, possibly in part via this proposed mechanism. CB_2 expression leads to increased rates of glycolysis, via increased HK3 and HKDC1 expression, which leads to increased levels of lactate, via LDH. The lack of pyruvate to provide acetyl-CoA to enter the tricarboxylic acid cycle (TCA), potentially leading to decreased levels of citrate. The TCA can continue to fuel the increased levels of oxidative phosphorylation in the absence of pyruvate derived acetyl-CoA via the entry of glutamine into the TCA via α-ketoglutarate. However, due to increased levels of glutathione, excess glutamine is likely being shunted into glutathione antioxidant purposes. Therefore, it is possible CB_2 expressing cells are producing acetyl-CoA via fatty acid oxidation, leading to increased reactive oxygen species (ROS) and the need for glutathione-mediated ROS reduction. More research is required to validate this model and test speculations.

5.4 Summary of Results

- CB_2 expression increases metabolic output through increased rates of glycolysis and oxidative phosphorylation.
- Increased expression of glycolytic enzymes, LDHB, HK3 and HKDC1 correlates with CB_2 expression in HER2+ breast cancer patients and increased *HK3* and *HKDC1* mRNA expression was observed after CB_2 induction in HCC1954^{iCB2} cells.
- CB_2 expression increases mitochondrial content in HCC1954^{iCB2} cells and is associated with *PPARG* and *DNM1P46* expression in HER2+ patients and HCC1954^{iCB2} cells, which are both genes involved in mitochondrial biogenesis.
- Metabolic rearrangement upon CB_2 expression results in decreased citrate and increased glutathione production.

Chapter 6 CB_2 expression induces stem like phenotype

6.1 CB_2-driven stemness

CSC typically compose around 0.1-1% of cancer cells in primary breast tumours[263]. These cells are highly tumourigenic, treatment resistant and can divide asymmetrically to repopulate tumours, leading to relapse[264]. Resistance of CSCs to chemotherapy and radiotherapy results from their lower turnover rate, expression of detoxifying enzymes such as the aldehyde dehydrogenase (ALDH) family and GPx[265], expression of ATP-binding cassette (ABC) transporter family members and high rates of DNA damage repair[266]. Therefore, CSCs have become a pivotal target in preventing tumour recurrence. Hence, identifying a CB_2+ population of CSCs in HER2+ breast cancer could allow for specific cannabinoid-based therapy and represents a novel way of targeting breast CSCs.

Stemness of cancer cells can be functionally determined *in vitro* with the mammosphere formation assay. Proliferative cancer cells cannot survive anchorage-independent growth and die via the programmed cell death pathway, anoikis, which regulated through integrin-mediated signalling pathways, activating apoptosis after integrin disengagement from ECM[267]. Upon detachment from ECM, anchorage dependent cells undergo this form of cell death, preventing the dissemination of detached cells. However, CSCs cells have the ability to survive anoikis and grow in suspension. When breast cancer cells are plated into an ultra-low attachment plate, CSCs will survive to form mammospheres. The mammosphere formation efficiency (MFE) is a quantitative readout of the stemness of a population of cells. Using this assay, the effect of CB_2 on regulating stemness can be determined. Firstly, HCC1954^{iCB2} cells were titrated to obtain the optimal cell number per well for mammosphere formation and quantification. HCC1954^{iCB2} cells were plated at 500-5000 cells/well in a 24-well ultra-low attachment plate, +/- 1 μg/ml dox (Appendix figure 8). After 7 days of culture, mammospheres were imaged and quantified. The cell density of 1000 cells/ml was chosen for further experiments as there was the greatest difference in MFE between

+/- CB_2 induction, less cell clumping and easier quantification than higher cell concentrations. HCC1954^{iCB2} cells were then plated at 1000 cells/well, +/- 1 μg/ml dox and cultured for 7 days, with 100 nM JWH133 or DMSO vehicle control added every other day (Figure 6.1.1). CB_2 expression significantly increased the MFE, which was abrogated with JWH133, suggesting that CB_2 regulates stemness in HER2+ breast cancer. To understand the mechanism conferring CB_2-mediated stemness, I sought to identify stem cell markers that could regulate this process.

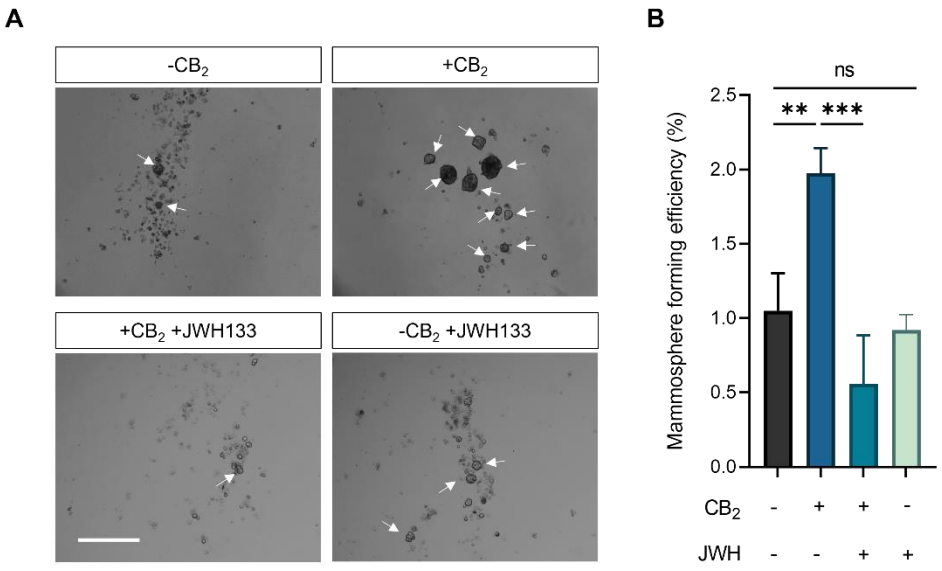

Figure 6.1.1: Mammosphere formation efficiency is increased by CB_2 expression and inhibited by JWH133.

(A) Light micrographs of mammosphere formation of HCC1954^{iCB2} cells in ultra-low attachment plates +/- 7 days CB_2 induction and after the addition of 100 nM JWH133 or vehicle (DMSO). White arrows indicating mammospheres (representative images of n=3 biological replicates). (B) Quantification of mammosphere formation efficiency from (A) (n=3, ordinary one-way ANOVA, mean ± SD). Scale bar 500 µm. * $p < 0.05$, ** $p < 0.01$

6.2 CB_2 modulates expression of stem cell markers

The Yamanaka factors are a set of well-established transcription factors highly expressed in embryonic stem cells. When expressed experimentally *in vitro*, these lead to the formation of induced pluripotent stem cells[268]. Pluripotency factors such as these are upregulated in CSCs[269]. Their expression in cancer has been associated with cancer stem cells in breast, bladder, liver and prostate cancer[270] and increased rates of chemoresistance and tumour recurrence in liver cancer[269]. Therefore, I investigated whether CB_2 expression was linked to these factors in HER2+ patients. TCGA analysis of *POU5F1* (OCT4), *KLF4*, *SOX2* and *MYC* revealed that only *POU5F1* was slightly elevated in high *CNR2* patients, with no statistical difference between high and low *CNR2* expression for *SOX2*, *KLF4* and *MYC*, nor was there any correlation with *CNR2* expression (Figure 6.2.1).

As *POU5F1* was upregulated in patient data and had a slight positive correlation with *CNR2* expression, I further explored the expression of OCT4 in $HCC1954^{iCB2}$ and $BT474^{iCB2}$ cells. Changes in protein levels were assessed, with no differences being observed, regardless of CB_2 expression (Appendix figure 9). Therefore, it was apparent that CB_2 was likely not conferring stemness via the expression of Yamanaka factors and likely relying on other pluripotency markers for the maintenance of stemness.

Consequently, I utilised TCGA dataset to interrogate the expression of other stem cell markers that correlate with *CNR2* expression in HER2+ breast cancer patients (Figure 6.2.2). High *CNR2*-expressing HER2+ patients had significantly higher expression of *CD44* and *ALDH1A1*, both well-established CSC markers in breast cancer[271,272]. Their expression in $HCC1954^{iCB2}$ cells was corroborated by qPCR analysis. Induction of CB_2 for 24 hours led to a significant increase in both *CD44* and *ALDH1A1* gene expression (Figure 6.2.2 C, F).

CD44 is a cell surface glycoprotein that binds hyaluronic acid and is involved in cell adhesion[273]. CD44 expression is frequently observed in breast CSCs and is associated with increased metastasis rates and decreased survival[274]. ALDH1A1 expression is also associated with poor patient outcomes[275], invasion and metastasis to the lymph nodes[276]. ALDH1A1 is responsible for converting aldehydes to carboxylic acids and reducing reactive oxygen species, vital steps in cellular detoxification[277]. These are critical protective actions in normal cells, and in cancer cells, it can reduce the effectiveness of cytotoxic drugs and result in the increased treatment resistance seen within CSC populations[278]. Further, ALDH1A1 oxidises retinal to retinoic acid (RA), which, once in the nucleus, binds to retinoid receptors, RXR and RARα, along with PPARs to regulate a variety of transcription events[279].

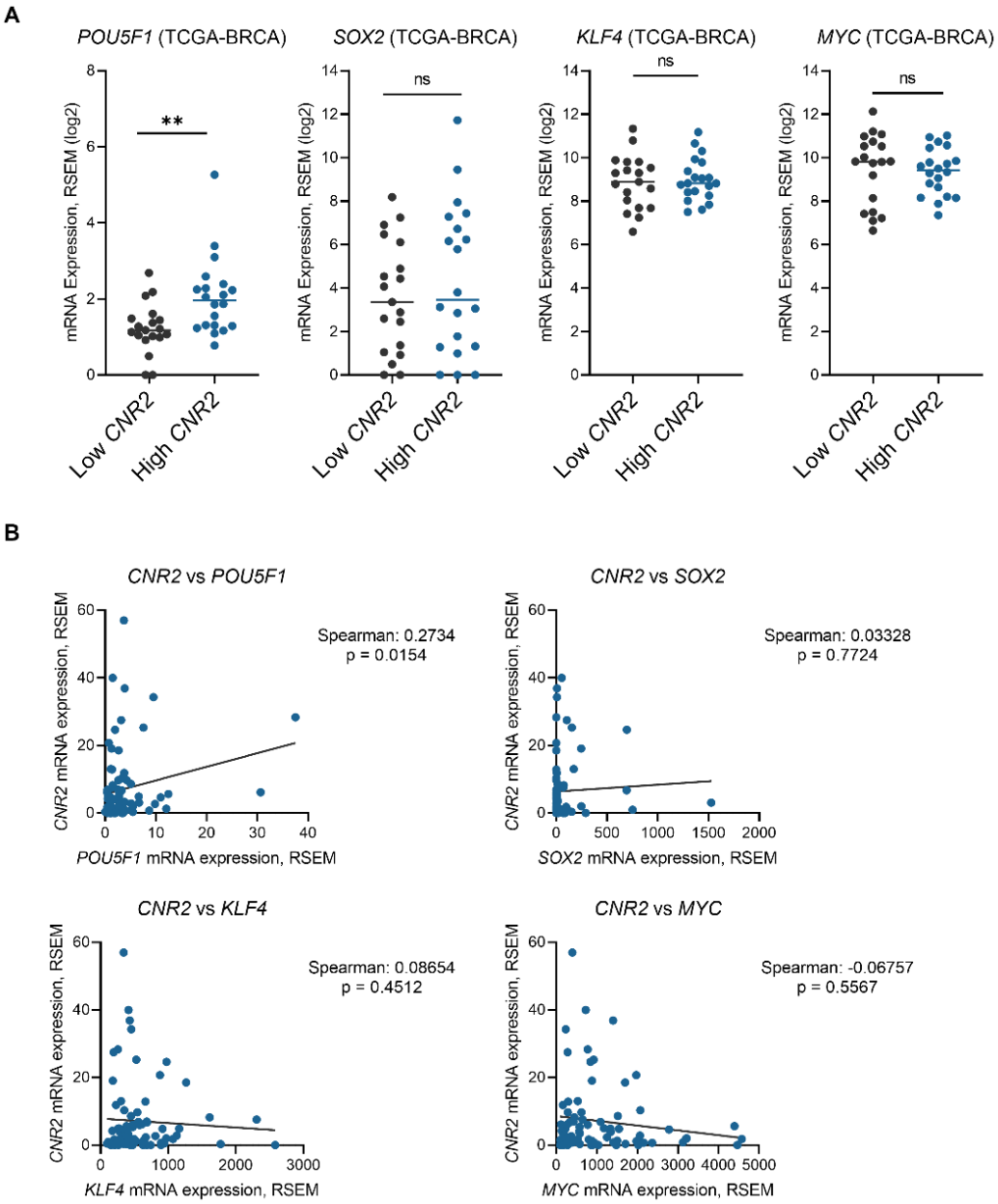

Figure 6.2.1: Expression changes in Yamanaka factors in HER2+ breast cancer patients with high and low CB_2 expression.

(A) Comparison of Yamanaka factor, *POUF5F1* (OCT4), *SOX2, KLF4* and *MYC*, mRNA expression in high (upper quartile) and low (lower quartile) *CNR2* expressing HER2+ breast cancer patients from the Breast Cancer Invasive TCGA dataset (unpaired t-test). (B) Breast Cancer Invasive TCGA HER2+ patient data of the correlation of mRNA expression between *POUF5F1*, *SOX2, KLF4* or *MYC* and *CNR2*. TCGA data generated using RNA-seq by Expectation Maximisation (RSEM). ** $p < 0.01$

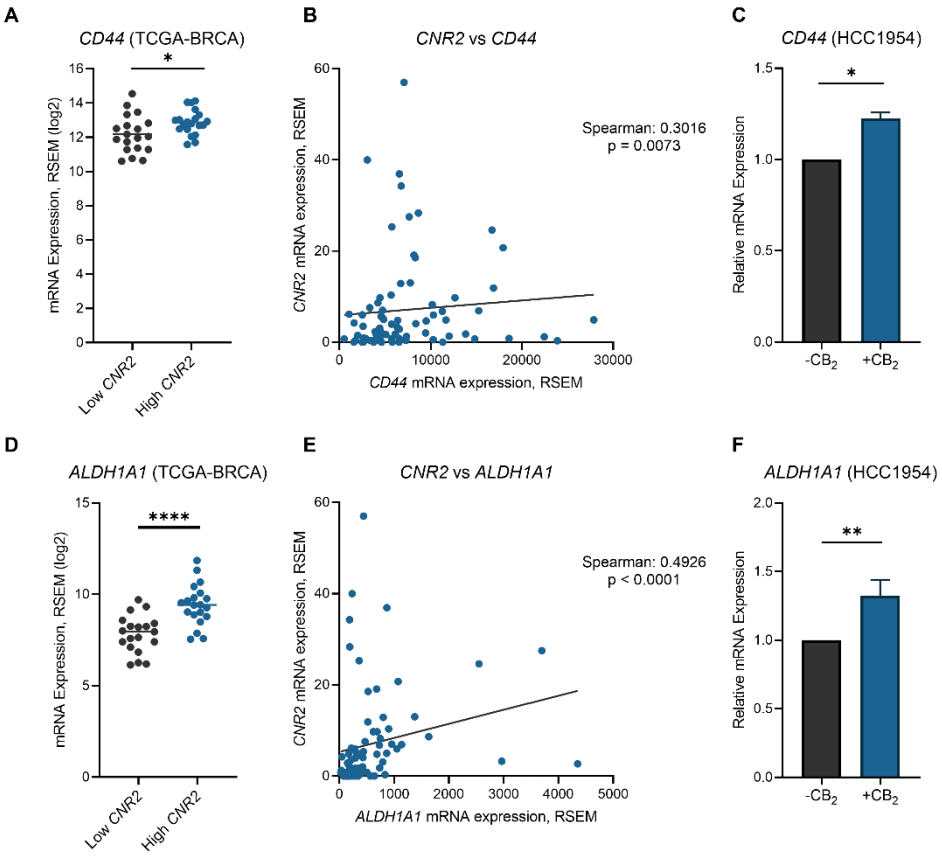

Figure 6.2.2: CB_2-driven increase in expression of cancer stem cell markers.

(A) Comparison of *CD44* mRNA expression between the upper and lower quartiles of *CNR2* expressing HER2+ patients in the Breast Cancer Invasive TCGA dataset (unpaired t-test). (B) Breast Cancer Invasive TCGA HER2+ patient data of the correlation of mRNA expression between *CD44* and *CNR2* (CB2). (C) *CD44* mRNA expression in HCC1954^{iCB2} cells by RT-qPCR +/- 24-hour CB_2 induction (n=3, unpaired t-test, mean ± SD). (D) Comparison of *ALDH1A1* mRNA expression between the upper and lower quartiles of *CNR2* expressing HER2+ patients in the Breast Cancer Invasive TCGA dataset (unpaired t-test). (E) Breast Cancer Invasive TCGA HER2+ patient data of the correlation of mRNA expression between *ALDH1A1* and *CNR2*. (F) *CD44* mRNA expression in HCC1954^{iCB2} cells by RT-qPCR +/- 24-hour CB_2 induction with 1 µg/ml dox (n=3, unpaired t-test, mean ± SD). TCGA data generated using RNA-seq by Expectation Maximisation (RSEM). * $p < 0.05$, ** $p < 0.01$, **** $p < 0.0001$.

6.3 ALDH1A1 is linked to pluripotency, ROS homeostasis and invasion

Due to the role of ALDH1A1 in RA-mediated transcription regulation and ROS homeostasis, protein expression of ALDH1A1 was initially validated by western blotting in HCC1954^{iCB2} cells. CB_2 induction resulted in increased ALDH1A1 expression, compared to HCC1954^{iCB2} cells lacking CB_2 expression. Further validation was carried out with ALDH1A1 immunofluorescence in HCC1954^{iCB2} cells +/- CB_2 induction, revealing significantly increased ALDH1A1 staining in the presence of CB_2 (Figure 6.3.1).

Interestingly, RA signalling has been shown to elevate glycolysis[280] and oxidative phosphorylation[281]. Indeed, PPARγ, the gene product of *PPARG*, is increased in high CB_2 HER2+ patients and associates with RARs to regulate transcription. This also suggests that ALDH1A1 RA signalling could lead to mitochondrial biogenesis through the action of PPARγ, highlighting the connections between these CB_2-regulated pathways. In addition, RA signalling regulates the expression of PYK2, a protein associated with increased invasion in HER2+ breast cancer, which is increased in HER2+ breast cancer patients with high CB_2 expression and had a strong positive correlation with *CNR2* mRNA expression (Figure 6.3.2 A, B). PYK2 has also been reported to be involved in chemotherapy resistance and the formation of breast CSCs in HER2+ patients and correlates with CD44 expression[282]. To determine if PYK2 regulates invasion, CB_2 expressing HCC1954^{iCB2} spheroids were treated with the PYK2 inhibitor, Defactinib, significantly reducing CB_2-driven invasion (Figure 6.3.2 C, D).

In addition, recent evidence has implicated RA signalling in regulating the expression and activity of AKT[283,284]. AKT is a vital signalling node in the CB_2 pathway and is implicated in many tumourigenic processes, including cell proliferation, survival, invasion, and in the formation of breast CSCs[285]. To determine if CB_2 expression in HER2+ breast cancer leads to AKT expression, AKT protein levels were assessed by

western blot. After 24 hours of CB_2 expression the levels of both phospho-AKT and total AKT increased, potentially mediated through increased RA signalling (Figure 6.3.3 A). To evaluate the role of the increased AKT expression on invasion in our model, HCC1954^{iCB2} spheroids were treated with an AKT1/2 inhibitor, significantly reducing CB_2-driven invasion into the surrounding 3D matrix (Figure 6.3.3 B, C).

Taken together, these data suggest that CB_2 expression can lead to increased invasive potential by controlling the expression of ALDH1A1. RA signalling can control the expression of pro-invasive and pluripotency genes, and the detoxification action of ALDH1A1 increases treatment resistance and decreases ROS-mediated cell death potentially leading to an increase in highly metastatic, stem-like population of cancer cells.

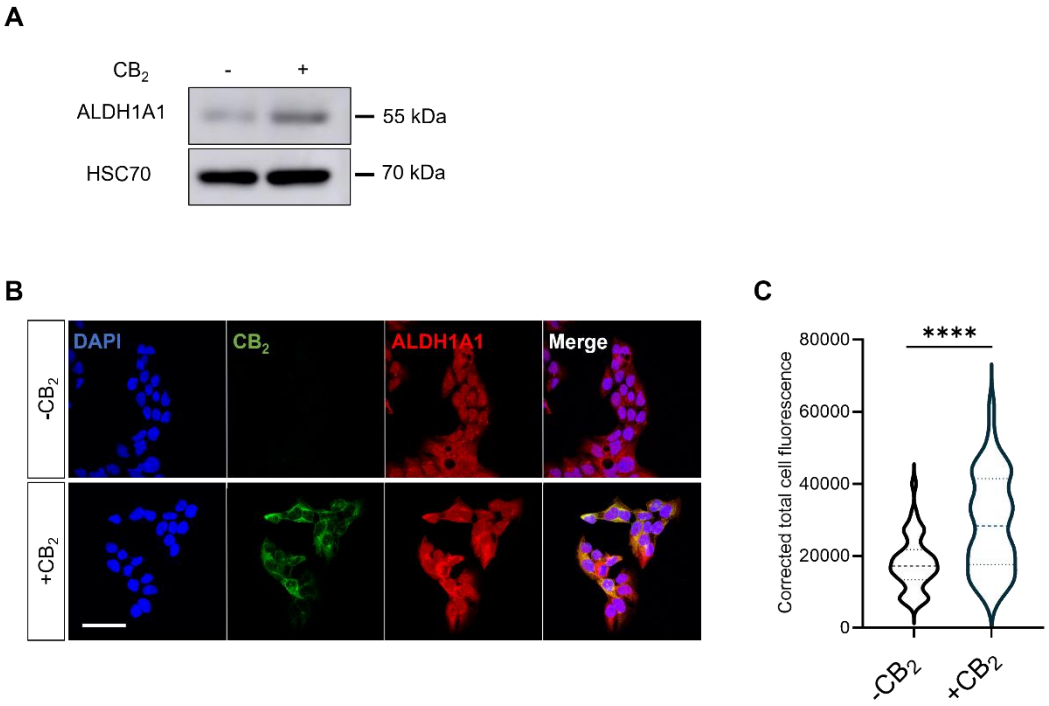

Figure 6.3.1: ALDH1A1 protein expression increases with CB_2 induction.

(A) Western blot analysis of ALDH1A1 protein expression +/- 24-hour CB_2 induction from HCC1954^{iCB2} whole cell lysates (representative image of n=3). (B) ALDH1A1 and CB_2 immunofluorescence of HCC1954^{iCB2} cells +/- 24-hour CB_2 induction with 1 µg/ml dox. (C) Corrected total cell fluorescence quantification of ALDH1A1 immunofluorescence from (B) with distribution of CTCF indicated by violin plot thickness. Mean CTCF and upper and lower quartiles indicated by dashed and dotted lines, respectively (n=3, unpaired t-test). **** $p < 0.0001$. Scale bar 50 µm.

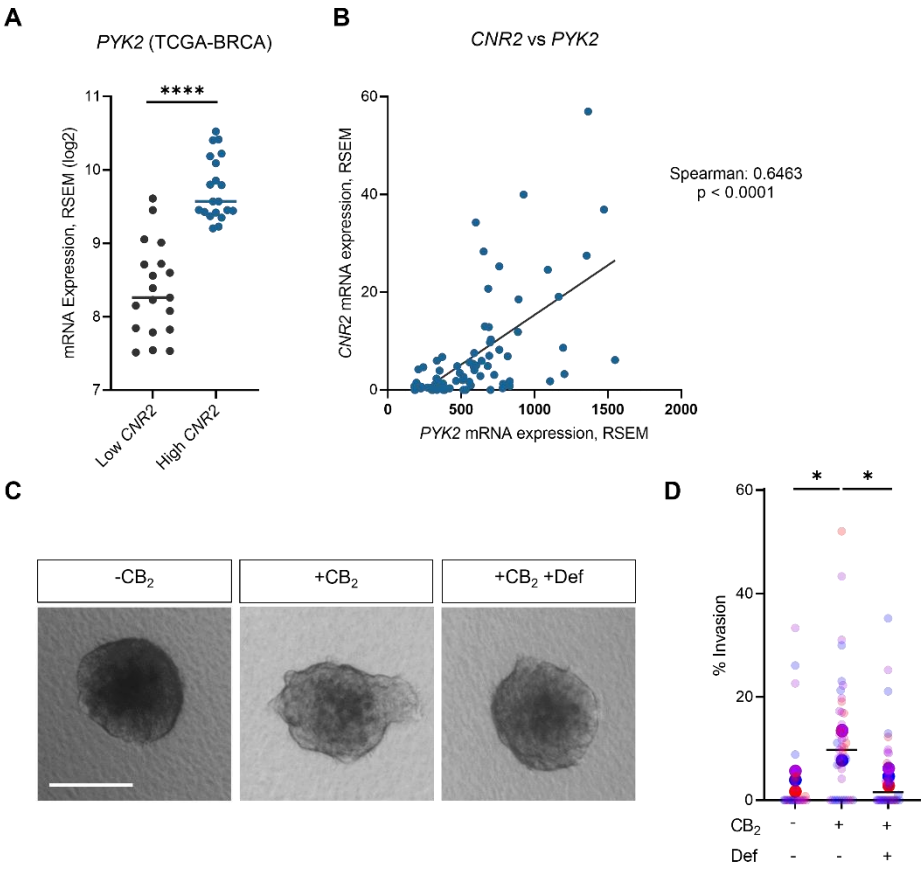

Figure 6.3.2: *PYK2* expression increases in high CB_2 expressing patients and contributes of CB_2-driven invasion.

(A) Comparison of *PYK2* mRNA expression between the upper and lower quartiles of *CNR2* expressing HER2+ patients in the Breast Cancer Invasive TCGA dataset (unpaired t-test, mean ± SD). (B) Breast Cancer Invasive TCGA HER2+ patient data of the correlation of mRNA expression between *PYK2* and *CNR2*. TCGA data generated using RNA-seq by Expectation Maximisation (RSEM). (C) Light micrographs of HCC1954^{iCB2} spheroids embedded in a collagen-Matrigel matrix. Spheroids +/- CB_2 induction and +/- 100 nM PYK2 inhibitor Defactinib or vehicle (DMSO). (D) Quantification of (C) with each colour representing biological repeats, translucent points representing a single spheroid and each larger solid point the mean invasion of each repeat, horizontal line represents median % invasion (n=3, ordinary one-way ANOVA). Scale bar 200 µm * $p < 0.05$, **** $p < 0.0001$.

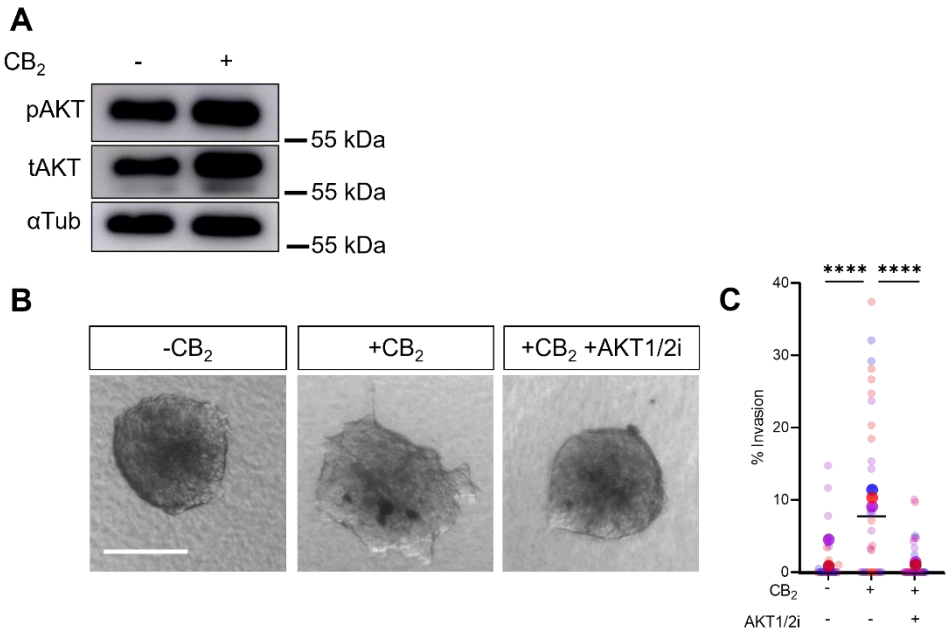

Figure 6.3.3: CB_2 increases expression and activation of AKT, leading to increased 3D invasion.

(A) Western blot analysis of phospho-AKT (Ser 473) and total-AKT protein using HCC1954^{iCB2} whole cell lysates +/- 24-hour CB_2 induction. αTubulin was used as a loading control (representative image of n=3 biological replicates). (B) Light micrographs of HCC1954^{iCB2} spheroids in collagen-Matrigel matrix, +/- CB_2 induction +/- 100 nM AKT1/2 inhibitor or vehicle (DMSO). (C) Quantification of AKT1/2 inhibitor treated spheroid invasion from (B), with each colour representing biological repeats, translucent points representing a single spheroid and each larger solid point the mean invasion of each repeat, horizontal line represents median % invasion (n=3, ordinary one-way ANOVA). Scale bar 200 µm. **** $p < 0.0001$.

6.4 CB_2 expression leads to the activation of the Wnt/ß-catenin pathway

As ALDH1A1 expression is linked to the outcome of HER2+ breast cancer, its association with cancer stem cells, invasion via PYK2 and potentially metabolism through PPARγ, I aimed to elucidate how ALDH1A1 expression is regulated by CB_2. ALDH1A1 expression can be controlled by the Wnt/β-catenin pathway, a signalling pathway that is often highly active in CSCs[286]. Therefore, to initially investigate whether CB_2 was increasing the activity of the Wnt/β-catenin pathway expression of Wnt ligands was examined in the HER+ breast cancer TCGA dataset (Figure 6.4.1). High *CNR2*-expressing patients have increased levels of various Wnt ligands, with the largest increase seen in *WNT10A*. Further analysis additionally revealed a positive correlation between *WNT10A* and *CNR2* mRNA expression (Figure 6.4.2 A, B). Expression of the Wnt ligands was verified by qPCR in HCC1954^{iCB2} cells and revealed a significant increase in mRNA expression of *WNT10A* after CB_2 induction (Figure 6.4.2 C).

As Wnt signalling leads to the activation of β-catenin, I investigated if CB_2 expression activated β-catenin in HCC1954^{iCB2} cells. In the absence of Wnt ligands, β-catenin is sequestered in the cytoplasm by a protein complex of glycogen synthase kinase 3 (GSK3), Axin, Adenomatous polyposis coli (APC) and casein kinase 1 (CK1). In its inactive state, β-catenin is phosphorylated and degraded through the proteasome. When Frizzled receptors are activated through Wnt ligand binding and associations with accessory protein LRP5/6, β-catenin separates from the inhibitory protein complex, activates and translocates to the nucleus, regulating the transcription of Wnt target genes through binding to TCF and LEF transcription factors[287]. Immunofluorescence of β-catenin revealed a significant increase in nuclear β-catenin after CB_2 induction, indicating β-catenin activity (Figure 6.4.3).

Subsequently, I verified if β-catenin was actively regulating gene transcription through the TOPFlash assay[288]. TOPFlash is a plasmid expressing firefly luciferase under the regulation of a TCF promoter. Following Wnt signalling, nuclear β-catenin regulates transcription through the activity of the TCF transcription factor (Figure 6.4.4). CB_2 expressing HCC1954^{iCB2} cells had significantly more luciferase activity compared to HCC1954^{iCB2} cells that lacked CB_2, indicating CB_2 induces β-catenin regulated gene transcription.

Together, these data suggest that CB_2 generates a cancer stem cell phenotype through CD44 and ALDH1A1 expression. ALDH1A1 could also contribute to the invasive potential of CB_2 expressing HER2+ cancer cells through driving the expression of PYK2. Moreover, the activation of the Wnt pathway is common in cancer stem cells and potentially controls the expression of ALDH1A1 and CD44, with CD44 acting as a positive regulator of Wnt/β-catenin signalling[286,289] (Figure 6.4.5). The resulting phenotype after CB_2 expression is a highly motile cancer stem cell that is at increased risk of forming metastases.

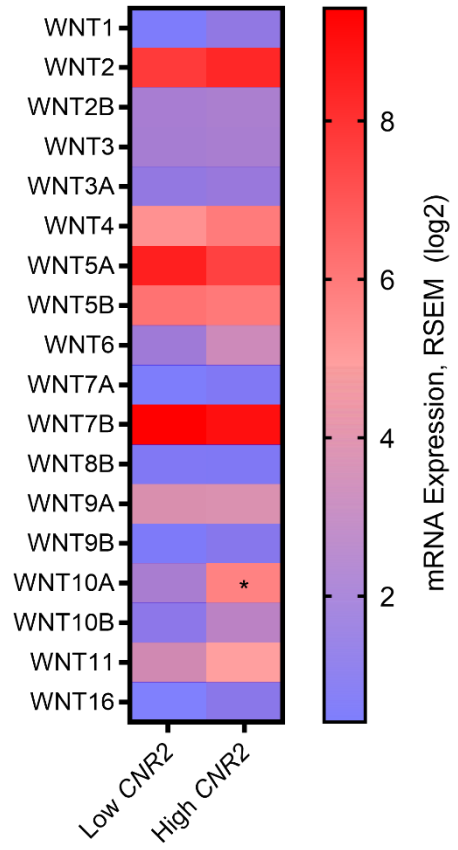

Figure 6.4.1: Wnt ligand expression changes in high and low CB_2 expression HER2+ patients.

Expression of Wnt ligand mRNA from the Breast Cancer Invasive TCGA dataset between the upper and lower quartiles of *CNR2* expressing HER2+ breast cancer patients. TCGA data generated using RNA-seq by Expectation Maximisation (RSEM). (* indicates significance of $p < 0.01$).

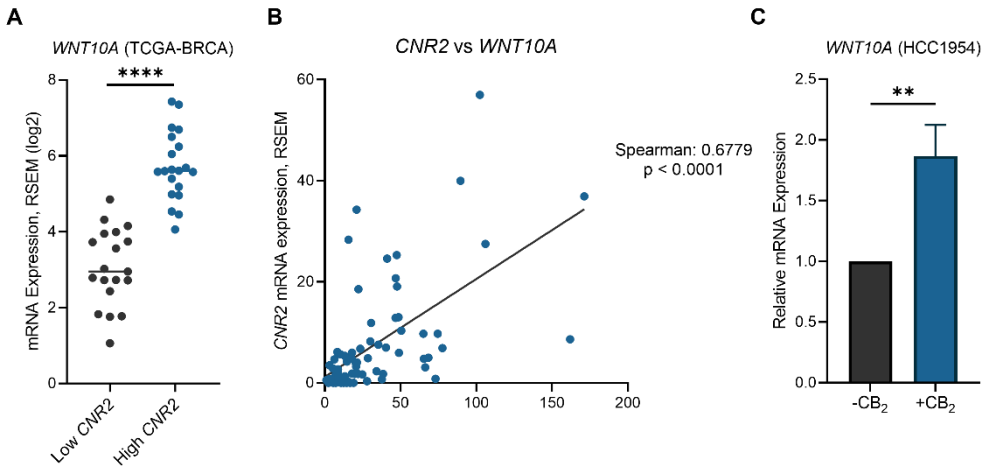

Figure 6.4.2: CB_2 expression leads to increased levels of WNT10A mRNA expression.

(A) Comparison of *WNT10A* mRNA expression between the upper and lower quartiles of *CNR2* expressing HER2+ patients in the Breast Cancer Invasive TCGA dataset (unpaired t-test) (B) Breast Cancer Invasive TCGA HER2+ patient data of the correlation of mRNA expression between *WNT10A* and *CNR2*. TCGA data generated using RNA-seq by Expectation Maximisation (RSEM). (C) RT-qPCR analysis of *WNT10A* mRNA expression in HCC1954^{iCB2} cells. Relative mRNA expression normalised to *ACTB* (β-actin) mRNA expression. +/- 24-hour CB_2 induction (n=3, unpaired t-test, mean ± SD). ** $p < 0.01$, **** $p < 0.0001$.

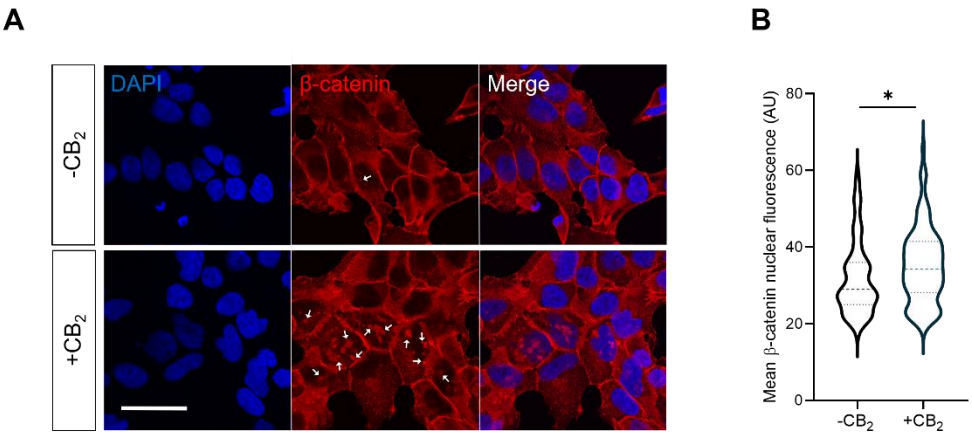

Figure 6.4.3: Activation of β-catenin upon CB2 expression.

(A) Subcellular localisation of β-catenin (red) by immunofluorescence +/- 24-hour CB2 induction in HCC1954^{iCB2} cells. White arrows indicating nuclear β-catenin staining (representative images of n=3). (B) Quantification of β-catenin nuclear localisation in HCC1954^{iCB2} cells from (A) (n=3 biological replicates, unpaired t-test, mean ± SD). Scale bar 40 µm * $p < 0.05$.

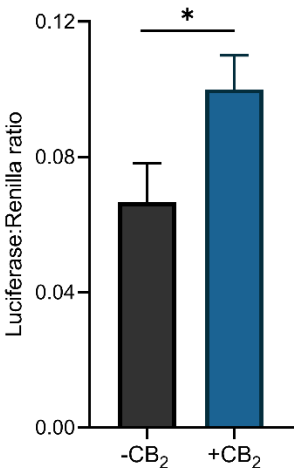

Figure 6.4.4: Activation of the Wnt/β-catenin pathway leads to TCF-mediated gene expression.

Analysis of TCF-mediated transcription in HCC1954^{iCB2} cells transfected with the TOPFlash reporter. Firefly luciferase activity normalised to Renilla luciferase. * $p < 0.05$.

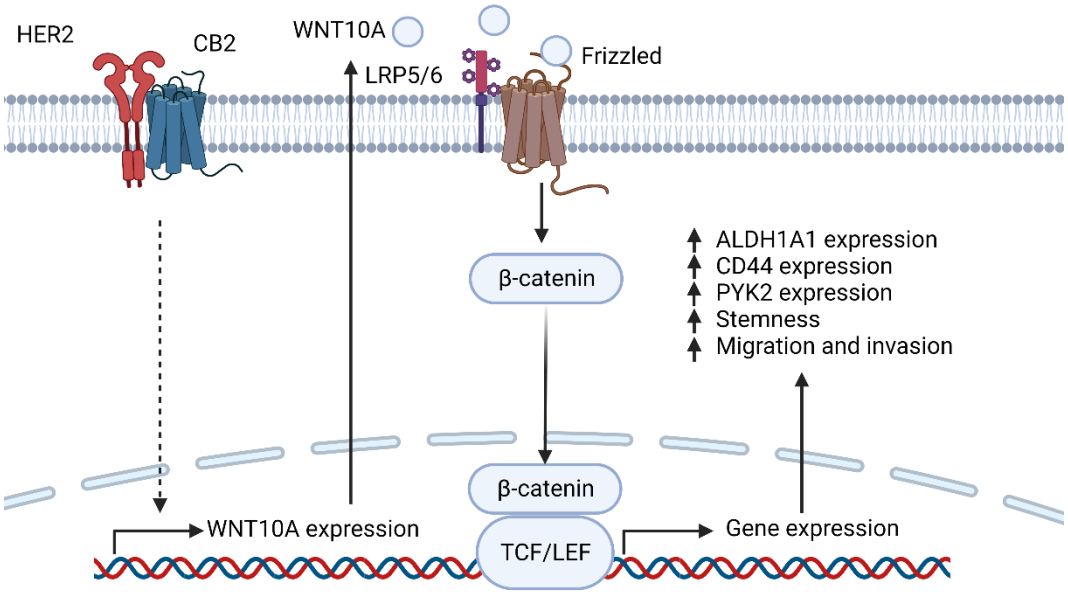

Figure 6.4.5: Proposed mechanism of CB_2-mediated autocrine Wnt/β-catenin pathway activation and induction of highly motile stem-like phenotype.

CB_2 expression in HER2+ breast cancer cells leads to increased WNT10A expression and β-catenin activation, potentially via autocrine stimulation of frizzled receptors. β-catenin translocates to the nucleus where it mediates TCF/LEF controlled transcription of *ALDH1A1*, *CD44* and *PYK2* resulting increased migration, invasion and stemness.

6.5 Summary of Results

- CB_2 expression increased the mammosphere formation efficiency of HCC1954^{iCB2} in low attachment culture.
- There were no changes in the expression of Yamanaka factors, regardless of CB_2 expression, however, CB_2 expression positively correlated with the breast cancer stem cell markers ALDH1A1 and CD44 in HER2+ breast cancer patients and HCC1954^{iCB2} cells.
- PYK2, a target of RA signalling, is correlated with CB_2 expression in HER2+ breast cancer patients, and inhibition of PYK2 inhibits 3D invasion of HCC1954^{iCB2} spheroids.
- CB_2 expression leads to increased AKT expression and activation, with AKT inhibition preventing invasion in 3D culture of HCC1954^{iCB2} spheroids.
- CB_2 expression increased *WNT10A* production, leading to activation and nuclear localisation of β-catenin and subsequent β-catenin-TCF mediated gene expression.

Chapter 7 CB_2 expression and immune evasion

7.1 CB_2 mediates immune evasion through PDL1 expression

The majority of CB_2 expression is localised to the tissues of the immune system, with high CB_2 expression present in the tonsils, spleen and on leukocytes[144]. The major role of CB_2 in these tissues is mediating the immune response and the resolution of inflammation. This was illustrated in CB_2-knockout mouse models, where bacterial infection leads to increased leukocyte recruitment and pro-inflammatory cytokine production, indicating CB_2 expression is important in mediating anti-inflammatory effects[144]. Therefore, I hypothesised whether CB_2 expression in cancer could reduce immune activity and increase immune evasion.

Metastasising cancer cells must avoid detection and destruction by the immune system to establish secondary tumour sites. To achieve this, cancer cells often upregulate immune checkpoint proteins that regulate immune cell function, such as programmed death-ligand 1 (PDL1) and cytotoxic T-lymphocyte-associated protein 4 (CTLA4). Engagement of PDL1 or CTLA4 with their receptors on immune cells promotes immune cell anergy and apoptosis, thereby preventing cancer cell killing. Expression of PDL1 and CTLA4 is linked with invasive breast cancer and worse patient prognosis, with HER2+ breast cancer highly associated with PDL1 expression[290–292]. Therefore, I aimed to determine whether CB_2 confers a selective advantage to invading cancer cells through the expression of immune checkpoint proteins, focusing on PDL1. Analysis of TCGA dataset revealed high *CNR2* expressing HER2+ breast cancer patients have significantly increased expression for *CD274* (the gene encoding PDL1), with its expression positively correlating with the expression of *CNR2* in HER2+ breast cancer patients (Figure 7.1.1 A, B). As PDL1 expression is highly prognostic for patient survival and the use of anti-PDL1 antibodies has high therapeutic potential[293], I investigated PDL1 expression in $HCC1954^{iCB2}$ cells. Recapitulating TCGA data suggesting *CD274* mRNA expression correlates with high CB_2 expression, I determined the levels of *CD274* in $HCC1954^{iCB2}$ cells by qPCR, with induction of CB_2 leading to

around a 50% increase in *CD274* mRNA expression (Figure 7.1.1 C). Additionally, PDL1 protein expression in HCC1954^{iCB2} was assessed by both western blot and flow cytometry and was increased after 24 hours of CB_2 expression (Figure 7.1.1 D, E).

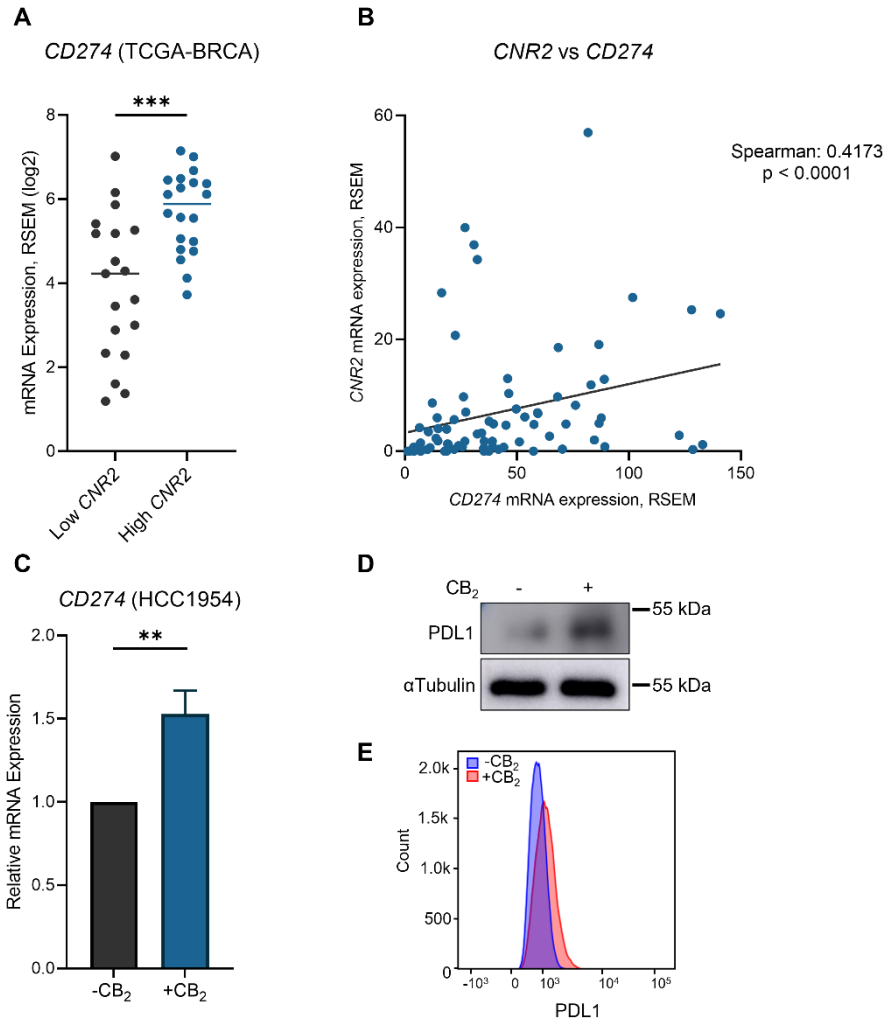

Figure 7.1.1: HER2+ breast cancer patients display a positive correlation between CB_2 and PDL1 expression.

(A) Analysis of *CD274* mRNA expression in high (upper quartile) and low (lower quartile) *CNR2* expressing HER2+ breast cancer patients from the Breast Cancer Invasive TCGA dataset (unpaired t-test). (B) Breast Cancer Invasive TCGA HER2+ patient data of the correlation of mRNA expression between *CD274* (PDL1) and *CNR2*. TCGA data generated using RNA-seq by Expectation Maximisation (RSEM). (C) *CD274* mRNA expression in HCC1954^{iCB2} cells by RT-qPCR +/- 24-hour CB_2 induction (n=3, unpaired t-test, mean ± SD). (D) Western blot analysis of PDL1 expression in HCC1954^{iCB2} whole cell lysates, +/- 24-hour CB_2 induction, αTubulin as a loading control (representative image of n=3). (E) Flow cytometry analysis of surface expression of PDL1 in HCC1954^{iCB2} cells with (red) and without (blue) 24 hours CB_2 induction (representative of n=3 biological replicates). Relative mRNA expression normalised to *ACTB* (β-actin) mRNA expression. ** $p < 0.01$, *** $p < 0.001$.

7.2 CB_2 leads to immune evasion via PDL1 expression in an AKT-dependent manner.

Increased PDL1 expression would facilitate invasive CB_2-expressing HER2+ CSCs evading the immune system, enabling metastasis. Interestingly, as CB_2 is linked to lymph node metastases in HER2+ patients (Figure 4.1.1 B), it is unsurprising that CB2 expression could lead to immune evasion, enabling lymph node colonisation. Therefore, I aimed to investigate whether PDL1 expression was present on $HCC1954^{iCB2}$ spheroids during invasion. Immunofluorescent staining of $HCC1954^{iCB2}$ revealed greater PDL1 staining on the invasive protrusions of CB_2-expressing spheroids, indicating CB_2-driven PDL1 expression may enhance immune evasion in HER2+ breast cancer patients, however, this should be examined experimentally (Figure 7.2.1).

Importantly, PDL1 expression can be controlled though the AKT signalling pathway, and therefore possibly through ALDH1A1 activity leading to increased AKT expression[283,284]. I sought to determine whether CB_2 expression impacted the expression of PDL1 in $HCC1954^{iCB2}$ cells via AKT. In addition to abrogating invasive potential of $HCC1954^{iCB2}$ spheroids, AKT inhibition also slightly decreased PDL1 staining, indicating CB_2 increases PDL1 expression, at least in part, through increased AKT expression and activity (Figure 7.2.1). Moreover, upon quantification, there was no difference in the total amount of PDL1 fluorescence between spheroids, regardless of CB_2 expression or AKT inhibition. However, quantification of the invasive protrusions revealed significantly higher PDL1 staining in CB_2-expressing spheres, which was reduced after AKT1/2 inhibition (Figure 7.2.2). Therefore, it appears that CB_2 expression is driving invasion and the expression of PDL1 in an AKT-dependent manner, possibly initiated via Wnt pathway, ALDH1A1 activity and retinoid signalling (Figure 7.2.3). Thus, expression of CB_2 could cause increased success of metastases and increased PDL1 expression may represent a mechanism of immune

evasion that could explain how CB_2 is linked to lymph node metastasis, increased relapse rates and decreased overall survival of HER2+ patients.

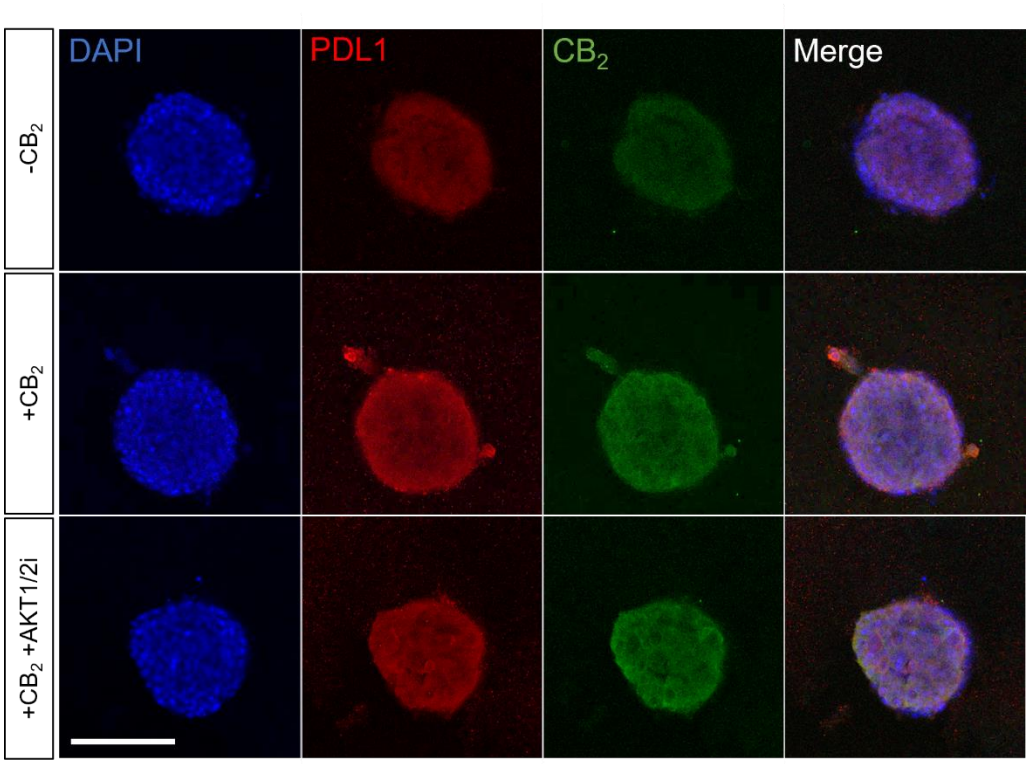

Figure 7.2.1: HCC1954^{iCB2} spheroids increase PDL1 expression after CB_2 expression, which is reduced by AKT inhibition.

Immunofluorescence of PDL1 (red) and CB_2 (green) in HCC1954^{iCB2} spheroids embedded in a collagen-Matrigel matrix, after 3 days +/- CB_2 induction and +/- 100 nM AKT1/2 inhibitor or vehicle (DMSO) (representative images of n=3). Scale bar 200 µm.

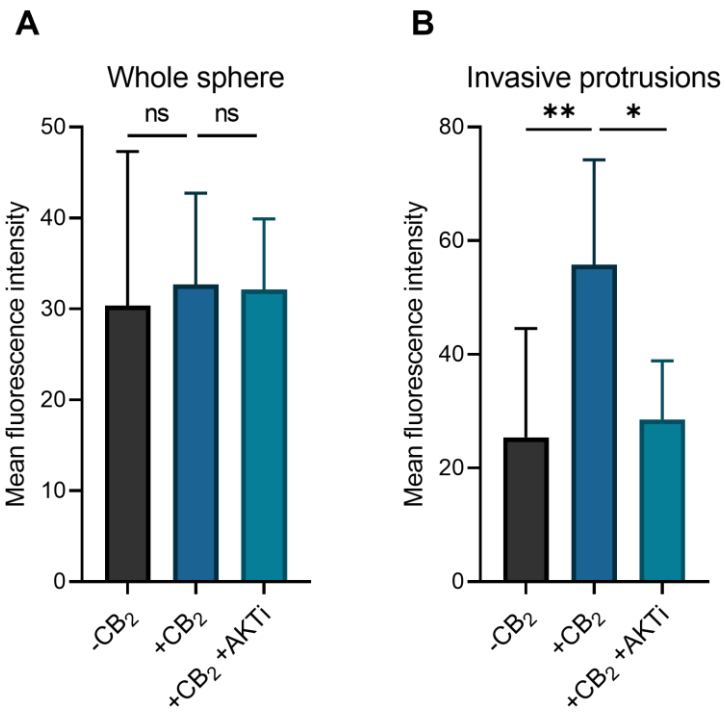

Figure 7.2.2: Increased PDL1 expression is localised to the invasive protrusions of CB_2 expressing spheroids.

Quantification of PDL1 immunofluorescence from Figure 7.2.1 in whole spheroids or invasive protrusions only, after 3 days +/- CB_2 induction and +/- 100 nM AKT1/2 inhibitor or vehicle (DMSO) (n=3 biological replicates, ordinary one-way ANOVA). * $p < 0.05$, ** $p < 0.01$.

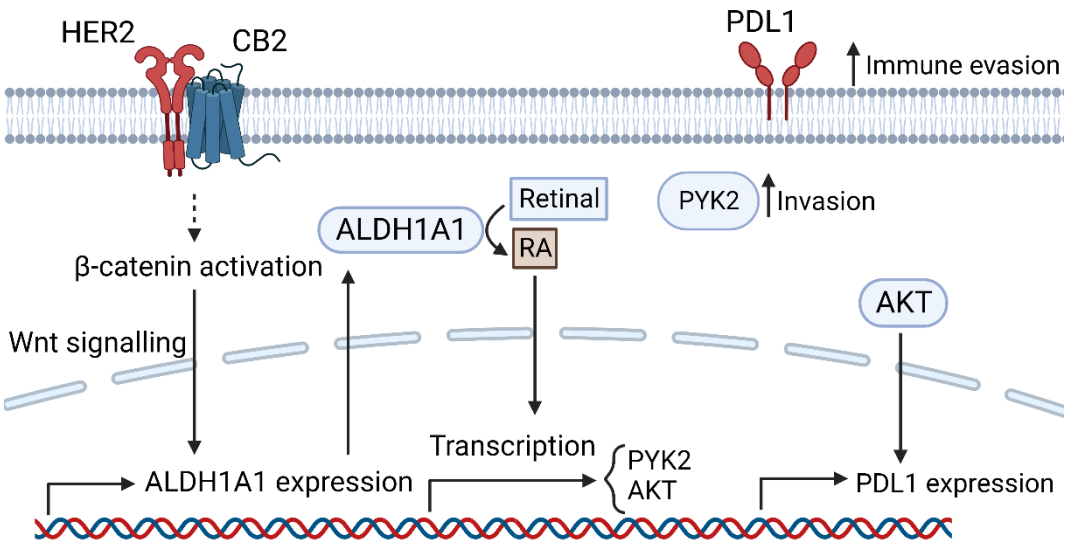

Figure 7.2.3: Proposed mechanism of CB_2-mediated tumourigenic signalling in HER2+ breast cancer.

CB_2 expression in HER2+ breast cancer leads to activation of the Wnt/β-catenin pathway and ALDH1A1 expression. ALDH1A1 catalyses the oxidation of retinal to retinoic acid (RA). Once in the nucleus RA can mediate signalling via the retinoic acid receptors to mediate the expression of *PYK2* and *AKT*. PYK2 and AKT activity results increased invasive potential and AKT signalling contributes to increased PDL1 expression leading to immune evasion.

7.3 Summary of Results

- CB_2 expression increases PDL1 expression in HER2+ patients and *in vitro* at the mRNA and protein level in $HCC1954^{iCB2}$ cells.
- In $HCC1954^{iCB2}$ spheroids, CB_2 expression increases PDL1 expression, which is localised to the invading protrusions.
- AKT inhibition of CB_2 expressing spheroids leads to reduced PDL1 expression on invasive protrusions.

Chapter 8 Discussion and conclusions

8.1 Introduction

The development of personalised medicine has provided many cancer patients with increasingly effective and tolerable therapies[294]. HER2+ breast cancer patients in particular have benefitted significantly from precision medicine. However, in many cases, resistance to targeted therapy leads to recurrence; thus, the identification of new targets and the development of new treatments is required. Cannabinoid signalling has become a target of increasing interest, as it is involved in many processes commonly exploited by cancer cells. In particular, CB_2 activity has diverse physiological roles that can be repurposed to benefit cancer growth, such as controlling the release of growth factors and cytokines to regulate development, wound repair and immune function[295]. As over 75% of HER2+ breast cancer patients display high CB_2 expression, and high levels of CB_2 are associated with decreased survival[172], CB_2 poses an attractive therapeutic target. For CB_2 targeting cannabinoid therapies to be efficacious in this context, understanding how CB_2 influences HER2+ breast cancer biology and progression is vital. To this end, I developed a CB_2 inducible system to interrogate the mechanism of CB_2-related tumourigenesis in HER2+ breast cancer and the potential of cannabinoid-based therapies as anti-breast cancer drugs. Herein, I describe a mechanism of CB_2-driven migration and invasion of HER2+ breast CSC with altered metabolism and increased potential for immune evasion. In this discussion, I will evaluate the CB_2 expression system and contextualise the findings of this thesis.

8.2 General limitations

Whilst the data presented in this thesis describe novel aspects of the role of CB_2 function in HER2+ breast cancer, there are certain limitations to be acknowledged,

with further research required to answer remaining research questions. Firstly, experimental data was obtained exclusively in *in vitro* models, and therefore conclusions drawn from this thesis should be further validated with the use of animal models and patient samples.

Furthermore, the dox-inducible system of CB_2 expression, whilst a useful tool, has some limitations. For example, some CB_2 mRNA expression was observed without dox treatment, indicating some leakiness of the pINDUCER20 vector. Additionally, further validation of CB_2 function could have been performed using CB_2 knockdown experiments, potentially rescuing the protumourigenic phenotype observed after CB_2 expression in a similar manner to cannabinoid treatment. The mechanism of CB_2 promoting invasion, metabolic rearrangement and stemness, whilst observed in the HER2+ subtype, may be common across different breast cancer subtypes. As such, it would have been prudent to examine similar changes upon CB_2 expression in HER2- breast cancer cell lines, such as MCF7, MDAMB231 or T47D.

Due to the importance of the CSC phenotype in metastasis and patient mortality, further confirmation of CSC markers, both on $HCC1954^{iCB2}$ cells, *in vivo* models and in patient samples would highlight the clinical relevance of CB_2+ breast CSCs. Methods for further analysis of the CSC phenotype are discussed later (Section 8.8 Future perspectives).

In addition to the limitations of the data, there remains many questions regarding the specific mechanism of CB_2 function in HER2+ breast cancer, with specific discussion of prospective experiments discussed in 8.8 Future perspectives. The mechanisms by which CB_2 leads to metabolic rewiring of HER2+ cancer cells are still no be determined. Whilst this thesis provides an indication that increased rates of glycolysis and oxidative phosphorylation could be influenced through ALDH1A1 function and RA signalling, this needs to be specifically examined. Furthermore, whist increased PDL1 expression was observed, whether its expression in this context would lead to

immune evasion is still unexplored. Finally, the presence and relevance of a population of CB_2+ CSC within HER2+ breast cancer patients is currently unknown.

8.3 CB_2 inducible expression system

8.3.1 Validation of CB_2 expression

In this thesis, most *in vitro* experimentation used the dox-inducible expression system for CB_2 in HER2+ breast cancer cell lines. This system enabled the investigation of the protumoural role of CB_2 in the context of HER2+ breast cancer and the applicability of cannabinoids as anti-cancer therapy. Whilst the inducible system showed robust CB_2 expression, and subsequent cannabinoid treatment led to changes in gene expression, metabolic rewiring and metastatic potential in HCC1954, SKBR3 and BT474 cell lines, there are some limitations to be considered, as this is an *in vitro* model of a complex and heterogenous disease.

8.3.2 Clinical relevance

The relevance of CB_2 expression levels in the dox-inducible *in vitro* system is difficult to compare to CB_2 expression levels in patient tumour tissue. However, the observed changes in our *in vitro* model have been cross-referenced via comparison to HER2+ breast cancer patients in TCGA datasets. Therefore, inducible CB_2 expression in HER2+ cell lines has similar consequences to CB_2 expression in patient cancers, supporting its clinical relevance. However, further validation of the CB_2-mediated metabolic rearrangement, stemlike phenotype and immune evasion in *in vivo* systems, such as tumourgenicity studies in immunodeficient and immunocompetent mouse models is warranted.

8.3.3 Heterogeneity of CB_2 expression

Before FACS, each cell line displayed considerable heterogeneity in CB_2 expression after induction with dox, possibly resulting from cells that incorporated different levels of *CNR2* into their genome during transfection. Alternatively, it is possible some cells were transduced with pINDUCER20 plasmid that did not contain the *CNR2* gene. In Figure 3.2.1, the brsG1 digestion of the *HA-CNR2*-pINDUCER20 plasmid, there is a presence of a fourth band at approximately 500 bp, indicating the presence of pINDUCER20 plasmid with four bsrG1 restriction sites that has not incorporated HA-*CNR2*. Therefore, it is possible the presence of this pINDUCER20 plasmid could affect the transduction efficiency of *HA-CNR2*-pINDUCER20 plasmid, leading to heterogeneity of CB_2 expression.

Although the CB_2 inducible expression system described here has certain limitations, it provides a valuable tool to study the effects of CB_2 expression in HER2+ breast cancer and the anti-tumourigenic effects of targeting CB_2 with cannabinoids.

8.3.4 JWH133 synthetic cannabinoid

The synthetic cannabinoid JWH133 was used to study CB_2 activation in most experiments due to its pharmacodynamic properties. JWH133 is a CB_2-specific cannabinoid, displaying 200-fold selectivity for CB_2 over CB_1[296]. Whilst other cannabinoids can also show high affinity to CB_2, such as β-caryophyllene[297] and AM-1241[298], JWH133 is highly potent, with a K_i value of 3.4 nM[295].

Moreover, JWH133 has low off-target effects at experimental concentrations, allowing for specific interrogation of CB_2 function[295]. Additionally, JWH133 has been demonstrated to have CB_2-specific anti-tumourigenic properties in a variety of cancer models, with JWH133 inhibiting growth of breast cancer cells *in vitro* and *in vivo*[183,295,299]. As such, JWH133 was the primary cannabinoid used to investigate CB_2

function. However, due to the relatively short half-life of JWH133, multiple treatments were required during longer culture periods.

8.4 Protumourigenic effects of CB_2 expression

Synthetic and phytocannabinoids have been used extensively *in vivo* and *in vitro* to interrogate the function of CB_2 in cancer. Treatment with cannabinoid agonists of CB_2 has revealed their pro-apoptotic, anti-proliferative and anti-invasive function[124,168,208]. However, the mechanisms by which CB_2 elicits its protumourigenic function are still being elucidated. Whilst increased CB_2 expression relates to decreased survival in HER2+ breast cancer, high CB_2 expression in HER2- cancer leads to improved patient prognosis (Figure 4.1.1 A). This dichotomy possibly indicates that the formation of HER2-CB_2 heteromers is more pathological than CB_2 expression alone. In addition, high CB_2 expression in HER2- cancer could indicate increased immune infiltration, a marker of better prognosis, as transcriptomic analysis of bulk tumour tissue cannot determine cell of origin.

In HER2+ breast cancer, CB_2 is thought to mediate some of its protumourigenic effects by stabilising HER2 at the membrane, leading to increased HER2 signalling, as administration of THC causes disruption of the HER2-CB_2 heteromer and HER2 internalisation and degradation[186]. However, CB_2 exhibits tumourigenic properties in other subtypes of breast cancer, such as TNBC, where it leads to increased migration, proliferation and decreased apoptosis in the absence of HER2[300]. Thus, CB_2 can mediate protumourigenic signalling independent of HER2, which is apparent in non-breast cancers such as prostate cancer and GBM[178,301], illustrating the complexity regarding the role of CB_2 in cancer.

8.4.1 CB_2 expression contributes to metastatic potential

Interestingly, patient data indicated that high CB_2 expression correlates with worse survival in HER2+ patients with lymph node metastases but not in HER2+ patients without metastases to the lymph nodes (Figure 4.1.1 B). This implies that CB_2 is an indicator of poor prognosis in particularly aggressive or advanced cancer. It also indicates that CB_2 expression may contribute to metastasis and lead to rapid deterioration of patient survival. In fact, CB_2 expression has been linked to increased metastases of colon, lung, pancreatic and breast cancers, amongst others, with cannabinoid treatment reducing the metastatic action of CB_2[172,204,302,303]. Consistent with the literature, CB_2 expression leads to increased metastatic potential in $HCC9154^{iCB2}$ and $BT474^{iCB2}$ cells, which was inhibited through activation with JWH133 (Figure 4.2.4). Similar *in vitro* results have also been reported in spheroid cultures of other cancers, including gastric cancer, hepatocellular carcinoma and NSCLC, in which invasion is inhibited with CB_2 agonists, highlighting the applicability of cannabinoid-based medicine to prevent metastatic disease in early-stage cancer patients [304–306].

Furthermore, CB_2 activity has been correlated with the expression of MMP2 and MMP9, mediators of tumour invasion via the degradation of the ECM[307]. Treatment with phytocannabinoids has been reported to inhibit MMP function via the activation of tissue inhibitors of metalloproteinase 1 (TIMP1) and TIMP4, which bind to and inhibit MMP proteolytic activity[308]. Additionally, analysis of HER2+ patient data shows an increase in PYK2 with CB_2 expression (Figure 6.3.2 A, B), which has been implicated in the invasiveness of HER2+ breast cancer and in the regulation of MMP9 expression. In the 3D hanging drop spheroid model, CB_2 expression increased invasion in a PYK2 dependent manner (Figure 6.3.2 C, D), emphasising the role of CB_2 in contributing to the metastatic potential of HER2+ breast cancer[282,309].

CB_2 expression has also been shown to cause increased expression of IGFR1 and the activation of its signalling pathway, resulting in increased metastasis[171,310]. This is of particular interest to HER2+ breast cancer as the compensatory increase in IGFR1 expression is a common mechanism of resistance to anti-HER2 therapies[109]. Therefore, this suggests that the inhibition of CB_2 would not only decrease the risk of metastasis but also the risk of acquired resistance to HER2-targeted therapy, highlighting the potential use of cannabinoids in combination therapy in HER2+ breast cancer.

8.4.2 Epithelial-mesenchymal transition is mediated through CB_2

Growing evidence suggests that CB_2 expression increases migration and invasion by triggering EMT in various cancers[310]. CB_2 expression has been reported to correlate with expression of the EMT transcription factor snail, vimentin and N-cadherin expression in the MCF7 breast cancer cell line[311], although there was no significant difference in *SNAI1* expression in TCGA data of HER2+ breast cancer patients. However, high CB_2 expression in HER2+ patients is linked with another EMT-regulating transcription factor ZEB2 (Figure 4.4.1), which regulates migration and invasion in breast cancer and has been shown to be regulated by CB_2 in NSCLC[312,313]. Further, synthetic cannabinoid WIN 55,212-2 has been shown to reduce EMT-led invasion in gastric and endometrial cancers[314], and CB_2 knockdown has also been reported to disrupt EMT by reducing N-cadherin, vimentin and snail expression in breast cancer[311].

There is growing evidence that CB_2 expression could be mediating EMT through Wnt signalling, which is further support by evidence presented in this thesis. Activation of the Wnt pathway is associated with EMT in breast cancer[315] with endo, phyto, and synthetic cannabinoid treatment preventing Wnt/β-catenin mediated EMT[181,316].

Moreover, in HCC1954^{iCB2} cells, CB_2 expression increased Wnt/β-catenin activity, indicative of the mechanism of CB_2-mediated EMT (Figure 6.4.3).

In BT474^{iCB2} cells, expression of CB_2 led to decreased E-cadherin and increased vimentin expression, indicating that CB_2 contributes to the transition to a mesenchymal phenotype in these cells. In contrast, HCC1954^{iCB2} cells already displayed a mesenchymal phenotype with high vimentin and low E-cadherin prior to CB_2 expression. HCC1954 cells have PTEN loss[317], which has been reported to induce EMT[228], and therefore CB_2 expression is not required for EMT. However, CB_2 expression still contributes to invasion in this cell line. These data indicate that although CB_2 expression is sufficient to trigger EMT, it is not absolutely required, as many different tumourigenic processes regulate EMT. Therefore, CB_2 can contribute to metastasis through increasing EMT, as well ats promoting the migratory and invasive potential of mesenchymal-like cancer cells. This may be driven through the expression or activation of PYK2, as PYK2 inhibition in 3D spheroids abrogated invasion (Figure 6.3.2 C, D).

8.4.3 CB_2 regulation of proliferation and cell survival

Cannabinoid receptor expression contributes to the proliferation and survival of cancer cells in many cancer types through the regulation of AKT activity and the BAX/BCL2 axis[124]. Neuronal CB_2 activation also promoted neuronal survival through the down regulation of BAX and upregulation of BCL2[318].

In breast cancer, CB_2 expression increases cancer proliferation through AKT signalling, and activation with JWH133 and phytocannabinoids leads to AKT inhibition through the ER stress pathway, resulting in autophagic cell death[208]. However, the data reported in this thesis highlight some discrepancies in how CB_2 impacts proliferation in different breast cancer subtypes, as seen in proliferation rates

of HCC1954^{iCB2} and BT474^{iCB2} cells (Figure 4.3.1). CB_2 expression in the inducible system did not increase proliferation in HCC1954^{iCB2} or BT474^{iCB2} cells. HCC1954^{iCB2} cells displayed no significant difference in proliferation, indicating CB_2 may not contribute to increased cell growth in the setting of cancers already displaying high rates of proliferation. In HCC1954^{iCB2} cells, CB_2 expression may lead to improved survival, possibly via the BAX/BCL2 axis, but not to cell proliferation, resulting in a slight, non-significant increase seen in the Incucyte assay (Figure 4.3.1). As the cell signalling pathways resulting in cell proliferation by CB_2 and HER2 (i.e., AKT and MAPK) overlap, the expression of CB_2 may not increase the activation of these pathways sufficiently to result in increased proliferation. However, I observed a CB_2-dependent increase in AKT expression and phosphorylation in HCC1954^{iCB2} cells, indicating increased activity of this pathway (Figure 6.3.3 A).

Interestingly in BT474^{iCB2} cells, CB_2 expression led to a decrease in cell proliferation. Whilst BT474 cells are HER2+, they also have expression of ER[319]. ER+ breast cancers with high CB_2 expression have been shown to have a better prognosis[171]. Furthermore, it has been demonstrated that CB_2 expression can interfere with ER signalling and gene expression, decreasing protumourigenic ERα expression and increasing anti-tumourigenic ERβ expression, reducing proliferation[134,320]. This disruption of protumourigenic ER signalling likely contributes to increased survival in CB_2 expressing luminal breast cancer patients and the observed decreased in BT474^{iCB2} proliferation following the induction of CB_2.

Due to these conflicting data on the role of CB_2 in proliferation, further research is required to elucidate the role of CB_2 in different breast cancer subtypes. Understanding the context in which CB_2 may contribute to improved or diminished patient survival is vital in the development of cannabinoid-based therapies.

8.4.4 Metabolic rearrangement in CB_2 expressing cancer cells

An emerging role of CB_2 is in the regulation of cellular metabolism in normal tissue, however, the role of CB_2 in cancer cell metabolism is still unclear. Here, I describe the effects of CB_2 in the metabolism of normal cells and the relevance to the novel role of CB_2 regulating HER2+ cancer cell metabolism identified in this thesis.

Much of the research into the function of CB_2 in metabolism has used the CB_2-specific phytocannabinoid β-caryophyllene, also found in cinnamon (*Cinnamomum* species*)*, pepper (*Piper nigrum)* and oregano (*Origanum vulgare)*[297]. β-caryophyllene has been shown to increase glucose uptake, glycolysis and oxidative phosphorylation pathways in C2C12 muscle myotubes[321]. CB_2 activation by β-caryophyllene leads to increased glycolytic enzyme activity, mitochondrial activity, and flux through the tricarboxylic acid cycle (TCA) and electron transport chain, leading to increased ATP production[321]. Similarly, induction of CB_2 in HCC1954^{iCB2} and BT474^{iCB2} cells leads to increased glycolysis, through upregulating HK3 and HKDC1 glycolytic enzymes, and oxidative phosphorylation, through increased mitochondrial content, leading to increased ATP production. Interestingly, HK3 expression also appears to regulate the expression of genes involved in mitochondrial biogenesis, reinforcing the observed increased oxidative phosphorylation[250]. Furthermore, in pancreatic cancer, CB_2 activation inhibits energetic metabolism and induces autophagy in an AMPK-dependent manner, corroborating the link between cannabinoid signalling and metabolism in cancer, and highlighting another potential mechanism of therapeutically targeting cannabinoid receptors[322].

CB_2 can also reduce oxidative stress by regulating expression of superoxide dismutase, catalase and glutathione peroxidase (GPx) enzymes[318]. This function of CB_2 is reflected in HER2+ breast cancers, with increased expression of *PPARG* and *GPX3*, indicating CB_2 expressing cells have increased antioxidant properties. Additionally, increased

expression of PPARγ, the protein encoded by *PPARG*, can lead to increased mitochondrial biogenesis through the interaction of Peroxisome proliferator-activated receptor gamma coactivator 1-alpha (PGC-1α)[323]. This may explain the observed increased mitochondrial content occurring in CB_2 HCC1954^{iCB2} cells. It has also been reported that CB_2 activation by JWH133 in obese mice can lead to a down regulation of PPARγ expression[295] and CB_2 activation in neurons has been shown to the upregulate PPARγ to mitigate oxidative stress[318], highlighting the link between CB_2, PPARγ and antioxidant activity.

Recent evidence suggests that CB_2 also regulates metabolism in dendritic cells (DCs), where CB_2 activation leads to metabolic rewiring[324]. CB_2 activation with synthetic cannabinoid WIN 55,212-2 decreased glycolytic flux and increased mitochondrial activity in DCs, with increased expression of genes involved in fatty acid metabolism, indicating fatty acid oxidation (FAO) was fuelling the TCA cycle, rather than glutamine[324]. Interestingly, mass spectrophotometry analysis of metabolites in HCC1954^{iCB2} cells revealed increased levels of glutathione (Figure 5.3.2 B), indicating that excess glutamine is available for conversion to glutathione, suggesting CB_2 expression in HER2+ breast cancer cells also leads to increased FAO. Increased glutathione levels indicate GPx-meditated antioxidant activity, possibly mediated by increased *GPX3* expression seen in HER2+ breast cancer patients expressing high levels of CB_2 (Figure 5.3.2 C). Supporting this, I observed decreased levels of glucose-derived citrate production in CB_2 expressing HCC1954^{iCB2} cells (Figure 5.3.2 A), associated with increased fatty acid uptake and oxidation and therefore increased need for ROS reduction and antioxidant activity.

The precise mechanism of how CB_2 regulates metabolism is still unclear, however, CB_2 has been linked to mitochondrial function in ageing renal cells of the kidney, through β-catenin activity[325]. Interestingly, in HCC1954^{iCB2} cells, CB_2 expression led to β-catenin activation, although no mitochondrial dysfunction was observed. However,

the above study highlights the interactions of CB_2 and Wnt/β-catenin pathways in the regulation of cellular metabolism. Interestingly, Wnt signalling is an important pathway in breast cancer and is involved in the formation of breast cancer CSCs.

CB_2 expression leads to metabolic rewiring of HCC1954^{iCB2} cells, leading to a highly energetic, plastic and anti-oxidative phenotype, resembling metabolic changes that occur in the formation of CSCs [248]. The high levels of both glycolysis and oxidative phosphorylation could indicate metabolic plasticity in HCC1954^{iCB2} and BT474^{iCB2} cells, suggesting that CB_2 confers a stem-like phenotype, as metabolic plasticity is a hallmark of cancer stem cells. Furthermore, increased mitochondrial content and activity are likely involved in decreased ROS production, which is required to maintain stemness[232]. However, heterogenous CB_2 expression levels could lead to different metabolic phenotypes, with a population showing high levels of glycolysis and another, more stem like population, displaying high levels of oxidative phosphorylation. Further investigation is necessary to fully elucidate how CB_2 expression impacts metabolism.

8.5 Cancer stem cells

CSCs constitute a small population of cells in solid tumours, maintaining pluripotency and the ability for self-renewal[326]. Cancer stem cells are thought to arise from progenitor cells that turn malignant, known as tumour-initiating cells, or from differentiated, non-stem cancer cells that de-differentiate and regain pluripotency[327]. Now, there is increasing evidence of bi-directional conversion of cancer stem cells, switching phenotypes from stem to non-stem and non-stem to stem[328]. Regardless of their origin, CSCs can produce heterogeneous daughter cells, contributing to the clonal evolution of tumours[329].

A hallmark of CSCs is the divergence from the Warburg effect seen in proliferating cancer cells, increasing metabolic plasticity that can switch from high rates of aerobic glycolysis to high levels of oxidative phosphorylation[248,330]. Metabolic switching can facilitate CSCs conversion from a low cell turnover, quiescent state, to a highly invasive migratory phenotype[330,331]. CSCs have widely been reported to have increased migration, invasion and angiogenic properties and significantly increased rates of metastasis compared to their non-stem counterparts [332]. Once at a metastatic site, CSCs can switch back to quiescence and low levels of proliferation, contributing to chemotherapy resistance and patient relapse[331].

CSCs mediate resistance to conventional chemo and radiotherapies partly due to their low levels of proliferation, which renders many chemotherapies less effective[266,333]. Furthermore, CSCs express high levels of ATP binding cassette (ABC) transporters that actively transport cytotoxic drugs out of the cell[334]. Many CSCs also display elevated expression of the ALDH family of detoxifying enzymes, such as ALDH1A1[335], which convert chemotherapeutic drugs such as cyclophosphamide and platinum-based therapies to inactive, more excretable forms[336]. Additionally, ALDH1A1 expression can confer radiotherapy resistance through increased levels of DNA repair and decreasing ROS-associated oxidative damage in prostate and breast cancer[337].

The prominence of CSCs in the progression and mortality of cancer is well recognised, although therapeutically targeting CSCs remains a significant challenge[338]. Here we report that CB_2 mediates stemness in HER2+ breast cancer, and therapeutic targeting of CB_2 could lead to well-tolerated anti-CSC therapies. However, although the ECS is emerging as a regulator of CSC phenotype, additional research is required to understand the mechanism of cannabinoid receptor-mediated stemness.

8.5.1 CB_2 function contributes to cancer stem cell formation

Whilst evidence on the role of individual cannabinoid receptors (i.e., CB_1 or CB_2) in stem cell function is limited, there is growing evidence that cannabinoid treatment has an anti-CSC action[328,334]. Cannabinoid signalling has been demonstrated in the normal maintenance of embryonic stem cells and in regulating the differentiation of hematopoietic stem cells[339]. Moreover, CB_2 activity has been shown to have roles in the survival, homing and migration of stem cells[339].

In cancer, phytocannabinoids such as CBD lead reduction in CSC number and function through triggering ER stress[334] and decreasing Wnt pathway activity[340]. THC and CBD have also been shown to reduce treatment therapy resistance mechanisms of CSCs via inhibiting the expression of ABC transporters and decreasing ALDH activity[334,341]. In glioblastoma (GBM) CSCs, which show increased levels of CB_2, THC and JWH133 treatment reduced their proliferation, invasiveness and tumourigenesis and promoted cell death[342,343]. Furthermore, non-lethal concentrations of JWH133 reduced the formation of GBM neurospheres in *in vitro* low attachment culture and the efficiency of *in vivo* tumourigenesis in mice[342], emphasizing CB_2 function in mediating cancer stemness.

Here I describe that CB_2 expression leads to an increased ability for mammosphere formation, which was inhibited by JWH133, validating a CB_2-mediated increase in stemness in HER2+ breast cancer (Figure 6.1.1). Whilst CB_2 expression did not change expression of the Yamanaka pluripotency factors, CB_2 expression in HER2+ breast cancer correlates with an increase of ALDH1A1 and CD44, two widely recognised breast CSC markers. Due to the low percentage of cancer cells that display stem like properties within a tumour, the change in CSC marker expression observed in TCGA data does not necessarily indicate an increase in the CSC population. Significant changes in ALDH1A1 and CD44 expression reported in this thesis, however, suggest

that there is a notable increase in the population of CSCs. Further assessment of the CB_2-dependent increase in CSC numbers in experimental cultures and patients is required, discussed later.

However, high ALDH1A1 and CD44 levels are observed in CTCs isolated from breast cancer patients, and their expression correlates with increased rates of lymph node metastases[344], indicating CB_2 expression could contribute to lymph node metastasis through the induction of ALDH1A1+/CD44+ CSC phenotype. The identification of CB_2+ CSC populations in HER2+ breast cancer patient would further reinforce the role of CB_2 function in the generation of CSCs, further highlighting the potential therapeutic benefit of CB_2 targeted cannabinoid therapy.

8.5.2 ALDH1A1 activity and Wnt signalling in breast cancer stem cells

In breast cancer, ALDH1A1 expression is associated with poor patient outcomes[275]. ALDH1A1 converts aldehydes to carboxylic acids and reduces reactive oxygen species, vital steps in cellular detoxification[277]. These are critical protective actions in normal cells and, in cancer cells, they can reduce the effectiveness of cytotoxic drugs and confer the treatment resistance seen within CSC populations, as mentioned previously[278]. Further, ALDH1A1 oxidises retinal to retinoic acid (RA), which, once in the nucleus, binds to retinoic acid receptors, RXR and RARα, along with PPARs to regulate a variety of transcription events[279]. Interestingly, RA signalling has been linked to elevated glycolysis[280] and oxidative phosphorylation[,281]. Indeed, PPARγ, which is increased in high CB_2 HER2+ cancer (Figure 5.2.7) associates with RARs to regulate transcription[279].

RA signalling also leads to the increase of PYK2. Thus, CB_2 could regulate invasion by increasing PYK2 expression via ALDH1A1-mediated RA signalling. Furthermore, RA signalling has been shown to regulate the expression and activation of AKT[283],

which can further promote cancer cell invasion and the maintenance of stemness. Supporting this, we observed increased AKT expression and phosphorylation in HCC1954^{iCB2} cells upon CB_2 induction and AKT-dependent 3D invasion (Figure 6.3.3).

ALDH1A1 has further been implicated in the maintenance of CSCs in oesophageal cancer through interactions with β-catenin and activation of the Wnt/β-catenin pathway[345]. ALDH1A1 activity led to increased β-catenin expression and the subsequent expression of Wnt target genes[283]. Interestingly, the expression of ALDH1A1 can also be controlled by Wnt signalling, as TCF/LEF transcription factors have been shown to interact with the *ALDH1A1* promoter[346]. This could represent a positive feedback loop between ALDH1A1 and β-catenin, which could be initiated by CB_2. Additionally, CB_2 has previously been associated with the Wnt pathway[347], with cannabinoids inhibiting ALDH activity *in vivo* in rat models, suspectedly via Wnt pathway inhibition[334].

Notably, CB_2 expression in HER2+ breast cancer leads to increased expression of the Wnt ligand WNT10A, potentially leading to the autocrine activation of the Wnt/β-catenin pathway and ALDH1A1 expression. WNT10A is important in the maintenance of stemness in normal mammary stem cells[348], in addition to controlling the pluripotency of embryonic stem cells in the developing foetus[349]. Hence, I postulated that CB_2 controlled stemness and increased metastatic potential via WNT10A production, Wnt/β-catenin signalling and subsequent ALDH1A1 expression, leading to increased PYK2 and AKT in HCC1954^{iCB2} cells. In support of this hypothesis, CB_2 induced the translocation of β-catenin to the nucleus in HCC1954^{iCB2} cells, leading to TCF-regulated transcription (Figure 6.4.4) and increased ALDH1A1 mRNA and protein expression (Figure 6.2.2 and Figure 6.3.1). Thus, ALDH1A1 activity leads to the expression of PYK2[350] and AKT[283], increasing the metastatic potential of HER2+ CB_2+ breast cancer cells and contributing to

pluripotency maintenance and tumourigenesis. Therefore, CB_2 is an attractive target for anti-CSC therapies, potentially reducing the population of CSCs, leading to decreased rates of tumour metastasis and treatment resistance in HER2+ patients.

8.6 Cancer immunoediting

Immune evasion is essential for successful metastasis and occurs through immunoediting of the anticancer response[351]. In the first stage of immunoediting, elimination, the immune system recognises tumour neoantigens and initiates the secretion of proinflammatory cytokines and tumour cell killing by innate immune cells such as natural killer and dendritic cells[352]. Elimination is compounded by neoantigen presentation in the lymph nodes by antigen-presenting cells such as dendritic cells, leading to an adaptive immune response and expansion of tumour-specific T cells, contributing to tumour cell killing[351,352]. During equilibrium, the second stage of tumour immunoediting, resistance to anti-tumour immunity develops through the production of immunosuppressive cytokines and immune checkpoint proteins, recruitment of immunosuppressive immune cells or reduction in the immunogenicity of the tumour cells[351,352]. In the equilibrium stage of immunoediting, whilst the immune system cannot eradicate the tumour, it prevents uncontrolled tumour growth. However, further selection of immune-resistant clones, exacerbated by the presence of CSCs generating new clonal populations, enables tumour cells to escape the immune response in the final stage of immune editing[351].

8.6.1 Immune suppression in breast cancer

In breast cancer, immune escape can occur through the production of transforming growth factor beta (TGFβ), interleukin 10 (IL-10) and indoleamine 2,3-dioxygenase (IDO)[353], inhibiting immune function and increasing the recruitment of immune

suppressive T regulatory cells (Tregs), myeloid-derived suppressor cells (MDSCs) and TAMs[354]. Breast cancer cells further exacerbate immune suppression through the upregulation of immune checkpoint molecules such as PDL1 and CTLA4[355,356]. PDL1 mediates immune suppression through binding Programmed cell death protein 1 (PD1) on immune cells, triggering immune cell anergy and apoptosis[357]. Furthermore, engagement of PDL1 to PD1 on naïve T cells promotes differentiation to suppressive Treg cells[358]. PDL1 can also mediate cell growth and survival through reverse signalling in tumour cells[359]. Therefore, due to the importance of immune checkpoints in mediating immune escape, immune checkpoint inhibitors and therapeutic antibodies have been developed, such as the anti-PD1 mAb Pembrolizumab and the anti-PDL1 mAb Avelumab, both indicated in the treatment of HER2+ breast cancer[360,361].

8.6.2 CB_2-mediated immune escape

Here I report that increased PDL1 levels are associated with CB_2 expression in HER2+ breast cancer and thus implicate CB_2 in immune evasion. Increased PDL1 is seen in high CB_2 expressing HER2+ patients and HCC1954^{iCB2} cells (Figure 7.1.1). Notably, PDL1 is upregulated by the cells in the invasive protrusions of spheroids, suggesting that invading cancer cells have an increased likelihood of evading the immune system (Figure 7.2.1).

PDL1 expression can be regulated through the AKT/mTOR pathway[362], and we observed PDL1 staining on spheroids in an AKT-dependent manner (Figure 7.2.1 and Figure 7.2.2). This indicates that CB_2 can potentially mediate immune evasion through increased ALDH1A1 activity, leading to increased AKT expression and the subsequent increase in PDL1 expression. Therefore, activation of CB_2 with cannabinoids could lead to a reduction in AKT activity and hence reduced PDL1 expression, and therefore has the potential improve tumour immunogenicity. Indeed,

previous research has indicated that *in vitro* treatment with cannabinoids reduces levels of PDL1 expression in pancreatic cancer and glioblastoma cells[363], validating the therapeutic potential of targeting CB_2 in breast cancer to reduce immune suppression. Consequently, cannabinoids offer an attractive alternative to regulating anti-tumour immunity, in addition to their anti-proliferative, anti-metastatic and anti-stem action.

8.7 Conclusions

The HER2+ subtype represents an aggressive form of breast cancer with high rates of metastasis and poor prognosis. Whilst HER2-targeted therapies have drastically improved patient survival, the development of resistance and tumour recurrence is inevitable. CB_2 expression has been implicated in proliferation, invasion and metastasis of HER2+ breast cancer and represents an attractive therapeutic target. Treatment with well-tolerated cannabinoids, either synthetic or those derived from *Cannabis sativa*, have already demonstrated potent anti-tumour activity in both *in vitro* and *in vivo* preclinical studies.

In this thesis, I have further elucidated the tumourigenic role of CB_2 and implicated its expression in metabolic rearrangement, leading to a highly energetic phenotype with enhanced antioxidant potential, reminiscent of cancer stem cell metabolism. Further, I have identified an ALDH1A1+ CD44+ cancer stem cell population with enhanced mammosphere formation efficiency, dependent on CB_2 expression. Additionally, I have highlighted the role of CB_2 in activating the Wnt/β-catenin pathway, potentially promoting EMT and ALDH1A1 expression. Consequently, CB_2 expression results in a highly migratory stem-like phenotype with an increased invasive capacity, dependent on PYK2 and AKT activity.

Finally, I report that the CB_2-dependent increase in AKT expression and activity leads to an increase in the expression of the immune checkpoint protein PDL1. Importantly, PDL1 expression is localised to the invasive protrusions of 3D spheroids in an AKT-dependent manner, indicating the relevance of CB_2 mediating immune evasion during local invasion and metastasis.

These data suggest that CB_2 is a highly valuable prognostic marker in HER2+ breast cancer, and therapeutic targeting of CB_2 could lead to decreased stemness, metastasis, immune evasion and treatment resistance. Therefore, further research and validation of the mechanisms of CB_2 expression in *in vitro* and animal models is of high importance before the development of safe and efficacious cannabinoid-based therapies for combination treatment and the stratification of HER2+ breast cancer patients that would benefit from such treatments.

8.8 Future perspectives

Further work in the continuation of this project will be performed to validate the proposed mechanism of CB_2 mediated metabolic rearrangement and stem-phenotype, and further examine the role of CB_2 in mediating immune evasion. CB_2 function could be more extensively examined in the inducible system through CB_2 induction with dox and subsequent knockdown with shRNA, or even by reducing CB_2 expression via the removal of dox from culture media.

TCGA hits such as ZEB2, which were unable to be confirmed in the laboratory should be pursued to confirm their relevance in *in vitro* through RT-qPCR and western blotting. Whilst certain EMT markers changed upon CB_2 expression, functional changes related to the EMT phenotype could be assessed through the identification of morphological changes of cells, changes in cytoskeleton arrangement and wound scratch assays. Further investigation into the mechanism of CB_2-mediated cancer

invasion through PYK2 expression and potential regulation of MMP activity could be explored through CB_2 knockdown experiments, mentioned earlier.

Additional classification of stemness in HCC1954^{iCB2}, through techniques such as flow cytometry to analyse CSC marker expression (such as CD133, ESA and CD24, in addition to ALDH1A1 and CD44), would further validate the formation of a CSC population after CB_2 expression, which could be further verified by immunofluorescence of mammosphere sections. Flow cytometry could also identify what proportion of CB_2 expressing cells transform into CSCs and whether this is dependent on amount of CB_2 expression. The cancer stem phenotype could further be studied *in vivo* by with tumourgenicity studies in nude mice using HCC1954^{iCB2} cells with and without CB_2 expression. The presence of CB_2+ CSCs in patient tissue via IHC, RNA scope and imaging mass cytometry would confirm the role of CB_2 in the formation of CSCs. Furthermore, using matched patient tissue of primary tumour and lymph node metastasis would help identify at which stage the function of CB_2 contributes to the formation of the highly migratory stem like phenotype.

While CB_2 expression does have an effect on metabolism, further research is required to elucidate the full scope of metabolic rewiring. Firstly, more extensive analysis of metabolite changes by increasing number of biological replicates, across several cell lines would help isolate CB_2-specific metabolism changes.

Additional experimentation in this regard could investigate the FAO pathway and reduction in ROS. The antioxidant role of CB_2 could be further studied using fluorescent oxidative stress indicator CM-H2DCFDA and the examination of GPX3 expression through ELISA. The relevance of ALDH1A1 activity could be further confirmed through the use of ALDEFLUOR™ fluorescent reporter for ALDH activity.

Investigation into CB_2 conferring immune suppression with 3D spheroid T-cell killing assays would validate CB_2 mediated immune evasion in HER2+ breast cancer and highlight the importance of CB_2 expression in regards to influencing immunotherapy. Moreover, it would solidify the applicability of CB_2 as a therapeutic target if activation of CB_2 with JWH133 in these assays prevented immune evasion, as anticipated. This could be further explored *in vivo* in immune competent mice to examine whether CB_2 expressing HER2+ cells express sufficient levels of PDL1 to establish tumours.

Finally, examining HER2+ patient tissues with matched lymph node metastases for CB_2, PDL1, ALDH1A1 and CD44 expression would corroborate the role of CB_2 increasing immune evasion, CSC formation and metastatic potential in relevant patient samples, reinforcing the applicability of CB_2 as a clinical target.

Chapter 9 References

1. Arnold, M. *et al.* Current and future burden of breast cancer: Global statistics for 2020 and 2040. *The Breast* **66**, 15–23 (2022).

2. Lukong, K. E. Understanding breast cancer – The long and winding road. *BBA Clin* **7**, 64–77 (2017).

3. di Lonardo, A., Nasi, S. & Pulciani, S. Cancer: We Should Not Forget The Past. *J Cancer* **6**, 29–39 (2015).

4. Winchester, D. J., Winchester, D. P., Hudis, C. A. & Norton, L. *Breast Cancer*. (PMPH-USA, 2006).

5. Papavramidou, N., Papavramidis, T. & Demetriou, T. Ancient Greek and Greco–Roman Methods in Modern Surgical Treatment of Cancer. *Ann Surg Oncol* **17**, 665–667 (2010).

6. HALSTED, W. S. THE RESULTS OF RADICAL OPERATIONS FOR THE CURE OF CARCINOMA OF THE BREAST.*. *Ann Surg* **46**, 1–19 (1907).

7. MADDEN, J. L., KANDALAFT, S. & BOURQUE, R.-A. Modified Radical Mastectomy. *Ann Surg* **175**, 624–634 (1972).

8. Veronesi, U. *et al.* Twenty-Year Follow-up of a Randomized Study Comparing Breast-Conserving Surgery with Radical Mastectomy for Early Breast Cancer. *New England Journal of Medicine* **347**, 1227–1232 (2002).

9. Pope, M. H. Bernardino Ramazzini: The Father of Occupational Medicine. *Spine (Phila Pa 1976)* **29**, 2335–2338 (2004).

10. Lane-Claypon, J. E. A further report on cancer of the breast, with special reference to its associated antecedent conditions. *Ministry of Health. Reports on Public Health and Medical Subjects* **32**, (1926).

11. Kamińska, M., Ciszewski, T., Łopacka-Szatan, K., Miotła, P. & Starosławska, E. Breast cancer risk factors. *Menopausal Review* **3**, 196–202 (2015).

12. Miki, Y. *et al.* A Strong Candidate for the Breast and Ovarian Cancer Susceptibility Gene BRCA1. *Science (1979)* **266**, 66–71 (1994).

13. Wooster, R. *et al.* Identification of the breast cancer susceptibility gene BRCA2. *Nature* **378**, 789–792 (1995).

14. Warner, E. Screening BRCA1 and BRCA2 Mutation Carriers for Breast Cancer. *Cancers (Basel)* **10**, 477 (2018).

15. Narod, S. A. & Foulkes, W. D. BRCA1 and BRCA2: 1994 and beyond. *Nat Rev Cancer* **4**, 665–676 (2004).

16. Alaofi, R. K., Nassif, M. O. & Al-Hajeili, M. R. Prophylactic mastectomy for the prevention of breast cancer: Review of the literature. *Avicenna J Med* **8**, 67–77 (2018).

17. McClurg, D. P. *et al.* Analysis of the Clinical Advancements for BRCA-Related Malignancies Highlights the Lack of Treatment Evidence for BRCA-Positive Male Breast Cancer. *Cancers (Basel)* **14**, 3175 (2022).

18. Fox, S., Speirs, V. & Shaaban, A. M. Male breast cancer: an update. *Virchows Archiv* **480**, 85–93 (2022).

19. Keinan-Boker, L., Levine, H., Leiba, A., Derazne, E. & Kark, J. D. Adolescent obesity and adult male breast cancer in a cohort of 1,382,093 men. *Int J Cancer* **142**, 910–918 (2018).

20. Shaaban, A. M. *et al.* A comparative biomarker study of 514 matched cases of male and female breast cancer reveals gender-specific biological differences. *Breast Cancer Res Treat* **133**, 949–958 (2012).

21. Feng, Y. *et al.* Breast cancer development and progression: Risk factors, cancer stem cells, signaling pathways, genomics, and molecular pathogenesis. *Genes Dis* **5**, 77–106 (2018).

22. Carter, E. P., Gopsill, J. A., Gomm, Jennifer. J., Jones, J. L. & Grose, R. P. A 3D in vitro model of the human breast duct: a method to unravel myoepithelial-luminal interactions in the progression of breast cancer. *Breast Cancer Research* **19**, 50 (2017).

23. Kalluri, R. Basement membranes: structure, assembly and role in tumour angiogenesis. *Nat Rev Cancer* **3**, 422–433 (2003).

24. Riggio, A. I., Varley, K. E. & Welm, A. L. The lingering mysteries of metastatic recurrence in breast cancer. *Br J Cancer* **124**, 13–26 (2021).

25. Gibson, S. v. *et al.* Everybody needs good neighbours: the progressive DCIS microenvironment. *Trends Cancer* (2023) doi:10.1016/j.trecan.2023.01.002.

26. Borgquist, S. *et al.* The prognostic role of HER2 expression in ductal breast carcinoma in situ (DCIS); a population-based cohort study. *BMC Cancer* **15**, 468 (2015).

27. Place, A. E., Jin Huh, S. & Polyak, K. The microenvironment in breast cancer progression: biology and implications for treatment. *Breast Cancer Research* **13**, 227 (2011).

28. Ma, X.-J. *et al.* Gene expression profiles of human breast cancer progression. *Proceedings of the National Academy of Sciences* **100**, 5974–5979 (2003).

29. Bombonati, A. & Sgroi, D. C. The molecular pathology of breast cancer progression. *J Pathol* **223**, 308–318 (2011).

30. Allinen, M. *et al.* Molecular characterization of the tumor microenvironment in breast cancer. *Cancer Cell* **6**, 17–32 (2004).

31. Ma, X.-J., Dahiya, S., Richardson, E., Erlander, M. & Sgroi, D. C. Gene expression profiling of the tumor microenvironment during breast cancer progression. *Breast Cancer Research* **11**, R7 (2009).

32. Chabottaux, V. & Noel, A. Breast cancer progression: insights into multifaceted matrix metalloproteinases. *Clin Exp Metastasis* **24**, 647–656 (2007).

33. Jedeszko, C., Victor, B. C., Podgorski, I. & Sloane, B. F. Fibroblast Hepatocyte Growth Factor Promotes Invasion of Human Mammary Ductal Carcinoma In situ. *Cancer Res* **69**, 9148–9155 (2009).

34. Orimo, A. *et al.* Stromal Fibroblasts Present in Invasive Human Breast Carcinomas Promote Tumor Growth and Angiogenesis through Elevated SDF-1/CXCL12 Secretion. *Cell* **121**, 335–348 (2005).

35. Hu, M. *et al.* Distinct epigenetic changes in the stromal cells of breast cancers. *Nat Genet* **37**, 899–905 (2005).

36. Fiegl, H. *et al.* Breast Cancer DNA Methylation Profiles in Cancer Cells and Tumor Stroma: Association with HER-2/neu Status in Primary Breast Cancer. *Cancer Res* **66**, 29–33 (2006).

37. Mantovani, A., Marchesi, F., Malesci, A., Laghi, L. & Allavena, P. Tumour-associated macrophages as treatment targets in oncology. *Nat Rev Clin Oncol* **14**, 399–416 (2017).

38. Jeong, H., Hwang, I., Kang, S. H., Shin, H. C. & Kwon, S. Y. Tumor-Associated Macrophages as Potential Prognostic Biomarkers of Invasive Breast Cancer. *J Breast Cancer* **22**, 38 (2019).

39. Yang, C. *et al.* Comparison of Overall Survival Between Invasive Lobular Breast Carcinoma and Invasive Ductal Breast Carcinoma: A Propensity Score Matching Study Based on SEER Database. *Front Oncol* **10**, (2020).

40. van Seijen, M. *et al.* Ductal carcinoma in situ: to treat or not to treat, that is the question. *Br J Cancer* **121**, 285–292 (2019).

41. Dillekås, H., Rogers, M. S. & Straume, O. Are 90% of deaths from cancer caused by metastases? *Cancer Med* **8**, 5574–5576 (2019).

42. Wei, Y.-N. *et al.* Clinicopathologic characteristics of HER2-positive pure mucinous breast carcinoma: a systematic investigation into an unusual tumor. *Int J Clin Exp Pathol* **12**, 1666–1677 (2019).

43. Talmadge, J. E. & Fidler, I. J. AACR Centennial Series: The Biology of Cancer Metastasis: Historical Perspective. *Cancer Res* **70**, 5649–5669 (2010).

44. Dasgupta, A., Lim, A. R. & Ghajar, C. M. Circulating and disseminated tumor cells: harbingers or initiators of metastasis? *Mol Oncol* **11**, 40–61 (2017).

45. Douma, S. *et al.* Suppression of anoikis and induction of metastasis by the neurotrophic receptor TrkB. *Nature* **430**, 1034–1039 (2004).

46. Valastyan, S. & Weinberg, R. A. Tumor Metastasis: Molecular Insights and Evolving Paradigms. *Cell* **147**, 275–292 (2011).

47. Luzzi, K. J. *et al.* Multistep Nature of Metastatic Inefficiency. *Am J Pathol* **153**, 865–873 (1998).

48. Chambers, A. F., Groom, A. C. & MacDonald, I. C. Dissemination and growth of cancer cells in metastatic sites. *Nat Rev Cancer* **2**, 563–572 (2002).

49. Gomis, R. R. & Gawrzak, S. Tumor cell dormancy. *Mol Oncol* **11**, 62–78 (2017).

50. Sosa, M. S., Bragado, P. & Aguirre-Ghiso, J. A. Mechanisms of disseminated cancer cell dormancy: an awakening field. *Nat Rev Cancer* **14**, 611–622 (2014).

51. Perou, C. M. *et al.* Molecular portraits of human breast tumours. *Nature* **406**, 747–752 (2000).

52. Sonnenblick, A., Fumagalli, D., Sotiriou, C. & Piccart, M. Is the differentiation into molecular subtypes of breast cancer important for staging, local and systemic therapy, and follow up? *Cancer Treat Rev* **40**, 1089–1095 (2014).

53. Cheang, M. C. U. *et al.* Ki67 Index, HER2 Status, and Prognosis of Patients With Luminal B Breast Cancer. *JNCI: Journal of the National Cancer Institute* **101**, 736–750 (2009).

54. Yersal, O. Biological subtypes of breast cancer: Prognostic and therapeutic implications. *World J Clin Oncol* **5**, 412 (2014).

55. Hennigs, A. *et al.* Prognosis of breast cancer molecular subtypes in routine clinical care: A large prospective cohort study. *BMC Cancer* **16**, 734 (2016).

56. Lindström, L. *et al.* Long-term benefit from tamoxifen therapy for patients with Luminal A and Luminal B breast cancer: Retrospective analysis of the STO-3 trial. *Journal of Clinical Oncology* **36**, 541–541 (2018).

57. Creighton, C. The molecular profile of luminal B breast cancer. *Biologics* 289 (2012) doi:10.2147/BTT.S29923.

58. Boyle, P. Triple-negative breast cancer: epidemiological considerations and recommendations. *Annals of Oncology* **23**, vi7–vi12 (2012).

59. Heitz, F. *et al.* Triple-negative and HER2-overexpressing breast cancers exhibit an elevated risk and an earlier occurrence of cerebral metastases. *Eur J Cancer* **45**, 2792–2798 (2009).

60. Pistelli, M. *et al.* Prognostic factors in early-stage triple-negative breast cancer: lessons and limits from clinical practice. *Anticancer Res* **33**, 2737–42 (2013).

61. Foulkes, W. D. *et al.* The Prognostic Implication of the Basal-Like (Cyclin Ehigh/p27low/p53+/Glomeruloid-Microvascular-Proliferation+) Phenotype of BRCA1-Related Breast Cancer. *Cancer Res* **64**, 830–835 (2004).

62. Cronin, K. A., Harlan, L. C., Dodd, K. W., Abrams, J. S. & Ballard-Barbash, R. Population-based Estimate of the Prevalence of HER-2 Positive Breast Cancer Tumors for Early Stage Patients in the US. *Cancer Invest* **28**, 963–968 (2010).

63. Fan, Y.-S. *et al.* HER2 FISH classification of equivocal HER2 IHC breast cancers with use of the 2013 ASCO/CAP practice guideline. *Breast Cancer Res Treat* **155**, 457–462 (2016).

64. Daemen, A. & Manning, G. HER2 is not a cancer subtype but rather a pan-cancer event and is highly enriched in AR-driven breast tumors. *Breast Cancer Research* **20**, 8 (2018).

65. Roskoski, R. The ErbB/HER family of protein-tyrosine kinases and cancer. *Pharmacol Res* **79**, 34–74 (2014).

66. Gutierrez, C. & Schiff, R. HER2: biology, detection, and clinical implications. *Arch Pathol Lab Med* **135**, 55–62 (2011).

67. Graus-Porta, D. ErbB-2, the preferred heterodimerization partner of all ErbB receptors, is a mediator of lateral signaling. *EMBO J* **16**, 1647–1655 (1997).

68. Grant, S. Roles of Erbb family receptor tyrosine kinases, and downstream signaling pathways, in the control of cell growth and survival. *Frontiers in Bioscience* **7**, d376 (2002).

69. Rexer, B. N. & Arteaga, C. L. Intrinsic and Acquired Resistance to HER2-Targeted Therapies in HER2 Gene-Amplified Breast Cancer: Mechanisms and Clinical Implications. *Crit Rev Oncog* **17**, 1–16 (2012).

70. Moasser, M. M. The oncogene HER2: its signaling and transforming functions and its role in human cancer pathogenesis. *Oncogene* **26**, 6469–6487 (2007).

71. Johnson, K. S., Conant, E. F. & Soo, M. S. Molecular Subtypes of Breast Cancer: A Review for Breast Radiologists. *J Breast Imaging* **3**, 12–24 (2021).

72. Fedorova, O. *et al.* Attenuation of p53 mutant as an approach for treatment Her2-positive cancer. *Cell Death Discov* **6**, 100 (2020).

73. Ellsworth, R. E. *et al.* Amplification of HER2 is a marker for global genomic instability. *BMC Cancer* **8**, 297 (2008).

74. Turpin, J. *et al.* The ErbB2ΔEx16 splice variant is a major oncogenic driver in breast cancer that promotes a pro-metastatic tumor microenvironment. *Oncogene* **35**, 6053–6064 (2016).

75. Scaltriti, M. *et al.* Expression of p95HER2, a Truncated Form of the HER2 Receptor, and Response to Anti-HER2 Therapies in Breast Cancer. *JNCI Journal of the National Cancer Institute* **99**, 628–638 (2007).

76. Dias, K. *et al.* Claudin-Low Breast Cancer; Clinical & Pathological Characteristics. *PLoS One* **12**, e0168669 (2017).

77. Dowsett, M. *et al.* Relationship Between Quantitative Estrogen and Progesterone Receptor Expression and Human Epidermal Growth Factor Receptor 2 (HER-2) Status With Recurrence in the Arimidex, Tamoxifen, Alone or in Combination Trial. *Journal of Clinical Oncology* **26**, 1059–1065 (2008).

78. Lal, P., Tan, L. K. & Chen, B. Correlation of HER-2 Status With Estrogen and Progesterone Receptors and Histologic Features in 3,655 Invasive Breast Carcinomas. *Am J Clin Pathol* **123**, 541–546 (2005).

79. Cardoso, F. *et al.* 70-Gene Signature as an Aid to Treatment Decisions in Early-Stage Breast Cancer. *New England Journal of Medicine* **375**, 717–729 (2016).

80. Paik, S. *et al.* A Multigene Assay to Predict Recurrence of Tamoxifen-Treated, Node-Negative Breast Cancer. *New England Journal of Medicine* **351**, 2817–2826 (2004).

81. Vu, T. & Claret, F. X. Trastuzumab: Updated Mechanisms of Action and Resistance in Breast Cancer. *Front Oncol* **2**, (2012).

82. Hudis, C. A. Trastuzumab — Mechanism of Action and Use in Clinical Practice. *New England Journal of Medicine* **357**, 39–51 (2007).

83. Junttila, T. T. *et al.* Ligand-Independent HER2/HER3/PI3K Complex Is Disrupted by Trastuzumab and Is Effectively Inhibited by the PI3K Inhibitor GDC-0941. *Cancer Cell* **15**, 429–440 (2009).

84. Krasniqi, E. *et al.* Immunotherapy in HER2-positive breast cancer: state of the art and future perspectives. *J Hematol Oncol* **12**, 111 (2019).

85. Collins, D. M. *et al.* Trastuzumab induces antibody-dependent cell-mediated cytotoxicity (ADCC) in HER-2-non-amplified breast cancer cell lines. *Annals of Oncology* **23**, 1788–1795 (2012).

86. Lo Nigro, C. *et al.* NK-mediated antibody-dependent cell-mediated cytotoxicity in solid tumors: biological evidence and clinical perspectives. *Ann Transl Med* **7**, 105–105 (2019).

87. Slamon, D. *et al.* Adjuvant Trastuzumab in HER2-Positive Breast Cancer. *New England Journal of Medicine* **365**, 1273–1283 (2011).

88. Takada, M. & Toi, M. Neoadjuvant treatment for HER2-positive breast cancer. *Chin Clin Oncol* **9**, 32–32 (2020).

89. Figueroa-Magalhães, M. C., Jelovac, D., Connolly, R. M. & Wolff, A. C. Treatment of HER2-positive breast cancer. *The Breast* **23**, 128–136 (2014).

90. Ali, S. *et al.* Efficacy of adjuvant trastuzumab in women with HER2-positive T1a or bN0M0 breast cancer: a population-based cohort study. *Sci Rep* **12**, 1068 (2022).

91. Untch, M. & Lück, H.-J. Lapatinib – Member of a New Generation of ErbB-Targeting Drugs. *Breast Care* **5**, 8–12 (2010).

92. Gui, X., Li, H., Yan, Y. & Zhang, R. Efficacy of lapatinib combined with capecitabine in patients with HER2-positive metastatic breast cancer in a real-world study. *Oncol Lett* **20**, 1–1 (2020).

93. Opdam, F. L., Guchelaar, H.-J., Beijnen, J. H. & Schellens, J. H. M. Lapatinib for advanced or metastatic breast cancer. *Oncologist* **17**, 536–42 (2012).

94. Xu, Z. *et al.* Efficacy and safety of lapatinib and trastuzumab for HER2-positive breast cancer: a systematic review and meta-analysis of randomised controlled trials. *BMJ Open* **7**, e013053 (2017).

95. Cortés, J. *et al.* Trastuzumab Deruxtecan versus Trastuzumab Emtansine for Breast Cancer. *New England Journal of Medicine* **386**, 1143–1154 (2022).

96. Moinard-Butot, F. *et al.* Efficacy of trastuzumab emtansine (T-DM1) and lapatinib after dual HER2 inhibition with trastuzumab and pertuzumab in patient with metastatic breast cancer: Retrospective data from a French multicenter real-life cohort. *The Breast* **63**, 54–60 (2022).

97. Modi, S. *et al.* Trastuzumab Deruxtecan in Previously Treated HER2-Positive Breast Cancer. *New England Journal of Medicine* **382**, 610–621 (2020).

98. Teicher, B. A. & Doroshow, J. H. The Promise of Antibody–Drug Conjugates. *New England Journal of Medicine* **367**, 1847–1848 (2012).

99. Iwata, T. N. *et al.* A HER2-Targeting Antibody–Drug Conjugate, Trastuzumab Deruxtecan (DS-8201a), Enhances Antitumor Immunity in a Mouse Model. *Mol Cancer Ther* **17**, 1494–1503 (2018).

100. Singh, A. P., Sharma, S. & Shah, D. K. Quantitative characterization of in vitro bystander effect of antibody-drug conjugates. *J Pharmacokinet Pharmacodyn* **43**, 567–582 (2016).

101. Xiao, W. *et al.* Breast cancer subtypes and the risk of distant metastasis at initial diagnosis: a population-based study. *Cancer Manag Res* **10**, 5329–5338 (2018).

102. Nahta, R. & Esteva, F. J. HER2 therapy: Molecular mechanisms of trastuzumab resistance. *Breast Cancer Research* **8**, 215 (2006).

103. Mitra, D. *et al.* An oncogenic isoform of HER2 associated with locally disseminated breast cancer and trastuzumab resistance. *Mol Cancer Ther* **8**, 2152–2162 (2009).

104. Castagnoli, L. *et al.* Activated d16HER2 Homodimers and SRC Kinase Mediate Optimal Efficacy for Trastuzumab. *Cancer Res* **74**, 6248–6259 (2014).

105. Nagy, P. *et al.* Decreased accessibility and lack of activation of ErbB2 in JIMT-1, a herceptin-resistant, MUC4-expressing breast cancer cell line. *Cancer Res* **65**, 473–82 (2005).

106. Nagata, Y. *et al.* PTEN activation contributes to tumor inhibition by trastuzumab, and loss of PTEN predicts trastuzumab resistance in patients. *Cancer Cell* **6**, 117–127 (2004).

107. Bachman, K. E. *et al.* The PIK3CA gene is mutated with high frequency in human breast cancers. *Cancer Biol Ther* **3**, 772–775 (2004).

108. Motoyama, A. B., Hynes, N. E. & Lane, H. A. The efficacy of ErbB receptor-targeted anticancer therapeutics is influenced by the availability of epidermal growth factor-related peptides. *Cancer Res* **62**, 3151–8 (2002).

109. Pohlmann, P. R., Mayer, I. A. & Mernaugh, R. Resistance to Trastuzumab in Breast Cancer. *Clin. Cancer Res.* **15**, 7479–7491 (2009).

110. Huang, X. *et al.* Heterotrimerization of the Growth Factor Receptors erbB2, erbB3, and Insulin-like Growth Factor-I Receptor in Breast Cancer Cells Resistant to Herceptin. *Cancer Res* **70**, 1204–1214 (2010).

111. Scaltriti, M. *et al.* Cyclin E amplification/overexpression is a mechanism of trastuzumab resistance in HER2 $^{+}$ breast cancer patients. *PNAS* **108**, 3761–3766 (2011).

112. Oliveras-Ferraros, C. *et al.* Inhibitor of Apoptosis (IAP) survivin is indispensable for survival of HER2 gene-amplified breast cancer cells with primary resistance to HER1/2-targeted therapies. *Biochem Biophys Res Commun* **407**, 412–419 (2011).

113. Tanizaki, J. *et al.* Roles of BIM induction and survivin downregulation in lapatinib-induced apoptosis in breast cancer cells with HER2 amplification. *Oncogene* **30**, 4097–4106 (2011).

114. Warmerdam, P. A., van de Winkel, J. G., Vlug, A., Westerdaal, N. A. & Capel, P. J. A single amino acid in the second Ig-like domain of the human Fc gamma receptor II is critical for human IgG2 binding. *J Immunol* **147**, 1338–43 (1991).

115. Luque-Bolivar, A., Pérez-Mora, E., Villegas, V. E. & Rondón-Lagos, M. Resistance and Overcoming Resistance in Breast Cancer. *Breast Cancer: Targets and Therapy* **12**, 211–229 (2020).

116. Yang, J. *et al.* Prediction of HER2-positive breast cancer recurrence and metastasis risk from histopathological images and clinical information via multimodal deep learning. *Comput Struct Biotechnol J* **20**, 333–342 (2022).

117. Blackwell, K. L. *et al.* Randomized Study of Lapatinib Alone or in Combination With Trastuzumab in Women With ErbB2-Positive, Trastuzumab-Refractory Metastatic Breast Cancer. *Journal of Clinical Oncology* **28**, 1124–1130 (2010).

118. Baselga, J. *et al.* Abstract S3-3: First Results of the NeoALTTO Trial (BIG 01-06/EGF 106903): A Phase III, Randomized, Open Label, Neoadjuvant Study of Lapatinib, Trastuzumab, and Their Combination Plus Paclitaxel in Women with HER2-Positive Primary Breast Cancer. *Cancer Res* **70**, S3-3-S3-3 (2010).

119. Newman, D. J. The “Utility” of Highly Toxic Marine-Sourced Compounds. *Mar Drugs* **17**, 324 (2019).

120. Skidmore, L. *et al.* ARX788, a Site-specific Anti-HER2 Antibody–Drug Conjugate, Demonstrates Potent and Selective Activity in HER2-low and T-DM1–resistant Breast and Gastric Cancers. *Mol Cancer Ther* **19**, 1833–1843 (2020).

121. Newman, D. & Cragg, G. Current Status of Marine-Derived Compounds as Warheads in Anti-Tumor Drug Candidates. *Mar Drugs* **15**, 99 (2017).

122. Barok, M. *et al.* ARX788, a novel anti-HER2 antibody-drug conjugate, shows anti-tumor effects in preclinical models of trastuzumab emtansine-resistant HER2-positive breast cancer and gastric cancer. *Cancer Lett* **473**, 156–163 (2020).

123. Nunnery, S. E. & Mayer, I. A. Management of toxicity to isoform α-specific PI3K inhibitors. *Annals of Oncology* **30**, x21–x26 (2019).

124. Velasco, G., Sánchez, C. & Guzmán, M. Anticancer Mechanisms of Cannabinoids. *Current Oncology* **23**, 23–32 (2016).

125. Lu, H.-C. & Mackie, K. An Introduction to the Endogenous Cannabinoid System. *Biol Psychiatry* **79**, 516–525 (2016).

126. De Petrocellis, L., Melck, D., Bisogno, T., Milone, A. & Di Marzo, V. Finding of the endocannabinoid signalling system in Hydra, a very primitive organism: possible role in the feeding response. *Neuroscience* **92**, 377–387 (1999).

127. Silver, R. J. The Endocannabinoid System of Animals. *Animals* **9**, 686 (2019).

128. Lu, H.-C. & Mackie, K. Review of the Endocannabinoid System. *Biol Psychiatry Cogn Neurosci Neuroimaging* **6**, 607–615 (2021).

129. di Marzo, V., de Petrocellis, L., Bisogno, T. & Melck, D. Metabolism of anandamide and 2-arachidonoylglycerol: An historical overview and some recent developments. *Lipids* **34**, S319–S325 (1999).

130. Murataeva, N., Straiker, A. & Mackie, K. Parsing the players: 2-arachidonoylglycerol synthesis and degradation in the CNS. *Br J Pharmacol* **171**, 1379–1391 (2014).

131. Blankman, J. L., Simon, G. M. & Cravatt, B. F. A Comprehensive Profile of Brain Enzymes that Hydrolyze the Endocannabinoid 2-Arachidonoylglycerol. *Chem Biol* **14**, 1347–1356 (2007).

132. Hermanson, D. J., Gamble-George, J. C., Marnett, L. J. & Patel, S. Substrate-selective COX-2 inhibition as a novel strategy for therapeutic endocannabinoid augmentation. *Trends Pharmacol Sci* **35**, 358–367 (2014).

133. Cravatt, B. F. *et al.* Supersensitivity to anandamide and enhanced endogenous cannabinoid signaling in mice lacking fatty acid amide hydrolase. *Proceedings of the National Academy of Sciences* **98**, 9371–9376 (2001).

134. Almeida, C. F., Teixeira, N., Correia-da-Silva, G. & Amaral, C. Cannabinoids in Breast Cancer: Differential Susceptibility According to Subtype. *Molecules* **27**, 156 (2021).

135. Laezza, C. *et al.* The Endocannabinoid System: A Target for Cancer Treatment. *Int J Mol Sci* **21**, 747 (2020).

136. Li, H.-L. An archaeological and historical account of cannabis in China. *Econ Bot* **28**, 437–448 (1973).

137. Atalay, S., Jarocka-Karpowicz, I. & Skrzydlewska, E. Antioxidative and Anti-Inflammatory Properties of Cannabidiol. *Antioxidants* **9**, 21 (2019).

138. Tham, M. *et al.* Allosteric and orthosteric pharmacology of cannabidiol and cannabidiol-dimethylheptyl at the type 1 and type 2 cannabinoid receptors. *Br J Pharmacol* **176**, 1455–1469 (2019).

139. Pisanti, S. *et al.* Cannabidiol: State of the art and new challenges for therapeutic applications. *Pharmacol Ther* **175**, 133–150 (2017).

140. di Marzo, V. New approaches and challenges to targeting the endocannabinoid system. *Nat Rev Drug Discov* **17**, 623–639 (2018).

141. Mackie, K. Distribution of Cannabinoid Receptors in the Central and Peripheral Nervous System. in *Cannabinoids* 299–325 (Springer-Verlag). doi:10.1007/3-540-26573-2_10.

142. Castillo, P. E., Younts, T. J., Chávez, A. E. & Hashimotodani, Y. Endocannabinoid Signaling and Synaptic Function. *Neuron* **76**, 70–81 (2012).

143. Wang, X., Dow-Edwards, D., Keller, E. & Hurd, Y. L. Preferential limbic expression of the cannabinoid receptor mRNA in the human fetal brain. *Neuroscience* **118**, 681–694 (2003).

144. Turcotte, C., Blanchet, M.-R., Laviolette, M. & Flamand, N. The CB2 receptor and its role as a regulator of inflammation. *Cellular and Molecular Life Sciences* **73**, 4449–4470 (2016).

145. Atwood, B. K. & Mackie, K. CB2: a cannabinoid receptor with an identity crisis. *Br J Pharmacol* **160**, 467–479 (2010).

146. Jean-Gilles, L. *et al.* Effects of pro-inflammatory cytokines on cannabinoid CB1and CB2receptors in immune cells. *Acta Physiologica* **214**, 63–74 (2015).

147. Ashton, J. & Glass, M. The Cannabinoid CB2 Receptor as a Target for Inflammation-Dependent Neurodegeneration. *Curr Neuropharmacol* **5**, 73–80 (2007).

148. Saroz, Y., Kho, D. T., Glass, M., Graham, E. S. & Grimsey, N. L. Cannabinoid Receptor 2 (CB2) Signals via G-alpha-s and Induces IL-6 and IL-10 Cytokine Secretion in Human Primary Leukocytes. *ACS Pharmacol Transl Sci* **2**, 414–428 (2019).

149. Miller, A. M. & Stella, N. CB2 receptor-mediated migration of immune cells: it can go either way. *Br J Pharmacol* **153**, 299–308 (2008).

150. Almogi-Hazan, O. & Or, R. Cannabis, the Endocannabinoid System and Immunity—the Journey from the Bedside to the Bench and Back. *Int J Mol Sci* **21**, 4448 (2020).

151. Pesce, M. *et al.* Endocannabinoid-related compounds in gastrointestinal diseases. *J Cell Mol Med* (2017) doi:10.1111/jcmm.13359.

152. Howlett, A. C. International Union of Pharmacology. XXVII. Classification of Cannabinoid Receptors. *Pharmacol Rev* **54**, 161–202 (2002).

153. Howlett, A., Blume, L. & Dalton, G. CB1 Cannabinoid Receptors and their Associated Proteins. *Curr Med Chem* **17**, 1382–1393 (2010).

154. Calandra, B. *et al.* Dual intracellular signaling pathways mediated by the human cannabinoid CB1 receptor. *Eur J Pharmacol* **374**, 445–455 (1999).

155. Ibsen, M. S., Connor, M. & Glass, M. Cannabinoid CB1 and CB2 Receptor Signaling and Bias. *Cannabis Cannabinoid Res* **2**, 48–60 (2017).

156. Howlett, A. C. *et al.* The cannabinoid receptor: biochemical, anatomical and behavioral characterization. *Trends Neurosci* **13**, 420–423 (1990).

157. Scarlett, K. A. *et al.* Agonist-induced CXCR4 and CB2 Heterodimerization Inhibits Gα13/RhoA-mediated Migration. *Molecular Cancer Research* **16**, 728–739 (2018).

158. Urbi, B. *et al.* Effects of cannabinoids in Amyotrophic Lateral Sclerosis (ALS) murine models: a systematic review and meta-analysis. *J Neurochem* **149**, 284–297 (2019).

159. Carroll, C. B., Zeissler, M.-L., Hanemann, C. O. & Zajicek, J. P. Δ 9-tetrahydrocannabinol (Δ9-THC) exerts a direct neuroprotective effect in a human cell culture model of Parkinson's disease. *Neuropathol Appl Neurobiol* **38**, 535–547 (2012).

160. Maurya, N. & Velmurugan, B. K. Therapeutic applications of cannabinoids. *Chem Biol Interact* **293**, 77–88 (2018).

161. Ware, M. A review of nabilone in the treatment of chemotherapy-induced nausea and vomiting. *Ther Clin Risk Manag* **Volume 4**, 99–107 (2008).

162. Keating, G. M. Delta-9-Tetrahydrocannabinol/Cannabidiol Oromucosal Spray (Sativex®): A Review in Multiple Sclerosis-Related Spasticity. *Drugs* **77**, 563–574 (2017).

163. Tomida, I. Cannabinoids and glaucoma. *British Journal of Ophthalmology* **88**, 708–713 (2004).

164. Mack, A. & Joy, J. MARIJUANA AND GLAUCOMA. in *Marijuana as Medicine? The Science Beyond the Controversy.* (National Academies Press (US), 2000).

165. Elikkottil, J., Gupta, P. & Gupta, K. The analgesic potential of cannabinoids. *J Opioid Manag* **5**, 341–57 (2009).

166. Guindon, J. & Hohmann, A. G. The endocannabinoid system and cancer: therapeutic implication. *Br J Pharmacol* **163**, 1447–1463 (2011).

167. Xu, F. *et al.* Cannabidiol promotes apoptosis of osteosarcoma cells in vitro and in vivo by activating the SP1-CBX2 axis. *Am J Transl Res* **14**, 1188–1203 (2022).

168. Ramer, R., Schwarz, R. & Hinz, B. Modulation of the Endocannabinoid System as a Potential Anticancer Strategy. *Front Pharmacol* **10**, (2019).

169. Pisanti, S., Picardi, P., D'Alessandro, A., Laezza, C. & Bifulco, M. The endocannabinoid signaling system in cancer. *Trends Pharmacol Sci* **34**, 273–282 (2013).

170. Khunluck, T. *et al.* Activation of cannabinoid receptors in breast cancer cells improves osteoblast viability in cancer-bone interaction model while reducing breast cancer cell survival and migration. *Sci Rep* **12**, 7398 (2022).

171. Elbaz, M., Ahirwar, D., Ravi, J., Nasser, M. W. & Ganju, R. K. Novel role of cannabinoid receptor 2 in inhibiting EGF/EGFR and IGF-I/IGF-IR pathways in breast cancer. *Oncotarget* **8**, 29668–29678 (2017).

172. Pérez-Gómez, E. *et al.* Role of cannabinoid receptor CB2 in HER2 pro-oncogenic signaling in breast cancer. *J Natl Cancer Inst* **107**, (2015).

173. Blasco-Benito, S. *et al.* Therapeutic targeting of HER2–CB 2 R heteromers in HER2-positive breast cancer. *Proc Natl Acad Sci U S A* **116**, 3863–3872 (2019).

174. Di Liberto, V., Mudò, G. & Belluardo, N. Crosstalk between receptor tyrosine kinases (RTKs) and G protein-coupled receptors (GPCR) in the brain: Focus on heteroreceptor complexes and related functional neurotrophic effects. *Neuropharmacology* **152**, 67–77 (2019).

175. Negro, A. *et al.* erbB2 is required for G protein-coupled receptor signaling in the heart. *Proceedings of the National Academy of Sciences* **103**, 15889–15893 (2006).

176. Munson, A. E., Harris, L. S., Friedman, M. A., Dewey, W. L. & Carchman, R. A. Antineoplastic Activity of Cannabinoids2. *JNCI: Journal of the National Cancer Institute* **55**, 597–602 (1975).

177. Salazar, M. *et al.* Cannabinoid action induces autophagy-mediated cell death through stimulation of ER stress in human glioma cells. *Journal of Clinical Investigation* **119**, 1359–1372 (2009).

178. Torres, S. *et al.* A Combined Preclinical Therapy of Cannabinoids and Temozolomide against Glioma. *Mol Cancer Ther* **10**, 90–103 (2011).

179. Caffarel, M. M., Andradas, C., Pérez-Gómez, E., Guzmán, M. & Sánchez, C. Cannabinoids: A new hope for breast cancer therapy? *Cancer Treat Rev* **38**, 911–918 (2012).

180. Caffarel, M. M., Sarrió, D., Palacios, J., Guzmán, M. & Sánchez, C. Δ9-Tetrahydrocannabinol Inhibits Cell Cycle Progression in Human Breast Cancer Cells through Cdc2 Regulation. *Cancer Res* **66**, 6615–6621 (2006).

181. Laezza, C. *et al.* Anandamide inhibits the Wnt/β-catenin signalling pathway in human breast cancer MDA MB 231 cells. *Eur J Cancer* **48**, 3112–3122 (2012).

182. Sulcova, E. Biphasic Effects of Anandamide. *Pharmacol Biochem Behav* **59**, 347–352 (1998).

183. Caffarel, M. M. *et al.* Cannabinoids reduce ErbB2-driven breast cancer progression through Akt inhibition. *Mol Cancer* **9**, 1–11 (2010).

184. Kisková, T., Mungenast, F., Suváková, M., Jäger, W. & Thalhammer, T. Future Aspects for Cannabinoids in Breast Cancer Therapy. *Int J Mol Sci* **20**, 1673 (2019).

185. Shrivastava, A., Kuzontkoski, P. M., Groopman, J. E. & Prasad, A. Cannabidiol Induces Programmed Cell Death in Breast Cancer Cells by Coordinating the Cross-talk between Apoptosis and Autophagy. *Mol Cancer Ther* **10**, 1161–1172 (2011).

186. Moreno, E. *et al.* Correction for Blasco-Benito et al., Therapeutic targeting of HER2–CB2R heteromers in HER2-positive breast cancer. *Proceedings of the National Academy of Sciences* **116**, 6505–6505 (2019).

187. Gazdar, A. F. *et al.* Characterization of paired tumor and non-tumor cell lines established from patients with breast cancer. *Int J Cancer* **78**, 766–774 (1998).

188. Fogh, J., Fogh, J. M. & Orfeo, T. One Hundred and Twenty-Seven Cultured Human Tumor Cell Lines Producing Tumors in Nude Mice23. *JNCI: Journal of the National Cancer Institute* **59**, 221–226 (1977).

189. Lasfargues, E. Y., Coutinho, W. G. & Redfield, E. S. Isolation of two human tumor epithelial cell lines from solid breast carcinomas. *J Natl Cancer Inst* **61**, 967–78 (1978).

190. DuBridge, R. B. *et al.* Analysis of mutation in human cells by using an Epstein-Barr virus shuttle system. *Mol Cell Biol* **7**, 379–387 (1987).

191. Katzen, F. Gateway ® recombinational cloning: a biological operating system. *Expert Opin Drug Discov* **2**, 571–589 (2007).

192. Lánczky, A. & Győrffy, B. Web-Based Survival Analysis Tool Tailored for Medical Research (KMplot): Development and Implementation. *J Med Internet Res* **23**, e27633 (2021).

193. Gao, J. *et al.* Integrative Analysis of Complex Cancer Genomics and Clinical Profiles Using the cBioPortal. *Sci Signal* **6**, (2013).

194. Cerami, E. *et al.* The cBio Cancer Genomics Portal: An Open Platform for Exploring Multidimensional Cancer Genomics Data. *Cancer Discov* **2**, 401–404 (2012).

195. Lombardo, Y., de Giorgio, A., Coombes, C. R., Stebbing, J. & Castellano, L. Mammosphere Formation Assay from Human Breast Cancer Tissues and Cell Lines. *Journal of Visualized Experiments* (2015) doi:10.3791/52671.

196. Schneider, C. A., Rasband, W. S. & Eliceiri, K. W. NIH Image to ImageJ: 25 years of image analysis. *Nat Methods* **9**, 671–675 (2012).

197. Kallunki, Barisic, Jäättelä & Liu. How to Choose the Right Inducible Gene Expression System for Mammalian Studies? *Cells* **8**, 796 (2019).

198. Meerbrey, K. L. *et al.* The pINDUCER lentiviral toolkit for inducible RNA interference in vitro and in vivo. *Proceedings of the National Academy of Sciences* **108**, 3665–3670 (2011).

199. Reece-Hoyes, J. S. & Walhout, A. J. M. Gateway Recombinational Cloning. *Cold Spring Harb Protoc* **2018**, pdb.top094912 (2018).

200. Bahassi, E. M. *et al.* Interactions of CcdB with DNA Gyrase. *Journal of Biological Chemistry* **274**, 10936–10944 (1999).

201. Cyr, C. *et al.* Cannabis in palliative care: current challenges and practical recommendations. *Ann Palliat Med* **7**, 463–477 (2018).

202. Dariš, B., Tancer Verboten, M., Knez, Ž. & Ferk, P. Cannabinoids in cancer treatment: Therapeutic potential and legislation. *Bosn J Basic Med Sci* **19**, 14–23 (2019).

203. Vidlarova, M. *et al.* Cannabinoid receptor 2 expression in early-stage non-small cell lung cancers identifies patients with good prognosis and longer survival. *Transl Lung Cancer Res* **11**, 2040–2050 (2022).

204. Martínez-Martínez, E. *et al.* Cannabinoids receptor type 2, CB2, expression correlates with human colon cancer progression and predicts patient survival. *Oncoscience* **2**, 131–141 (2015).

205. Sánchez, C. *et al.* Inhibition of glioma growth in vivo by selective activation of the CB(2) cannabinoid receptor. *Cancer Res* **61**, 5784–9 (2001).

206. Khan, M. I. *et al.* Involvement of the CB2 cannabinoid receptor in cell growth inhibition and G0/G1 cell cycle arrest via the cannabinoid agonist WIN 55,212–2 in renal cell carcinoma. *BMC Cancer* **18**, 583 (2018).

207. Ravi, J., Elbaz, M., Wani, N. A., Nasser, M. W. & Ganju, R. K. Cannabinoid receptor-2 agonist inhibits macrophage induced EMT in non-small cell lung cancer by downregulation of EGFR pathway. *Mol Carcinog* **55**, 2063–2076 (2016).

208. Velasco, G., Hernández-Tiedra, S., Dávila, D. & Lorente, M. The use of cannabinoids as anticancer agents. *Prog Neuropsychopharmacol Biol Psychiatry* **64**, 259–266 (2016).

209. Hinz, B. & Ramer, R. Cannabinoids as anticancer drugs: current status of preclinical research. *Br J Cancer* **127**, 1–13 (2022).

210. Tomko, A. M., Whynot, E. G., Ellis, L. D. & Dupré, D. J. Anti-Cancer Potential of Cannabinoids, Terpenes, and Flavonoids Present in Cannabis. *Cancers (Basel)* **12**, 1985 (2020).

211. Rahman, S. *et al.* The onus of cannabinoids in interrupting the molecular odyssey of breast cancer: A critical perspective on UPRER and beyond. *Saudi Pharmaceutical Journal* **27**, 437–445 (2019).

212. Jones, D., Pereira, E. R. & Padera, T. P. Growth and Immune Evasion of Lymph Node Metastasis. *Front Oncol* **8**, 36 (2018).

213. Nathanson, S. D. Insights into the mechanisms of lymph node metastasis. *Cancer* **98**, 413–423 (2003).

214. Alves, A. M., Paredes, J. & Schmitt, F. Expression of PD-L1 in primary breast carcinoma and lymph node metastases. *Surgical and Experimental Pathology* **2**, 7 (2019).

215. Kamiya, S. *et al.* Association between PD-L1 expression and lymph node metastasis in cutaneous squamous cell carcinoma. *Asia Pac J Clin Oncol* **16**, (2020).

216. Chen, J. *et al.* Drug concentrations in axillary lymph nodes after lymphatic chemotherapy on patients with breast cancer. *Breast Cancer Res* **6**, R474-7 (2004).

217. Jonkman, J. E. N. *et al.* An introduction to the wound healing assay using live-cell microscopy. *Cell Adh Migr* **8**, 440–51 (2014).

218. Jenei, V., Nystrom, M. L. & Thomas, G. J. Measuring Invasion in an Organotypic Model. in *Methods Mol Biol* vol. 769 223–232 (2011).

219. del Duca, D., Werbowetski, T. & del Maestro, R. F. Spheroid preparation from hanging drops: characterization of a model of brain tumor invasion. *J Neurooncol* **67**, 295–303 (2004).

220. Frantz, C., Stewart, K. M. & Weaver, V. M. The extracellular matrix at a glance. *J Cell Sci* **123**, 4195–200 (2010).

221. Kalluri, R. & Weinberg, R. A. The basics of epithelial-mesenchymal transition. *J Clin Invest* **119**, 1420–8 (2009).

222. Roche, J. The Epithelial-to-Mesenchymal Transition in Cancer. *Cancers (Basel)* **10**, 52 (2018).

223. Loh, C.-Y. *et al.* The E-Cadherin and N-Cadherin Switch in Epithelial-to-Mesenchymal Transition: Signaling, Therapeutic Implications, and Challenges. *Cells* **8**, 1118 (2019).

224. Klymkowsky, M. W. & Savagner, P. Epithelial-Mesenchymal Transition. *Am J Pathol* **174**, 1588–1593 (2009).

225. Brabletz, T., Kalluri, R., Nieto, M. A. & Weinberg, R. A. EMT in cancer. *Nat Rev Cancer* **18**, 128–134 (2018).

226. Ribatti, D., Tamma, R. & Annese, T. Epithelial-Mesenchymal Transition in Cancer: A Historical Overview. *Transl Oncol* **13**, 100773 (2020).

227. Giordano, A. *et al.* Epithelial–Mesenchymal Transition and Stem Cell Markers in Patients with HER2-Positive Metastatic Breast Cancer. *Mol Cancer Ther* **11**, 2526–2534 (2012).

228. Burnett, J. P. *et al.* Trastuzumab resistance induces EMT to transform HER2+ PTEN− to a triple negative breast cancer that requires unique treatment options. *Sci Rep* **5**, 15821 (2015).

229. Ingthorsson, S. *et al.* HER2 induced EMT and tumorigenicity in breast epithelial progenitor cells is inhibited by coexpression of EGFR. *Oncogene* **35**, 4244–4255 (2016).

230. D'Amato, V. *et al.* Mechanisms of lapatinib resistance in HER2-driven breast cancer. *Cancer Treat Rev* **41**, 877–883 (2015).

231. Palm, W. Metabolic plasticity allows cancer cells to thrive under nutrient starvation. *Proceedings of the National Academy of Sciences* **118**, (2021).

232. Ghanbari Movahed, Z., Rastegari-Pouyani, M., Mohammadi, M. H. & Mansouri, K. Cancer cells change their glucose metabolism to overcome increased ROS: One step from cancer cell to cancer stem cell? *Biomedicine & Pharmacotherapy* **112**, 108690 (2019).

233. Wu, W. & Zhao, S. Metabolic changes in cancer: beyond the Warburg effect. *Acta Biochim Biophys Sin (Shanghai)* **45**, 18–26 (2013).

234. Warburg, O., Wind, F. & Negelein, E. The metabolism of tumors in the body. *Journal of General Physiology* **8**, 519–530 (1927).

235. Hanahan, D. & Weinberg, R. A. Hallmarks of Cancer: The Next Generation. *Cell* **144**, 646–674 (2011).

236. Sreedhar, A. & Zhao, Y. Dysregulated metabolic enzymes and metabolicï¿½reprogramming in cancer cells (Review). *Biomed Rep* (2017) doi:10.3892/br.2017.1022.

237. Nowak, N., Kulma, A. & Gutowicz, J. Up-regulation of key glycolysis proteins in cancer development. *Open Life Sci* **13**, 569–581 (2018).

238. Tu, S.-H. *et al.* Increased expression of enolase α in human breast cancer confers tamoxifen resistance in human breast cancer cells. *Breast Cancer Res Treat* **121**, 539–553 (2010).

239. LeBleu, V. S. *et al.* PGC-1α mediates mitochondrial biogenesis and oxidative phosphorylation in cancer cells to promote metastasis. *Nat Cell Biol* **16**, 992–1003 (2014).

240. Mosier, J. A., Wu, Y. & Reinhart-King, C. A. Recent advances in understanding the role of metabolic heterogeneities in cell migration. *Fac Rev* **10**, (2021).

241. DeWane, G., Salvi, A. M. & DeMali, K. A. Fueling the cytoskeleton – links between cell metabolism and actin remodeling. *J Cell Sci* **134**, (2021).

242. Mosier, J. A., Schwager, S. C., Boyajian, D. A. & Reinhart-King, C. A. Cancer cell metabolic plasticity in migration and metastasis. *Clin Exp Metastasis* **38**, 343–359 (2021).

243. Parlani, M., Jorgez, C. & Friedl, P. Plasticity of cancer invasion and energy metabolism. *Trends Cell Biol* (2022) doi:10.1016/j.tcb.2022.09.009.

244. Riss, T. *et al.* Cell Viability Assays. in *Assay Guidance Manual* (eds. Markossian, S., Grossman, A. & Brimacombe, K.) (Eli Lilly & Company and the National Center for Advancing Translational Sciences, 2013).

245. Errede, B., Kamen, M. D. & Hatefi, Y. Preparation and properties of complex IV (Ferrocytochrome c: Oxygen oxidoreductase EC 1.9.3.1). in 40–47 (1978). doi:10.1016/S0076-6879(78)53011-5.

246. TeSlaa, T. & Teitell, M. A. Techniques to Monitor Glycolysis. in 91–114 (2014). doi:10.1016/B978-0-12-416618-9.00005-4.

247. Ahler, E. *et al.* Doxycycline Alters Metabolism and Proliferation of Human Cell Lines. *PLoS One* **8**, e64561 (2013).

248. Sancho, P., Barneda, D. & Heeschen, C. Hallmarks of cancer stem cell metabolism. *Br J Cancer* **114**, 1305–1312 (2016).

249. Chen, W., Dong, J., Haiech, J., Kilhoffer, M.-C. & Zeniou, M. Cancer Stem Cell Quiescence and Plasticity as Major Challenges in Cancer Therapy. *Stem Cells Int* **2016**, 1–16 (2016).

250. Wyatt, E. *et al.* Regulation and Cytoprotective Role of Hexokinase III. *PLoS One* **5**, e13823 (2010).

251. Ludvik, A. E. *et al.* HKDC1 Is a Novel Hexokinase Involved in Whole-Body Glucose Use. *Endocrinology* **157**, 3452–3461 (2016).

252. Li, G.-H. & Huang, J.-F. Inferring therapeutic targets from heterogeneous data: HKDC1 is a novel potential therapeutic target for cancer. *Bioinformatics* **30**, 748–752 (2014).

253. Wang, X. *et al.* HKDC1 promotes the tumorigenesis and glycolysis in lung adenocarcinoma via regulating AMPK/mTOR signaling pathway. *Cancer Cell Int* **20**, 450 (2020).

254. Mishra, D. & Banerjee, D. Lactate Dehydrogenases as Metabolic Links between Tumor and Stroma in the Tumor Microenvironment. *Cancers (Basel)* **11**, 750 (2019).

255. Liu, D. *et al.* Prognostic significance of serum lactate dehydrogenase in patients with breast cancer: a meta-analysis. *Cancer Manag Res* **Volume 11**, 3611–3619 (2019).

256. Mozdy, A. D., McCaffery, J. M. & Shaw, J. M. Dnm1p Gtpase-Mediated Mitochondrial Fission Is a Multi-Step Process Requiring the Novel Integral Membrane Component Fis1p. *Journal of Cell Biology* **151**, 367–380 (2000).

257. Corona, J. C. & Duchen, M. R. PPARγ as a therapeutic target to rescue mitochondrial function in neurological disease. *Free Radic Biol Med* **100**, 153–163 (2016).

258. O'Sullivan, S. E. An update on PPAR activation by cannabinoids. *Br J Pharmacol* **173**, 1899–1910 (2016).

259. Bouaboula, M. *et al.* Anandamide induced PPARγ transcriptional activation and 3T3-L1 preadipocyte differentiation. *Eur J Pharmacol* **517**, 174–181 (2005).

260. Sonego, A. B., Prado, D. da S. & Guimarães, F. S. PPARγ receptors are involved in the effects of cannabidiol on orofacial dyskinesia and cognitive dysfunction induced by typical antipsychotic in mice. *Prog Neuropsychopharmacol Biol Psychiatry* **111**, 110367 (2021).

261. Rouillard, A. D. *et al.* The harmonizome: a collection of processed datasets gathered to serve and mine knowledge about genes and proteins. *Database* **2016**, baw100 (2016).

262. Chang, C., Worley, B. L., Phaëton, R. & Hempel, N. Extracellular Glutathione Peroxidase GPx3 and Its Role in Cancer. *Cancers (Basel)* **12**, 2197 (2020).

263. Wu, X. *et al.* Alteration of endocannabinoid system in human gliomas. *J Neurochem* **120**, 842–849 (2012).

264. Li, Z. *et al.* Asymmetric Cell Division and Tumor Heterogeneity. *Front Cell Dev Biol* **10**, (2022).

265. Kim, D., Choi, B., Ryoo, I. & Kwak, M.-K. High NRF2 level mediates cancer stem cell-like properties of aldehyde dehydrogenase (ALDH)-high ovarian cancer cells: inhibitory role of all-trans retinoic acid in ALDH/NRF2 signaling. *Cell Death Dis* **9**, 896 (2018).

266. Zhou, H.-M., Zhang, J.-G., Zhang, X. & Li, Q. Targeting cancer stem cells for reversing therapy resistance: mechanism, signaling, and prospective agents. *Signal Transduct Target Ther* **6**, 62 (2021).

267. Frisch, S. M. & Ruoslahti, E. Integrins and anoikis. *Curr Opin Cell Biol* **9**, 701–706 (1997).

268. Takahashi, K. & Yamanaka, S. Induction of Pluripotent Stem Cells from Mouse Embryonic and Adult Fibroblast Cultures by Defined Factors. *Cell* **126**, 663–676 (2006).

269. Fatma, H. & Siddique, H. R. Pluripotency inducing Yamanaka factors: role in stemness and chemoresistance of liver cancer. *Expert Rev Anticancer Ther* **21**, 853–864 (2021).

270. Gong, L. *et al.* Cancer cell reprogramming: a promising therapy converting malignancy to benignity. *Cancer Commun* **39**, 48 (2019).

271. Horimoto, Y. *et al.* Combination of Cancer Stem Cell Markers CD44 and CD24 Is Superior to ALDH1 as a Prognostic Indicator in Breast Cancer Patients with Distant Metastases. *PLoS One* **11**, e0165253 (2016).

272. Kong, Y. *et al.* Breast cancer stem cell markers CD44 and ALDH1A1 in serum: distribution and prognostic value in patients with primary breast cancer. *J Cancer* **9**, 3728–3735 (2018).

273. Sneath, R. J. & Mangham, D. C. The normal structure and function of CD44 and its role in neoplasia. *Molecular Pathology* **51**, 191–200 (1998).

274. McFarlane, S. *et al.* CD44 increases the efficiency of distant metastasis of breast cancer. *Oncotarget* **6**, 11465–11476 (2015).

275. Khoury, T. *et al.* Aldehyde dehydrogenase 1A1 expression in breast cancer is associated with stage, triple negativity, and outcome to neoadjuvant chemotherapy. *Modern Pathology* **25**, 388–397 (2012).

276. Li, X., Xu, Q., Fu, X. & Luo, W. ALDH1A1 overexpression is associated with the progression and prognosis in gastric cancer. *BMC Cancer* **14**, 705 (2014).

277. Yue, H. *et al.* ALDH1A1 in Cancers: Bidirectional Function, Drug Resistance, and Regulatory Mechanism. *Front Oncol* **12**, (2022).

278. Tomita, H., Tanaka, K., Tanaka, T. & Hara, A. Aldehyde dehydrogenase 1A1 in stem cells and cancer. *Oncotarget* **7**, 11018–11032 (2016).

279. Vassalli, G. Aldehyde Dehydrogenases: Not Just Markers, but Functional Regulators of Stem Cells. *Stem Cells Int* **2019**, 1–15 (2019).

280. Saumet, A. *et al.* Estrogen and retinoic acid antagonistically regulate several microRNA genes to control aerobic glycolysis in breast cancer cells. *Mol Biosyst* **8**, 3242 (2012).

281. Doan, T. B. *et al.* A tumour suppressive relationship between mineralocorticoid and retinoic acid receptors activates a transcriptional program consistent with a reverse Warburg effect in breast cancer. *Breast Cancer Research* **22**, 122 (2020).

282. Al-Juboori, S. IK. *et al.* PYK2 promotes HER2-positive breast cancer invasion. *Journal of Experimental & Clinical Cancer Research* **38**, 210 (2019).

283. Wang, W. *et al.* ALDH1A1 maintains the cancer stem-like cells properties of esophageal squamous cell carcinoma by activating the AKT signal pathway and interacting with β-catenin. *Biomedicine & Pharmacotherapy* **125**, 109940 (2020).

284. Ghyselinck, N. B. & Duester, G. Retinoic acid signaling pathways. *Development* **146**, (2019).

285. Xia, P. & Xu, X.-Y. PI3K/Akt/mTOR signaling pathway in cancer stem cells: from basic research to clinical application. *Am J Cancer Res* **5**, 1602–9 (2015).

286. Poturnajova, M., Kozovska, Z. & Matuskova, M. Aldehyde dehydrogenase 1A1 and 1A3 isoforms – mechanism of activation and regulation in cancer. *Cell Signal* **87**, 110120 (2021).

287. Komiya, Y. & Habas, R. Wnt signal transduction pathways. *Organogenesis* **4**, 68–75 (2008).

288. Veeman, M. T., Slusarski, D. C., Kaykas, A., Louie, S. H. & Moon, R. T. Zebrafish Prickle, a Modulator of Noncanonical Wnt/Fz Signaling, Regulates Gastrulation Movements. *Current Biology* **13**, 680–685 (2003).

289. Orian-Rousseau, V. & Schmitt, M. CD44 regulates Wnt signaling at the level of LRP6. *Mol Cell Oncol* **2**, e995046 (2015).

290. Peng, Z. *et al.* Identification of CTLA-4 associated with tumor microenvironment and competing interactions in triple negative breast cancer by co-expression network analysis. *J Cancer* **11**, 6365–6375 (2020).

291. Cirqueira, M. B. *et al.* Prognostic Role of PD-L1 Expression in Invasive Breast Cancer: A Systematic Review and Meta-Analysis. *Cancers (Basel)* **13**, 6090 (2021).

292. Litvin, I. E., Paganella, M. P., Wendland, E. M. & Roehe, A. V. Prognosis of PD-L1 in human breast cancer: protocol for a systematic review and meta-analysis. *Syst Rev* **9**, 66 (2020).

293. de Sousa Linhares, A. *et al.* Therapeutic PD-L1 antibodies are more effective than PD-1 antibodies in blocking PD-1/PD-L1 signaling. *Sci Rep* **9**, 11472 (2019).

294. Jackson, S. E. & Chester, J. D. Personalised cancer medicine. *Int J Cancer* **137**, 262–266 (2015).

295. Hashiesh, H. M., Sharma, C., Goyal, S. N., Jha, N. K. & Ojha, S. Pharmacological Properties, Therapeutic Potential and Molecular Mechanisms of JWH133, a CB2 Receptor-Selective Agonist. *Front Pharmacol* **12**, (2021).

296. Huffman, J. W. *et al.* 3-(1′,1′-Dimethylbutyl)-1-deoxy-Δ 8 -THC and related compounds: synthesis of selective ligands for the CB 2 receptor. *Bioorg Med Chem* **7**, 2905–2914 (1999).

297. Gertsch, J. *et al.* Beta-caryophyllene is a dietary cannabinoid. *Proceedings of the National Academy of Sciences* **105**, 9099–9104 (2008).

298. Ibrahim, M. M. *et al.* Activation of CB2 cannabinoid receptors by AM1241 inhibits experimental neuropathic pain: Pain inhibition by receptors not present in the CNS. *Proceedings of the National Academy of Sciences* **100**, 10529–10533 (2003).

299. Qamri, Z. *et al.* Synthetic cannabinoid receptor agonists inhibit tumor growth and metastasis of breast cancer. *Mol Cancer Ther* **8**, 3117–3129 (2009).

300. Zhang, J. *et al.* Combined CB2 receptor agonist and photodynamic therapy synergistically inhibit tumor growth in triple negative breast cancer. *Photodiagnosis Photodyn Ther* **24**, 185–191 (2018).

301. Singh, K., Jamshidi, N., Zomer, R., Piva, T. J. & Mantri, N. Cannabinoids and Prostate Cancer: A Systematic Review of Animal Studies. *Int J Mol Sci* **21**, 6265 (2020).

302. Carracedo, A. *et al.* Cannabinoids Induce Apoptosis of Pancreatic Tumor Cells via Endoplasmic Reticulum Stress–Related Genes. *Cancer Res* **66**, 6748–6755 (2006).

303. Preet, A., Ganju, R. K. & Groopman, J. E. Δ9-Tetrahydrocannabinol inhibits epithelial growth factor-induced lung cancer cell migration in vitro as well as its growth and metastasis in vivo. *Oncogene* **27**, 339–346 (2008).

304. Xu, S., Ma, H., Bo, Y. & Shao, M. The oncogenic role of CB2 in the progression of non-small-cell lung cancer. *Biomedicine & Pharmacotherapy* **117**, 109080 (2019).

305. Pourkhalili, N. *et al.* Evaluation of anti-invasion effect of cannabinoids on human hepatocarcinoma cells. *Toxicol Mech Methods* **23**, 120–126 (2013).

306. Xian, X.-S. *et al.* Effect of a synthetic cannabinoid agonist on the proliferation and invasion of gastric cancer cells. *J Cell Biochem* (2010) doi:10.1002/jcb.22540.

307. Adhikary, S., Kocieda, V. P., Yen, J.-H., Tuma, R. F. & Ganea, D. Signaling through cannabinoid receptor 2 suppresses murine dendritic cell migration by inhibiting matrix metalloproteinase 9 expression. *Blood* **120**, 3741–3749 (2012).

308. Hinz, B. & Ramer, R. Anti-tumour actions of cannabinoids. *Br J Pharmacol* **176**, 1384–1394 (2019).

309. Fan, H. & Guan, J.-L. Compensatory Function of Pyk2 Protein in the Promotion of Focal Adhesion Kinase (FAK)-null Mammary Cancer Stem Cell Tumorigenicity and Metastatic Activity. *Journal of Biological Chemistry* **286**, 18573–18582 (2011).

310. Glogauer, J. & Blay, J. Cannabinoids, their cellular receptors, and effects on the invasive phenotype of carcinoma and metastasis. *Cancer Rep* **5**, (2022).

311. Li, L.-T. *et al.* Cannabinoid receptors promote chronic intermittent hypoxia-induced breast cancer metastasis via IGF-1R/AKT/GSK-3β. *Mol Ther Oncolytics* **23**, 220–230 (2021).

312. Milian, L. *et al.* Cannabinoid receptor expression in non-small cell lung cancer. Effectiveness of tetrahydrocannabinol and cannabidiol inhibiting cell proliferation and epithelial-mesenchymal transition in vitro. *PLoS One* **15**, e0228909 (2020).

313. Burks, H. E. *et al.* ZEB2 regulates endocrine therapy sensitivity and metastasis in luminal a breast cancer cells through a non-canonical mechanism. *Breast Cancer Res Treat* **189**, 25–37 (2021).

314. Xian, X. *et al.* WIN 55,212-2 Inhibits the Epithelial Mesenchymal Transition of Gastric Cancer Cells via COX-2 Signals. *Cellular Physiology and Biochemistry* **39**, 2149–2157 (2016).

315. Xu, X., Zhang, M., Xu, F. & Jiang, S. Wnt signaling in breast cancer: biological mechanisms, challenges and opportunities. *Mol Cancer* **19**, 165 (2020).

316. Pagano, C., Navarra, G., Coppola, L., Bifulco, M. & Laezza, C. Molecular Mechanism of Cannabinoids in Cancer Progression. *Int J Mol Sci* **22**, 3680 (2021).

317. Jernström, S. *et al.* Drug-screening and genomic analyses of HER2-positive breast cancer cell lines reveal predictors for treatment response. *Breast Cancer: Targets and Therapy* **Volume 9**, 185–198 (2017).

318. Ullah, H., Di Minno, A., Santarcangelo, C., Khan, H. & Daglia, M. Improvement of Oxidative Stress and Mitochondrial Dysfunction by β-Caryophyllene: A Focus on the Nervous System. *Antioxidants* **10**, 546 (2021).

319. Dai, X., Cheng, H., Bai, Z. & Li, J. Breast Cancer Cell Line Classification and Its Relevance with Breast Tumor Subtyping. *J Cancer* **8**, 3131–3141 (2017).

320. Ruh, M. F., Taylor, J. A., Howlett, A. C. & Welshons, W. V. Failure of cannabinoid compounds to stimulate estrogen receptors. *Biochem Pharmacol* **53**, 35–41 (1997).

321. Geddo, F. *et al.* Plant-Derived Trans-β-Caryophyllene Boosts Glucose Metabolism and ATP Synthesis in Skeletal Muscle Cells through Cannabinoid Type 2 Receptor Stimulation. *Nutrients* **13**, 916 (2021).

322. Dando, I. *et al.* Cannabinoids inhibit energetic metabolism and induce AMPK-dependent autophagy in pancreatic cancer cells. *Cell Death Dis* **4**, e664–e664 (2013).

323. Galbraith, L. C. A. *et al.* PPAR-gamma induced AKT3 expression increases levels of mitochondrial biogenesis driving prostate cancer. *Oncogene* **40**, 2355–2366 (2021).

324. Angelina, A. *et al.* Cannabinoids induce functional Tregs by promoting tolerogenic DCs via autophagy and metabolic reprograming. *Mucosal Immunol* **15**, 96–108 (2022).

325. Zhou, S. *et al.* Cannabinoid receptor 2 plays a central role in renal tubular mitochondrial dysfunction and kidney ageing. *J Cell Mol Med* **25**, 8957–8972 (2021).

326. Yu, Z., Pestell, T. G., Lisanti, M. P. & Pestell, R. G. Cancer stem cells. *Int J Biochem Cell Biol* **44**, 2144–2151 (2012).

327. Friedmann-Morvinski, D. & Verma, I. M. Dedifferentiation and reprogramming: origins of cancer stem cells. *EMBO Rep* **15**, 244–253 (2014).

328. Peeri, H. & Koltai, H. Cannabis Biomolecule Effects on Cancer Cells and Cancer Stem Cells: Cytotoxic, Anti-Proliferative, and Anti-Migratory Activities. *Biomolecules* **12**, 491 (2022).

329. Marzagalli, M., Fontana, F., Raimondi, M. & Limonta, P. Cancer Stem Cells—Key Players in Tumor Relapse. *Cancers (Basel)* **13**, 376 (2021).

330. Fiorillo, M., Sotgia, F. & Lisanti, M. P. 'Energetic' cancer stem cells (e-CSCs): A new hyper-metabolic and proliferative tumor cell phenotype, driven by mitochondrial energy. *Front Oncol* **9**, (2019).

331. Yadav, A. K. & Desai, N. S. Cancer Stem Cells: Acquisition, Characteristics, Therapeutic Implications, Targeting Strategies and Future Prospects. *Stem Cell Rev Rep* **15**, 331–355 (2019).

332. Agliano, A., Calvo, A. & Box, C. The challenge of targeting cancer stem cells to halt metastasis. *Semin Cancer Biol* **44**, 25–42 (2017).

333. Jagust, P., Alcalá, S., Jr, B. S., Heeschen, C. & Sancho, P. Glutathione metabolism is essential for self-renewal and chemoresistance of pancreatic cancer stem cells. *World J Stem Cells* **12**, 1410–1428 (2020).

334. Koltai, H. & Shalev, N. Anti-Cancer Activity of Cannabis sativa Phytocannabinoids: Molecular Mechanisms and Potential in the Fight against Ovarian Cancer and Stem Cells. *Cancers (Basel)* **14**, 4299 (2022).

335. Ginestier, C. *et al.* ALDH1 Is a Marker of Normal and Malignant Human Mammary Stem Cells and a Predictor of Poor Clinical Outcome. *Cell Stem Cell* **1**, 555–567 (2007).

336. Hilton, J. Role of aldehyde dehydrogenase in cyclophosphamide-resistant L1210 leukemia. *Cancer Res* **44**, 5156–60 (1984).

337. Clark, D. W. & Palle, K. Aldehyde dehydrogenases in cancer stem cells: potential as therapeutic targets. *Ann Transl Med* **4**, 518–518 (2016).

338. Turdo, A. *et al.* Meeting the Challenge of Targeting Cancer Stem Cells. *Front Cell Dev Biol* **7**, (2019).

339. Choi, H. Y. *et al.* G protein-coupled receptors in stem cell maintenance and somatic reprogramming to pluripotent or cancer stem cells. *BMB Rep* **48**, 68–80 (2015).

340. Nalli, Y. *et al.* Analyzing the role of cannabinoids as modulators of Wnt/β-catenin signaling pathway for their use in the management of neuropathic pain. *Bioorg Med Chem Lett* **29**, 1043–1046 (2019).

341. Marselos, M., Vasiliou, V., Malamasi, M., Alikaridis, F. & Kefalas, T. Effects of Cannabis and Tobacco on the Ezymes of Alcohol Metabolism in the Rat. *Rev Environ Health* **9**, (1991).

342. Peeri, H. *et al.* Specific Compositions of Cannabis sativa Compounds Have Cytotoxic Activity and Inhibit Motility and Colony Formation of Human Glioblastoma Cells In Vitro. *Cancers (Basel)* **13**, 1720 (2021).

343. Aguado, T. *et al.* Cannabinoids Induce Glioma Stem-like Cell Differentiation and Inhibit Gliomagenesis. *Journal of Biological Chemistry* **282**, 6854–6862 (2007).

344. Li, W. *et al.* Unraveling the roles of CD44/CD24 and ALDH1 as cancer stem cell markers in tumorigenesis and metastasis. *Sci Rep* **7**, 13856 (2017).

345. Valkenburg, K. C., Graveel, C. R., Zylstra-Diegel, C. R., Zhong, Z. & Williams, B. O. Wnt/β-catenin Signaling in Normal and Cancer Stem Cells. *Cancers (Basel)* **3**, 2050–2079 (2011).

346. Condello, S. *et al.* β-Catenin-regulated ALDH1A1 is a target in ovarian cancer spheroids. *Oncogene* **34**, 2297–2308 (2015).

347. Zhou, S. *et al.* Cannabinoid receptor type 2 promotes kidney fibrosis through orchestrating β-catenin signaling. *Kidney Int* **99**, 364–381 (2021).

348. Ji, H. *et al.* Proteomic profiling of secretome and adherent plasma membranes from distinct mammary epithelial cell subpopulations. *Proteomics* **11**, 4029–4039 (2011).

349. Reddy, S. *et al.* Characterization of Wnt gene expression in developing and postnatal hair follicles and identification of Wnt5a as a target of Sonic hedgehog in hair follicle morphogenesis. *Mech Dev* **107**, 69–82 (2001).

350. Ovcharenko, A., Granot, G., Shpilberg, O. & Raanani, P. Retinoic acid induces adhesion and migration in NB4 cells through Pyk2 signaling. *Leuk Res* **37**, 956–62 (2013).

351. Gil Del Alcazar, C. R., Alečković, M. & Polyak, K. Immune Escape during Breast Tumor Progression. *Cancer Immunol Res* **8**, 422–427 (2020).

352. Bates, J. P., Derakhshandeh, R., Jones, L. & Webb, T. J. Mechanisms of immune evasion in breast cancer. *BMC Cancer* **18**, 556 (2018).

353. Drake, C. G., Jaffee, E. & Pardoll, D. M. Mechanisms of Immune Evasion by Tumors. in 51–81 (2006). doi:10.1016/S0065-2776(06)90002-9.

354. Wang, M. *et al.* Mechanism of immune evasion in breast cancer. *Onco Targets Ther* **Volume 10**, 1561–1573 (2017).

355. Yu, H. *et al.* Cytotoxic T lymphocyte antigen 4 expression in human breast cancer: implications for prognosis. *Cancer Immunology, Immunotherapy* **64**, 853–860 (2015).

356. Zitvogel, L. & Kroemer, G. Targeting PD-1/PD-L1 interactions for cancer immunotherapy. *Oncoimmunology* **1**, 1223–1225 (2012).

357. Han, Y., Liu, D. & Li, L. PD-1/PD-L1 pathway: current researches in cancer. *Am J Cancer Res* **10**, 727–742 (2020).

358. Cai, J., Wang, D., Zhang, G. & Guo, X. The Role Of PD-1/PD-L1 Axis In Treg Development And Function: Implications For Cancer Immunotherapy. *Onco Targets Ther* **12**, 8437–8445 (2019).

359. Jalali, S. *et al.* Reverse signaling via PD-L1 supports malignant cell growth and survival in classical Hodgkin lymphoma. *Blood Cancer J* **9**, 22 (2019).

360. Agostinetto, E. *et al.* Immunotherapy for HER2-Positive Breast Cancer: Clinical Evidence and Future Perspectives. *Cancers (Basel)* **14**, 2136 (2022).

361. Dirix, L. Y. *et al.* Avelumab, an anti-PD-L1 antibody, in patients with locally advanced or metastatic breast cancer: a phase 1b JAVELIN Solid Tumor study. *Breast Cancer Res Treat* **167**, 671–686 (2018).

362. Lastwika, K. J. *et al.* Control of PD-L1 Expression by Oncogenic Activation of the AKT–mTOR Pathway in Non–Small Cell Lung Cancer. *Cancer Res* **76**, 227–238 (2016).

363. Yang, Y. *et al.* Cannabinoids Inhibited Pancreatic Cancer via P-21 Activated Kinase 1 Mediated Pathway. *Int J Mol Sci* **21**, 8035 (2020).

Chapter 10 Appendix

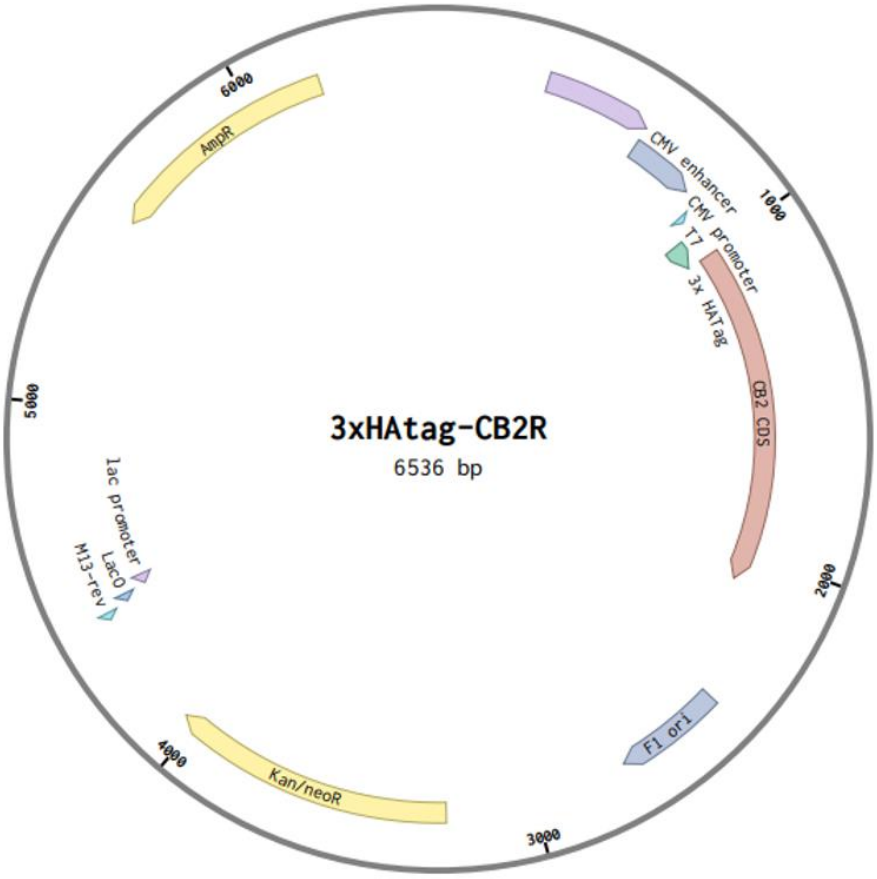

Appendix figure 1: The pcDNA3.1 vector containing the gene for CB2 with a 5' sequence for a 3x hemagglutinin (HA) tag (3xHA tag-CB2R).

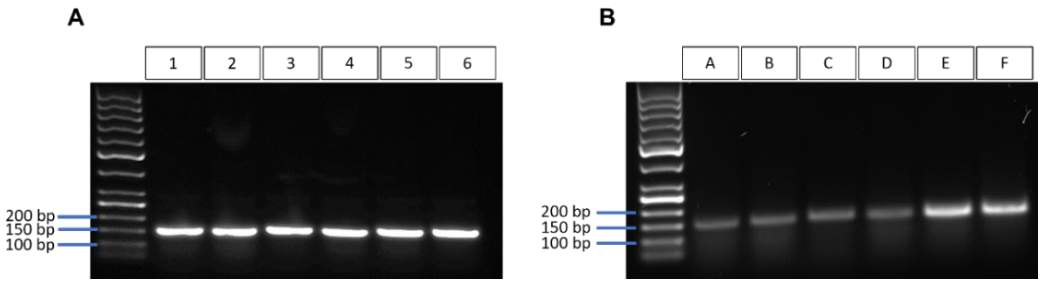

Appendix figure 2: DNA gels of colony PCR products.

DNA agarose gels of colony PCR from bacterial colonies 1-6 of the BP reaction (A) and colonies A-F (B)of the LR reaction, using *CNR2* qPCR primers, with an amplicon of 120 bp.

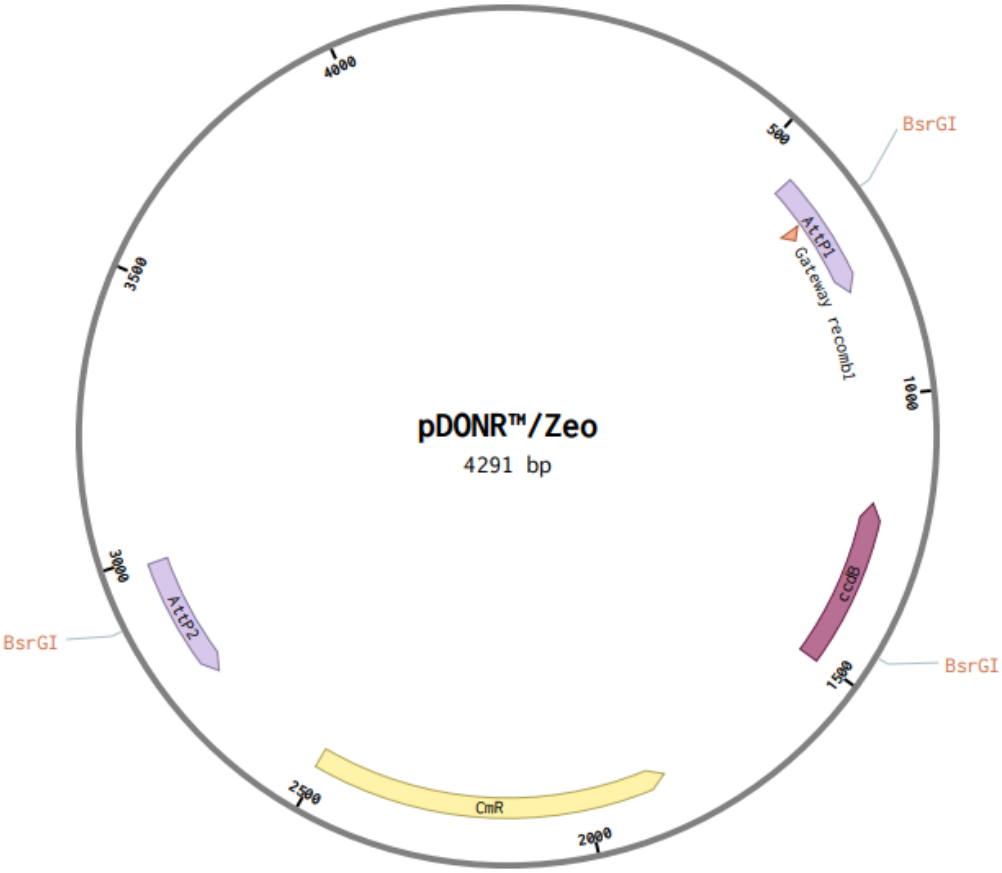

Appendix figure 3: The pDONR plasmid used in Gateway cloning, containing three bsrG1 restriction sites.

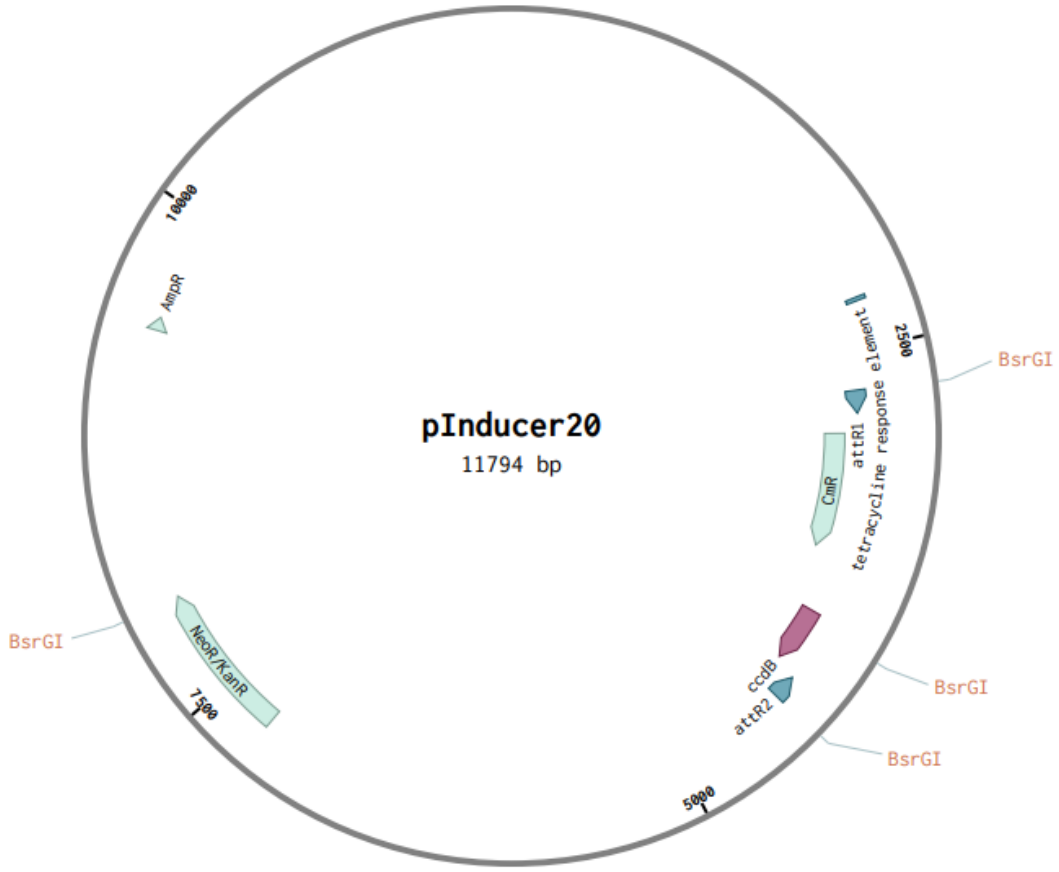

Appendix figure 4: The pINDUCER plasmid HA-*CNR2* was inserted into during in Gateway cloning, containing four bsrG1 restriction sites.

Appendix Table 1: Cell line information

Cell Line	Derivation	Stage	Origin Patient	Molecular Subtype	Mutations
HCC1954	Breast ductal carcinoma	Stage IIa	61-year-old Asian woman	HER2+ ER- PR-	PTEN (loss) TP53 (Y163C) PIK3CA (H1047R)
BT474	Invasive breast ductal carcinoma	Stage II	60-year-old white woman	HER2+ ER+ PR+	TP53 (E285K) PIK3CA (L111N)
SKBR3	Pleural effusion	-	43-year-old white woman	HER2+ ER- PR-	PTEN (loss) TP53 (R175H)

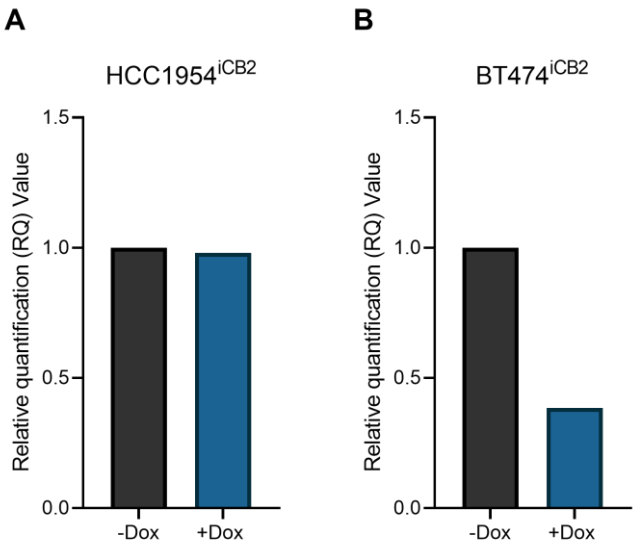

Appendix figure 5: CB_2 expression following dox treatment not due to genomic DNA contamination.

RT-qPCR analysis of HCC1954^{iCB2} (A) and BT474^{iCB2} (B) cells +/- 24-hour CB_2 induction with 1 µg/ml dox, using MMP13 genomic DNA primers. n=1

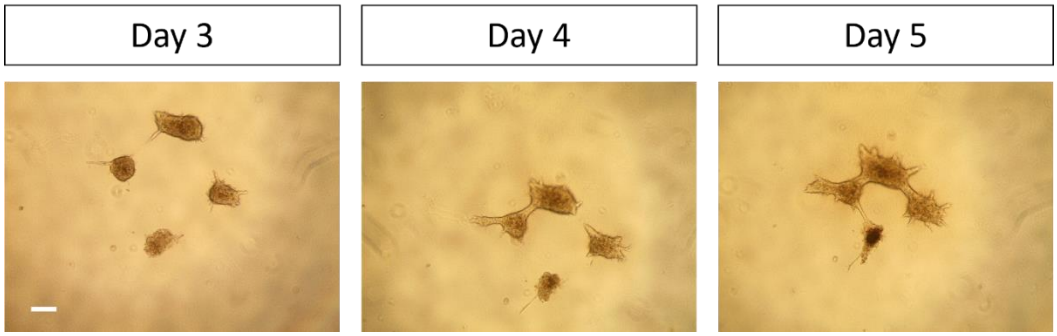

Appendix figure 6: Coalescence of spheroids in the hanging drop model.

Brightfield images of HCC1954^{iCB2} spheroids growing into one another, captured at day 3, day4 and day 5 of culture.

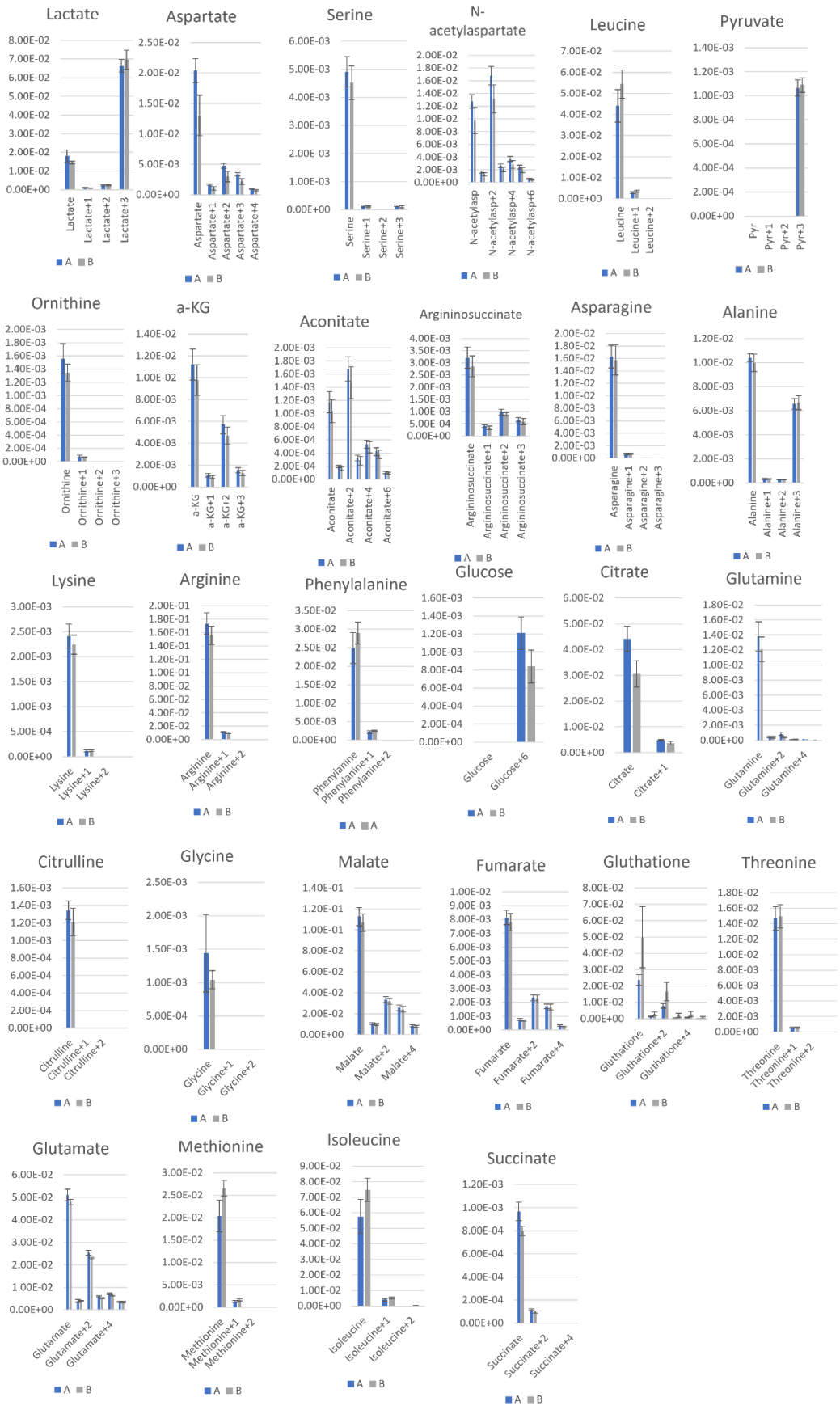
Lactate
Lactate
Lactate+1
Lactate+2
Lactate+3
Aspartate
Aspartate
Aspartate+1
Aspartate+2
Aspartate+3
Aspartate+4
Serine
Serine
Serine+1
Serine+2
Serine+3
N-acetylaspartate
N-acetylasp
N-acetylasp+2
N-acetylasp+4
N-acetylasp+6
Leucine
Leucine
Leucine+1
Leucine+2
Pyruvate
Pyr
Pyr+1
Pyr+2
Pyr+3
A
B
Ornithine
Ornithine
Ornithine+1
Ornithine+2
Ornithine+3
a-KG
a-KG
a-KG+1
a-KG+2
a-KG+3
Aconitate
Aconitate
Aconitate+2
Aconitate+4
Aconitate+6
Argininosuccinate
Argininosuccinate
Argininosuccinate+1
Argininosuccinate+2
Argininosuccinate+3
Asparagine
Asparagine
Asparagine+1
Asparagine+2
Asparagine+3
Alanine
Alanine
Alanine+1
Alanine+2
Alanine+3
Lysine
Lysine
Lysine+1
Lysine+2
Arginine
Arginine
Arginine+1
Arginine+2
Phenylalanine
Phenylalanine
Phenylalanine+1
Phenylalanine+2
Glucose
Glucose
Glucose+6
Citrate
Citrate
Citrate+1
Glutamine
Glutamine
Glutamine+2
Glutamine+4
Citrulline
Citrulline
Citrulline+1
Citrulline+2
Glycine
Glycine
Glycine+1
Glycine+2
Malate
Malate
Malate+2
Malate+4
Fumarate
Fumarate
Fumarate+2
Fumarate+4
Gluthatione
Gluthatione
Gluthatione+2
Gluthatione+4
Threonine
Threonine
Threonine+1
Threonine+2
Glutamate
Glutamate
Glutamate+2
Glutamate+4
Methionine
Methionine
Methionine+1
Methionine+2
Isoleucine
Isoleucine
Isoleucine+1
Isoleucine+2
Succinate
Succinate
Succinate+2
Succinate+4

Appendix figure 7: Fluxomic mass spectrometry analysis of HCC1954^{iCB2} cells with and without CB_2 expression.

Total Ion Count (TIC), y-axis, values of targeted metabolites containing ^{13}C-glucose in HCC1954^{iCB2} cells without (A) and with (B) 24-hours of CB_2 expression. The x-axis, metabolite + n indicates the presence of additional ^{13}C atoms in the metabolite. Note Lactate with the highest proportion of ^{13}C atoms of all metabolites.

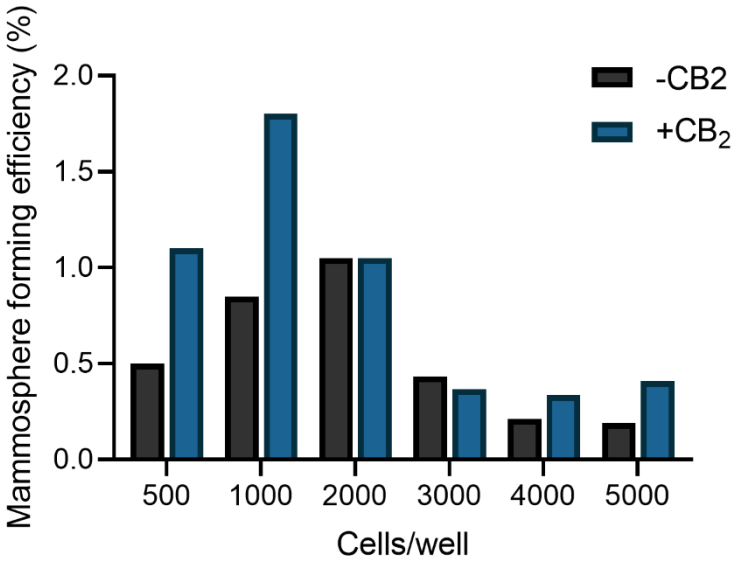

Appendix figure 8: Mammosphere formation assay cell titration.

Mammosphere forming efficiency in HCC1954^{iCB2} cells +/- 7-day CB_2 induction with 1 µg/ml dox at different cell concentrations per well.

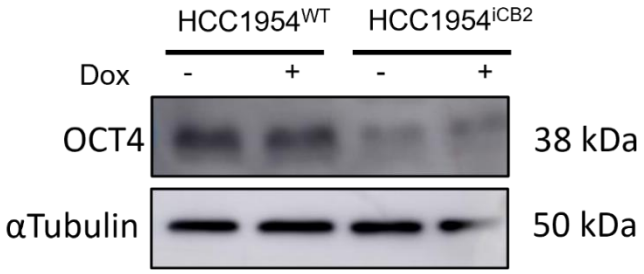

Appendix figure 9: No detectable change in OCT4 expression irrespective of CB_2 expression

Western blot of using anti-OCT4 antibody in HCC1954WT and HCC1954iCB2 cells with and without 24-hour CB2 induction. αTubulin used as loading control. Representative of n=2. Experiment performed by QMUL BSc student Hema Mall.